SYNTHESIS, STRUCTURE AND REACTIVITY OF W(IV) COMPLEXES: DEVELOPMENT OF AN OLEFIN DIMERIZATION CATALYST

By

RYAN C. MILLS

A DISSERTATION PRESENTED TO THE GRADUATE SCHOOL
OF THE UNIVERSITY OF FLORIDA IN PARTIAL FULFILLMENT
OF THE REQUIREMENTS FOR THE DEGREE OF
DOCTOR OF PHILOSOPHY

UNIVERSITY OF FLORIDA

2001

ACKNOWLEDGMENTS

The individuals deserving thanks from the author for their role in the completion of this dissertation are innumerable. First and foremost, I would like to thank my parents, Olin and Lynne for their unwavering support throughout this long and enduring process. Their love and guidance has helped me to be successful not only in chemistry, but also in life. The values that they have instilled in me have and will always guide me in every facet of life.

My most sincere respect and gratitude are extended to my research advisor, Dr. James M. Boncella, for his support and guidance. His advice and encouragement during the frustrating times and his excitement over the successes realized during this journey have been a constant source of motivation. More importantly, his willingness to allow me to learn from my mistakes and generate my own ideas of what was important to investigate has molded me into the chemist I am today. I believe that if Jim had not taken this approach, the skills and knowledge that I would have obtained could not have compared to the actual results of this educational process.

I also wish to thank Dr. Khalil A. Abboud. He solved and helped explain all of the structures presented in this dissertation as well as the many structures that are not included here. Khalil has not only taught me everything I know about crystallography, but he has also been the source of many valuable personal and professional discussions.

Many people have passed through the Boncella group during my time here. I would like to thank each and every one of them, for they have all played a role in the

completion of this dissertation. I give special thanks to Dr. Shu-Yu Steve Wang, Dr. Carlos Ortiz and Dr. David Knoeppel as they taught me all of the skills that made this work possible. I also give thanks to Ken Weakley for being a constant source of friendship during these five years. This is greatly appreciated because it was a tough task for him to convince his wife that the appropriate activities for a fall Saturday afternoon were to drink a lot of beer and watch football.

I also would like to thank all of the friends that I have made in my time at the University of Florida. Each and every one of them has played an important role and will always be remembered. Without them any semblance of a normal life would have been impossible.

Finally, I wish to thank a very special person, Kimberly Deters, who has been the driving force for the completion of this dissertation. Kimberly has been a constant source of strength and motivation throughout this process and I am extremely grateful for this because her endeavors are just as demanding. She has always said that good things happen to good, hard-working people and I now believe that to be true.

TABLE OF CONTENTS

page

ACKNOWLEDGMENTS ii

ABSTRACT viii

CHAPTERS

1 INTRODUCTION AND BACKGROUND 1

Hydroformylation 5
Acetic Acid Synthesis 7
Alkene Hydrogenation 8

2 HYDROGENOLYSIS OF β-HYDROGEN CONTAINING DIALKYLS: SYNTHESIS OF d^2 TUNGSTEN ARENE COMPLEXES AND THEIR REACTION WITH DIPHENYLACETYLENE 13

Introduction 13
Synthesis and Characterization of W(IV)-arene Complexes 15
[2+2] Cycloaddition of Diphenylacetylene and Styrene 20
Proposed Mechanism for Coupling 21
Synthesis of a W(IV) Mixed-dialkyl Complex 24
Cycloaddition and Rearrangement Steps 25
Conclusions 26

3 COORDINATIVELY UNSATURATED W(IV) BIS-PYRIDINE COMPLEXES: A REACTIVE SOURCE OF W(IV) 28

Introduction 28
Arene Displacement Reactions 29
Spectroscopic and X-ray Crystallographic Studies 30
Bonding Explanation for Hindered Rotation 33
Improved Synthesis of $W(IV)L_2$ Compounds 35
Addition of a Sixth Ligand to $W(IV)L_2$ 36
Ligand Substitution Reactivity 41
Substitution of One Pyridine Ligand 41
Synthesis of $W(IV)(PMe_3)_2L$ Complexes 42
Conclusions 45

4 REACTION OF THE W(IV)L_2 COMPLEXES WITH VARIOUS UNSATURATED SUBSTRATES: UNDERSTANDING THE REACTIVITY OF THE W(NPh)[o-$(Me_3SiN)_2C_6H_4$] FRAGMENT 46

Introduction 46
Early-Transition Metal Acetylene Complexes 46
Early-Transition Metal Butadiene Complexes 48
Early-Transition Metal Olefin Complexes 49
Synthesis and Characterization of a W-alkyne Complex 51
X-ray Structural Analysis 53
Ligand Fold Angle 55
Hydrogenation Reactions 56
Synthesis and Characterization of W(IV)(butadiene) Complexes 57
X-ray Structural Analysis of **17** 58
NMR Spectroscopic Analysis of **17** and **18** 61
Description of Fluxionality 62
Acetone Insertion 69
Reactions of W(IV)L_2 with Olefins 73
Mechanism for Oxidative Coupling 74
Initial Olefin Coordination 74
Ligand Displacement and Oxidative Coupling 77
Conclusions 79

5 CARBON-SULFUR BOND ACTIVATION OF THIOPHENES BY W(NPh)[o-$(Me_3SiN)_2C_6H_4$](PYRIDINE)$_2$ 80

Introduction 80
C-S Bond Activation Reactions 83
Thiophene C-S Bond Activation 83
2-Methylthiophene and Benzothiophene 87
3-Methylthiophene 89
Mechanistic Considerations 91
Conclusions 92

6 TUNGSTEN CATALYZED OLEFIN DIMERIZATION AND CODIMERIZATION 95

Introduction 95
Metallacyclopentane Decomposition 99
Catalytic Ethylene Dimerization and Codimerization with Butene 101
Product Characterization 102
W(NPh)[o-$(Me_3SiN)_2C_6H_4$]Cl_2 as a Catalyst Precursor 106
Activation of W($CH_2CH_2CH_2CH_2$)(NPh)[o-$(Me_3SiN)_2C_6H_4$] (**20**) 107
Alkylidene Formation for the Aniline/W/Al System 108
Activation of W(NPh)[o-$(Me_3SiN)_2C_6H_4$]Cl_2 (**28**) 110

Alkylidene Decomposition 113
Ligand C-H Activation 114
Bimolecular Decomposition 116
Ethylidene Rearrangement 117
Proposed Activation of **28** 118
Dimerization Substrate Selectivity 119
Straight-Chain α-Olefins 120
Cyclic Olefins and Dienes as Substrates 123
Alkene Oligomerization 124
Conclusions 127

7 SUMMARY AND CONCLUSIONS 129

8 EXPERIMENTAL PROCEDURES 134

General Methods 134
Synthesis of W(NPh)($CH_2CH_2CH_2Ph$)$_2$(o-(Me_3SiN)$_2C_6H_4$) (**2**) 135
Synthesis of W(NPh)(η^4-ethylbenzene)(o-(Me_3SiN)$_2C_6H_6$) (**3**) 135
Synthesis of W(NPh)(η^4-propylbenzene)(o-(Me_3SiN)$_2C_6H_6$) (**4**) 136
Synthesis of [o-(Me_3SiN)$_2C_6H_4$)(NPh)W$CH_2C(Ph)=C(Ph)CHPh$] (**5**) 137
Synthesis of [o-(Me_3SiN)$_2C_6H_4$)(NPh)W$CH_2C(Ph)=C(Ph)CHPh$] (**5**) From W(NPh)[o-(Me_3SiN)$_2C_6H_6$](CH$_2$CH$_2$Ph)(Me) (**7**) 137
Synthesis of W(NPh)[o-(Me_3SiN)$_2C_6H_4$](CH$_2$CH$_2$Ph)Cl (**6**) 138
Synthesis of W(NPh)[o-(Me_3SiN)$_2C_6H_4$](CH$_2$CH$_2$Ph)Me (**7**) 138
Synthesis of [W(NPh)(o-(Me_3SiN)$_2C_6H_4$)(C_5H_5N)$_2$] (**8**) 139
Synthesis of **8** From W(NPh)(o-(Me_3SiN)$_2C_6H_4$)Cl$_2$ 140
Synthesis of W(NPh)(o-(Me_3SiN)$_2C_6H_4$)(p-C_6H_7N)$_2$ (**9**) 140
Synthesis of **9** From W(NPh)(o-(Me_3SiN)$_2C_6H_4$)Cl$_2$ 141
Synthesis of W(NPh)(o-(Me_3SiN)$_2C_6H_4$)(C_9H_7N)$_2$ (**10**) 141
Synthesis of [W(NPh)(o-(Me_3SiN)$_2C_6H_4$)Ph$_2$] (**11**) 142
Synthesis of [W(NPh)(o-(Me_3SiN)$_2C_6H_4$)(C_5H_5N)$_2$(CO)] (**12a**) 142
Synthesis of [W(NPh)(o-(Me_3SiN)$_2C_6H_4$)(C_6H_7N)$_2$(CO)] (**12b**) 143
Synthesis of [W(NPh)(o-(Me_3SiN)$_2C_6H_4$)(C_5H_5N)(PMe$_3$)(CO)] (**13a**) 143
Synthesis of [W(NPh)(o-(Me_3SiN)$_2C_6H_4$)(C_6H_7N)(PMe$_3$)(CO)] (**13b**) 144
Synthesis of [W(NPh)(o-(Me_3SiN)$_2C_6H_4$)(C_5H_5N)(PMe$_3$)$_2$] (**14a**) 144
Synthesis of [W(NPh)(o-(Me_3SiN)$_2C_6H_4$)(C_6H_7N)(PMe$_3$)$_2$] (**14b**) 145
Synthesis of [W(NPh)(o-(Me_3SiN)$_2C_6H_4$)(PhC≡CPh)] (**15**) 146
Reaction of **15** With H_2 to make **16** 146
Synthesis of W(NPh)[o-(Me_3SiN)$_2C_6H_4$][η^4-(CH$_2$=C(CH$_3$)C(CH$_3$)=CH$_2$)] (**17**) 146
Synthesis of W(NPh)[o-(Me_3SiN)$_2C_6H_4$](η^4-(CH$_2$=CHCH=CH$_2$) (**18**) 147
Synthesis of W[OC(CH$_3$)$_2$CH$_2$C(CH$_3$)C(CH$_3$)CH$_2$](NPh)[o-(Me_3SiN)$_2C_6H_4$] (**19**) . 148
Synthesis of W(CH$_2$CH$_2$CH$_2$CH$_2$)(NPh)[o-(Me_3SiN)$_2C_6H_4$] (**20**) 148
Synthesis of [W(NPh)(o-(Me_3SiN)$_2C_6H_4$)(C_5H_5N)$_2$(η^2-ethylene)] (**21**) 149
Synthesis of [o-(Me_3SiN)$_2C_6H_4$](NPh)W(SC_4H_4) (**22**) 149

Synthesis of [o-$(Me_3SiN)_2C_6H_4$](NPh)W(SC_5H_6) (**23**) 150
Synthesis of [o-$(Me_3SiN)_2C_6H_4$](NPh)W(SC_8H_6) (**24**) 151
Synthesis of [o-$(Me_3SiN)_2C_6H_4$](NPh)W(SC_5H_6) (**25a,b**) 151
Reaction of W($CH_2CH_2CH_2CH_2$)(NPh)[o-$(Me_3SiN)_2C_6H_4$] (**20**) with $EtAlCl_2$..... 152
Ethylene Dimerization 152
Hexene Dimerization 153
Additional Dimerization Experiments 153
Crystallographic Studies 153
X-ray Data Collection and Structure Refinement for Compounds **4** and **5** 153
X-ray Data Collection and Structure Refinement for Compounds **9** and **12a** 154
X-ray Data Collection and Structure Refinement for Compound **14a**..... 155
X-ray Data Collection and Structure Refinement for Compound **15**..... 156
X-ray Data Collection and Structure Refinement for Compound **17**..... 157
X-ray Data Collection and Structure Refinement for Compound **19**..... 158
X-ray Data Collection and Structure Refinement for Compound **22**..... 159

APPENDICES

A NUCLEAR MAGNETIC RESONANCE SPECTRA 160

B TABLES OF CRYSTALLOGRAPHIC DATA 209

LIST OF REFERENCES 287

BIOGRAPHICAL SKETCH 299

Abstract of Dissertation Presented to the Graduate School
of the University of Florida in Partial Fulfillment of the
Requirements for the Degree of Doctor of Philosophy

SYNTHESIS, STRUCTURE AND REACTIVITY OF W(IV) COMPLEXES:
DEVELOPMENT OF AN OLEFIN DIMERIZATION CATALYST

By

Ryan C. Mills

August 2001

Chairman: James M. Boncella
Major Department: Chemistry

Two unique series of W(IV) imido complexes containing the chelating diamido ligand [o-$(Me_3SiN)_2C_6H_4$] have been synthesized. W(IV) arene complexes with the formulae: W(NPh)(η^4-ethylbenzene)(o-$(Me_3SiN)_2C_6H_6$) (**3**) and W(NPh)(η^4-propylbenzene)(o-$(Me_3SiN)_2C_6H_6$) (**4**) were generated through hydrogenolysis of the W(VI) dialkyl complexes, W(NPh)$(CH_2CH_2Ph)_2$(o-$(Me_3SiN)_2C_6H_4$) (**1**) and W(NPh)$(CH_2CH_2CH_2Ph)_2$(o-$(Me_3SiN)_2C_6H_4$) (**2**). The W(IV)L_2 complexes, [W(NPh)(o-$(Me_3SiN)_2C_6H_4)(C_5H_5N)_2$] (**8**) and W(NPh)(o-$(Me_3SiN)_2C_6H_4$)(p-$C_6H_7N)_2$ (**9**) were synthesized by Na^o reduction of W(NPh)(o-$(Me_3SiN)_2C_6H_4)Cl_2$ in the presence of pyridine or 4-picoline. These compounds have been fully characterized by NMR spectroscopy, and X-ray crystal structures of **4** and **9** have been determined.

Compounds **8** and **9** readily incorporated additional ligands, PMe_3 and CO, and undergo ligand substitution reactions with PMe_3 to give a series of six-coordinate W(IV) complexes that demonstrate the coordinative unsaturation of **8** and **9**. The solid state

structures of [W(NPh)(o-$(Me_3SiN)_2C_6H_4$)$(C_5H_5N)_2$(CO)] (**12a**) and [W(NPh)(o-$(Me_3SiN)_2C_6H_4$)$(C_5H_5N)$$(PMe_3)_2$] (**14a**) are described.

The reactivity of [W(NPh)(o-$(Me_3SiN)_2C_6H_4$)$(C_5H_5N)_2$] (**8**) toward unsaturated substrates was examined. Compound **8** reacted with diphenylacetylene to give the metallocylopropene complex, [W(NPh)(o-$(Me_3SiN)_2C_6H_4$)(PhC≡CPh)] (**15**). Likewise compound **8** also displayed reactivity towards butadienes resulting in the formation of W(NPh)[o-$(Me_3SiN)_2C_6H_4$][η^4-$(CH_2=C(CH_3)C(CH_3)=CH_2)$] (**17**) and W(NPh)[o-$(Me_3SiN)_2C_6H_4$]($\eta^4$-$(CH_2=CHCH=CH_2)$ (**18**). Reduction of the unsaturated ligands in **15** and **17** was observed in the crystal structures of these compounds.

Carbon-sulfur bond activation of thiophenes promoted by [W(NPh)(o-$(Me_3SiN)_2C_6H_4$)$(C_5H_5N)_2$] (**8**) was also studied. Reaction of **8** with thiophene, 2-methylthiophene, benzothiophene or 3-methylthiophene resulted in oxidative addition of the C-S bond to the W(IV) metal center. The solid-state structure of [o-$(Me_3SiN)_2C_6H_4$](NPh)W(SC_4H_4) (**22**) is also discussed. Oxidation of the W(IV) center of the WL_2 complexes was also observed in their reactions with olefins. These reactions led to oxidative coupling of two olefin molecules to give a series of metallacyclopentane complexes.

Using the ability of Lewis acids such as $EtAlCl_2$ to decompose these metallacycles, a catalytic olefin dimerization/codimerization catalyst system was devloped based on the W(VI)Cl_2 complex. Initial studies regarding the dimerization of a series of linear α-olefins, internal and terminal olefins, dienes and cyclic olefins are also discussed. In addition to dimerization, the $WCl_2/EtAlCl_2$ catalyst also promotes oligomerization of alkenes to highly branched products.

CHAPTER 1
INTRODUCTION AND BACKGROUND

Organometallic chemistry, a field dedicated to achieving a better understanding of the interactions of organic molecules with transition metals, has become a bridge between the classical fields of organic and inorganic chemistry. Consequently, organometallic compounds are defined as materials that posses a direct bond (σ or π) between metal and carbon atoms. Organo-transition metal chemistry has been one of the most important areas of research for chemists because of its application in catalysis of oxidation, hydrogenation, olefin metathesis and polymerization reactions as well as numerous additional organic transformations.[1-4] Therefore, synthesis and study of the reactivity and properties of transition metal compounds plays an integral role in expanding the general understanding of the field of organometallic chemistry.

The broad applications of organometallic complexes are in part due to the diversity of the metals in the transition series. Simply by changing the metal, the properties of the resulting complexes can be drastically altered. Moving from left to right across the periodic table, the electronegativity of the elements increases substantially. This means that the orbitals in which the electrons reside, decrease in energy across the transition series. As a result, the early transition metals are electropositive and readily lose all of their valence electrons and are commonly found in higher oxidation states. Lower oxidation states of these metals are easily oxidized because the electrons are in high-energy orbitals. This process does not always occur at the hand of an oxidizing

agent. Early-transition metal complexes with a d^2 electronic configuration can lose these electrons to the π^* orbitals of unsaturated ligands through back bonding. This makes d^2 early-transition metals very π–basic and able to bind π-acceptor ligands strongly.

On the other hand, later-transition metals are electronegative and tend to maintain their valence electrons. Therefore, lower oxidation states tend to be more stable and complexes of higher oxidation states readily find a means to attain a lower more stable oxidation state. As a result, back donation from these metals is limited and coordination of an unsaturated ligand usually places positive character on the ligand making it susceptible to nucleophilic attack.

Although the properties of transition metals are diverse, discussions of organometallic reaction sequences may be categorized by the definition of five general reaction types and their reverse reactions (Table 1-1).[5] Characteristic variables that pertain to these reactions are as follows:

1. ΔVE: Change in the number of valence electrons at the metal center.
2. ΔOS: Change in the oxidation state of the metal.
3. ΔCN: Change in the coordination number about the central metal atom.

Two-electron processes where the metal center is either reduced or oxidized by two units are at the heart of many organometallic reactions. As shown in Table 1-1, oxidative addition/reductive elimination and oxidative coupling/reductive decoupling represent a generalization of reaction types that involve a two-electron process. These reaction types have been observed both individually in stoichiometric situations and in tandem to facilitate a catalytic reaction. During the time spent compiling the results to be presented in this dissertation, the importance of two-electron processes became even more apparent. Because of the enormous volume of literature regarding this type of

reactivity, this introduction will demonstrate the significance of two-electron processes in catalysis as it is our ultimate goal to demonstrate catalytic activity in several of the systems that were investigated. Discussions of stoichiometric reactions that rely on two-electron oxidation or reduction are reserved for the relevant chapters. I think this strategy builds a more effective foundation for each type of reactivity and aids in the reader's understanding of the significance of the chemistry discussed in each chapter.

Table 1-1. Generalization of the types of organometallic reactions.

Reaction	ΔVE	ΔOS	ΔCN
Lewis-acid ligand dissociation	0	0	-1
Lewis-acid ligand association	0	0	+1
Lewis-base ligand dissociation	-2	0	-1
Lewis-base ligand association	+2	0	+1
Oxidative addition	+2	+2	+2
Reductive elimination	-2	-2	-2
Migratory insertion	-2	0	-1
Extrusion	+2	0	+1
Oxidative coupling	-2	+2	0
Reductive decoupling	+2	-2	0

Of the many applications of organometallic chemistry, the homogeneous catalysis of organic reactions is of great importance in both academia and industry.[6-8] Homogeneous catalysis proceeds via a series of reaction steps, coupled to each other to form a complete loop. In industry these reactions allow the formation of products in a very efficient manner whereas the academic study of these processes generates new

insights into the understanding and optimization of these catalyst systems through modeling studies.

Many reactions in chemistry are favorable thermodynamically, yet occur at extremely slow rates. The presence of a catalyst dramatically increases these rates. Many of the known catalytic cycles involve changes in the oxidation state of the metal center. Transition metals, with their d valence electrons, usually posses a large number of available oxidation states, particularly in comparison to main group elements and therefore can be tailored into very efficient catalysts. The most common oxidation state change found in catalytic systems of this type is a two-electron process (eg. M^n-M^{n+2}-M^n) where the metal cycles between two readily available oxidation states. Typically, the two key steps in a catalytic cycle that proceeds through a reversible two-electron change are oxidative addition and its reverse, reductive elimination (Figure 1-1). The metals in groups 8 to 10 especially possess a tendency for rapid, reversible two-electron oxidation/reduction (such as from $18e^-$ to $16e^-$ and back), and thus it is not surprising that they are often involved in homogeneous catalysis.[4] On the other hand, although early-transition metals (Groups 4, 5 and 6) are known to undergo stoichiometric oxidative addition or reductive elimination reactions, catalytic reactions involving these complexes typically do not involve a change in the oxidation state of the metal during the catalytic cycle (e.g., alkene or alkyne metathesis and polymerization for which there is no oxidation state change during the catalytic cycle).

Figure 1-1. Reversible oxidative addition/reductive elimination.

Hydroformylation

The hydroformylation of olefins (Figure 1-2), was discovered by Roelen in 1938 while studying the mechanism of the Fisher-Tropsch synthesis.[9,10] It was found that an alkene could be converted to the homologous aldehyde by the addition of H_2 and CO in the presence of $Co_2(CO)_8$. Since then this reaction has become one of the largest volume, homogeneously catalyzed processes.[11-13] Today, C_3-C_{15} aldehydes are produced by this process and then converted into amines, carboxylic acids and primary alcohols with the most desirable products being butanol and 2-ethylhexanol.[14]

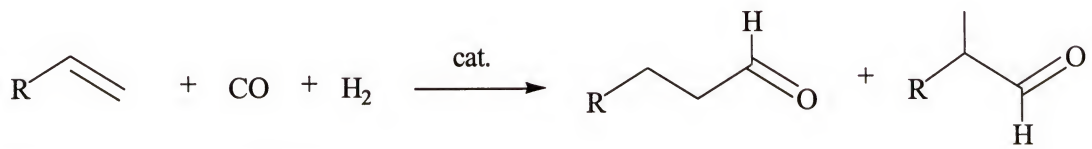

Figure 1-2. Catalytic hydroformylation of alkenes.

Much of the early work, including the proposal of a rational mechanism, regarding this process focused on the Co catalyzed reaction (Figure 1-3). What was initially thought to be oxidative addition of H_2 followed by reductive elimination of aldehyde (Steps 6 and 7), a $2e^-$ cycle, is now believed to involve coordination of H_2 followed by heterolytic H_2 cleavage.[15,16] Through this mechanism, oxidative addition of H_2, which has a high activation energy in this system, is avoided.

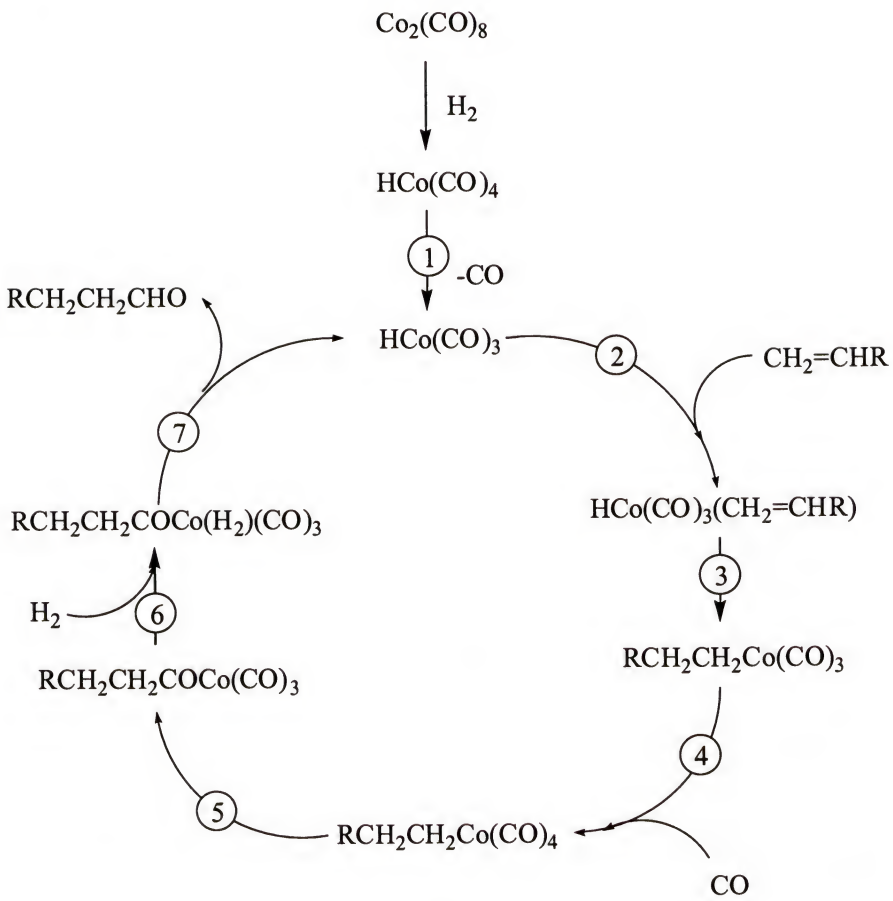

Figure 1-3. Cobalt catalyzed hydroformylation.

More recently, rhodium based catalyst systems have replaced those derived from Co complexes. The rhodium catalysts have the advantages of very mild reaction conditions, high conversion rates of olefin and high selectivity for n-aldehyde.[3] Another advantage of this system is that it is more amenable to mechanistic studies,[17] as exemplified by Wilkinson's pioneering work with $RhH(CO)(PPh_3)_3$.[18] The key steps in this reaction are the oxidative addition of H_2 to an Rh(I) intermediate acyl complex followed by reductive elimination of the product aldehyde. Shortly after these developments, Union Carbide commercialized the first phosphine-modified rhodium

catalysts for hydroformylation.[14] Figure 1-4 displays a reaction scheme for this process, where the rapid and reversible Rh(I)-Rh(III) redox couple (Steps 5 and 6) is the basis for the exceptionally high reactivity of this catalyst.

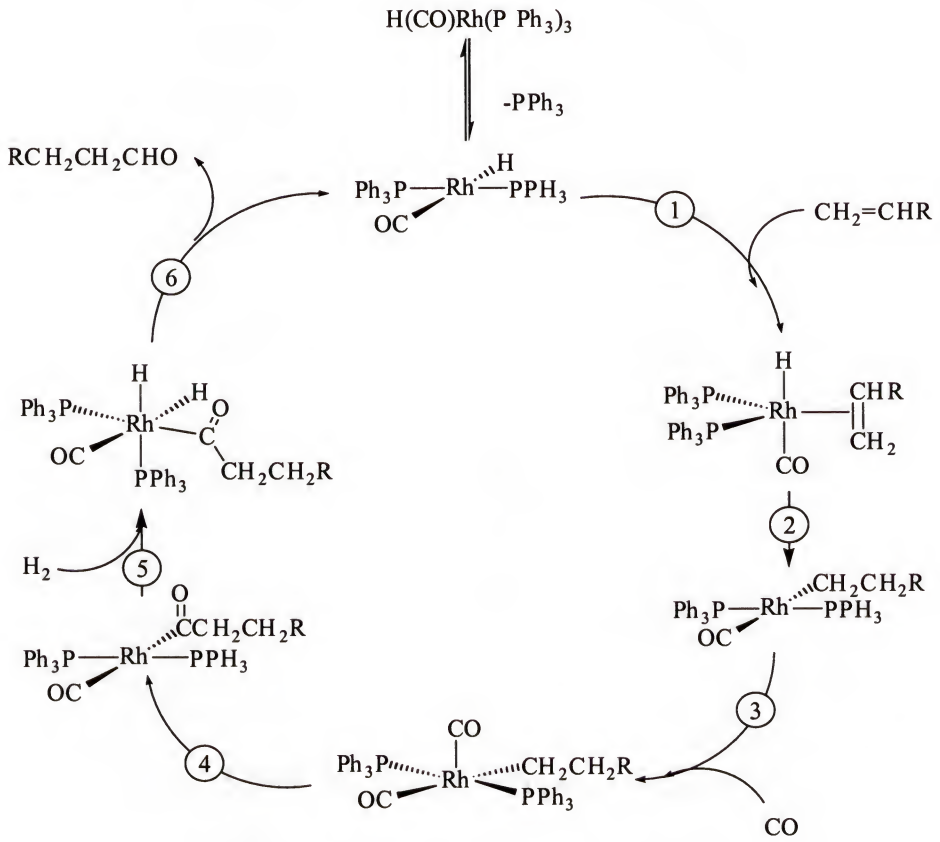

Figure 1-4. Union Carbide hydroformylation process.

Acetic Acid Synthesis

Another example of how reversible two-electron processes can facilitate an organic transformation in a catalytic manner is the synthesis of acetic acid from methyliodide. The rhodium catalyzed synthesis of acetic acid, which was commercialized by Monsanto in the late 1960s also relies on the ability of rhodium to cycle between Rh(I) and Rh(III).[19,20] Mechanistic studies of this process led to the proposal of the catalytic cycle shown in Figure 1-5.[21-23] The rhodium catalyst precursor,

RhX_3, is converted into the Rh(I) anion, $[RhI_2(CO)_2]^-$ in the system which contains both CO and an iodide ions. At this juncture, the reversible $2e^-$ electron process begins with the oxidative addition of CH_3I to the Rh(I) anion intermediate. It has been suggested that the high rate at which this step occurs accounts for the observed catalyst activity.[21-23] Subsequent CO migratory insertion precedes completion of the Rh(I)-Rh(III)-Rh(I) two-electron cycle through reductive elimination of acetyliodide, which regenerates the Rh(I) anion. Acetyliodide is then hydrolyzed to produce the desired product, acetic acid.

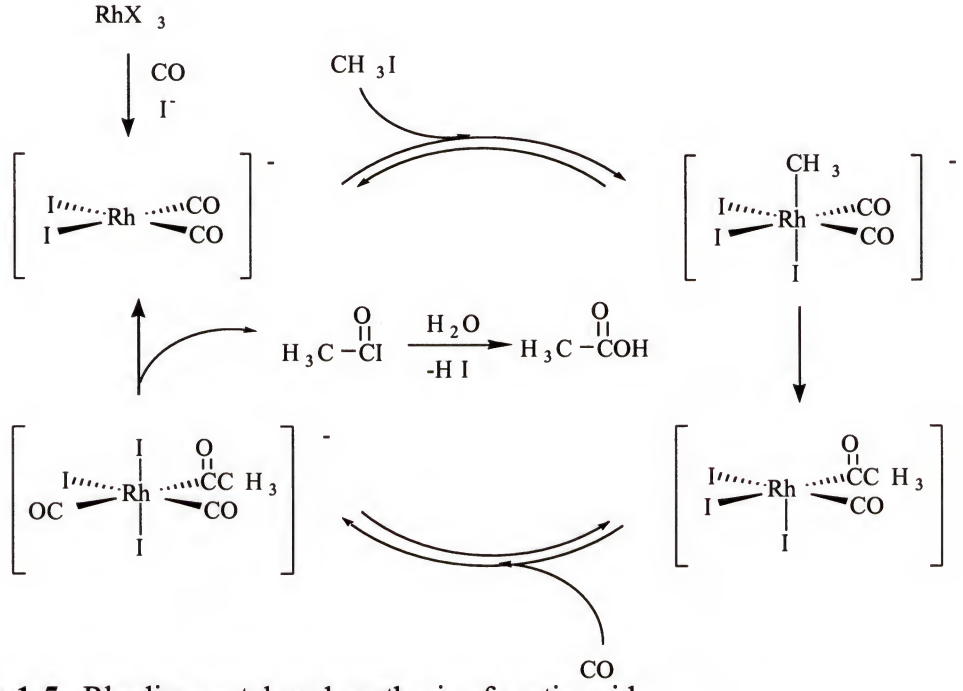

Figure 1-5. Rhodium catalyzed synthesis of acetic acid.

Alkene Hydrogenation

Further support for the importance of reversible two-electron reduction/oxidation processes in organometallic chemistry resides in the ability of homogeneous catalysts to facilitate the hydrogenation of carbon-carbon double bonds. Still today, the single most important development in the field of homogeneously catalyzed hydrogenation was that

reported by both Coffey[24] and Wilkinson[25] in 1965. At the same time in different labs, it was observed that $RhCl(PPh_3)_3$ was a very efficient hydrogenation catalyst. Their observations stimulated a large amount of research on rhodium, iridium and ruthenium complexes containing tertiary phosphine ancillary ligands as possible hydrogenation catalysts. Included in this work were several very exquisite and detailed mechanistic studies that have established reaction pathways for some of these hydrogenation catalysts.[26-29]

As was discussed for the hydroformylation and acetic acid reactions, the rhodium-catalyzed hydrogenation of olefins also involves a cycling between oxidation states that are two units apart. Figure 1-6 shows the mechanism for alkene hydrogenation known as the dihydride pathway. For this catalytic cycle, oxidative addition of H_2 to $RhCl(PPh_3)_3$ results in the formation of a Rh(III) dihydride species. Olefin coordination followed by insertion into the M-H bond generates an intermediate Rh(III) alkyl hydride complex. Similar to hydroformylation and the acetic acid synthesis, the Rh(I)-Rh(III)-Rh(I) cycle found in catalytic alkene hydrogenation is completed via reductive elimination of in this case alkane.

The three examples of homogeneous catalysts described above are by no means an exhaustive representation of the intimate role that the ability of transition metals to cycle between oxidation states plays in organometallic chemistry. Numerous additional examples of two-electron processes could be cited. For example, catalytic hydrosilation and hydrocyanation also involve transition metal complexes that have this type of oxidation state cycling at the heart of their respective reactivities.[15] These examples clearly demonstrate that the ability of transition metals to undergo facile oxidation state

changes is of the utmost importance in the catalysis of organic reactions. This dissertation is focused on the investigation of a similar two-electron process (W(IV)-W(VI)) and its potential use in catalytic transformations of organic substrates.

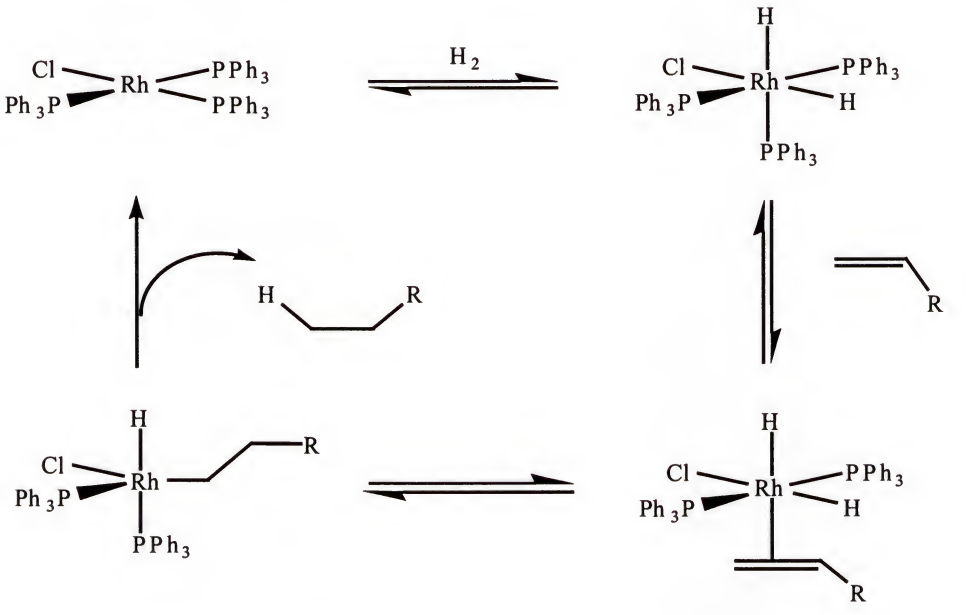

Figure 1-6. Homogeneously catalyzed alkene hydrogenation.

The chemistry of tungsten imido dialkyl complexes, stabilized by the chelating diamide ligand, *ortho*-$(Me_3SiN)_2C_6H_4$ has been a major focus of our research group for some time.[30-32] However, with a single observation, the direction of this project was significantly altered and resulted in the wide array of reactivities demonstrated by the [W(NPh)(o-$(Me_3SiN)_2C_6H_4$)] fragment discussed in this dissertation. It was observed that when an NMR sample of the W(VI)-bisphenethyl complex was exposed to a positive pressure of H_2, a new W(IV)-arene complex was formed.[33] Although the arene complex was not isolated and fully characterized at this point, an interesting reaction was noted.

After *in situ* generation of the W(IV)-arene complex, the reaction mixture was exposed to an excess of both H_2 and styrene and warmed to 50° C. The NMR analysis of

the product mixture revealed that the arene complex had catalyzed the hydrogenation of styrene to ethylbenzene. Subsequently, this catalyst was also found to facilitate the hydrogenation of 2,3-dimethylbutadiene to a mixture of *cis*-2,3-dimethyl-2-butene and 2,3-dimethylbutane. Although the activity of the catalyst was determined to be small, the catalyst was found to be rather robust in nature, remaining active for periods up to two weeks with total turnover numbers greater than 5000.[33]

With our research group's knowledge of W(VI) alkyl and hydride complexes and a general understanding of alkene hydrogenation, a plausible mechanism was proposed to rationalize this reactivity. The proposed pathway for the hydrogenation, shown in Figure 1-7, involves initial oxidative addition of H_2 to the arene complex resulting in the loss of ethylbenzene. Coordination of styrene followed by insertion into the W-H bond gives a W(VI) alkyl monohydride intermediate that undergoes reductive elimination to reform the arene complex.

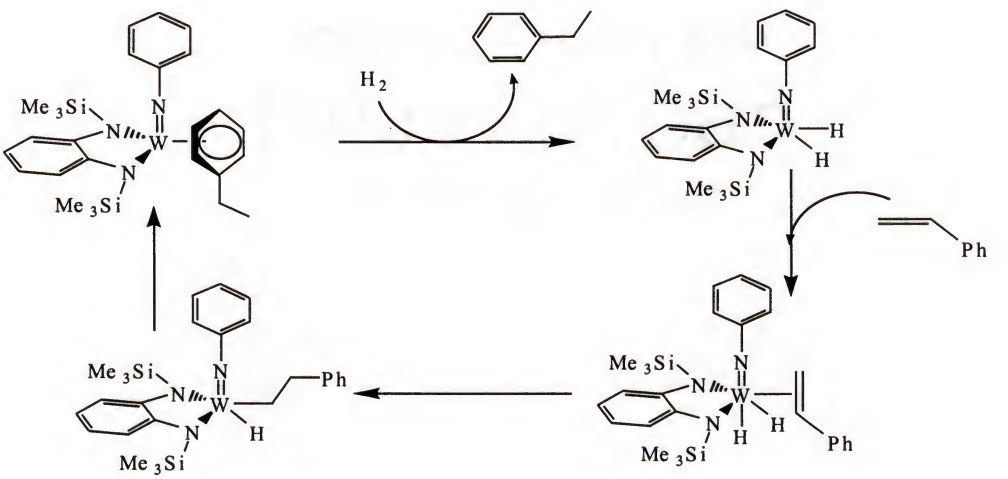

Figure 1-7. Proposed mechanism for the W(IV)-arene catalyzed hydrogenation of styrene.

Two important pieces of information that have greatly affected the content of this dissertation were obtained from these reactions. First, the observation of a W(IV)-arene

complex suggested the possibility of synthesizing a variety of W(IV) complexes that could generate many new avenues for research in our group. The catalytic hydrogenation of styrene although slow, demonstrated the feasibility of promoting catalytic reactions through the exploitation of what appeared to be an accessible W(IV)-W(VI), reversible two-electron process. In lieu of this, we undertook the task of exploring the chemistry of the chelate stabilized W(IV) imido system, W(NPh)(o-$(Me_3SiN)_2C_6H_4$).

In this dissertation, my research regarding the synthesis, characterization and subsequent reactivity studies of this fragment is presented. Included in these discussions are the syntheses of two unique W(IV) systems and their intriguing spectroscopic and structural characteristics. Although the reactivity of one of the W(IV) systems was found to be limited, the other displayed a rich variety of reactivities, including ligand substitution, substrate reduction, C-S bond activation and oxidative coupling. In addition, an alkene dimerization catalyst is presented that had its origins in the knowledge gained through these studies.

CHAPTER 2
HYDROGENOLYSIS OF β-HYDROGEN CONTAINING DIALKYLS: SYNTHESIS OF d^2 TUNGSTEN ARENE COMPLEXES AND THEIR REACTION WITH DIPHENYLACETYLENE

Introduction

The chemistry of metal complexes containing six membered π–arene ligands has been thoroughly developed since Fischer and Hafner first characterized $Cr(\eta^6\text{-benzene})_2$, generated from the $Al/AlCl_3$ reduction of $CrCl_3$ in the presence of benzene.[2,34-36] Stable arene complexes have now been characterized for virtually all of the transition metals.[1] Although most early examples of transition metal arene complexes were limited to compounds containing low valent metals,[37-45] more recently d^0-metal-arenes have become more common.[46-51] Surprisingly, examples of d^2-arene complexes have been limited. However, the few examples of d^2 arene complexes are representative of typical syntheses for high-oxidation state early transition metal arene complexes, namely reduction of a metal halide in the presence of arene and the metal mediated cyclotrimerization of alkynes.

Troyanov has reported the synthesis of the d^2 arene complexes $[Zr(\eta^6\text{-}C_6H_6)_2(AlCl_3)_2Cl_2]$ and $[Ti(\eta^6\text{-}C_6H_6)(AlCl_3)_2Cl_2]$,[52,53] which were generated through reduction of $ZrCl_4$ and $TiCl_4$ with $Al/AlCl_3$ in benzene (Figure 2-1). This is different from the conditions (Na/K, PMe_3, toluene) used by Green to synthesize the Zr(II) arene complex $Zr(\eta^6\text{-toluene})Cl_2(PMe_3)_2$.[54] In addition to metal halide reduction, metal mediated alkyne

cyclotrimerization is another common method for the synthesis of early- transition metal arene complexes.[2] Bruck *et al.* applied this methodology to the synthesis of [Ta(η^6-C_6R_6)$(OAr)_2Cl$],[55] from $Ta(OAr)_2Cl_3$ and 2-alkyne with Na/Hg as the reducing agent (Figure 2-2). In order to address the question of whether or not the coordinated arene of the product was formed at the metal center, the reaction of $Ta(OAr)_2Cl_3$ with hexaethylbenzene under similar conditions was examined. The absence of $Ta(C_6R_6)(OAr)_2Cl$ in the product mixture supported the proposed metal assisted cyclotrimerization mechanism for the formation of [Ta(η^6-C_6R_6)$(OAr)_2Cl$].

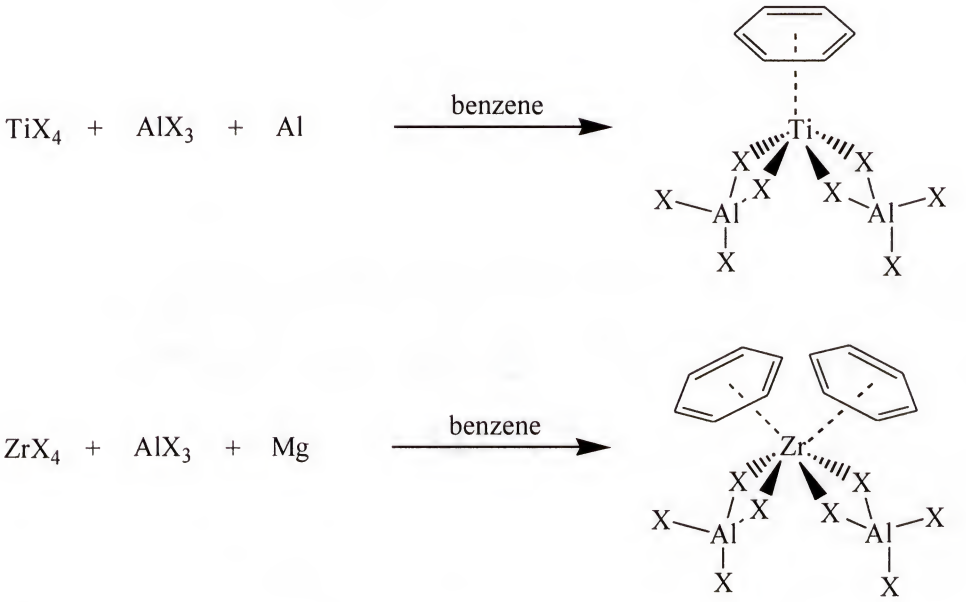

Figure 2-1. Troyanov synthesis of metal arenes by reduction.

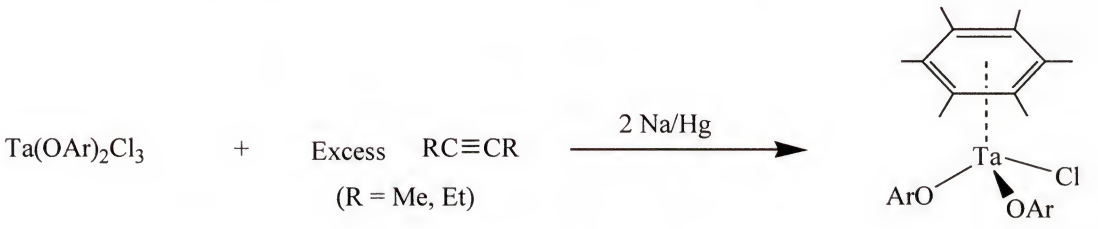

Figure 2-2. Metal mediated alkyne cyclotrimerization.

Following earlier work from our group on the reactivity of β-hydrogen containing W(VI)-dialkyl complexes of the type [W(NPh)(o-$(Me_3SiN)_2C_6H_4$)R_2] (where R = CH_2CH_3, CH_2CMe_3)[31,56] with H_2,[30] we became interested in similar reactions where the alkyl groups have pendant arene rings (R = CH_2CH_2Ph, $CH_2CH_2CH_2Ph$).

Synthesis and Characterization of W(IV)-arene Complexes

In order to study the hydrogenolysis chemistry of W(VI)-dialkyl complexes with arene containing alkyl groups, the complexes [W(NPh)(o-$(Me_3SiN)_2C_6H_4$)$(CH_2CH_2C_6H_5)_2$][33] (**1**), and [W(NPh)(o-$(Me_3SiN)_2C_6H_4$) $(CH_2CH_2CH_2C_6H_5)_2$] (**2**) were synthesized from the reaction of [W(NPh)(o-$(Me_3SiN)_2C_6H_4$)Cl_2] with the corresponding Grignard reagent (Figure 2-3).

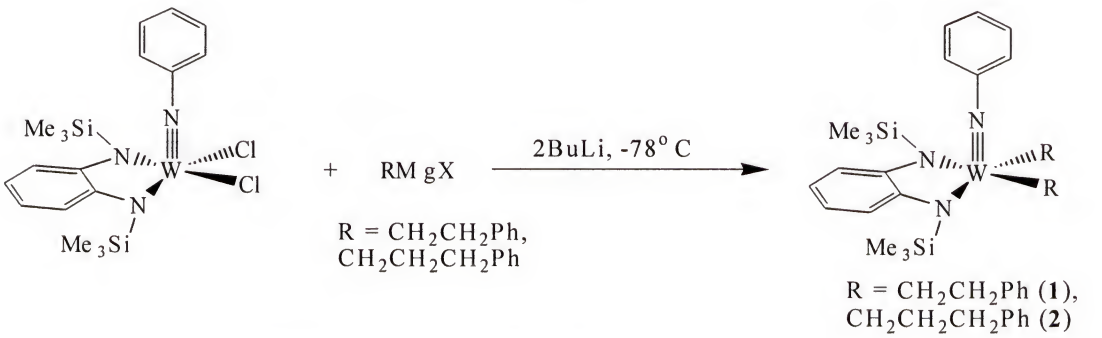

Figure 2-3. Synthesis of W(VI)-dialkyl complexes.

Room temperature hydrogenolysis (34psi, H_2) of a toluene solution of [W(NPh)(o-$(Me_3SiN)_2C_6H_4$)$(CH_2CH_2C_6H_5)_2$] (**1**), or [W(NPh)(o-$(Me_3SiN)_2C_6H_4$) $(CH_2CH_2CH_2C_6H_5)_2$] (**2**) (Figure 2-4), results in a slow color change from orange to dark purple over several days. From these solutions, the d^2-arene complexes [W(NPh)(η^4-ethylbenzene)(o-$(Me_3SiN)_2C_6H_4$)] (**3**) and [W(NPh)(η^4-propylbenzene)(o-$(Me_3SiN)_2C_6H_4$)] (**4**) were isolated as dark purple solids by washing the crude reaction

products with cold $(Me_3Si)_2O$. Attempts to decrease the long reaction times by increasing the reaction temperature or the H_2 pressure, led to the formation of significantly more complicated product mixtures.

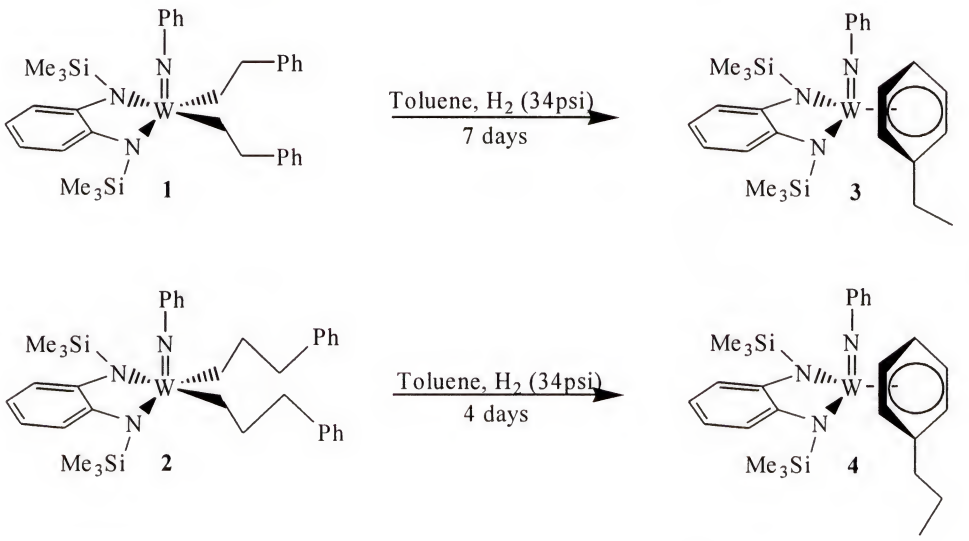

Figure 2-4. Synthesis of W(IV)-arene complexes.

Compounds **3** and **4** are indefinitely stable at room temperature in the solid state when stored under an inert atmosphere. In addition, solutions of both **3** and **4** display surprising stability toward arene–arene exchange reactions which have been observed to readily occur at room temperature for analogous molybdenum arene complexes,[57] suggesting a more robust interaction between tungsten and the arene ring.

The new π-bound arene ring is clearly indicated in the ^{1}H NMR spectra of **3** and **4** (Figure 2-5). The aromatic resonances for the protons of the coordinated ring display typical upfield chemical shifts (δ 4.27(t), 4.65(d), 4.73(t) (**3**) and 4.29(t), 4.68(d), 4.74(t) for (**4**)) associated with arene complexes due to the depletion of π-electron density from the ring upon coordination to the electropositive metal center.[1] To a lesser extent, the

resonances corresponding to the substituent alkyl hydrogens of **3** and **4** are also shifted upfield upon coordination (0.55(t), 1.66(q) (**3**) and 0.65(t), 1.03(m), 1.67(t) (**4**)).

Single crystals of **4** suitable for an X-ray diffraction study were obtained through slow evaporation of a concentrated C_6D_6 solution of **4**. The crystal structure of **4** shows that the arene ring is coordinated in an η^4 fashion (Figure 2-6). Selected bond lengths and angles are summarized in Table 2-1. The W-C distances of four of the ring carbons C3(2.251Å), C4(2.363 Å), C5(2.382 Å) and C6(2.267 Å) are significantly shorter than those for ring carbons C1(2.533 Å) and C2(2.503 Å). As a result, a considerable distortion from planarity of the coordinated arene ring is observed (the angle between the planes formed by C2-C1-C6-C5 and C2-C3-C4-C5 is 20.4°). Furthermore, the short ring C-C distances for C4-C5 (1.372Å) and C1-C2 (1.371Å), consistent with C-C double bonds, coupled with the fold of the arene ring indicate that there is a significant disruption of aromaticity upon coordination. Overall, the interaction of the arene ring with the tungsten center in **4** is similar to the ($\sigma_2\pi$) bonding extreme of a 1,3-butadiene-metal interaction.[37] Despite the inherent stability of the coordinated arene ring in **3** and **4** as demonstrated by the lack of arene displacement chemistry, compound **3** was found to undergo a unique coupling reaction with diphenylacetylene.

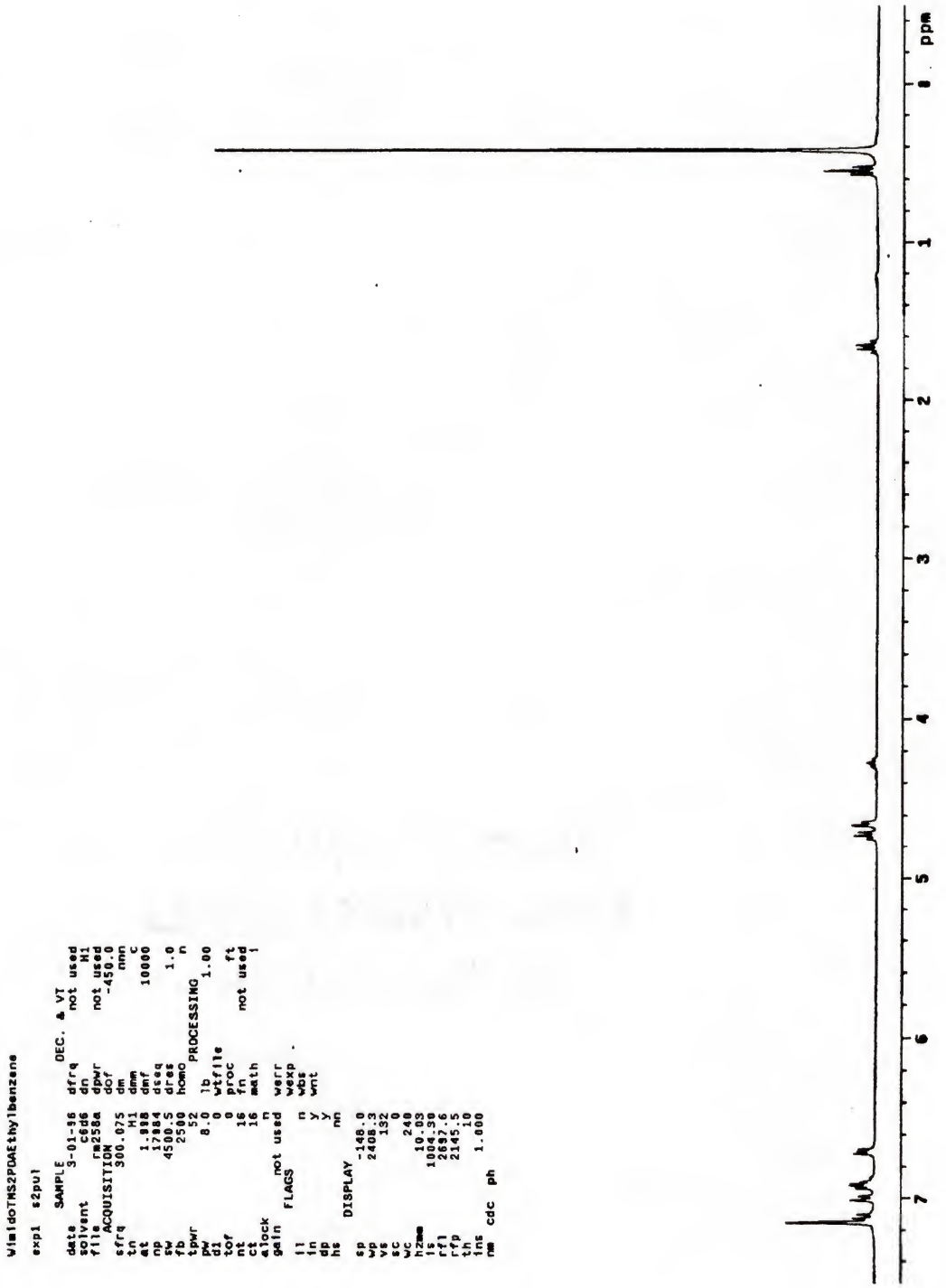

Figure 2-5. ^{1}H NMR spectrum (C_6D_6) of [W(NPh)(η^4-ethylbenzene)(o-$(Me_3SiN)_2C_6H_4$)] (**3**).

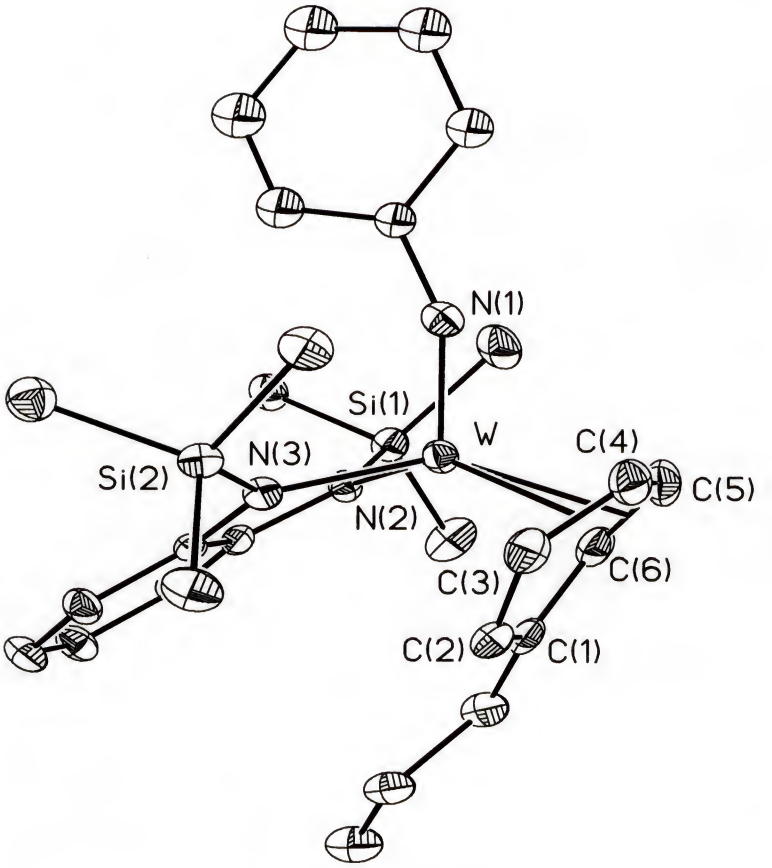

Figure 2-6. Molecular structure of [W(NPh)(η^4-propylbenzene)(o-$(Me_3SiN)_2C_6H_4$)] (**4**). Thermal ellipsoids are drawn at 40 % probability and the hydrogen atoms have been removed for clarity.

Table 2.1. Summary of selected bond lengths (Å) and angles (deg) for **4**.

W-N1	1.762(4)	W-C5	2.382(5)	C6-C1	1.459(7)
W-N2	2.057(4)	W-C6	2.267(5)	W-N1-C7	155.2(6)
W-N3	2.056(4)	C1-C2	1.371(6)	N1-W-N2	102.50(16)
W-C1	2.533(5)	C2-C3	1.459(7)	N1-W-N3	103.44(16)
W-C2	2.503(5)	C3-C4	1.416(7)	N3-W-N2	77.66(14)
W-C3	2.251(5)	C4-C5	1.372(7)		
W-C4	2.363(5)	C5-C6	1.434(7)		

[2 + 2] Cycloaddition of Diphenylacetylene and Styrene

Thermolysis (60° C) of a toluene solution containing equimolar amounts of [W(NPh)(η^4-ethylbenzene)(o-$(Me_3SiN)_2C_6H_4$)] (**3**) and PhC≡CPh for 12 hours, afforded the W(VI)-metallacyclopent-3-ene species [o-$(Me_3SiN)_2C_6H_4$)(NPh)WCH$_2$C(Ph)=C(Ph)CHPh] (**5**) in 54% yield (Figure 2-7). The ^{1}H NMR spectrum of **5** displays two doublet resonances (2.58 and 2.81ppm, ^2J = 10.8 Hz) and a singlet resonance (4.77ppm, $^2J_{W\text{-}H}$ = 4.8 Hz), for the α-CH$_2$ and α-CH protons of the metallacycle, respectively. In the $^{13}C\{^1H\}$NMR spectrum, the two α-carbons bonded to the metal center resonate at δ 57.74 ppm as a triplet with $^1J(^{13}C\text{-}^1H)$ = 143.0 Hz and 73.72 ppm as a doublet with $^1J(^{13}C\text{-}^1H)$ = 137.36 Hz. The coupling constants measured for the α-carbons in compound **5** are similar those observed for strongly $\sigma_2\pi$-bound group 4 and 5 butadiene complexes (138-150 Hz).[58-60]

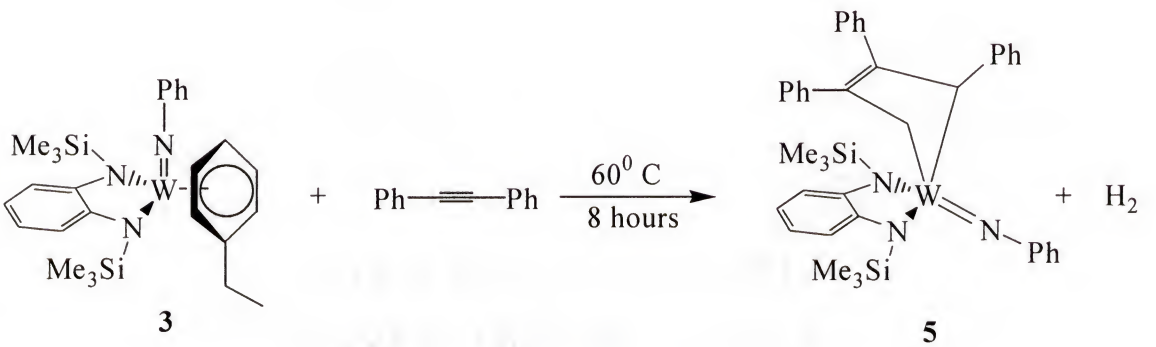

Figure 2-7. Synthesis of metallacyclopent-3-ene, **5**.

An X-ray diffraction study of a single crystal of **5** grown by slow evaporation of a saturated pentane solution of **5**, confirmed the metallacyclopent-3-ene structure which was deduced from the spectroscopic data (Figure 2-8). Selected bond lengths and angles are summarized in Table 2-2. Compound **5** adopts a distorted square pyrimadal geometry

about the W center with the imido group occuping the apical position. A short W-imido nitrogen bond length of 1.745(3) Å is indicative of a W-N triple bond.[61-63] The W-N2 (2.034(3) Å) and W-N3 (2.037 Å) bond distances are within the normal range observed for W complexes of this type.[61-63] The W-α-carbon (W-C1 and W-C4) bond distances are 2.162(4) and 2.204(4) Å respectively. This small difference in the W-C1, W-C4 bond lengths can be attributed to a steric interaction between the phenyl substituent of C4 and the Me_3Si group of the diamide ligand. Also, the fact that C1 is a secondary carbon whereas C4 is tertiary may be a contributing factor in the observed elongation of the W-C4 bond length with respect to the W-C1 distance. Localization of metallacyclopentene double bond between C2 and C3 is indicated by the short C2-C3 bond distance of 1.364(5) Å, which is consistent with a typical C-C double bond. Involvement of this double bond in the stabilization of the metal center in compound **5** is minimal as suggested by the relatively long W-C2 and W-C3 distances of 2.589(4) and 2.582(3) Å respectively.

Proposed Mechanism for Coupling

It has been demonstrated that early transition metal complexes facilitate the metal mediated [2+2] cycloaddition alkynes and olefins to generate metallacyclopentenes.[64-67] The formation of **5**, appears to proceed by initial side-chain C-H bond activation of the coordinated ethylbenzene in **3**, followed by β abstraction of H, to generate a W(IV)-styrene intermediate (Figure 2-9). Presumably, the intermediate η^2-styrene complex then undergoes the expected cycloaddition reaction with PhC≡CPh followed by rearrangement to generate **5**.

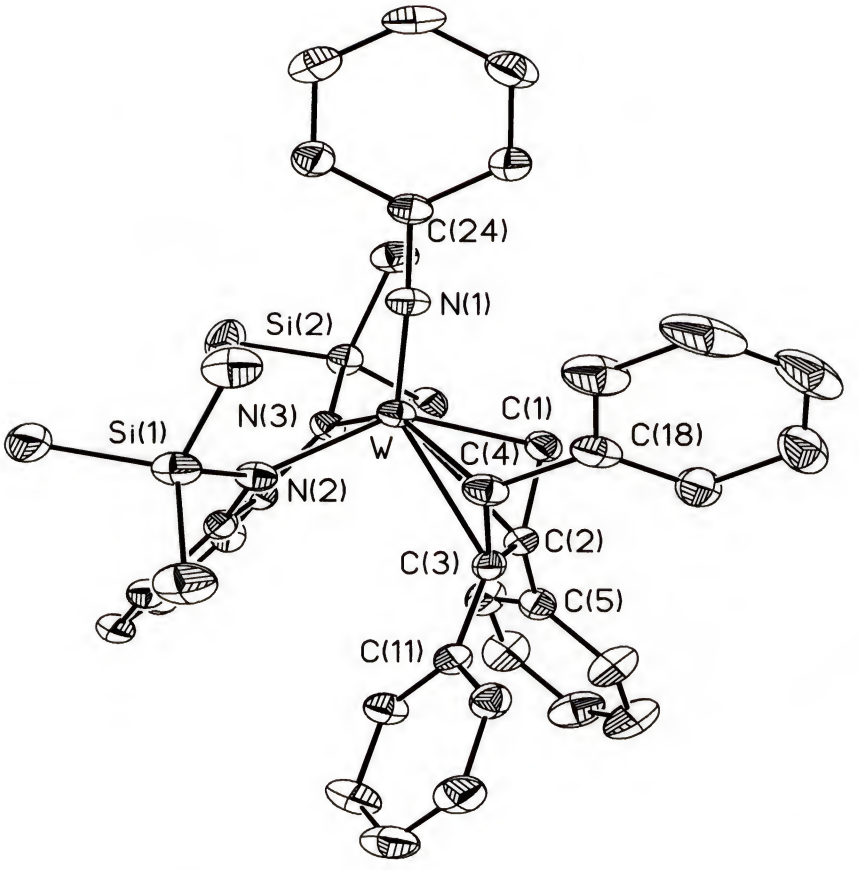

Figure 2-8. Molecular structure of [o-$(Me_3SiN)_2C_6H_4$)(NPh) $WCH_2C(Ph)=C(Ph)CHPh$] (**5**). Thermal ellipsoids are drawn at 40 % probability and the hydrogen atoms have been removed for clarity.

Table 2-2. Summary of selected bond lengths (Å) and angles (deg) for **5**.

W-N1	1.745(3)	W-C3	2.582(3)	W-N1-C24	176.2(3)
W-N2	2.034(3)	W-C4	2.204(4)	C1-W-C4	76.97(15)
W-N3	2.037(3)	C1-C2	1.497(5)	N2-W-N3	79.43(15)
W-C1	2.162(4)	C2-C3	1.364(5)	N1-W-N2	115.76(14)
W-C2	2.589(4)	C3-C4	1.495(5)	N1-W-N3	112.17(13)

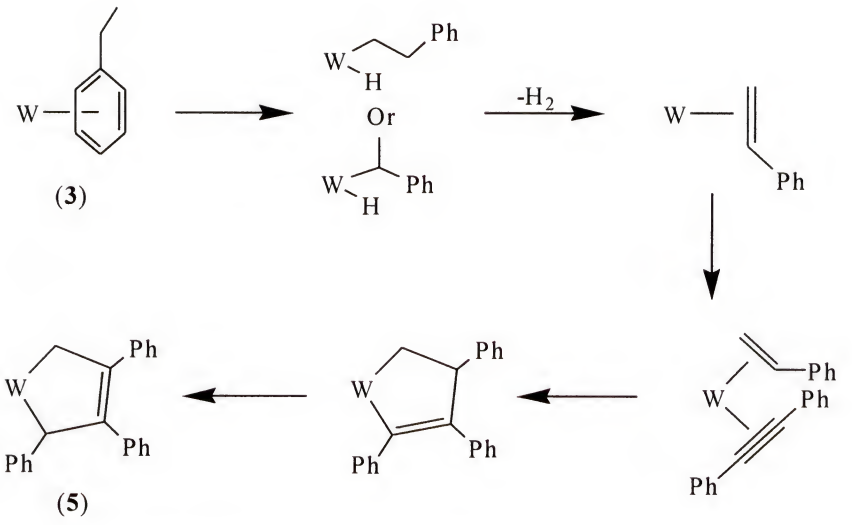

Figure 2-9. Proposed mechanism for the formation of **5**.

W(IV)-olefin complexes are not new to our research group. During our investigation of the β-hydrogen transfer chemistry of W(VI)-dialkyl complexes, the η^2-styrene complex W(NPh)[o-$(Me_3SiN)_2$(η^2-styrene)$(PMe_3)_2$ was isolated from the reaction of [W(NPh)(o-$(Me_3SiN)_2C_6H_4$)$(CH_2CH_2C_6H_5)_2$] (**1**) with two equivalents of PMe_3.[33] However, attempts to isolate a pure sample of base free styrene complex, in order to study its reaction with diphenylacetylene, have proved difficult. Thermolysis of a toluene solution of the bis-(phenethyl) complex **1** produces a intractable mixture of products, which as determined by ^{1}H NMR spectroscopy, includes W(IV)-styrene complex, W(IV)-ethylbenzene complex **3**, styrene and ethylbenzene as well as other uncharacterized products (Figure 2-10). To circumvent this problem and be able to generate the styrene complex *in situ,* a W(VI)-dialkyl system was synthesized such that the only products of β-hydrogen transfer chemistry would be styrene complex and a volatile alkane.

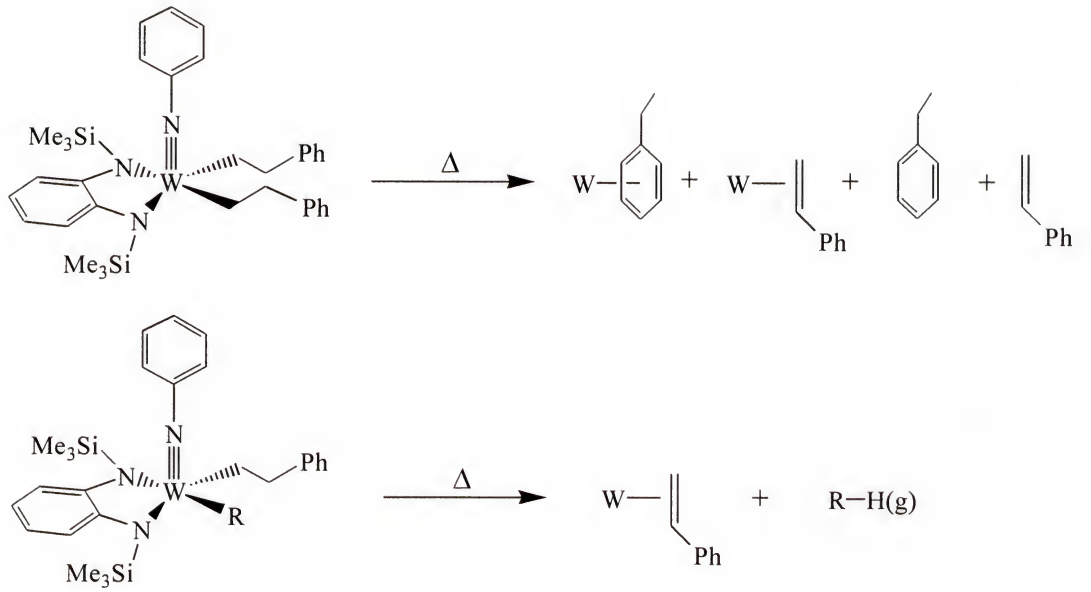

Figure 2-10. Styrene complex formation from bis-(phenethyl) and an ideal system.

Synthesis of a W(VI) Mixed-dialkyl Complex

In order to determine the validity of the proposed formation of an η^2-styrene intermediate through loss of H_2, the chemistry of the mixed dialkyl complex [W(NPh)(o-$(Me_3SiN)_2C_6H_6$)($CH_2CH_2C_6H_5$)(Me)] (**7**) was examined. Synthesis of compound **7** followed a procedure in which the monoalkyl complex [W(NPh)(o-$(Me_3SiN)_2C_6H_6$)($CH_2CH_2C_6H_5$)(Cl)] (**6**) was isolated from the reaction of [W(NPh)(o-$(Me_3SiN)_2C_6H_4)Cl_2$] with one equivalent of $PhCH_2CH_2MgCl$. Subsequent alkylation of **6** with one equivalent of MeMgI led to the formation of **7** in *ca.* 75 % yield.

Thermolysis (70°) of an NMR sample (C_7D_8) of **7** led to the formation of the η^2-styrene complex W(NPh)[o-$(Me_3SiN)_2C_6H_4$](η^2-styrene) through the liberation of CH_4. Once again attempts to isolate and fully characterize this reaction on preparatory scale were hindered by the instability of the styrene complex. In agreement with the proposed mechanism for the formation of the metallacyclopentene complex **5**, reaction of the mixed-dialkyl [W(NPh)(o-$(Me_3SiN)_2C_6H_6$)($CH_2CH_2C_6H_5$)(Me)] (**7**) with one equivalent

of diphenylacetylene at 70° C for several hours gave the metallacyclopentene complex, **5** in good yield (70 %) (Figure 2-11).

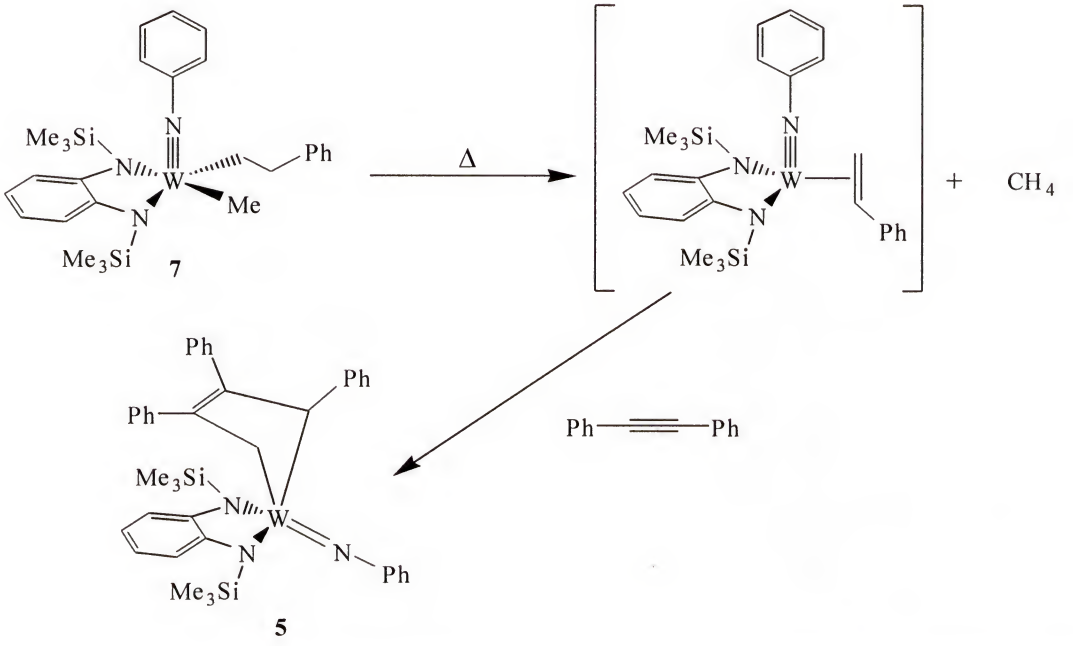

Figure 2-11. *In situ* generation of styrene complex to synthesize metallacyclopent-3-ene.

Cycloaddition and Rearrangement Steps

Once the styrene complex has been generated by side-chain C-H activation and reductive elimination of H_2 from **3** (Figure 2-9), rapid coupling of this intermediate with diphenylacetylene takes place to give the metallacyclopent-2-ene. In addition to the numerous reports of metal mediated olefin-alkyne coupling present in the literature,[64-67] this type of reactivity has also been demonstrated in our lab with a Mo(IV) system. In contrast to the tungsten system, the analogous Mo-styrene complex Mo(NPh)[o-$(Me_3SiN)_2C_6H_4$](η^2-styrene) is stable and has been isolated and fully characterized.[57] Reaction of the Mo-styrene complex with diphenylacetylene at room temperature initially (after 2 h) yields the expected olefin-alkyne coupling product a metallacyclopent-2-ene

complex. Over a period of 2 days this product is slowly converted to a metallacyclopent-3-ene species analogous to compound **5** (Figure 2-12). These observations not only support styrene-alkyne coupling in the reaction of **3** with PhC≡CPh, but they also demonstrate the likelihood of the proposed final rearrangement of the metallacyclopent-2-ene species to compound **5**.

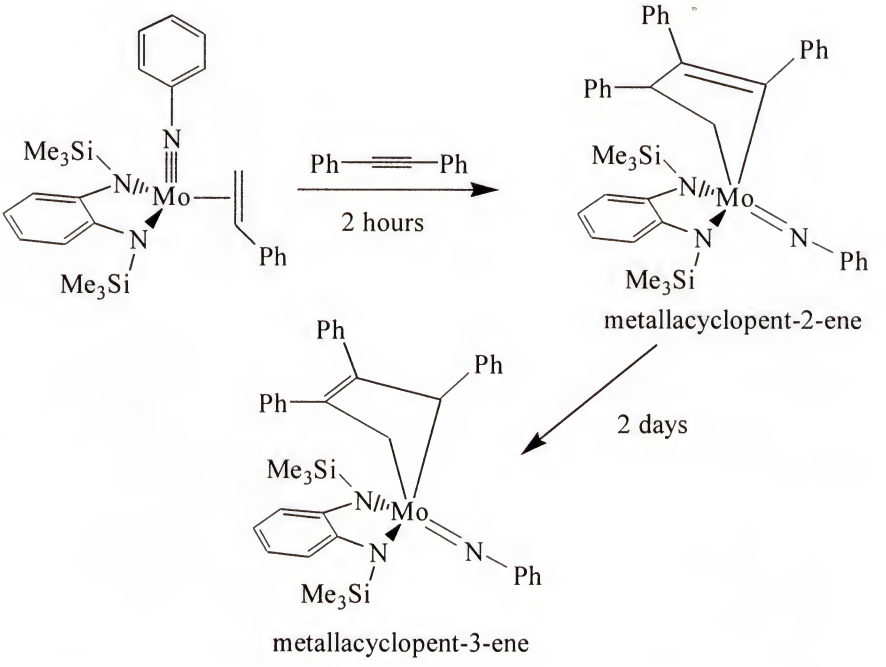

Figure 2-12. Molybdenum mediated [2 +2] cycloaddition.

Conclusions

The chemistry of d^2-arene complexes of early transition metals has not been a very thoroughly studied field. In this chapter the results of hydrogenolysis of β-hydrogen containing W(VI)-dialkyl complexes supported by imido and diamide ligands were presented. It was found that dialkyl compounds **1** and **2** are slowly converted to the corresponding arene complexes **3** and **4** over several days. Unfortunately the presence of a strong W-arene interaction has limited the subsequent chemistry of these complexes in comparison to their Mo analogs, which undergo rapid arene-arene exchange reactions.

The unexpected reaction of [W(NPh)(η^6-ethylbenzene)(o-$(Me_3SiN)_2C_6H_4$)] (**3**) with diphenylacetylene to give the metallacyclopentene complex **5**, has allowed us to apply our knowledge of both W and Mo chemistry to propose a mechanism for this transformation. Included in this proposed mechanism is a reaction that is of industrial significance. The initial step in the reaction of **3** with diphenylacetylene involves the C-H bond activation of the ethylbenzene side-chain, followed by reductive elimination of H_2. If correct, this process mimics the industrial preparation of styrene which is accomplished via ethylbenzene dehydrogenation in the presence of an iron-oxide based catalyst.[68] The extreme conditions required to facilitate the reaction on an industrial scale (600° C, in a steam atmosphere) demonstrate the difficulty in removing H_2 from ethylbenzene. This was also found to be the case in the reaction of **3** with diphenylacetylene, which only proceeded at elevated temperatures (> 60° C).

CHAPTER 3
COORDINATIVELY UNSATURATED W(IV) BIS-PYRIDINE COMPLEXES: A REACTIVE SOURCE OF W(IV)

Introduction

As discussed in Chapter 2, through the reaction of the β-hydrogen containing W(VI)-dialkyl complexes with H_2,[69] we have established that d^2 tungsten-arene complexes with the general formula W(NPh)(η^4-arene)(o-$(Me_3SiN)_2C_6H_4$) (arene = $CH_3CH_2C_6H_5$ (**3**), $CH_3CH_2CH_2C_6H_5$ (**4**)) can be synthesized by hydrogenolysis of the β-hydrogen containing dialkyl complexes W(NPh)(o-$(Me_3SiN)_2C_6H_4$)$(CH_2CH_2C_6H_5)_2$ (**1**) and W(NPh)(o-$(Me_3SiN)_2C_6H_4$) $(CH_2CH_2CH_2C_6H_5)_2$ (**2**).

Since its beginnings in the mid 50's, the chemistry of transition metal π-arene complexes has been investigated in considerable detail.[2] Reports have demonstrated that a coordinated arene can behave as a spectator ligand, labile ligand or substrate ligand.[1] For these reasons, we became interested in further examining the chemistry of the chelate stabilized W(IV)-arene complexes W(NPh)[o-$(Me_3SiN)_2C_6H_4$)](η^4-ethylbenzene) (**3**) and W(NPh)[o-$(Me_3SiN)_2C_6H_4$)](η^4-propylbenzene) (**4**) as well as other W(IV) derivatives of these complexes. As was stated in Chapter 2, we were disappointed in the limited reactivity demonstrated by compounds **3** and **4**, presumably due to a robust metal-arene interaction. However, as has been observed and well studied for other transition metal arene complexes,[44,48,70,71] compounds **3** and **4** were found to be susceptible to arene displacement by σ-donor ligands. In this chapter, the synthesis of a series of

coordinatively unsaturated W(IV)L_2 compounds through arene displacement as well as initial reactivity studies that suggests these compounds are a more reactive source of W(IV) than the arene complexes will be presented.

Arene Displacement Reactions

Pentane solutions of the W(IV)-arene complexes W(NPh)[o-$(Me_3SiN)_2C_6H_4$)](η^4-ethylbenzene) (**3**) and W(NPh)[o-$(Me_3SiN)_2C_6H_4$)](η^4-propylbenzene) (**4**) rapidly react with 2 eq. of pyridine, 4-picoline or quinoline at room temperature to give the W(IV)L_2 compounds [W(NPh)(o-$(Me_3SiN)_2C_6H_4$)$(C_5H_5N)_2$] (**8**) and [W(NPh)(o-$(Me_3SiN)_2C_6H_4$)(p-$C_6H_7N)_2$] (**9**) as dark purple solids and [W(NPh)(o-$(Me_3SiN)_2C_6H_4$)$(C_9H_7N)_2$] (**10**) as a black solid in good yield (60-75 %) (Figure 3-1). Additional purification of the crude products was possible through subsequent washings with cold pentane (0° C) followed by drying the resulting solid *in vacuo*. However, the highly unstable nature of these complexes significantly hinders the purification process.

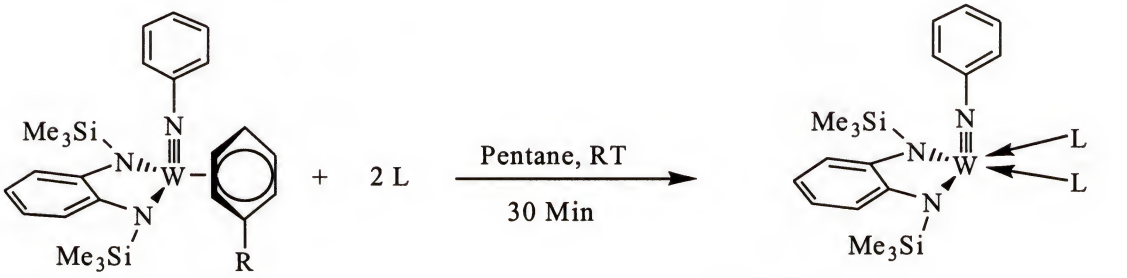

R = CH_2CH_2Ph (**3**) or $CH_2CH_2CH_2Ph$ (**4**)

L = C_5H_5N (**8**), p-C_6H_7N (**9**) and C_9H_7N (**10**)

Figure 3-1. Synthesis of W(IV)L_2 complexes via arene displacement.

Attempts to generate W(IV)L_2 compounds analogous to compounds **8-10** with other picoline derivatives and bipyridine were unsuccessful. Reaction of 2 equivalents of either 2-picoline or 3-picoline with W(NPh)[o-$(Me_3SiN)_2C_6H_4$)](η^4-propylbenzene) (**4**)

gave intractable mixtures of products, which by ^{1}H NMR spectroscopy contained small amounts of the desired W(IV)L_2 products. The exact nature of the remaining products has yet to be determined. However, based on observations of C-H bond activation chemistry, which will be presented in Chapter 4, it is possible that some of the undesired products are a result of C-H activation of the picoline CH_3 group. Compound **4** does not react with bipyridine at room temperature and at elevated temperatures only decomposition of the arene complex is observed.

Spectroscopic and X-ray Crystallographic Studies

The room temperature ^{1}H and ^{13}C NMR spectra of **8, 9** and **10** are consistent with monomeric L_2 adducts where the donor ligands are coordinated in an η^1(N) fashion. In particular, upon coordination, the resonances for the donor ligand protons are shifted up field with respect to the free ligand.[72] Interestingly, the ortho ring protons of the nitrogen donor ligands for compounds **8** and **9** display significantly different chemical shifts (5.69 and 7.80 ppm, (**8**), 5.78 and 7.88 ppm (**9**)), suggesting that there is hindered rotation of the rings about the W-N bonds on the timescale of the NMR experiment. This hindered rotation renders the ortho protons of each ring inequivalent, but the corresponding ortho protons on adjacent rings are equivalent due to the presence of a mirror plane, which exists between the two pyridine ligands. Figure 3-2 shows the proton assignment scheme for the W(IV)(pyridine)$_2$ (**8**) complex whereas Table 3-1 is a compilation of the proton resonances for the pyridine ligands of compounds **8-10**.

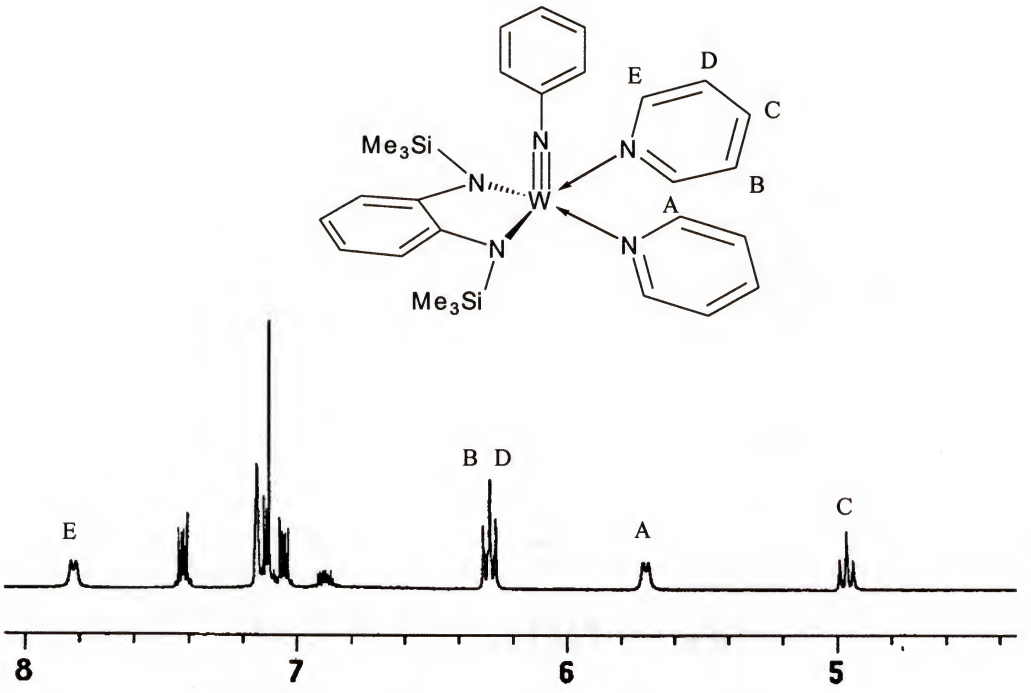

Figure 3-2. Proton assignment for W(IV)(pyridine)$_2$ (**8**).

Table 3-1. Summary of ^{1}H NMR chemical shifts of the pyridine ligands for compounds **8-10**. All spectra were obtained in C_6D_6.

W(IV)L_2 Complex	**8**	**9**	**10**
Ortho	5.69 d, 7.80 d	5.78 d, 7.88 d	5.55 d
Meta	6.27 t	6.28 t	6.50 dd
Para	4.95 t	N/A	4.99 d

The structure of the L_2 adducts was confirmed by an X-ray diffraction analysis of a single crystal of [W(NPh)(o-(Me$_3$SiN)$_2$C$_6$H$_4$)(p-C$_6$H$_7$N)$_2$] (**9**), grown from an unstirred reaction mixture in pentane at room temperature (Figure 3-3). Selected bond lengths and angles are summarized in Table 3-2. The coordination geometry about the W atom in **9** is best described as distorted square pyramidal with the W atom displaced 0.69Å out of the N2-N3-N4-N5 plane. The W-N1 bond length of 1.753(3) Å is consistent with typical

W-N imido bond lengths[31,61,69] while the W-N(pic) distances of 2.083(3) and 2.109(3) Å are shorter than what is typically found (2.30 Å) for W(IV)-N(py) bond lengths.[72-75]

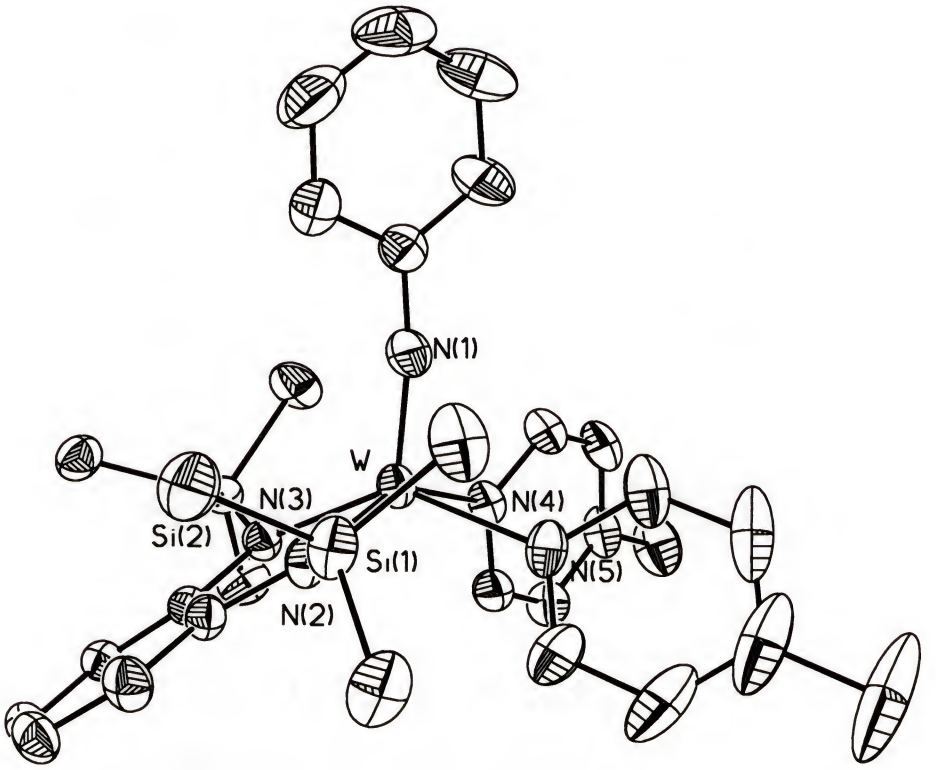

Figure 3-3. Molecular structure of [W(NPh)(o-$(Me_3SiN)_2C_6H_4$)(p-$C_6H_7N)_2$] (**9**). Thermal ellipsoids are drawn at 40 % probability and the hydrogen atoms have been removed for clarity.

Table 3-2. Summary of selected bond lengths (Å) and angles (deg) for **9**.

W-N1	1.753(3)	N3-W-N2	78.34(10)
W-N3	2.060(2)	N5-W-N4	80.33(10)
W-N2	2.062(3)	N2-W-N5	87.91(10)
W-N5	2.083(3)	N3-W-N4	88.80(10)
W-N4	2.109(3)	C1-N1-W	169.7(3)

Bonding Explanation for Hindered Rotation

The structural data for $[W(NPh)(o\text{-}(Me_3SiN)_2C_6H_4)(p\text{-}C_6H_7N)_2]$ (**9**) combined with a basic understanding of the bonding in these complexes provides an explanation for the unexpected slow rotation of the pyridine rings at room temperature that is observed in the ^1H NMR spectra of **8**, **9** and **10**. The conformation of the diamido ligand in **9** is significantly different from that observed in the W(VI) compounds we have previously studied.[31] In the W(VI) complexes, an angle of *ca.* 50° is formed by the plane defined by the W and two amide N atoms and the plane defined by the two amide N atoms and the phenylene ring (Figure 3-4). We suggested that the folding of the TMS_2pda ligand in the d^0 complexes arises because of π donation from the amide N atoms to the LUMO (d_{xy}) on the W center.[56] Maximum π donation occurs when the N p_π orbitals are rotated into the xy plane of the metal center (Figure 3-4). In order to approach this conformation, the ligand folds along the N-N vector giving the observed structures. Recently, DFT calculations performed by Galindo[76] confirmed these qualitative arguments.

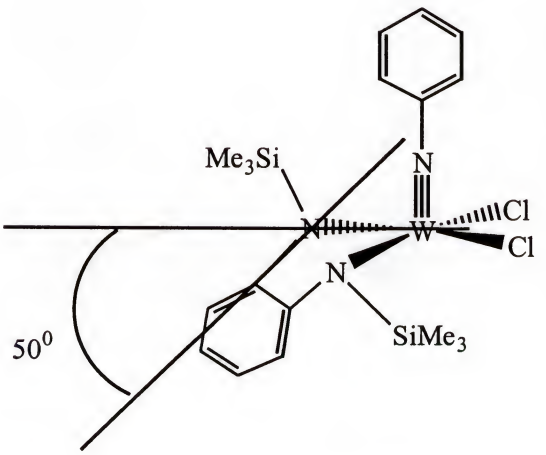

Figure 3-4. Pictorial representation of ligand fold angle for W(VI) complexes.

In contrast to the W(VI) complexes, compound **9** has an almost planar diamide ligand (fold angle = 5.3°). The structural difference arises because in **9** the d_{xy} orbital contains a pair of electrons. In order to avoid a filled-filled interaction between the d_{xy} orbital and nitrogen p_{π} orbitals, the nitrogen p_{π} orbitals rotate out of the xy plane, away from the d_{xy} orbital (Figure 3-5). Upon rotation, the diamide ligand is flattened. This conformation moves the $SiMe_3$ groups into the xy plane (The plane of the pyridine rings.). This creates a steric interaction between the $SiMe_3$ groups and the Py ligands that is the source of the observed hindered rotation of the pyridine rings about the W-N bonds.

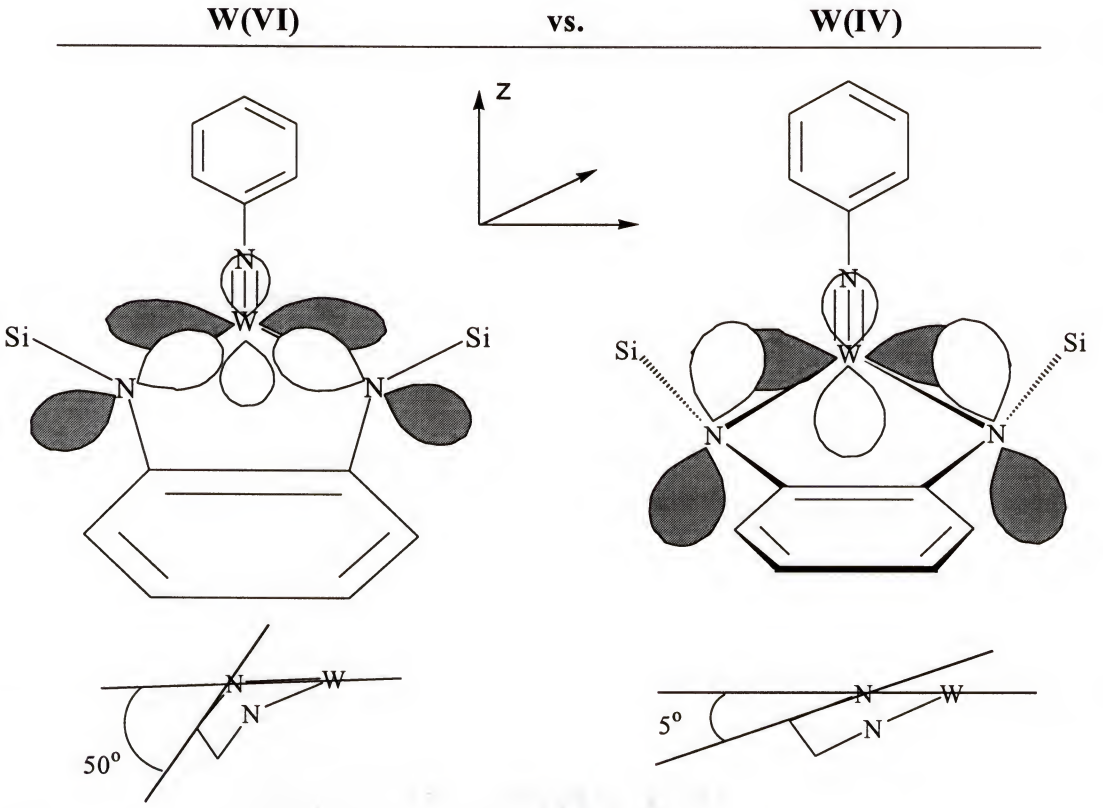

Figure 3-5. Pictorial representation of W(VI) vs. W(IV) N p_{π} - M d_{xy} orbital overlap.

We have previously synthesized the complex W(NPh)[o-$(Me_3SiN)_2C_6H_4$]Ph_2 (**11**),[33,77] which can be used as a W(VI) model of compounds **8-10** and we observe free rotation of the phenyl rings about the W-C bonds (Figure 3-6). Because this compound has a d^0 electronic configuration, we would expect that the o-$(Me_3SiN)_2C_6H_4$ ligand is folded along the N-N vector as it is in all other M(VI) (M= Mo, W) complexes of this type. This folding of the ligand moves the $SiMe_3$ groups out of the xy plane of the molecule thus relieving the steric congestion in the complex that would cause hindered rotation about the W-C bonds.

This bonding model combined with structural features obtained from X-ray crystallographic analysis will be used in Chapters 4 and 5 as a tool towards understanding the properties of several of the pentacoordinate complexes presented in these chapters. Specifically, we can use this information to characterize the oxidation state of the metal center and rationalize the observed reactivities.

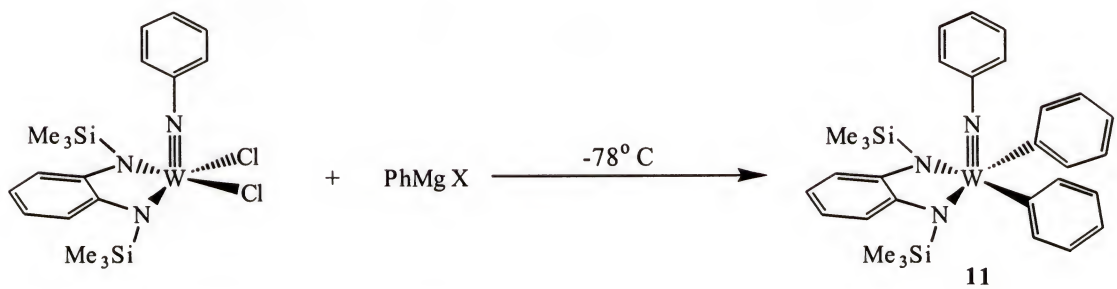

Figure 3-6. Synthesis of W(VI)(phenyl)$_2$ (**11**).

Improved Synthesis of W(IV)L_2 Compounds

Although our initial discovery of the W(IV)L_2 compounds through arene displacement from either **3** or **4** allowed us to characterize compounds **8, 9** and **10**, in order to study their chemistry more easily, a more efficient synthetic pathway was

necessary. In light of this, we have discovered that compounds **8** and **9** can be generated from the W(VI)-dichloride complex W(NPh)(o-$(Me_3SiN)_2C_6H_4$)Cl_2 in one step. Na^0 reduction of a THF solution of the W(VI)-dichloride, in the presence of pyridine or 4-picoline produces **8** and **9** with improved purity and yield (> 90 %) (Figure 3-7). Isolation of pure **8** and **9** is accomplished by removal of the THF *in vacuo* followed by toluene extraction to separate the desired products from NaCl, the major byproduct of the reaction. Subsequent removal of toluene from the filtrate solution followed by drying the resulting solid *in vacuo* for 3 hours yields **8** and **9** as dark purple, crystalline solids.

This synthetic route eliminates the need to generate the W(IV)-arene complexes **3** and **4** which require 4-7 days to synthesize. In addition, the difficulty encountered in both the purification of the arene complexes and the purification of the W(IV)L_2 complexes when generated from the arene complexes are circumvented.

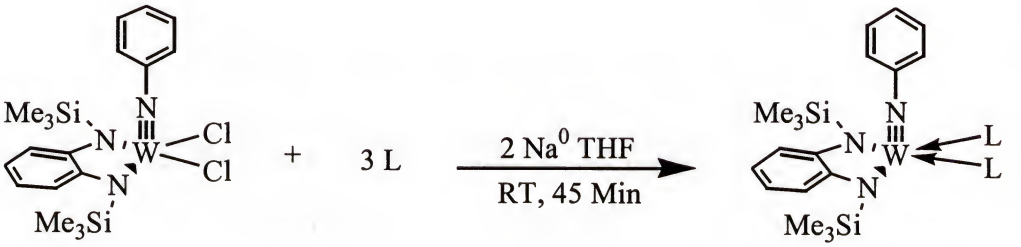

Figure 3-7. Synthesis of **8** and **9** by Na^0 reduction of W(NPh)(o-$(Me_3SiN)_2C_6H_4$)Cl_2.

Addition of a Sixth Ligand to W(IV)L_2

We have found that the W(IV)L_2 compounds **8** and **9** are coordinatively unsaturated and readily accommodate additional ligands. For example, reaction of [W(NPh)(o-$(Me_3SiN)_2C_6H_4$)$(C_5H_5N)_2$] (**8**) or [W(NPh)(o-$(Me_3SiN)_2C_6H_4$)$(p\text{-}C_6H_7N)_2$]

(**9**) with CO (20 psi) results in the rapid formation of the six coordinate complexes [W(NPh)(o-$(Me_3SiN)_2C_6H_4$)$(C_5H_5N)_2$(CO)] (**12a**) and [W(NPh)(o-$(Me_3SiN)_2C_6H_4$)$(C_6H_7N)_2$(CO)] (**12b**), which are isolated as dark brown, crystalline solids (Figure 3-8). Pure samples of **12a** and **12b** are obtained simply by removing the pentane reaction solvent, subsequent purification was not necessary in this case.

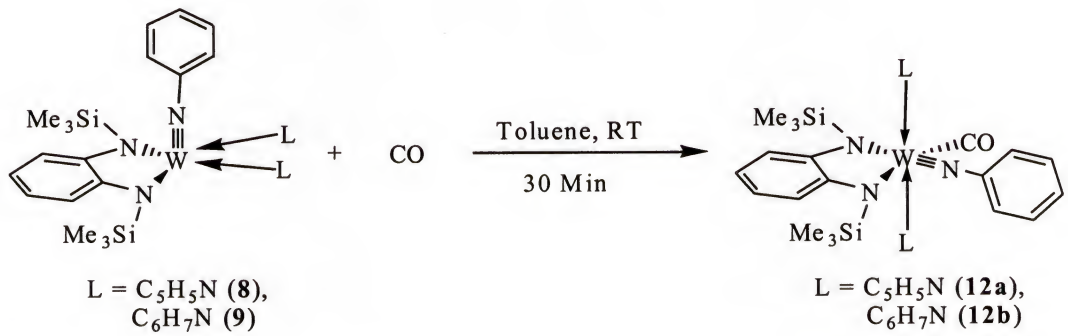

L = C_5H_5N (**8**), C_6H_7N (**9**)

L = C_5H_5N (**12a**), C_6H_7N (**12b**)

Figure 3-8. Synthesis of six-coordinate W(IV) complexes.

An X-ray diffraction study was performed on a single crystal of [W(NPh)(o-$(Me_3SiN)_2C_6H_4$)$(C_5H_5N)_2$(CO)] (**12a**), grown from a concentrated Et_2O solution at -40° C over a 1 week period. The molecular structure is shown in Figure 3-9 and a summary of selected bond lengths and angles is presented in Table 3-3. Complex **12a** adopts a pseudo-octahedral geometry about the W-atom, with the pyridine groups occupying mutually *trans* positions. Consequently, the phenyl-imido is *cis* and *trans* to the $NSiMe_3$ groups, and CO occupies the remaining coordination site. The largest distortions from a purely octahedral geometry are the N1-W-N2 (110.34(14)°) and N2-W-N3 (78.08(12)°) bond angles, which can be attributed to the restricted bite of the chelate ring.

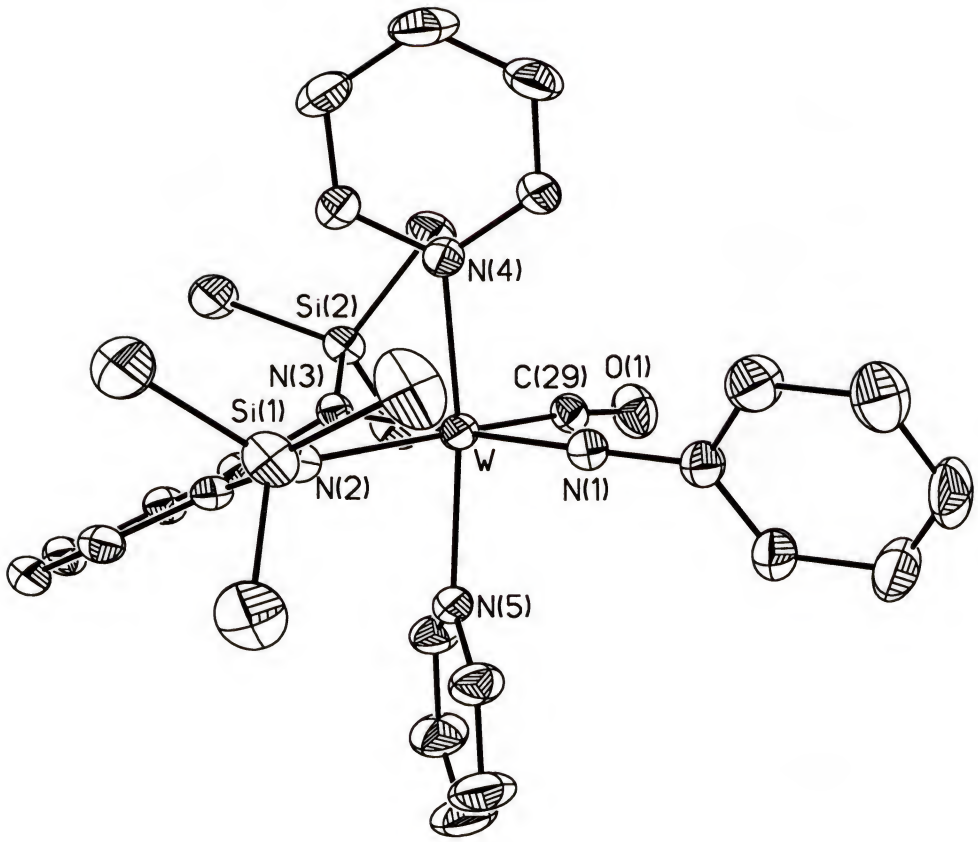

Figure 3-9. Molecular structure of [W(NPh)(o-$(Me_3SiN)_2C_6H_4$)(p-$C_6H_7N)_2$(CO)] (**12a**). Thermal ellipsoids are drawn at 40 % probability and the hydrogen atoms have been removed for clarity.

Table 3.3. Summary of selected bond lengths (Å) and angles (deg) for **12a**.

W-N1	1.787(3)	N1-W-N4	92.67(14)	C29-W-N4	96.07(14)
W-N2	2.139(3)	N1-W-N5	92.18(14)	C29-W-N5	88.85(15)
W-N3	2.112(3)	N4-W-N5	173.39(12)	N3-W-N4	89.23(12)
W-N4	2.203(3)	N1-W-C29	84.62(16)	N3-W-N5	86.63(12)
W-N5	2.215(3)	C29-W-N3	86.83(15)	N2-W-N4	88.77(12)
W-C29	1.985(4)	N1-W-N2	110.34(14)	N2-W-N5	85.34(13)
C29-O1	1.165(5)	N2-W-N3	78.08(12)		

The value of the CO stretching frequencies, ν_{CO} = 1890 cm^{-1} (**12a**) and 1878 cm^{-1} (**12b**), are unusually low for what might be expected for high oxidation state (W(IV), d^2) complexes. It is likely that the ability of the W to back-bond to the CO ligand is significantly enhanced relative to what might be expected because the amide N that is *trans* to the CO ligand is a π donor ligand, which enhances the back-bonding thereby relieving an unfavorable N pπ - Wdπ filled-filled interaction.

The room temperature ^{1}H NMR spectra of **12a** and **12b** display two peaks (0.34 and 0.37 ppm (**12a**), 0.41 and 0.45 ppm (**12b**)) that are assigned to inequivalent $Si(CH_3)_3$ groups. The inequivalence of the $Si(CH_3)_3$ groups is consistent with the structural results that place the $NSiMe_3$ groups *cis* and *trans* to the imido group.[30] In contrast to the ^{1}H NMR spectra of the W(IV)L_2 compounds **8**, **9** and **10**, there is only one set of pyridine ring protons for **12a** and **12b** due to the equivalency of the rings in the octahedral geometry. Consistent with the NMR spectra of compounds **8** and **9**, the meta and para ring proton resonances of the pyridine ligands of **12a** and **12b** are shifted upfield with respect to free ligand and the ortho protons experience a downfield shift. The ^{1}H NMR spectrum of **12b** (Figure 3-10) displays this chemical shift pattern as the ortho protons are shifted downfield (8.7 ppm) and the meta protons are shifted upfield (6.2 ppm). This pattern of the chemical shifts of the pyridine ligands in six-coordinate W(IV) complexes became instrumental in characterizing additional six-coordinate complexes presented in this chapter as well as those found in Chapter 4. The ^{13}C NMR spectra of **12a** and **12b** display resonances at 281 and 284 ppm respectively corresponding to the CO ligands.

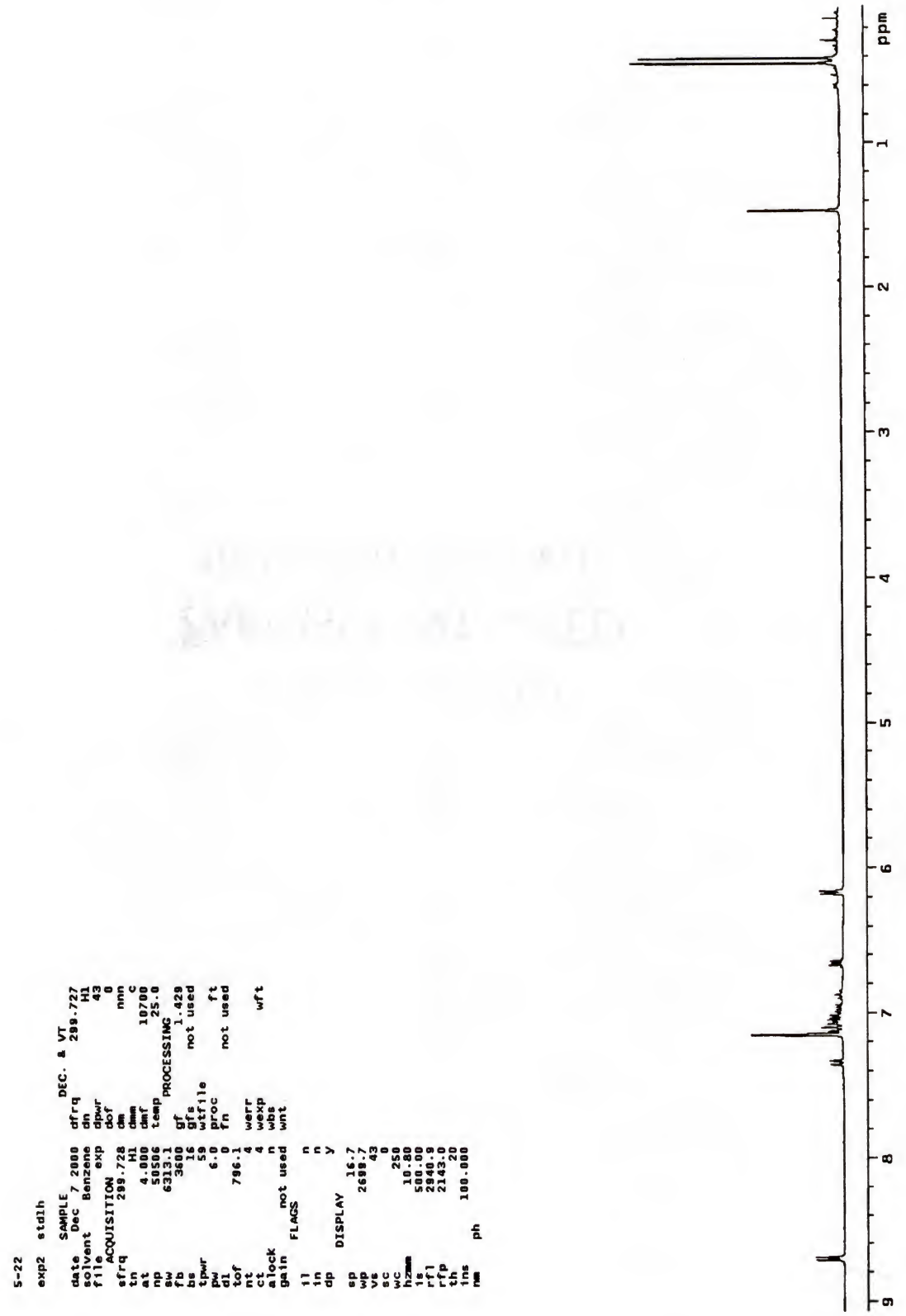

Figure 3-10. ^{1}H NMR spectrum of $[W(NPh)(o\text{-}(Me_3SiN)_2C_6H_4)(C_6H_7N)_2(CO)]$ (**12b**).

Ligand Substitution Reactivity

Substitution of One Pyridine Ligand

Examination of the chemistry of the six coordinate compounds **12a** and **12b** led to the observation that one of the N-donor ligands is labile and can be displaced. This was demonstrated by the reaction of $[W(NPh)(o\text{-}(Me_3SiN)_2C_6H_4)(C_5H_5N)_2(CO)]$ (**12a**) and $[W(NPh)(o\text{-}(Me_3SiN)_2C_6H_4)(C_6H_7N)_2(CO)]$ (**12b**) with PMe_3 to give the substitution products $[W(NPh)(o\text{-}(Me_3SiN)_2C_6H_4)(C_5H_5N)(CO)(PMe_3)]$ (**13a**) and $[W(NPh)(o\text{-}(Me_3SiN)_2C_6H_4)(C_6H_7N)(CO)(PMe_3)]$ (**13b**) (Figure 3-11). Due to the coordinative saturation of **12a** and **12b**, we believe that the reaction proceeds through a dissociative pathway in which a five coordinate $[W(NPh)(o\text{-}(Me_3SiN)_2C_6H_4)(CO)L]$ intermediate is trapped by the incoming PMe_3 ligand.

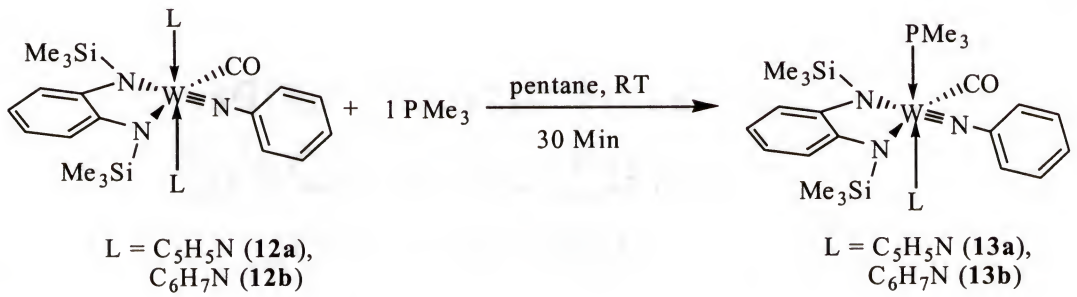

L = C_5H_5N (**12a**), C_6H_7N (**12b**)

L = C_5H_5N (**13a**), C_6H_7N (**13b**)

Figure 3-11. Pyridine substitution with PMe_3.

The ^1H NMR spectra of compounds **13a** and **13b** display two peaks (0.21 and 0.30 ppm (**13a**), 0.25 and 0.34 ppm (**13b**)) that are assigned to inequivalent $Si(CH_3)_3$ groups. Resonances corresponding to the PMe_3 ligands appear at 0.98 for **13a** and 1.00 for **13b** with $^2J_{P\text{-}H}$ coupling constants of 9.0 and 9.3 Hz respectively. The resonances for the pyridine protons of **13a** and **13b** display a similar pattern to that which was observed for compounds **12a** and **12b**. The ^{31}P NMR spectra of these complexes display a single

resonance for the PMe_3 ligands (-10.76 ppm (**13a**), -10.71 ppm (**13b**)) with a $^1J_{W-P}$ coupling constant of 188 Hz for both compounds.

Synthesis of $W(IV)(PMe_3)_2L$ Complexes

In agreement with the proposed lability of one of the N-donor ligands in the six coordinated complexes $[W(NPh)(o\text{-}(Me_3SiN)_2C_6H_4)(C_5H_5N)_2(CO)]$ (**12a**) and $[W(NPh)(o\text{-}(Me_3SiN)_2C_6H_4)(C_6H_7N)_2(CO)]$ (**12b**), reaction of $[W(NPh)(o\text{-}(Me_3SiN)_2C_6H_4)(C_5H_5N)_2]$ (**8**) or $[W(NPh)(o\text{-}(Me_3SiN)_2C_6H_4)(C_6H_7N)_2]$ (**9**) with 2 eq. of PMe_3 results in the rapid formation of $[W(NPh)(o\text{-}(Me_3SiN)_2C_6H_4)(C_5H_5N)(PMe_3)_2]$ (**14a**) and $[W(NPh)(o\text{-}(Me_3SiN)_2C_6H_4)(C_6H_7N)(PMe_3)_2]$ (**14b**) respectively with loss of 1 eq. of pyridine or picoline (Figure 3-12). Displacement of pyridine or 4-picoline by a second PMe_3 group to generate compounds **14a** and **14b** instead of complexes of the type $W(IV)L_2(PMe_3)$ is preferred as demonstrated by the reaction of compound **8** or **9** with 1 eq. of PMe_3, which produces a 1:1 mixture of the bis-phosphine complexes **14a** or **14b** and $W(IV)L_2$ (starting material) as determined by NMR spectroscopy.

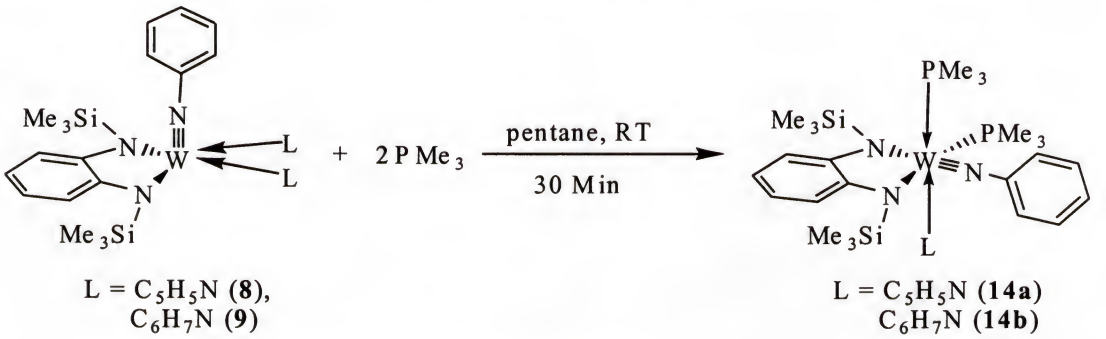

L = C_5H_5N (**8**), C_6H_7N (**9**)

L = C_5H_5N (**14a**) C_6H_7N (**14b**)

Figure 3-12. Synthesis of $W(IV)L(PMe_3)_2$ complexes.

An X-ray diffraction study was performed on a single crystal of $[W(NPh)(o\text{-}(Me_3SiN)_2C_6H_4)(C_5H_5N)(PMe_3)_2]$ (**14a**), grown from a concentrated pentane solution at -40° C over 3 days. The molecular structure is shown in Figure 3-13 and a summary of

selected bond lengths and angles is presented in Table 3-4. Complex **14a** adopts a pseudo-octahedral geometry about the W-atom, with the PMe_3 groups occupying mutually *cis* positions. Consequently, the phenyl-imido group is *cis* and *trans* to the $NSiMe_3$ groups, and pyridine occupies the remaining coordination site *trans* to one of the PMe_3 ligands. The largest distortions from a purely octahedral geometry are the N1-W-N3 (102.06(17)°), N2-W-N3 (76.76(15)°), N3-W-N4 (82.60(16)°) and N3-W-P2 (170.40(11)°) bond angles, which can be attributed to the restricted bite of the chelate ring.

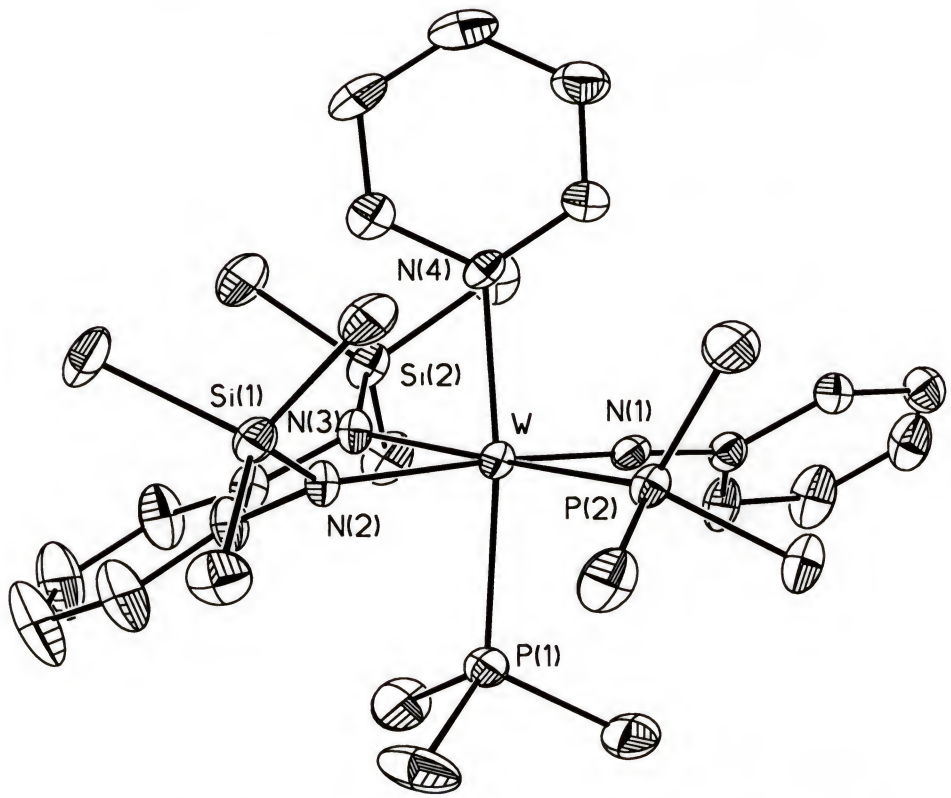

Figure 3-13. Molecular structure of $[W(NPh)(o\text{-}(Me_3SiN)_2C_6H_4)(C_5H_5N)(PMe_3)_2]$ (**14a**). Thermal ellipsoids are drawn at 40 % probability and the hydrogen atoms have been removed for clarity.

Table 3-3. Summary of selected bond lengths (Å) and angles (deg) for **14a**.

W-N1	1.795(4)	N1-W-N3	102.06(17)	N4-WN2	90.73(16)
W-N2	2.151(4)	N2-W-N3	76.76(15)	N4-W-N3	82.60(16)
W-N3	2.166(4)	N2-W-P2	94.51(11)	P1-W-N1	89.83(13)
W-N4	2.232(4)	N1-W-P2	86.96(14)	P1-W-N2	85.68(12)
W-P1	2.4757(14)	N4W-N1	93.61(17)	P1-W-N3	91.10(12)
W-P2	2.4950(13)	N4-W-P2	93.65(11)	P1-W-P2	92.23(5)

Similar to the W(IV)L_2(CO) compounds **12a** and **12b** and the W(IV)L(CO)(PMe_3) compounds **13a** and **13b**, the room temperature ^{1}H NMR spectra of **14a** and **14b** display two peaks (0.14 and 0.20 ppm (**14a**), 0.17 and 0.24 ppm (**14b**), assigned to the inequivalent $Si(CH_3)_3$ groups, again due to a *cis* and *trans* orientation with respect to the imido group.[30] The PMe_3 protons appear as doublets at 1.09 ppm ($^2J_{P-H}$ = 7.3 Hz) and 1.43 ppm ($^2J_{P-H}$ = 6.3 Hz) for **14a** and 1.12 ppm ($^2J_{P-H}$ = 8.1 Hz) and 1.46 ($^2J_{P-H}$ = 6.3 Hz) for **14b**, consistent with inequivalent PMe_3 groups. The ^{31}P NMR spectra of **14a** and **14b** confirm this inequivalency as the PMe_3 groups appear as two doublets (-40.31, -24.09 ppm, $^2J_{P-P}$ = 9.5 Hz) for **14a** and (-39.93, -24.09 ppm, $^2J_{P-P}$ = 10.0 Hz) for **14b** that have ^{183}W satellites ($^1J_{W-P}$ = 190 and 158 Hz (**14a**), $^1J_{W-P}$ = 193 and 159 Hz (**14b**)). The small $^2J_{P-P}$ values are consistent with a *cis* orientation of the PMe_3 groups,[3] leaving the pyridine group as the remaining ligand of the octahedral complex. A *cis*-orientation of the PMe_3 groups also accounts for the difference in the $^1J_{W-P}$ values. The larger $^1J_{W-P}$ value corresponds to the PMe_3 group which is *trans* to pyridine and the smaller value for the PMe_3 *trans* to amide as would be expected with the amide group

having a greater *trans* influence than pyridine. This was also observed in the solid-state structure, where the W-P distance for the PMe_3 group *trans* to amide (2.4950(13) Å) is longer than that for the PMe_3 group trans to pyridine (2.4757(14) Å).

Conclusions

The Na^0 reduction of $[W(NPh)[o\text{-}(Me_3SiN)_2C_6H_4]Cl_2]$ in the presence of donor ligands such as pyridine or 4-picoline, provides a simple and efficient means for producing the coordinatively unsaturated $W(IV)L_2$ compounds $[W(NPh)(o\text{-}(Me_3SiN)_2C_6H_4)(C_5H_5N)_2]$ (**8**) or $[W(NPh)(o\text{-}(Me_3SiN)_2C_6H_4)(C_6H_7N)_2]$ (**9**). The reactions of compounds **8** and **9** with additional ligands (CO, PMe_3), presented in this chapter, serve to demonstrate the reactive nature of these compounds as well as suggesting patterns of ligand substitution that will become important in subsequent chapters. Based on the initial observations of the lability of the N-donor ligands upon formation of six coordinate complexes, we believe that $W(IV)L_2$ compounds will display very rich chemistry. Chapters 4 and 5 will discuss in more detail the reactivity of these complexes with certain organic substrates.

In addition to the increased reactivity with respect to the W(IV)-arene complexes, the $W(IV)L_2$ compounds **8** and **9** are to the author's knowledge, very rare examples of bis-pyridine complexes where there is hindered rotation about the M-N(py) bonds. Using the bonding model that was presented, we were able to suggest that a steric interaction between the Me_3Si groups and the pyridine ligands causes the observed hindered rotation of the pyridine ligands. This bonding model and the fold angle of the diamide ligand become important tools in the discussion of the chemistry presented in the following chapters.

CHAPTER 4
REACTION OF THE W(IV)L_2 COMPLEXES WITH VARIOUS UNSATURATED SUBSTRATES: UNDERSTANDING THE REACTIVITY OF THE W(NPh)[o-$(Me_3SiN)_2C_6H_4$] FRAGMENT

Introduction

The interaction of early-transition metal complexes with unsaturated organic substrates has been an active area of research for many years. The focus of this chapter will be expanding our understanding of the chemistry of the W(IV)L_2 complexes W(NPh)(o-$(Me_3SiN)_2C_6H_4$)$(C_5H_5N)_2$ (**8**) and W(NPh)(o-$(Me_3SiN)_2C_6H_4$)$(C_6H_7N)_2$ (**9**) in the presence of various unsaturated organic substrates. Included in the discussion of this topic will be the reactions of compounds **8** and **9** with acetylenes, butadienes and olefins and the structural and spectroscopic properties of the resulting products.

Early-Transition Metal Acetylene Complexes

Acetylene complexes of group 4,[78-83] 5[84-90] and 6[87,91-104] transition metals with a d^2electronic configuration are well known and have been investigated in detail.[105,106] Typically, the alkyne ligands in these complexes are considered to be π-bound to the metal center. The magnitude of the ligand-to-metal π-donor interaction can range from two to four electrons, depending on the involvement of the alkyne perpendicular π-bonding component. Research has also shown that the metal-to-ligand interactions may be sufficiently strong to change the formal oxidation state of the metal and reduce the alkyne ligand.[85,89,90] The extent of this reduction is such that alkyne complexes have been used as a source of 1,2-alkene dianions in organic synthesis.[88]

In contrast to the synthesis of d^2 arene complexes of the early transition metals (Chapter 2), acetylene complexes are most commonly generated through displacement reactions where a ligand is displaced by an acetylinic substrate. For example, Nielson[96] *et al.* used the reaction of $WCl_2(NPh)(PMe_3)_3$ with diphenylacetylene to generate the W(IV)-acetylene complex $WCl_2(NPh)(PhC{\equiv}CPh)(PMe_3)_2$ (Figure 4-1). Ligand displacement has also been employed in the synthesis of Group 5 acetylene complexes such as $Nb(THF)_2Cl_3(RC{\equiv}CR)$.[88]

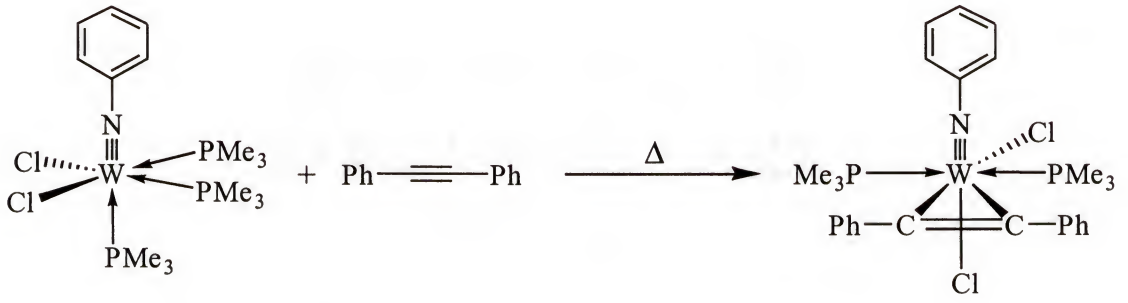

Figure 4-1. Synthesis of acetylene complex by ligand displacement.

Acetylene complexes can also be generated by reduction of a metal halide in the presence of alkynes as demonstrated by Rothwell's[98] synthesis of a series of alkyne complexes of the type $W(OAr)_2Cl_2(C_2R_2)$ from the reaction of $W(OAr)_2Cl_4$ with an alkyne using Na^o as the reductant. Among the well-characterized d^2, Group 4 metallocene-acetylene complexes the Ti complexes $Cp^*_2Ti(\eta^2$-acetylene) or $Cp_2Ti(\eta^2$-acetylene), were the first to be generated without additional donor ligands. Analogous complexes of zirconium are less common. Rosenthal was able to isolate and characterize the first zirconacene-acetylene complex, *rac*-[1,2-ethylene-1,1'-bis(η^5-tetrahydroindenyl)]Zr(η^2-acetylene) through the Mg^o reduction of *rac*-[1,2-ethylene-1,1'-bis(η^5-tetrahydroindenyl)]$ZrCl_2$ with bis(trimethylsilyl)-acetylene.[82]

Early-Transition Metal Butadiene Complexes

1,3-Butadiene complexes of early-transition metals, especially titanium, zirconium and tantalum, have been shown to be distinctively different from those of late-transition metals.[107] Therefore, the considerable interest in diene complexes of Group 4 and 5 metals is not surprising.[108,109,58,59] From this area of research has come a number of significant discoveries, such as the first mononuclear diene complex with the diene moiety bound in an s-trans conformation $Cp_2Zr(diene)$ [110] as well as a host of new reagents for organic[111-113] and organometallic[114-120] transformations. In addition, these studies have shown that the bonding displayed by Group 4 and 5 diene complexes has demonstrated the effect of periodicity on the coordination modes of unsaturated ligands. As with complexes of other unsaturated ligands, butadiene complexes are typically generated by either ligand displacement or metal halide reduction in the presence of diene, but they can also be synthesized by the addition of Mg-butadiene$(THF)_3$ to metal dihalides as well.

1,3-Butadiene, the simplest acyclic conjugated diene, is a common ligand particularly for complexes of the later transition metals.[121] Coordination of 1,3-butadiene to these electron rich metals takes the form of a π-bound, cis-planar group of carbon atoms, which are all nearly equidistant from the metal center. Consistent with this are the very similar carbon-carbon bond lengths of the butadiene fragment. This π^4 type of bonding is typical for the 1,3-diene complexes of those metal to the right of the periodic table (Figure 4-2).

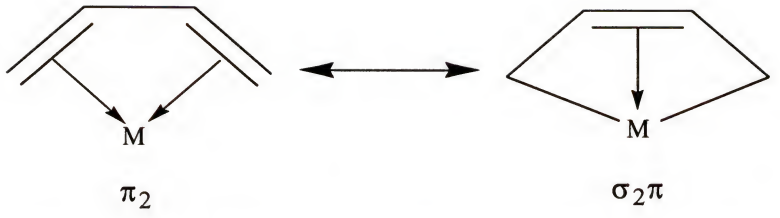

Figure 4-2. Bonding extremes for transition metal butadiene complexes.

For early transition metals, a completely different mode of coordination is observed, which includes both σ and π components. In this type of $\sigma_2\pi$ geometry, the four carbon atoms of the butadiene are not equidistant from the metal center and the carbon-carbon bond lengths are dissimilar, alternating as long-short-long. An extreme of this type of bonding is the metallacyclopentene having only a minimal interaction of the carbon-carbon double bond with the metal center (Figure 4-2).

Diene complexes usually display dynamic behavior and the nature of these processes also appears to be dependant on the position of the metal center in the transition series. For later, electron rich metals, the diene fragment normally undergoes rotation around the metal-butadiene centroid axis while for early-transition metals, a process known as envelope flipping is observed. The latter process has also been induced in late-transition metal complexes of the type CpCo(diene) under photochemical conditions.[122] Additional reports have also suggested the possibility of diene rotation coupled with envelope flipping to explain the fluxional behavior of low valent diene complexes of Mo[123] and W.[124]

Early-Transition Metal Olefin Complexes

Similar to π_2-butadiene complexes, stable π-olefin complexes are more common for late-transition metals than for early-transition metals, due to increased back bonding

capabilities of the more electron rich late-transition metals. However, the proposed involvement of olefin complexes as intermediates in many industrial processes[1] and synthetic reactions[3,79] has increased interest in early-transition metal olefin complexes.

Several groups have studied the equilibrium between bis-olefin complexes and metallacyclopentanes.[125-127] Typically, this equilibrium lies towards the metallacyclopentane isomer for early-transition metal species. Therefore, in order to isolate high-oxidation state early-transition metal π-olefin complexes, additional donor ligands such as PR_3 groups are usually required. Bercaw[125] was able to isolate and characterize the monomeric $Cp^*_2Ti(\eta^2$-ethylene) complex from the reduction of $Cp^*_2TiCl_2$ under ethylene pressure. This complex was also found to undergo subsequent oxidative coupling with additional ethylene to generate a metallacyclopentane species (Figure 4-3).

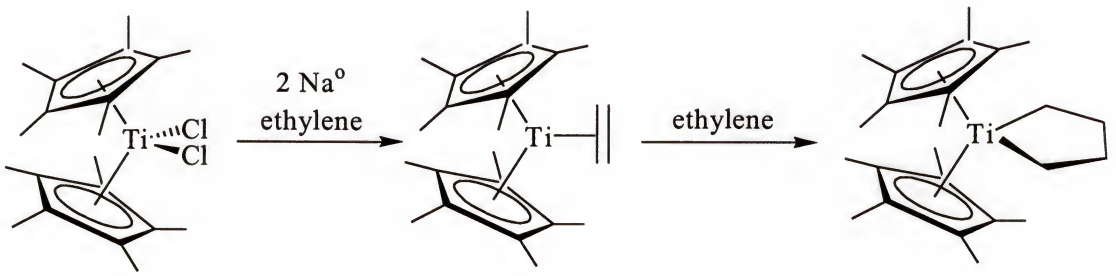

Figure 4-3. Synthesis of Ti-ethylene and Ti-metallacyclopentane complexes.

Group 5 and 6 d^2 olefin complexes are also common in the literature, but once again these compounds require additional stabilization in the form of donor ligands. Examples of these types of complexes include, but are not limited to: $Ta(NPh)(\eta^2$-olefin$)(PMe_3)_3Cl$,[128] $Cp^*Ta(=C(H)(t\text{-butyl}))(\eta^2$-ethylene$)(PMe_3)$,[129] $Mo(NAr)(OR)_2(\eta^2$-ethylene$)(PMe_3)$[130] and $W(NAr)Cl_2(PMe_3)_2(\eta^2$-olefin$)$.[102,131]

In recent years, members of our research group synthesized a series of stable Mo(IV)-η^2-olefin complexes of the type [Mo(NPh)(η^2-olefin)(o-$(Me_3SiN)_2C_6H_4$)] (olefin = propylene, isobutylene, 1-butene, 2-butene, styrene).[57,132] In addition, analogous Mo(IV)-acetylene and Mo(IV)-butadiene complexes have been synthesized from the Mo(IV)-arene complexes by simple ligand displacement. Our observations of the ability of the W(IV)L_2 complexes to readily accommodate a sixth ligand and undergo ligand substitution reactions combined with a desire to compare the reactivity of the Mo(IV) complexes with the W(IV) system prompted us to investigate the reactivity of these complexes with unsaturated substrates.

Synthesis and Characterization of a W-alkyne Complex

The W-alkyne complex [W(NPh)(o-$(Me_3SiN)_2C_6H_4$)(PhC≡CPh)] (**15**) was prepared by heating an equimolar toluene solution of W(NPh)(o-$(Me_3SiN)_2C_6H_4$)$(C_5H_5N)_2$ (**8**) and diphenylacetylene at 55° C for 4 hours. Purification of the crude product by pentane extraction gave **15** as an air and moisture sensitive brown solid in 68 % yield (Figure 4-4). The ^{1}H NMR spectrum for **15** displays overlapping aromatic resonances for the diamide, imido and coordinated diphenylacetylene moieties with integration values that are consistent with a monomeric W(IV)-alkyne complex. The $SiMe_3$ protons resonate as a singlet at 0.41 ppm.

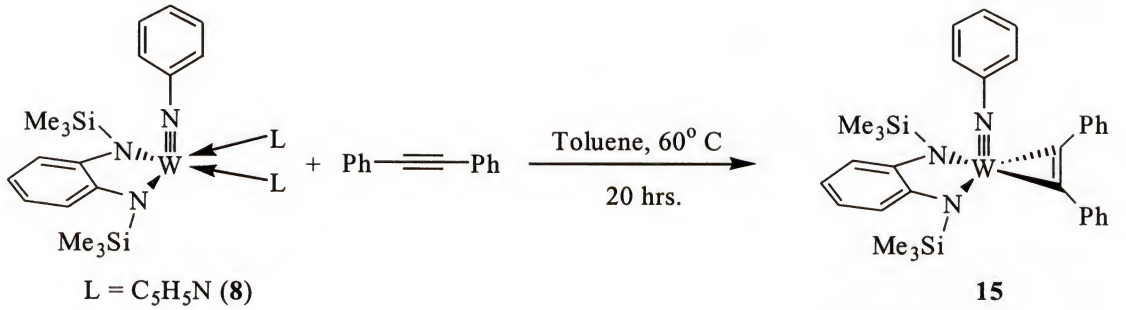

L = C_5H_5N (**8**) **15**

Figure 4-4. Synthesis of W-alkyne complex **15**.

Table 4-1. ^{13}C NMR chemical Shifts for Selected Tungsten Alkyne complexes

Complex	$\delta(R^{13}C{\equiv}CCR)$
$[WCl_4(C_2Ph_2)]$[85]	270.0
$W(NPh)(o\text{-}(Me_3SiN)_2C_6H_4)(PhC{\equiv}CPh)$ this work	198.5
$[W(OC_6H_3Pr_2\text{-}2,6)_2Cl_2(C_2Et_2)$[98]	191.7
$[W(OC_6H_3Pr^i_2\text{-}2,6)_2Cl_2(C_2Ph_2)$[98]	183.4
$[Tp'W(O)(I)(C_2Me_2)]$[103]	162.0
$[Tp'W(O)(I)(PhC{\equiv}CMe)]$[96]	167.0
$[WCl_2(NPh)(C_2Ph_2)(PMe_3)_2]$[96]	155.8
$[WCl_2(NNCHMe_2)(C_2Ph_2)(PMe_3)_2]$[96]	151.4
$[WCl_2(NC_6H_3Pr^i_2\text{-}2,6)(C_2Ph_2)(PMe_3)_2]$[101]	154.4

A more detailed explanation of the ^{13}C NMR spectrum is warranted here due to its importance in understanding the nature of the metal-alkyne interaction. Table 4-1 lists the ^{13}C NMR chemical shifts of the alkyne carbon atoms for a variety of W(IV) alkyne complexes. It can be seen (Table 4-1) that the ^{13}C NMR resonance for the alkyne carbons of **15** is downfield (198.5 ppm) of the W-alkyne complexes that are considered to contain 3 electron donor alkynes ligands (140-190 ppm).[105] Even though the resonance for the alkyne carbons of **15** is within the range for $4e^-$ donor alkyne complexes, the shift is not as dramatic as that observed for $[WCl_4(C_2Ph_2)]$ (270 ppm)[85] Of significance is the large chemical shift difference (~ 45 ppm) observed when comparing **15** to other reported (imido)W-alkyne complexes. However, in comparison to **15** most of these complexes

contain additional donor ligands. The lack of donor ligands such as PMe_3 in compound **15** results in a decreased electron density at the tungsten center. This increases the magnitude of the W-alkyne interaction, resulting in a more significant downfield shift of the alkyne resonance. Therefore, based on literature reports and the observed ^{13}C NMR spectrum for **15**, the alkyne ligand of this complex can be considered a $4e^-$ donor.

X-ray Structural Analysis

An X-ray diffraction study was performed on a single crystal of [W(NPh)(o-$(Me_3SiN)_2C_6H_4$)(PhC≡CPh)] (**15**), grown from a concentrated Et_2O solution of **15**, which was left undisturbed at -40° C for one week. The data obtained from this study was found to be in agreement with the spectroscopic findings, specifically the nature of the W-alkyne interaction. A summary of selected bond lengths and angles for **15** are presented in Table 4-2. Compound **15** adopts a distorted square pyramidal geometry about the W metal center with the imido group occupying the apical position (Figure 4-5). The W-N1(imido) (1.756(2) Å), W-N2(amido) (1.984(2) Å) and W-N3(amido) (2.017(2) Å) bond distances are all consistent with what has been previously observed for these types of bonds. The W-C(alkyne) bond distances of 2.054(3) Å, which are consistent with W-C single bonds[31] and the acetylene C-C distance of 1.332(4) Å (1.34 Å is the generally accepted value for a C=C bond) suggest a metallacyclopropene structure for the interaction of diphenylacetylene with W in compound **15**.

The bonding of the acetylene moiety in compound **15** is similar to that which has been observed for analogous Mo-acetylene complexes that have been prepared in our lab. The compounds [Mo(NPh)(o-$(Me_3SiN)_2C_6H_4$)(MeC≡CMe)] and [Mo(NPh)(o-$(Me_3SiN)_2C_6H_4$)($Me_3SiC{\equiv}CMe_3Si$)] display short Mo-C_{ave} distances of 2.054 and 2.078

Å respectively.[133] Also, the C-C bond distances of 1.297 and 1.305 Å for the Mo complexes are in good agreement with that found for **15** (1.332 Å).

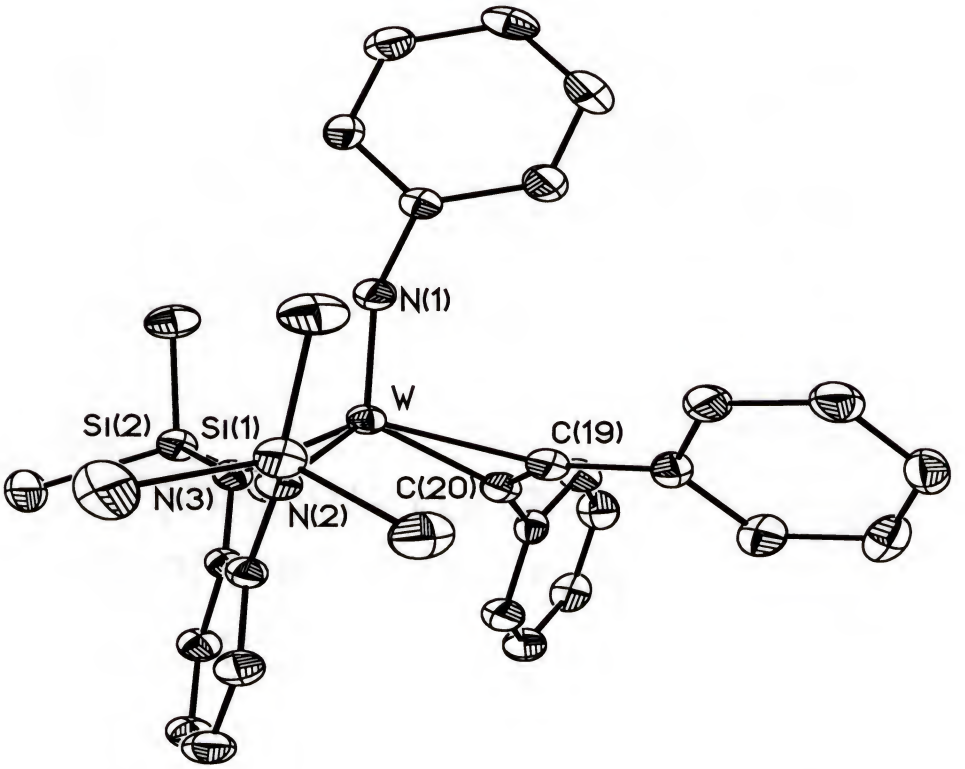

Figure 4-5. Molecular structure of [W(NPh)(o-$(Me_3SiN)_2C_6H_4$)(PhC≡CPh)] (**15**). Thermal ellipsoids are drawn at 40 % probability and the hydrogen atoms have been removed for clarity.

Table 4-2. Summary of bond lengths (Å) and angles (deg) for **15**.

W-N1	1.756(2)	N2-W-N3	85.42(8)
W-N2	1.984(2)	N2-W-C19	103.19(9)
W-N3	2.0168(19)	N3-W-C20	94.05(9)
W-C19	2.054(3)	C1-W-N1	161.77(18)
W-C20	2.054(3)	C20-C19-C21	137.0(3)
C19-C20	1.332(4)	C19-C20-C27	142.5(3)

Ligand Fold Angle

Using the bonding model that was described in Chapter 3 provides additional support for the proposed reduction of the diphenylacetylene ligand in compound **15**. In compound **15** an angle of 45° is formed between the plane defined by the W and two amide N atoms and the plane defined by the two amide N atoms and the phenylene ring (Figure 4-6). We suggested that the folding of the TMS_2pda ligand in this and other d^0 tungsten complexes arises because of π donation from the amide N atoms to the LUMO (d_{xy}) on the W center. In order to maximize the overlap of the N p_π and the W d_{xy} orbitals the ligand folds along the N-N vector. The structural data combined with the ^{13}C NMR spectrum suggests significant back bonding from the metal d_{xy} orbital to effectively reduce the diphenylacetylene ligand. Therefore, the diphenylacetylene behaves as a dianionic ligand and W(VI) best describes the oxidation state of the metal in compound **15**.

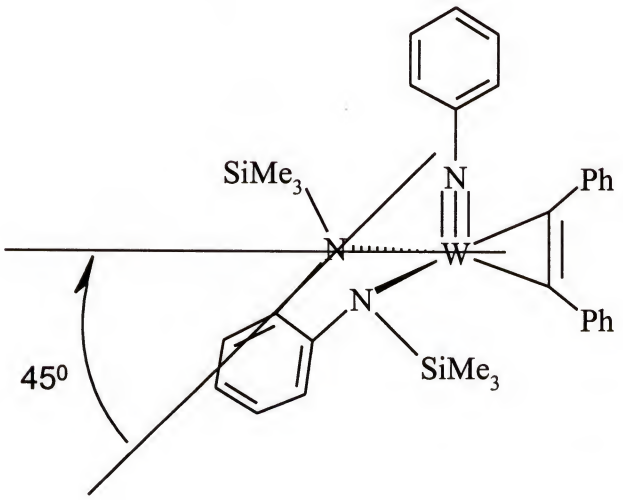

Figure 4-6. Pictorial representation of the ligand fold angle for **15**.

Hydrogenation Reactions

Preliminary results show that compound **15** is active towards the hydrogenation of alkynes and olefins. An NMR sample (C_6D_6) of [W(NPh)(o-$(Me_3SiN)_2C_6H_4$)(PhC≡CPh)] (**15**) after standing at room temperature under a positive pressure of H_2 (34 psi) for 10 hours displayed several new resonances. Among these new resonances were peaks between 4 and 5 ppm consistent with a π-coordinated arene group and two triplets (2.0, 2.21 ppm, bibenzyl CH_2 groups) corresponding to the W(IV)-bibenzyl complex [W(NPh)(o-$(Me_3SiN)_2C_6H_4$)(η^4-bibenzyl) (**16**) (Figure 4-7). The proton assignments for compound **16** were made by comparison with the analogous Mo(IV)-bibenzyl complex, which has been synthesized and fully characterized.[132] Unfortunately, isolation and characterization of **16** was hindered because the compound is unstable and readily decomposes.

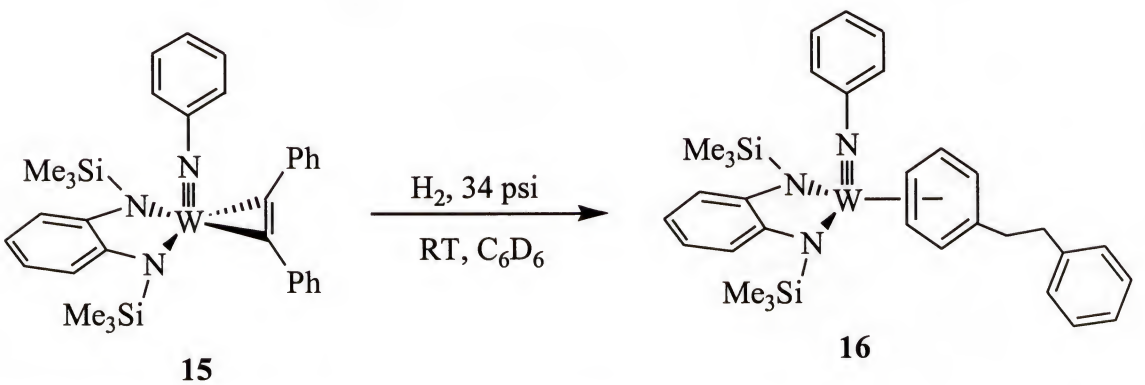

Figure 4-7. Synthesis of W(IV)-bibenzyl complex **16**.

Catalytic hydrogenation of diphenylacetylene and styrene has been achieved by exposing C_6D_6 solutions of **15** and diphenylacetylene or styrene to 1-2 atm of hydrogen. Catalytic conversion of styrene to ethylbenzene was observed at room temperature. After only 30 min, free ethylbenzene was present in the NMR spectrum. At this early stage of

the reaction, there is still bibenzyl complex, **16** present. After two hours compound **16** had disappeared and the W(IV)-ethylbenzene complex, **3** was observed in the ^{1}H NMR spectrum of the reaction mixture. We believe that since compound **3** is a more stable arene complex than **16**, once a sufficient amount of ethylbenzene is produced, compound **3** becomes the resting state of the catalyst.

This observation is not surprising considering the fact that W(NPh)[o-$(Me_3SiN)_2C_6H_4$](η^4-ethylbenzene) (**3**) has shown activity towards the hydrogenation of styrene, Chapter 1.[33] Under 1000 psi of hydrogen (50° C) compound **3** hydrogenates styrene at a rate of 40 turnovers per hour with total turnover numbers greater than 5000.

In the presence of excess diphenylacetylene, compound **15** is also a catalyst for the catalytic hydrogenation of diphenylacetylene (RT, 34 psi H_2). After 2 hours the reaction mixture contained free bibenzyl and compound **16**. Over extended periods of time decomposition products were also observed presumably due to the instability of **16**. Stilbene, the product of the first addition of H_2 to diphenylacetylene was never observed, suggesting that the addition of a second equivalent of H_2 is rapid in comparison to the formation of stilbene.

Synthesis and Characterization of W(IV)(butadiene) Complexes

In continuation of our investigation of the reactivity of the W(IV)L_2 complexes with unsaturated substrates, we found that W-diene complexes could be isolated from the reaction of compound **8** with butadienes. An equimolar toluene solution of W(NPh)(o-$(Me_3SiN)_2C_6H_4)(C_5H_5N)_2$ (**8**) and 2,3-dimethyl-1,3-butadiene was heated at 60° C for 20 hrs, during which time the solution became red-brown in color. Removal of the reaction solvent followed by pentane extraction gave the 2,3-dimethyl butadiene complex

W(NPh)[o-$(Me_3SiN)_2C_6H_4$][η^4-$(CH_2=C(CH_3)C(CH_3)=CH_2)$] (**17**) as an air and moisture sensitive dark brown solid in 73 % yield (Figure 4-8). Under significantly less forcing conditions (room temperature, 30 min), a toluene solution of W(NPh)(o-$(Me_3SiN)_2C_6H_4)(C_5H_5N)_2$ (**8**), when exposed to a positive pressure of 1,3-butadiene rapidly changes color. Removal of reaction solvent gave W(NPh)[o-$(Me_3SiN)_2C_6H_4$](η^4-$(CH_2=CHCH=CH_2)$ (**18**) in 93 % yield (Figure 4-8). Compound **18** is significantly less stable than **17**, and slowly decomposes at room temperature whereas **17** only decomposes at elevated temperatures.

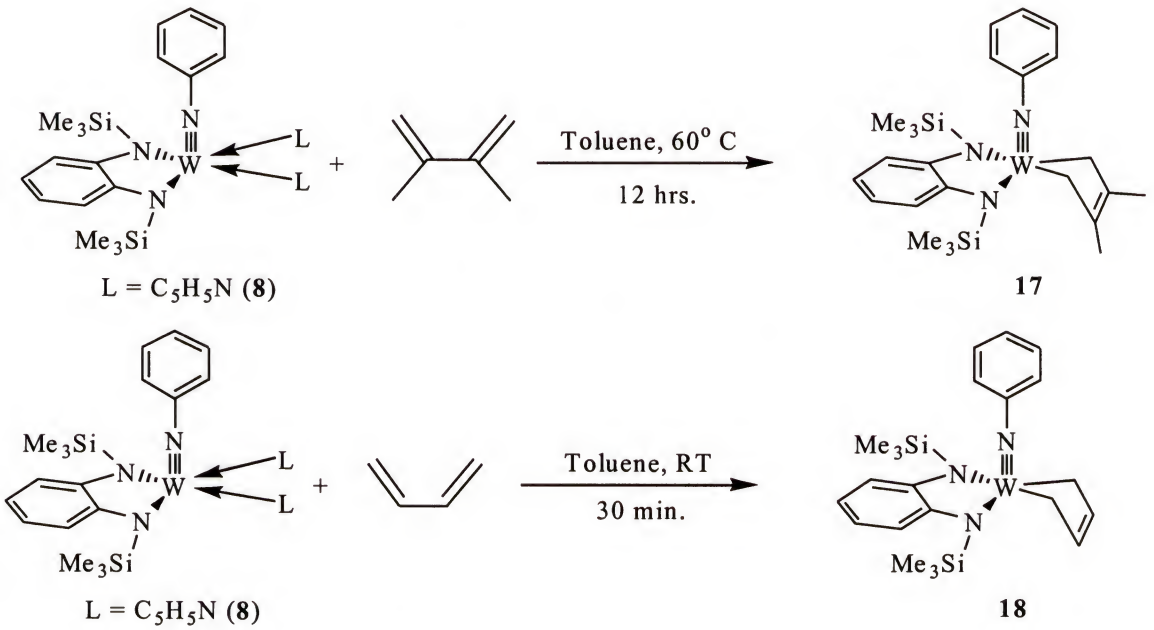

Figure 4-8. Synthesis of W-(butadiene) complexes **17** and **18**.

X-ray Structural Analysis of **17**

An X-ray diffraction analysis was performed on a single crystal of W(NPh)[o-$(Me_3SiN)_2C_6H_4$][η^4-$(CH_2=C(CH_3)C(CH_3)=CH_2)$ (**17**), grown from a concentrated pentane solution of **17**, which was left undisturbed at -40° C for one week. A summary

of selected bond lengths and angles for **17** is given in Table 4-3. Compound **17** adopts a distorted square pyramidal geometry about the W metal center with the imido group occupying the apical position and N2, N3, C19 and C22 forming the basal plane (Figure 4-9). The displacement of the W atom from the basal plane was calculated to be 0.73 Å. The W-N1(imido) (1.755(3) Å), W-N2(amido) (2.040(3) Å) and W-N3(amido) (2.045(3) Å) bond distances are all consistent with what has been previously observed for these types of bonds.[61-63]

The bond distances associated with the butadiene fragment are in good agreement for what has been determined for high-oxidation state group 4 and 5 butadiene complexes.[58,59,108,110,134,135] Specifically, the terminal C19-C20 (1.475(7) Å) and C21-C22 (1.472(7) Å) bond distances are significantly longer than the internal C20-C21 (1.375(7) Å) distance and the W-C19 and W-C22 (2.183(5), 2.178(5) Å) distances are shorter than that for W-C20 and W-C21 (2.460(4), 2.459(5) Å). This suggests that the interaction of the butadiene fragment with the W center is strongly distorted towards the $\sigma_2\pi$ bonding extreme for butadiene-metal complexes. In comparison to Cp_2Zr(2,3-dimethylbutadiene),[58] compound **17** displays a greater distortion towards this bonding extreme. The difference between the terminal and internal C-C bond lengths of a coordinated butadiene is commonly used as a tool to compare the extent of butadiene bonding in complexes with different metal centers. For example, in **17** the difference between the C19-C20 or C21-C22 bond and the C20-C21 bond is 0.10Å where that measured for Cp_2Zr(2,3-dimethylbutadiene) is 0.08 Å.

The fold angle of the phenylene-diamine ligand for compound **17** was observed to be 31° as described in Chapter 3. This angle is smaller than that which was calculated for the acetylene complex **15** (45°), suggesting a smaller amount of W(VI) character in **17,** but it is significantly larger than that for the purely W(IV) complex W(NPh)(o-$(Me_3SiN)_2C_6H_4)(C_6H_7N)_2$ (**9**) (5.3°). The difference in the amount of W(VI) character in **17** as compared to **15** is also evident in the bond lengths of the butadiene fragment, which is not as significantly reduced as the diphenylacetylene fragment in **15**.

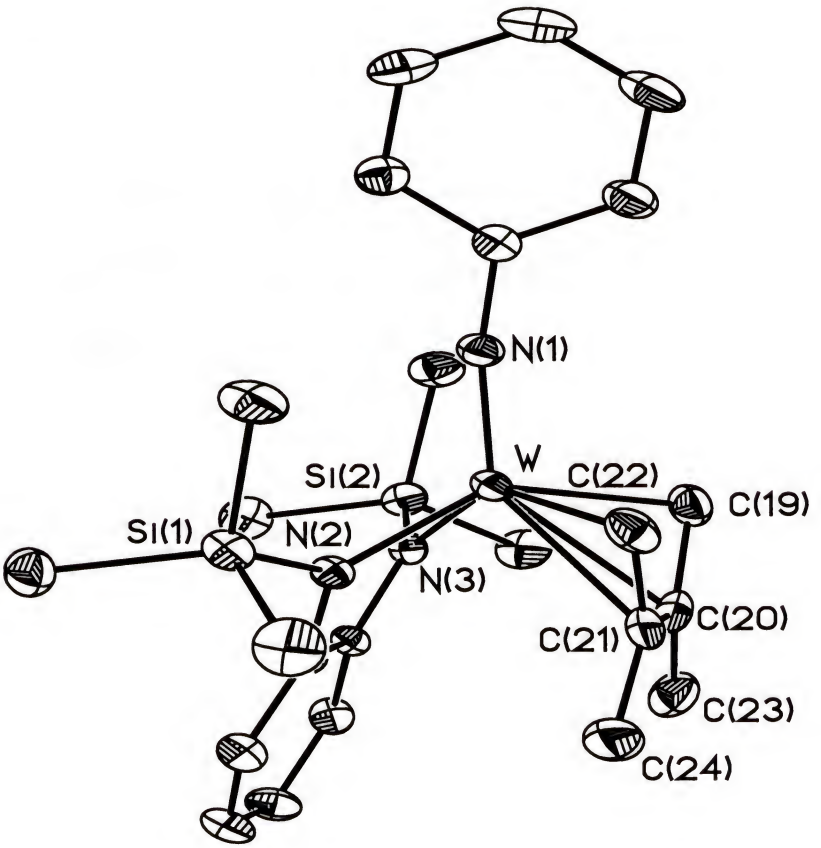

Figure 4-9. Molecular structure of W(NPh)[o-$(Me_3SiN)_2C_6H_4$][η^4-$(CH_2=C(CH_3)C(CH_3)=CH_2)$ (**17**). Thermal ellipsoids are drawn at 40 % probability and the hydrogen atoms have been removed for clarity.

Table 4-3. Summary of selected bond lengths (Å) and angles (deg) for **17**.

W-N1	1.755(3)	W-C22	2.178(5)	N2-W-C22	89.31(18)
W-N2	2.040(3)	C19-C20	1.475(7)	N3-W-C19	88.61(17)
W-N3	2.045(3)	C20-C21	1.375(7)	C19-W-C22	76.2(2)
W-C19	2.183(5)	C21-C22	1.472(7)	C21-C22-W	82.3(3)
W-C20	2.460(4)	C1-N1-W	169.3(3)	C20-C19-W	82.1(3)
W-C21	2.459(5)	N2-W-N3	78.77(13)		

NMR Spectroscopic Analysis of **17** and **18**

^{13}C and ^{1}H NMR parameters for **17** and **18** also revealed significant σ-bond character, consistent with other early-transition metal-diene complexes. When the spectra of $CpTaCl_2(C_4H_6)$,[59] $Cp_2Zr(C_4H_6)$,[58] $Cp_2Hf(C_4H_6)$,[114] and $Fe(CO)_3(C_4H_6)$[136] are compared, the magnitude of the ^{13}C-^{1}H coupling constants for the terminal carbons of the diene ligand increase from 145 to 170 Hz in the order Hf < Zr < Ta < Fe, indicating that the σ-bond character decreases in this order. The coupling constants of 143 and 149 Hz for compounds **17** and **18** are in agreement with the structural results for **17**, which suggest considerable σ-bond character of the terminal carbons. ^{1}H NMR parameters for these compounds also support the proposed structure. It has been observed that the magnitude of the vicinal coupling constant ($^{3}J_{H\text{-}H}$) varies by changing the metal.[58] For early-transition metal-butadiene complexes, the vicinal *cis* coupling constant is larger than the corresponding *trans* value. The order is reversed for late-transition metal complexes. For the W(1,3-butadiene) complex (**18**) the vicinal coupling constants were determined to be 5.1 Hz (*cis*) and 1.8 Hz (*trans*). The values of the geminal coupling constant ($J_{H\text{-}H'}$) for **17** (8.5 Hz) for the terminal CH_2 is between that determined for

$CpTaCl_2(C_4H_6)$ (6.5 Hz) and $Cp_2Zr(C_4H_6)$ (10 Hz) and considerably larger than that for $Fe(CO)_3(C_4H_6)$ (2.4 Hz).

Description of Fluxionality

Early-transition metal-diene complexes often display fluxional behavior in solution. An envelope flipping mechanism which proceeds through a planar metallacyclopentene transition state has been proposed to rationalize this behavior (Figure 4-10).[58,59,110] W-(diene) complexes **17** and **18** also exhibit dynamic behavior in solution as revealed by NMR spectroscopy.

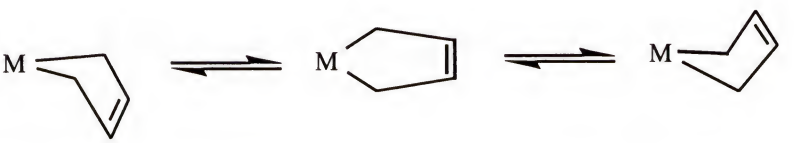

Figure 4-10. Envelope flipping mechanism for M-(butadiene) fluxionality.

Inspection of the room temperature ^1H NMR spectrum of $W(NPh)[o\text{-}(Me_3SiN)_2C_6H_4](\eta^4\text{-}(CH_2{=}CHCH{=}CH_2)$ (**18**) and comparison to the structure of $W(NPh)[o\text{-}(Me_3SiN)_2C_6H_4][\eta^4\text{-}(CH_2{=}C(CH_3)C(CH_3){=}CH_2)$ (**17**) as determined in the solid state (Figure 4-9) necessitates that some fluxional process be invoked to rationalize the observed spectroscopic properties. The room temperature ^1H NMR spectrum (C_6D_6) of **18** is shown in Figure 4-11. Besides the expected pattern for the imido and diamide aromatic protons, downfield, and the Me_3Si singlet at 0.37 ppm, the spectrum only contains one resonance, which is assigned to the butadiene β-CH protons (m, 4.59 ppm). The resonances corresponding to the α-CH_2 protons are broadened into the baseline (1.3-1.9 ppm). This determination was made using a ^1H COSY correlation experiment (Figure 4-11). Assuming a solid-state structure similar to that for compound **17** and no

fluxional processes are active, the spectrum should contain two multiplets for the α-CH_2 protons (H_{anti} and H_{syn}), in addition to the multiplet for the β-CH protons. For the W-(2,3-dimethylbutadiene) complex, **17** the expected pattern of two doublets for the α-CH_2 protons (H_{anti} and H_{syn}) are observed in addition to a singlet resonance for the CH_3 protons of the butadiene (Figure 4-12). These observations suggest that in solution at room temperature compound **18** is fluxional and **17** adopts the solid-state conformation.

Based on the results of several ^1H NMR experiments, including those that have already been mentioned and those presented in the following discussion, it was determined that a single fluxional process was insufficient in describing the room temperature behavior of **18**. Instead we propose that envelope flipping and diene rotation act in conjunction to produce the observed spectroscopic properties.

At -90° C the ^1H NMR spectrum of **18** displays two broad resonances, each integrating to two protons (1.0, 2.43 ppm), which correspond to the α-CH_2 protons (H_{anti} and H_{syn}) of the butadiene (Figure 4-13). The fact that at this temperature the syn and anti protons are inequivalent, but the corresponding resonances are still broadened suggests that the overall dynamic behavior of the molecule cannot be adequately explained by invoking only the envelope flip mechanism that is typical for early metal diene complexes.

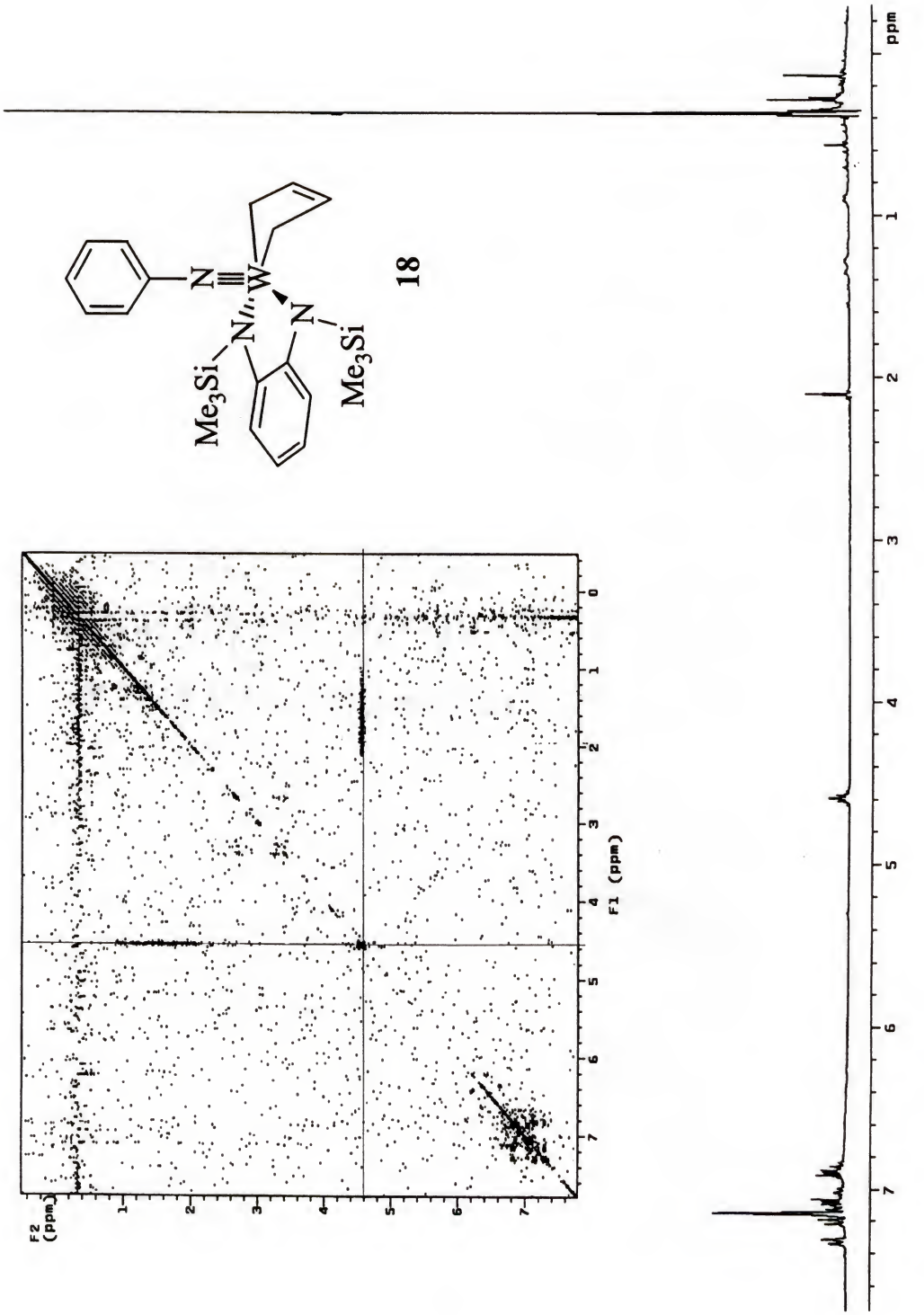

Figure 4-11. Room temperature ^{1}H NMR and ^{1}H COSY spectra of compound **18.**

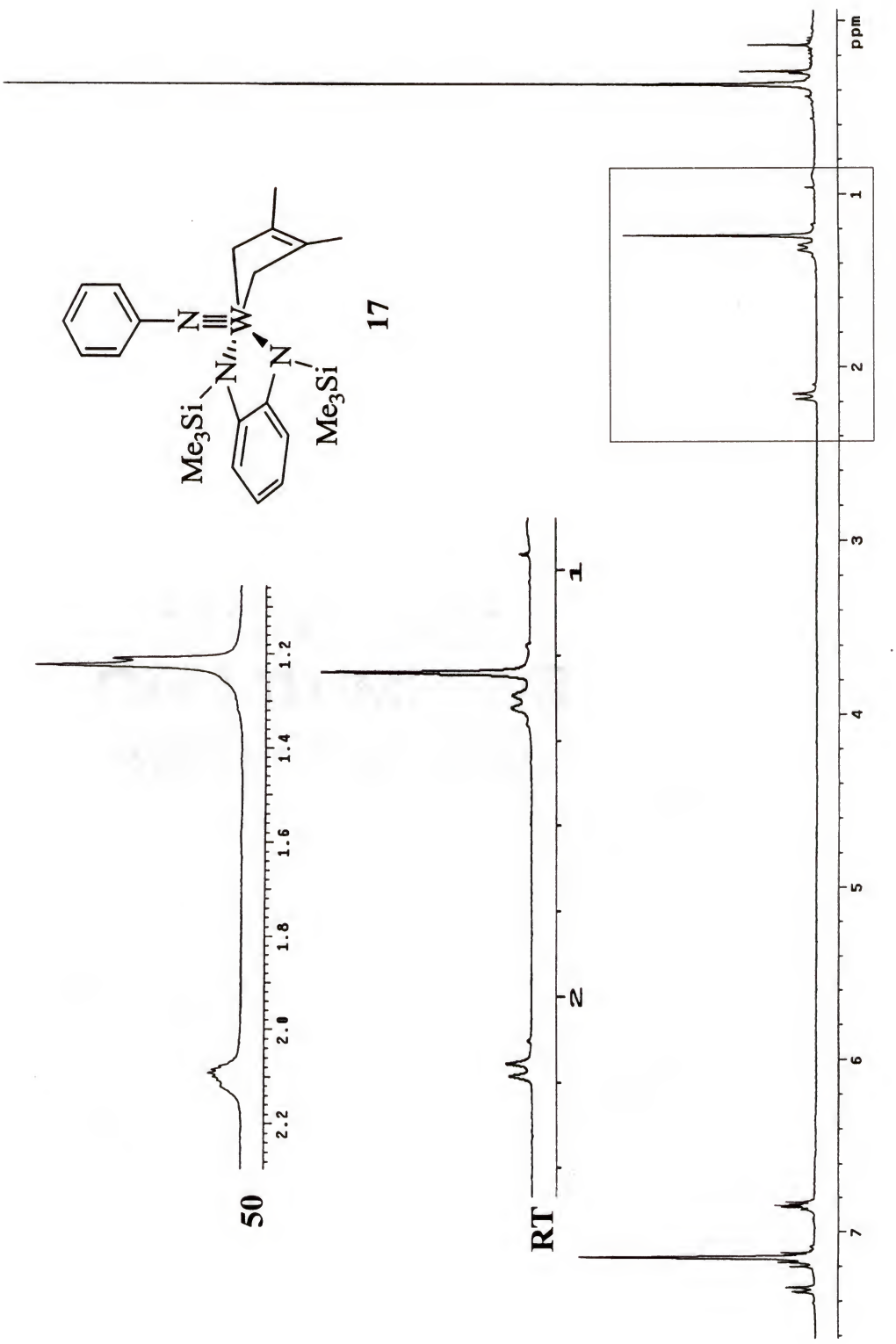

Figure 4-12. Room temperature and 50^0 C ^{1}H NMR spectra of compound **17.**

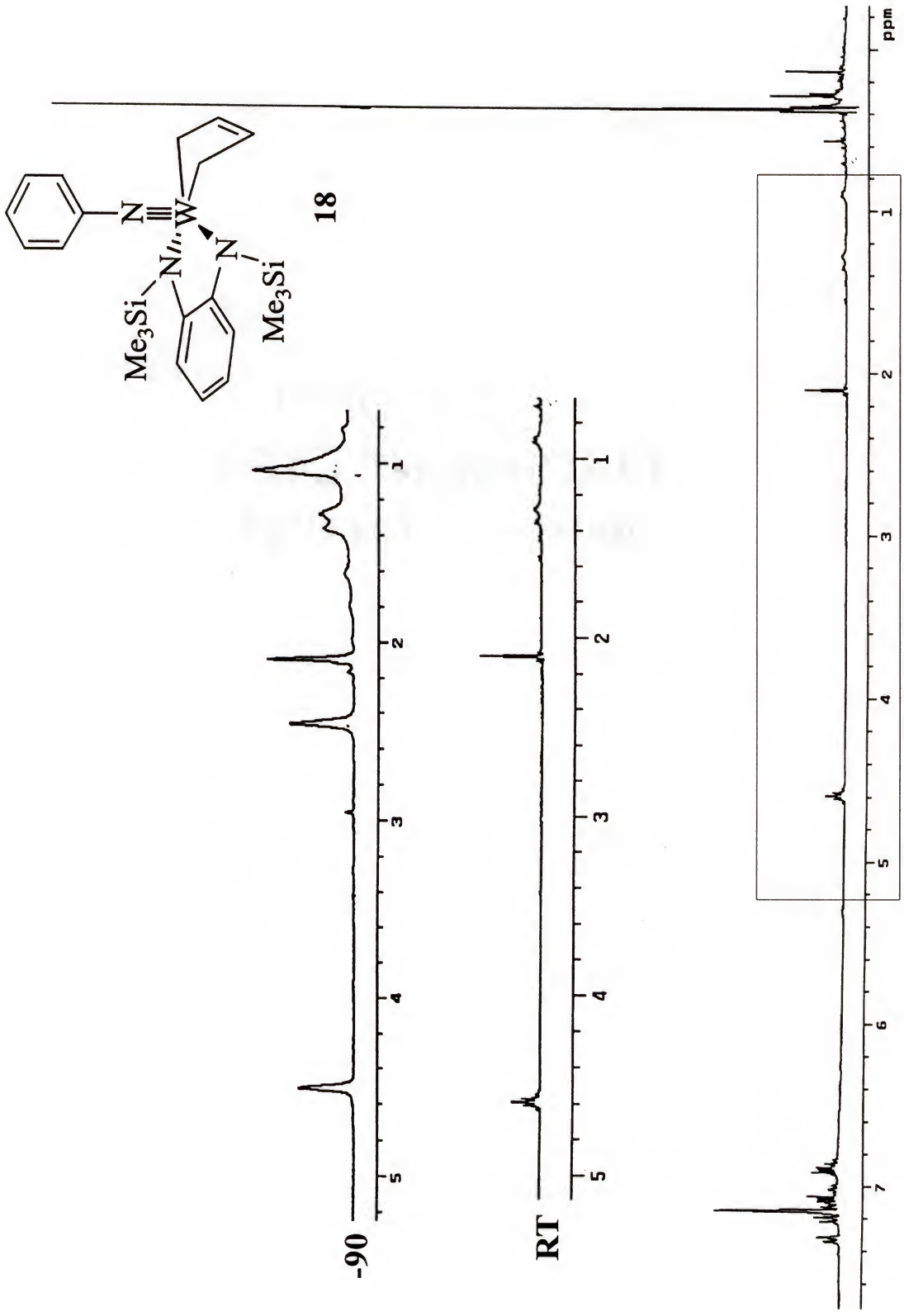

Figure 4-13. Variable temperature ^{1}H NMR spectra of compound **18.**

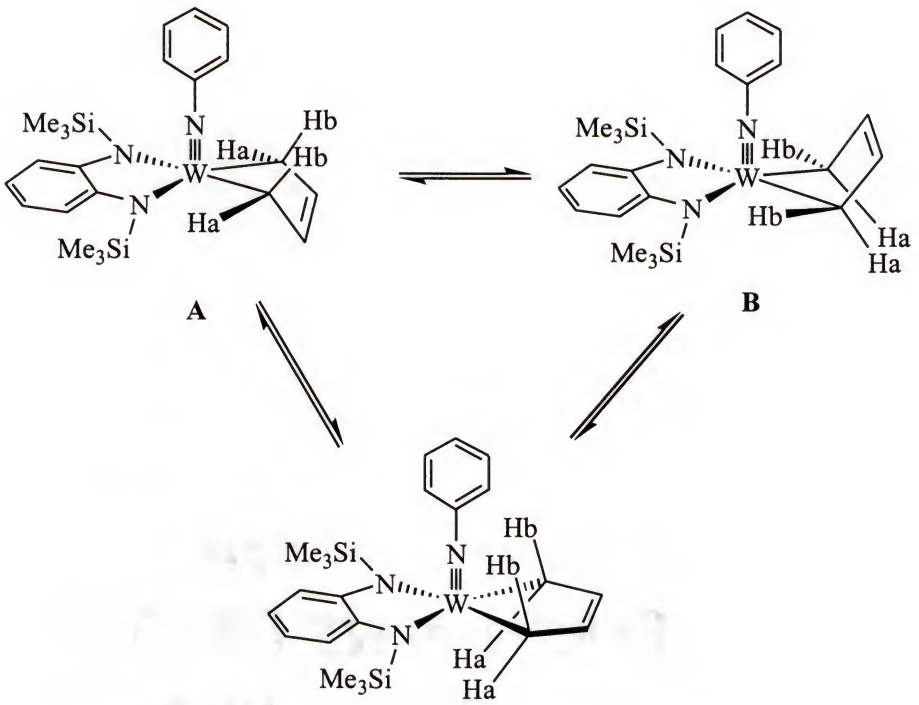

Figure 4-14. Envelope flipping mechanism to rationalize the fluxionality of **18** at low temperature.

Even though the envelope flip mechanism does not completely explain the fluxional behavior of **18**, we propose that this mechanism is one component of the observed fluxionality. At -90° C, the presence of two broad resonances for the α-CH_2 protons can be rationalized by invoking an envelope flip mechanism (Figure 4-14). This mechanism changes the proton environments of H_{syn} (Ha) and H_{anti} (Hb). However, since there is no symmetry element, which equilibrates the Ha and Hb protons in the two conformations (A and B, Figure 4-14), two resonances are observed. This inequivalence is a result of the molecule possessing two distinct faces, one on the side of the imido and the other opposite the imido group. As shown in Figure 4-14, in both conformation A and conformation B, Hb is on the imido face of the molecule and Ha is on the side *trans* to the imido group. Therefore, the observed spectrum at -90° C is an average of conformations A and B, resulting in a broadening of the α-CH_2 resonances.

At room temperature the α-CH_2 resonances are broadened into the baseline of the ^{1}H NMR spectrum suggesting that all of these protons are being exchanged slowly on the NMR timescale. As a result, at the high temperature limit (rapid exchange on the NMR timescale) only a single resonance (4 protons) should be present for the CH_2 protons. Analysis of this limit was hindered by the stability of the complex. At room temperature and above, compound **18** decomposes; therefore, elevated temperature NMR experiments were inconclusive.

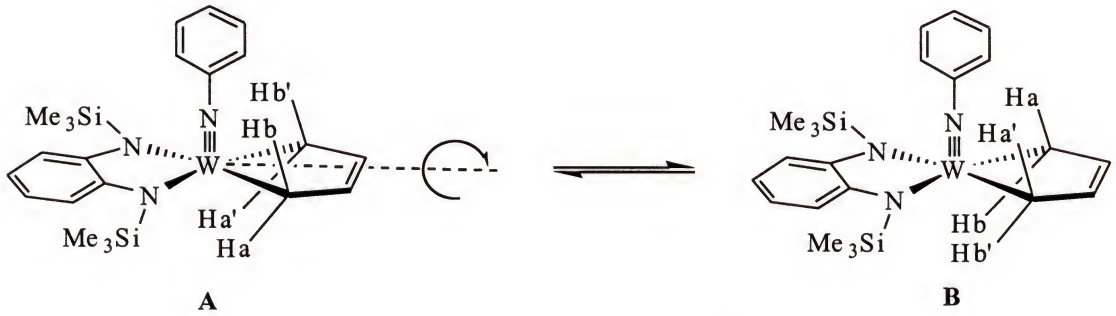

Figure 4-15. Butadiene rotation mechanism for **18**.

As stated above, there is not a symmetry element present which equilibrates the H_{syn} and H_{anti} protons through an envelope flipping mechanism. Therefore, another process must be active which equilibrates the protons on opposite faces of the molecule at room temperature. We propose that the simplest process, which accounts for the equilibration of these protons, is diene rotation (Figure 4-15). In the fast-exchange limit (not observed due to complex decomposition), diene rotation equilibrates all four α-CH_2 protons. Specifically, through rotation from conformation A to B (Figure 4-15), H_{up} (Hb) on one terminal butadiene carbon is exchanged with H_{down} (Ha') of the other terminal carbon and H_{down} (Hb') is exchanged with H_{up} (Ha) of the other terminal carbon. If the high temperature limited could be attained, this process would be fast on the NMR

timescale and all four CH_2 protons would be equivalent and resonate as a single peak. Therefore, to explain the observed spectroscopic properties, we propose that at or below -90° C only the envelope flipping mechanism is active and above this temperature both fluxional processes are active.

The 2,3-dimethylbutadiene complex **17** displays no fluxionality at room temperature and the ^1H NMR spectrum is consistent with the solid-state structure. At elevated temperature (50° C) the ^1H NMR spectrum of **17** displays broad resonances for the α-CH_2 protons similar to that observed for compound **18** at -90° C and consistent with the envelope flipping mechanism (Figure 4-12). Compound **17** begins to decompose at temperatures above 50° C, therefore, the temperature at which the diene rotation mechanism becomes active was not determined. This drastic difference in the activation energy associated with the diene fluxionality in compounds **17** and **18** was surprising considering the only difference between these complexes is the substituants at the 2 and 3 positions of the butadiene (CH_3 (**17**), H (**18**)).

Acetone Insertion

Butadiene complexes of early-transition metals are known to offer enhanced reactivity, reflecting their polar metal-carbon bonds and therefore have found interesting applications in organic synthesis. One area of interest lies in the regioselective insertion of unsaturated compounds such as carbonyls to give functionalized metallacyclic species, where the metallacycle has been expanded to a seven-membered ring.[111,114,117,118,137-139] Since X-ray structural analysis has shown that the W-2,3-dimethylbutadiene complex **17** exhibits substantial alkyl-metal character, it was tempting to consider the coupling of 2,3-

dimethylbutadiene with ketones at the W(NPh)[o-$(Me_3SiN)_2C_6H_4$] fragment as being a further example of this type of chemistry.

When one equivalent of acetone was added to a toluene solution of W(NPh)[o-$(Me_3SiN)_2C_6H_4$][η^4-$(CH_2=C(CH_3)C(CH_3)=CH_2)$ (**17**) at room temperature, a slow color change from brown to red was observed. After stirring at ambient temperature for 5 hours the reaction solvent was removed and the resulting red-brown solid was washed with several portions of cold (0° C) pentane. Subsequent drying of the remaining solid *in vacuo* gave the 1:1 addition product W[$OC(CH_3)_2CH_2C(CH_3)C(CH_3)CH_2$](NPh)[o-$(Me_3SiN)_2C_6H_4$] (**19**) (Figure 4-16).

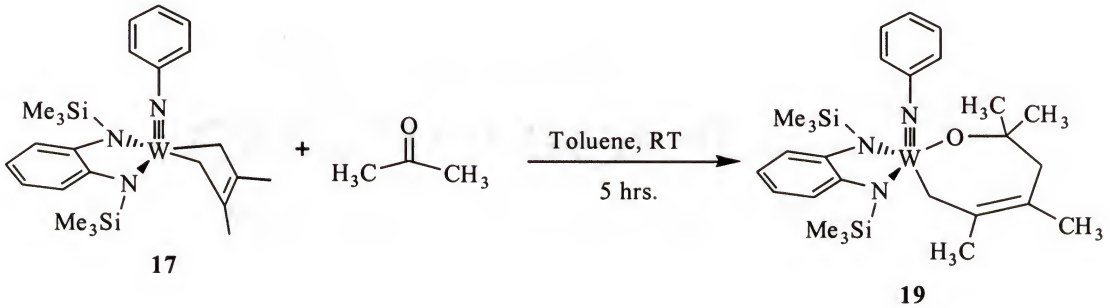

Figure 4-16. Synthesis of compound **19**.

An X-ray diffraction analysis was performed on a single crystal of W[$OC(CH_3)_2CH_2C(CH_3)C(CH_3)CH_2$](NPh)[o-$(Me_3SiN)_2C_6H_4$] (**19**), grown from a concentrated pentane solution of **19**, which was left undisturbed at -40° C for one week. A summary of selected bond lengths and angles for **19** are presented in Table 4-4. Compound **19** adopts a distorted square pyramidal geometry about the W metal center with the imido group occupying the apical position and N2, N3, C19 and O1 forming the basal plane (Figure 4-17). The W atom is displaced 0.60 Å above the basal plane. The W-N1(imido) (1.744(3) Å), W-N2(amido) (2.034(3) Å) and W-N3(amido) (2.030(3) Å)

bond distances are all consistent with what has been previously observed for W(VI) complexes.[61-63] Compound **19** exhibits an envelope-shaped core of atoms that is typical for many early-transition metal seven-membered ring systems.[117,140] To a first approximation, the atoms C19, W, O1, C23, C22 are almost coplanarly arranged. A second plane is comprised of the atoms C19, C20, C21, C22, which originate from the butadiene building block. These two planes are arranged relative to each other at an angle of *ca.* 50°. The bond lengths of the metallacyclic framework of complex **19** are within the expected ranges (Table 4-4).

The room temperature ^{1}H NMR spectrum of **19** is consistent with the solid-state structure. In addition to the expected resonances for the diamide and imido aromatic protons (downfield), two singlet resonances are observed (0.48 and 0.38 ppm), which correspond to the inequivalent Me_3Si groups. The ring protons of the seven-membered oxametallacycloheptane fragment appear as four doublets at 1.24 and 1.83 ppm (γ-CH_2) and 2.54 and 3.02 ppm (α-CH_2). Four singlet resonances, two for the butadiene CH_3 protons (1.19, 1.28 ppm) and two corresponding to the acetone CH_3 protons (1.59, 1.67 ppm) complete the spectral assignment.

Reaction of the 1,3-butadiene complex, W(NPh)[o-$(Me_3SiN)_2C_6H_4$](η^4-(CH_2=CHCH=CH_2) (**18**) with acetone under similar conditions led to the formation of a complex mixture of products that has not been fully characterized. The observed difference in reactivity of **17** and **18** with acetone was not completely unexpected. As was explained earlier, these complexes displayed very different properties in solution that could in part account for the dissimilar results observed in the reaction with acetone.

Currently we are working to determine the exact cause of this difference as well as expanding this chemistry to include other carbonyl compounds.

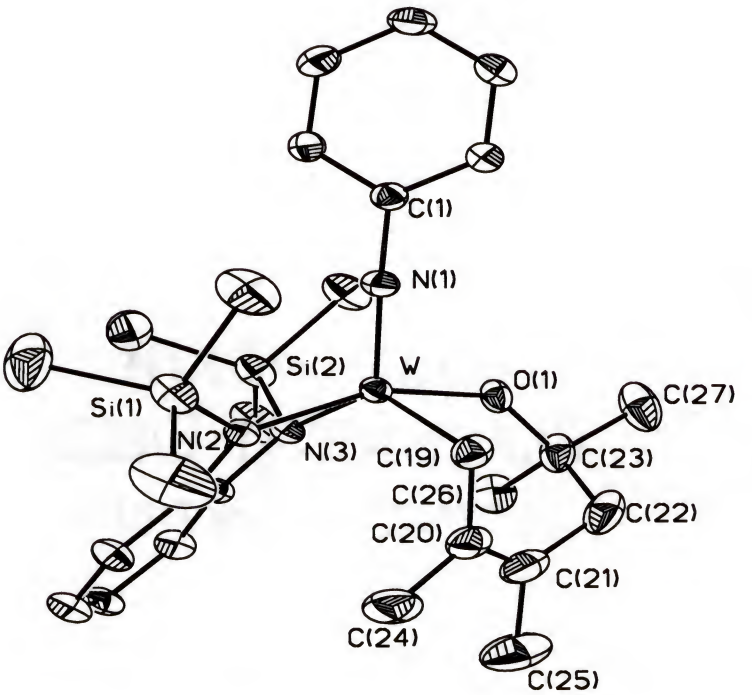

Figure 4-17. Molecular structure of $W[OC(CH_3)_2CH_2C(CH_3)C(CH_3)CH_2](NPh)[o\text{-}(Me_3SiN)_2C_6H_4]$ (**19**). Thermal ellipsoids are drawn at 40 % probability and the hydrogen atoms have been removed for clarity.

Table 4-4. Summary of bond lengths (Å) and angles (deg) for **19**.

W-N1	1.744(3)	O1-C23	1.431(5)	W-N1-C1	169.0(3)
W-N2	2.034(3)	C19-C20	1.502(6)	N2-W-N3	78.68(12)
W-N3	2.030(3)	C20-C21	1.336(7)	O1-W-C19	86.72(15)
W-O1	1.895(3)	C21-C22	1.510(8)	W-O1-C23	140.9(3)
W-C19	2.160(4)	C22-C23	1.536(8)	W-C19-C20	100.8(3)

Reactions of $W(IV)L_2$ with Olefins

Based on the reactivity of the $W(IV)L_2$ complexes with acetylene and butadiene, we became interested in the chemistry of these complexes in the presence of olefins. When a Young's ampoule containing a toluene solution of either $W(NPh)(o\text{-}(Me_3SiN)_2C_6H_4)(C_5H_5N)_2$ (**8**) or $W(NPh)(o\text{-}(Me_3SiN)_2C_6H_4)(C_6H_7N)_2$ (**9**) was exposed to a positive pressure of ethylene, an immediate color change from purple to orange-brown was observed. Upon mixing for 30 minutes, the solution became yellow brown in color. Removal of the reaction solvent followed by pentane extraction gave the metallacyclopentane complex $W(CH_2CH_2CH_2CH_2)(NPh)[o\text{-}(Me_3SiN)_2C_6H_4]$ (**20**) as a yellow-brown solid in 70% yield (Figure 4-18). Compound **20** has been previously prepared and characterized in our lab using several other synthetic schemes.[32]

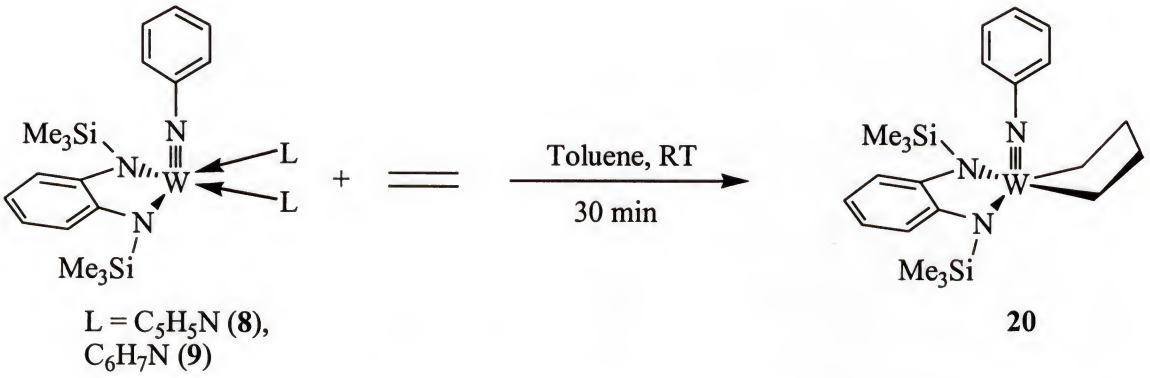

Figure 4-18. Synthesis of W-metallacyclopentane.

The oxidative coupling reaction of ethylene with the $W(IV)L_2$ described above is not substrate selective. Analogous reactions of $W(NPh)(o\text{-}(Me_3SiN)_2C_6H_4)(C_5H_5N)_2$ (**8**) with other olefinic substrates (propylene, 1-butene, 1-pentene, 1-hexene, styrene, cyclohexene) yielded metallacyclic species. Full characterization of the products from

these reactions was hindered by the complexity of the room temperature ^{1}H NMR spectra. For compound **20** all of the metallacycle substituants are hydrogens, therefore, the ^{1}H NMR spectrum is relatively simple. When other substituents are introduced the number of possible products is increased. Based on the orientation of the incoming olefins, α–α, α–β and β–β substitution patterns are possible for the product metallacycle (Figure 4-19). Due to the square pyramidal geometry of the metallacyclopentane complexes the substituants on the top face of the metallacycle are inequivalent to those on the opposite face. This serves to increase the complexity of the product mixture because the R groups can orient themselves either *syn* or *anti* to the imido group.

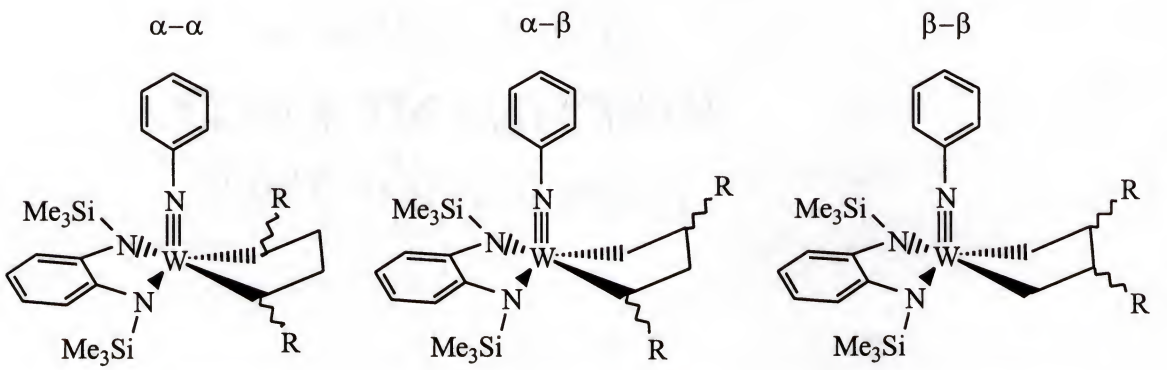

Figure 4-19. Possible products of oxidative coupling for olefins other than ethylene.

Mechanism for Oxidative Coupling

Initial Olefin Coordination

To generate a plausible mechanism for the observed oxidative coupling of alkenes by the W(IV)L_2 complexes we must first revisit the substitution chemistry presented in Chapter 3. It was found that the W(IV)L_2 complexes **8** and **9** rapidly incorporate an additional ligand to generate six coordinate octahedral complexes. With this knowledge in hand, it was proposed that the initial step in the oxidative coupling reactions involves

coordination of alkene to yield an octahedral complex similar to the complexes $[W(NPh)(o\text{-}(Me_3SiN)_2C_6H_4)(C_5H_5N)_2(CO)]$ (**12a**) and $[W(NPh)(o\text{-}(Me_3SiN)_2C_6H_4)(C_6H_7N)_2(CO)]$ (**12b**). To test this theory we undertook the task of synthesizing a $W(IV)L_2$(olefin) complex.

Due to the greater donor ability of 4-picoline with respect to pyridine the rate of the oxidative coupling reaction is slower for $W(NPh)(o\text{-}(Me_3SiN)_2C_6H_4)(C_6H_7N)_2$ (**9**). This is expressed in the way of slightly longer reaction times for the formation of metallacycles from compound **9** as compared to **8**. Therefore, it was proposed that an octahedral olefin complex generated from compound **9** would be longer lived than the analogous complex generated from **8** which could possibly allow its characterization. In a Young's ampoule compound **9** was dissolved in toluene and cooled to -78° C. The solution was exposed to a positive pressure of ethylene and an immediate color change was observed. Evacuation of the ampoule to remove the excess ethylene, followed by solvent removal allowed the isolation of the six-coordinate olefin complex $[W(NPh)(o\text{-}(Me_3SiN)_2C_6H_4)(C_5H_5N)_2(\eta^2\text{-ethylene})]$ (**21**) (Figure 4-20).

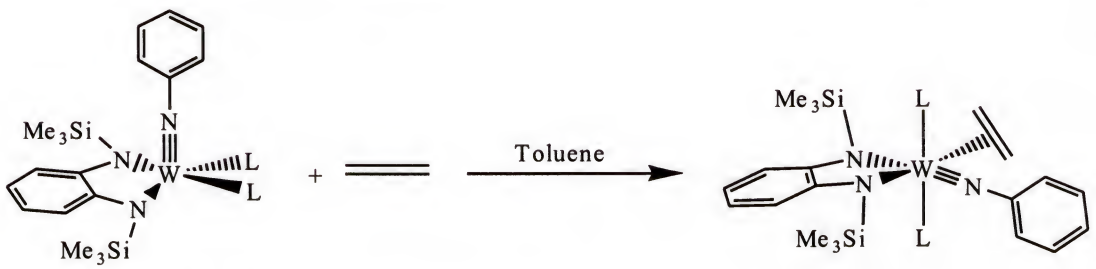

L = C_6H_7N (**9**) **21**

Figure 4-20. Synthesis of $W(IV)L_2$(ethylene) complex **21**.

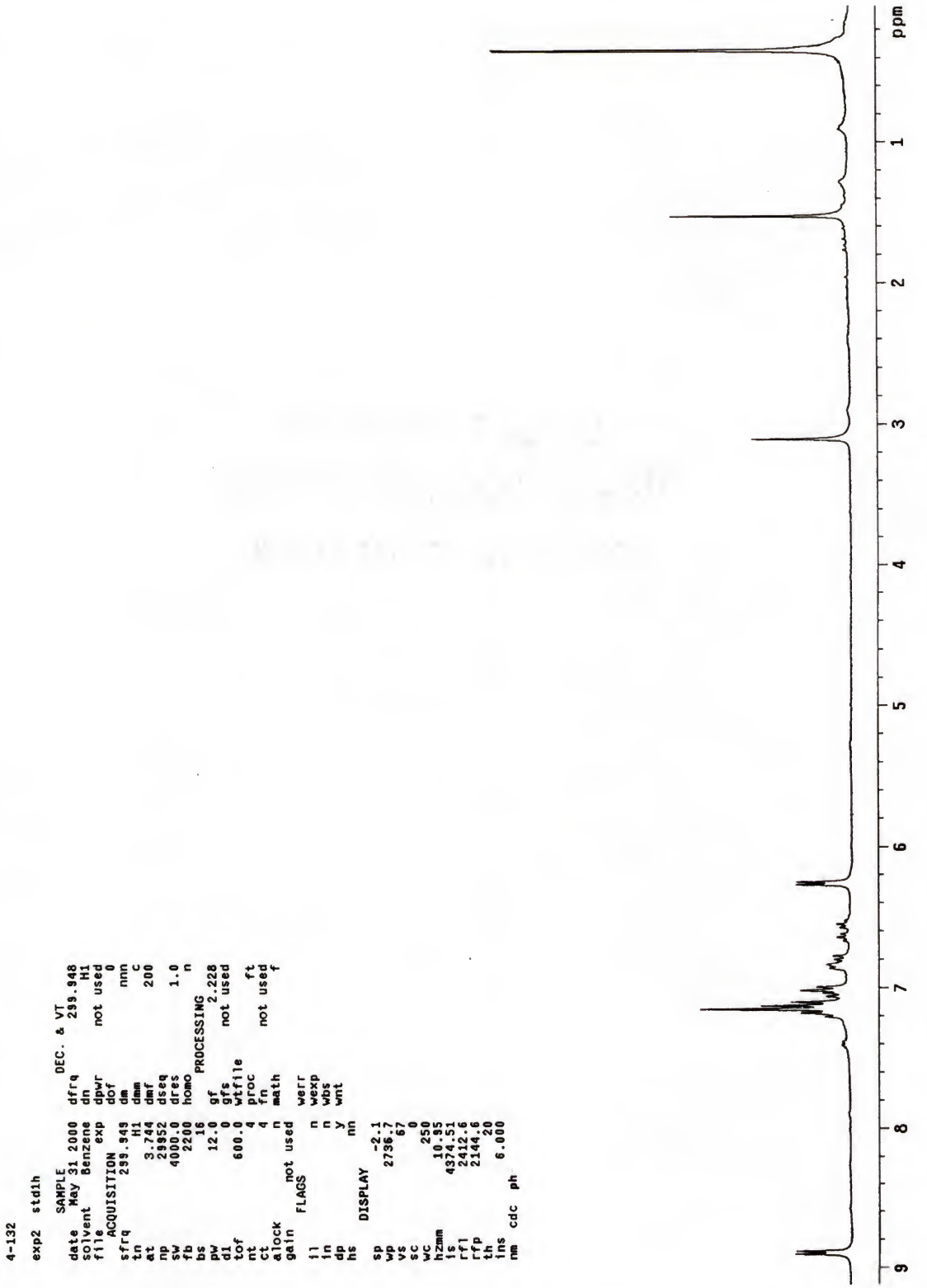

Figure 4-21. Room temperature ^{1}H NMR spectrum of compound **21.**

The room temperature ^{1}H NMR spectrum of **21** displays two resonances (0.34, 0.35 ppm) corresponding to inequivalent $SiMe_3$ groups, consistent with the $NSiMe_3$ groups being *cis* and *trans* to the imido ligand, and a singlet resonance (1.50 ppm) for the *para*-methyl groups of the 4-picoline ligands. The picoline *meta* and *ortho* protons resonate as doublets at 6.26 and 8.89 ppm respectively (Figure 4-21). This pattern of resonances for the 4-picoline and $NSiMe_3$ groups are consistent with that observed for $[W(NPh)(o\text{-}(Me_3SiN)_2C_6H_4)(C_6H_7N)_2(CO)]$ (**12b**) and places the ethylene group *trans* to amide. Consistent with a rapidly rotating ethylene group, the ethylene protons resonate as a singlet at 3.10 ppm. In the ^{13}C NMR spectrum the ethylene group resonates at 61.32 ppm.

Analogous reactions of $W(NPh)(o\text{-}(Me_3SiN)_2C_6H_4)(C_6H_7N)_2$ (**9**) with other olefins (propylene, 1-butene, 1-pentene, 1-hexene, styrene, cyclohexene) gave ^{1}H NMR spectra with similar resonances for 4-picoline and the Me_3Si groups as that observed for **12b** and **21**. Although none of these complexes were successfully isolated, the spectral data supports initial coordination of these olefins, giving six-coordinate complexes similar to **21**, prior to oxidative coupling with another molecule of olefin.

Ligand Displacement and Oxidative Coupling

As was the case for the proposed first step in the oxidative coupling reaction (olefin coordination), it is useful to revisit the ligand substitution chemistry of compounds **8** and **9** in order to understand the remainder of the coupling mechanism. It was observed that one of the pyridine or 4-picoline ligands of $[W(NPh)(o\text{-}(Me_3SiN)_2C_6H_4)(C_5H_5N)_2(CO)]$ (**12a**) or $[W(NPh)(o\text{-}(Me_3SiN)_2C_6H_4)(C_6H_7N)_2(CO)]$ (**12b**) could be readily displaced by another donor ligand such as PMe_3, suggesting

lability of these ligands in the six-coordinate complexes. Since the six-coordinate olefin complexes are coordinatively saturated, this lability is necessary in order to incorporate another olefin molecule into the coordination sphere to allow for oxidative coupling. In addition, through the reaction of the $W(IV)L_2$ complexes with two equivalents of PMe_3, we have demonstrated that the addition of two ligands to compounds **8** or **9** is possible and that the new ligands adopt a *cis* orientation. This is in agreement with the oxidative coupling of olefins, which requires a *cis* orientation of the olefin molecules to facilitate this reaction.[3] Based on these observations, we propose that the oxidative coupling of olefin with the $W(IV)L_2$ complexes follows a mechanism similar to that shown in Figure 4-22.

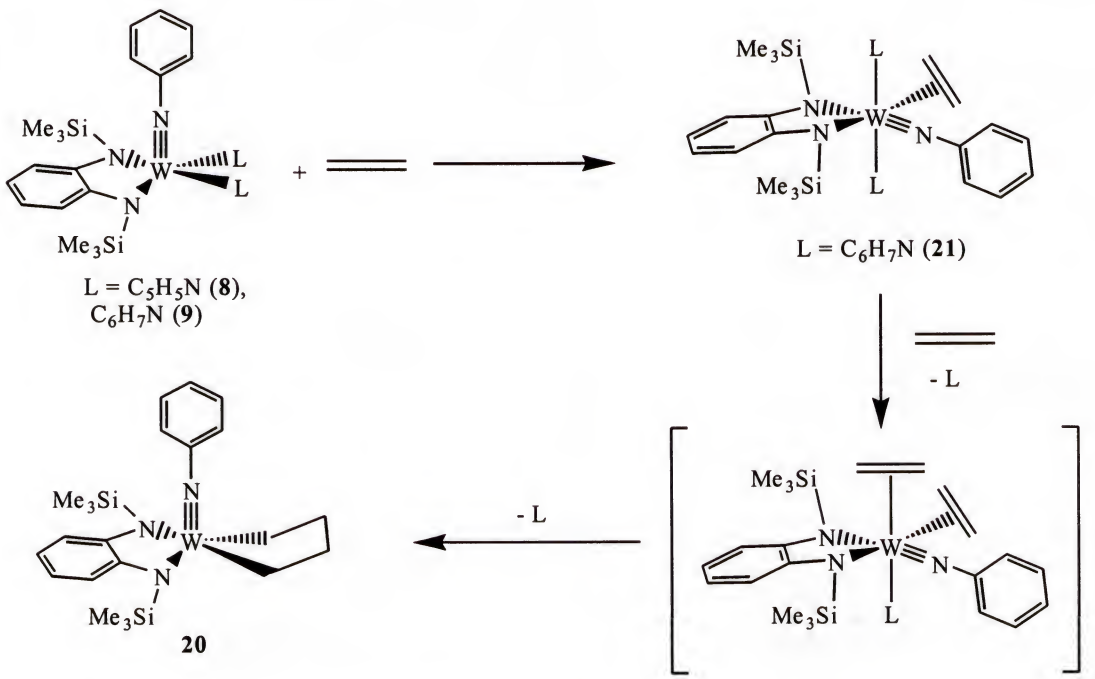

Figure 4-22. Proposed mechanism for the oxidative coupling of olefins.

Conclusions

The ligand substitution reactivity presented in Chapter 3 prompted us to examine the reactivity of the W(IV)L_2 complexes with unsaturated substrates. In this chapter the reactions of the complexes, W(NPh)(o-$(Me_3SiN)_2C_6H_4$)$(C_5H_5N)_2$ (**8**) and W(NPh)(o-$(Me_3SiN)_2C_6H_4$)$(C_6H_7N)_2$ (**9**) with diphenylacetylene, butadienes and olefins was discussed. For the reaction with diphenylacetylene and butadienes, the monomeric acetylene [W(NPh)(o-$(Me_3SiN)_2C_6H_4$)(PhC≡CPh)] (**15**) and butadiene W(NPh)[o-$(Me_3SiN)_2C_6H_4$][η^4-$(CH_2=C(CH_3)C(CH_3)=CH_2)$ (**17**) and W(NPh)[o-$(Me_3SiN)_2C_6H_4$](η^4-$(CH_2=CHCH=CH_2)$ (**18**) complexes were isolated. Structural and spectroscopic studies revealed that the unsaturated ligands in these complexes were reduced upon coordination to the metal center. The reduction of the incoming ligands was also evident in the fold angle of the diamide ligand, which was significantly larger (30-45°) than that for the W(IV)L_2 compound (**9**) (5.3°) suggesting the oxidation state of the W center in compounds **15**, **17** and **18** is best described as W(VI). In regard to the subsequent chemistry of these complexes, we have only scratched the surface and believe that the chemistry of these complexes will be very rich. With olefins, compounds **8** and **9** facilitate the oxidative coupling of two olefin molecules to generate metallacyclopentane complexes, of which the most basic derivative, compound **20** was isolated and fully characterized. The overall reactivity discussed in this chapter not only demonstrates the reactive nature of the W(IV)L_2 complexes, but also the propensity of these complexes to reduce incoming substrates whereby generating W(VI) metal complexes. The following chapters discuss chemistry that was developed using the knowledge gained from the experiments presented here and in Chapter 3.

CHAPTER 5
CARBON-SULFUR BOND ACTIVATION OF THIOPHENES BY W(NPh)[o-$(Me_3SiN)_2C_6H_4$](PYRIDINE)$_2$

Introduction

Hydrodesulfurization (HDS), the process by which sulfur is removed from petroleum feedstocks, represents one of the largest-scale industrial processes that utilizes transition metal catalysts. This process is of prime importance to the petroleum industry because of the growing need to process feedstocks of high sulfur content (1-4%) with the aim of producing fuels with the smallest possible sulfur content. The presence of sulfur in petroleum feedstocks causes two major problems, first, sulfur containing compounds can contaminate precious metal catalysts used later in the refining process and secondly, the combustion of fuels containing sulfur generates hazardous emissions. On an industrial scale, the HDS process involves treatment of crude oil with a high pressure of hydrogen gas (up to 200 atm) in the presence of an alumina-supported catalyst, typically Mo/Co, at elevated temperatures (300-450° C), Figure 5.1.[141-145]

$$\text{"R-S"} + H_2 \xrightarrow[H_2,\ 200\ \text{atm}]{\text{catalyst, 300-450}^\circ\text{ C}} \text{R-H} + H_2S$$

Catalyst = MoS_2 and Co_9S_8

Figure 5.1. Industrial process for the hydrdesulfurization of petroleum feedstocks.

Of the sulfur containing impurities present in petroleum feedstocks, thiophene, benzothiophene, dibenzothiophene and their derivatives are among the most difficult compounds to desulfurize. To improve the efficiency of the HDS process, a better understanding of the interaction of thiophenes with transition metal complexes is necessary. As a result, homogeneous modeling of HDS has become an active area of research, especially during the past decade.[144]

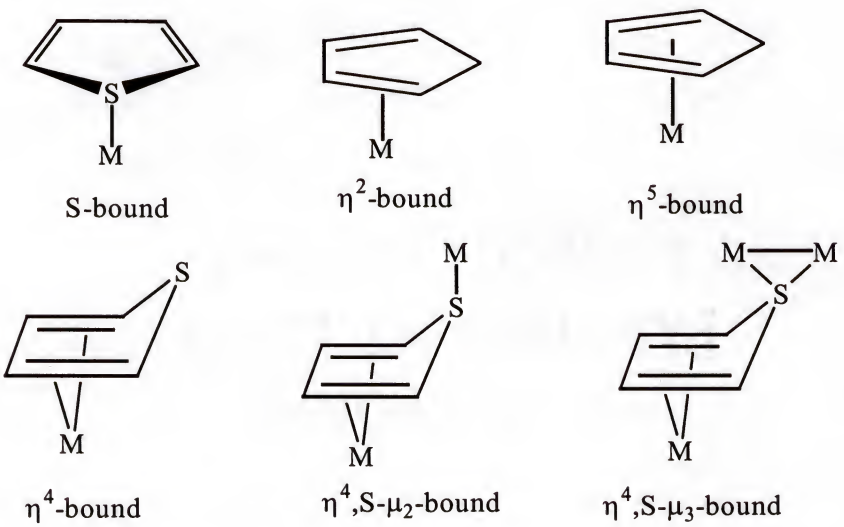

Figure 5-2. Coordination modes of thiophenes.

Many research groups have studied the coordination and activation of thiophenes by transition metals, which are believed to be the initial steps in the HDS process. A significant number of thiophene complexes have been prepared and studied where thiophene is coordinated in a variety of modes, including η^1(S)-coordinated, η^2, η^4 and η^5 (Figure 5-2).[145-148] In addition, several metal complexes have been found to promote direct C-S bond activation of thiophenes.[149] These studies, however, have focused on complexes of Mn, Fe, Co, Ni, Rh, Ru and Ir. From these studies have come significant advances in the modeling of HDS. For example, Bianchini[150] reported the first example

of catalytic HDS of dibenzothiophene (DBT) in the homogeneous phase. This report described the C-S bond activation of DBT by the (triphos)IrH fragment to give (triphos)IrH(η^2-C,S-DBT). By treating this complex with H_2, Bianchini was able to facilitate the HDS of dibenzothiophene to yield 2-phenylthiophenol, biphenyl and H_2S. Surprisingly, thiophene complexes of Group 6 metals (Mo and W), an integral component of an industrial HDS catalysts, have been almost nonexistent.

Low valent Mo and W-DBT complexes have been prepared through the photolysis of $Mo(CO)_6$ or $W(CO)_6$ in the presence of DBT. However, Parkin's[151] recent report of thiophene and benzothiophene C-S bond activation by the molybdocene complexes $[Me_2Si(C_5Me_4)_2]MoH_2$ and $[Me_2Si(C_5Me_4)_2]Mo(Ph)H$ (Figure 5-3), represents the first homogeneous example of such chemistry with molybdenum. The analogous Cp_2WH_2 system has also been shown to facilitate the C-S bond activation of thiophene (Figure 5-3).[152] Unfortunately these complexes also facilitate C-H bond activation of thiophenes as a competing process in these reactions.

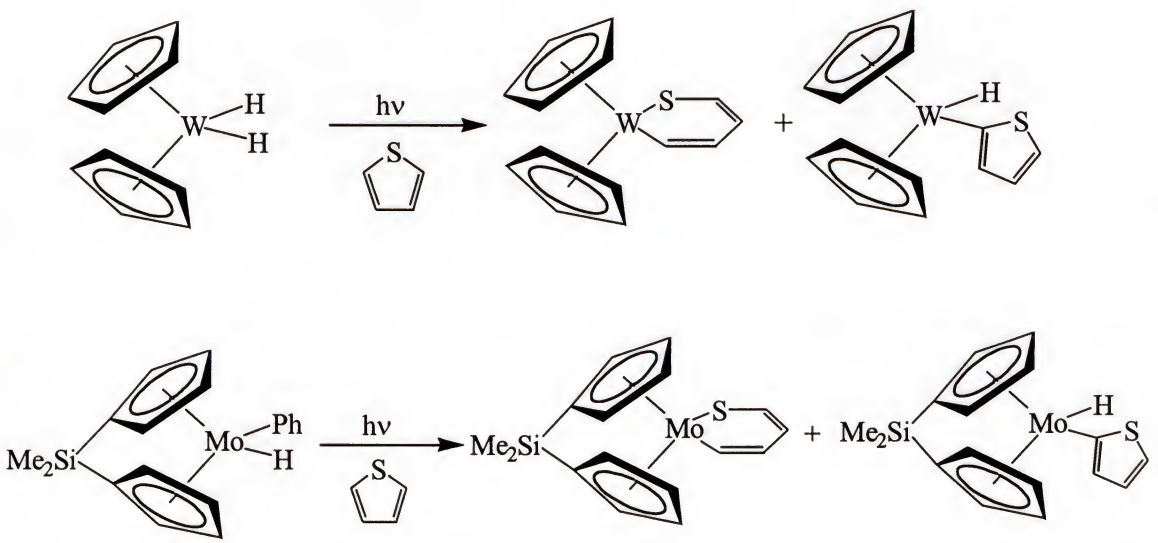

Figure 5-3. Tungsten and molybdenum promoted C-S bond activation.

In Chapter 3, the preparation of the coordinatively unsaturated W(NPh)[o-$(Me_3SiN)_2C_6H_4$]L_2 (L = pyridine (**8**), 4-picoline (**9**) or quinoline (**10**)) complexes was presented.[76] Subsequent investigation of ligand substitution chemistry of the W(IV)L_2 complexes with unsaturated substrates (Chapter 4) has demonstrated the propensity of the W metal center to reduce the unsaturated ligand upon coordination, thereby increasing the W(VI) character of the resulting compounds. The oxidative coupling of olefins to give W(VI)-metallacyclopentane complexes also demonstrates the ability of the W(IV) metal center to reduce unsaturated substrates. These results have prompted us to examine the activity of these W(IV)L_2 complexes towards substrate oxidative addition, more specifically the activation of the C-S bonds of thiophene and its derivatives.

C-S Bond Activation Reactions

Thiophene C-S Activation

Thermolysis (65° C, 8-12 hrs.) of a toluene solution containing [W(NPh)(o-$(Me_3SiN)_2C_6H_4$)$(C_5H_5N)_2$] (**8**) and 2 equivalents of thiophene afforded the carbon-sulfur bond activation product [(o-$(Me_3SiN)_2C_6H_4$)(NPh)W(SC_4H_4)] (**22**) in *ca.* 60% yield as a dark red solid (Figure 5-4). Isolation of a pure sample of compound **22** was accomplished through pentane extraction of the crude reaction mixture. Significantly decreased reaction times (3-4 hrs.) and increased yields (85%) have been observed for this reaction when the molar amount of thiophene was increased from 2 to 10 equivalents.

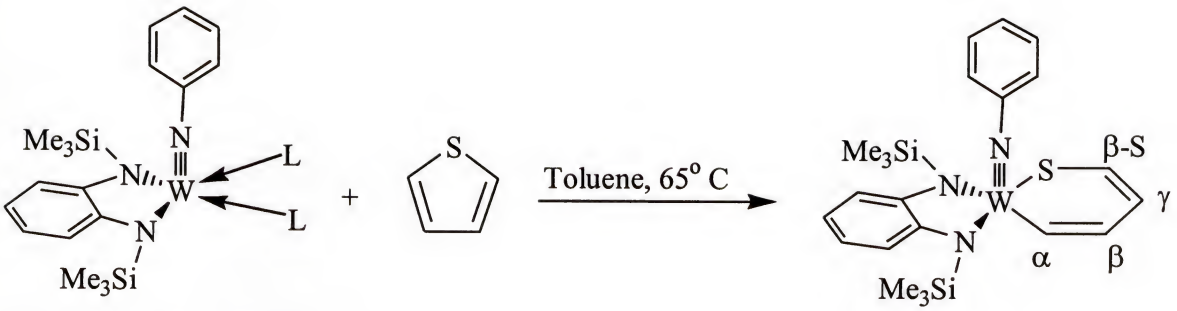

L = C_5H_5N (**8**) **22**

Figure 5-4. Synthesis of **22** through C-S bond activation.

Characterization of the reaction product by ^1H NMR spectroscopy was straightforward due to the distinct resonances and coupling constants associated with the metallathiacycle ring protons. The room temperature ^1H NMR spectrum of **22** displays two resonances (0.39 and 0.50 ppm), which correspond to the inequivalent Me_3Si groups. The metallathiacycle protons (positions are labeled in Figures 5-4 and 5-5) are shifted downfield with respect to free thiophene and appear as a doublet of doublets (6.70 ppm, $^3J_{H\text{-}H}$ = 7 and 9 Hz) corresponding to the β-CH proton, a doublet (8.01 ppm, $^3J_{H\text{-}H}$ = 9 Hz) for the α-CH proton, a doublet of doublets (8.20 ppm, $^3J_{H\text{-}H}$ = 13 and 7 Hz) for the γ-CH proton, and a doublet (9.00 ppm, $^3J_{H\text{-}H}$ = 13 Hz) for the β-CH proton adjacent to the S atom (Figure 5-5). The observed downfield shift of the metallathiacycle protons for compound **22** contrasts the reported upfield shift with respect to free thiophene found for the complex $(C_5H_5)_2W(SC_4H_4)$.[152] This is presumably due to the increased electron deficiency of the d^0 W(VI) center in compound **22** relative to the d^2 metal center of the $Cp_2W(IV)$ system.

An X-ray diffraction study of a single crystal of **22** grown from a concentrated pentane solution at -40° C confirmed the nature of C-S bond activation product. Due to disorder in the S1 and C22, the positions of the metallathiacycle atoms were solved

independently in two parts. A molecular drawing of **22** with the atom-labeling scheme is shown in Figure 5-6. Compound **22** adopts a five-coordinate, distorted square pyramidal geometry with the imido ligand occupying the apical position. The short W-N(imido) bond length of 1.734(3) Å, consistent with a W-N triple bond and the W-N(amido) bond lengths of 2.016(3) and 2.008(3) Å are similar to that observed for other W(VI) complexes.[31] Consistent with a W(VI) metal center, the diamide fold angle of **22** was observed to be 42°. Bonding within the metallathiacycle fragment appears to be localized as demonstrated by the alternating (short (C19-C20 1.192(16) Å)-long (C20-C21, 1.600(16) Å)-short (C21-C22 1.289(14) Å)) C-C bond lengths of the butadiene portion of the metallathiacycle (Figure 5-6).

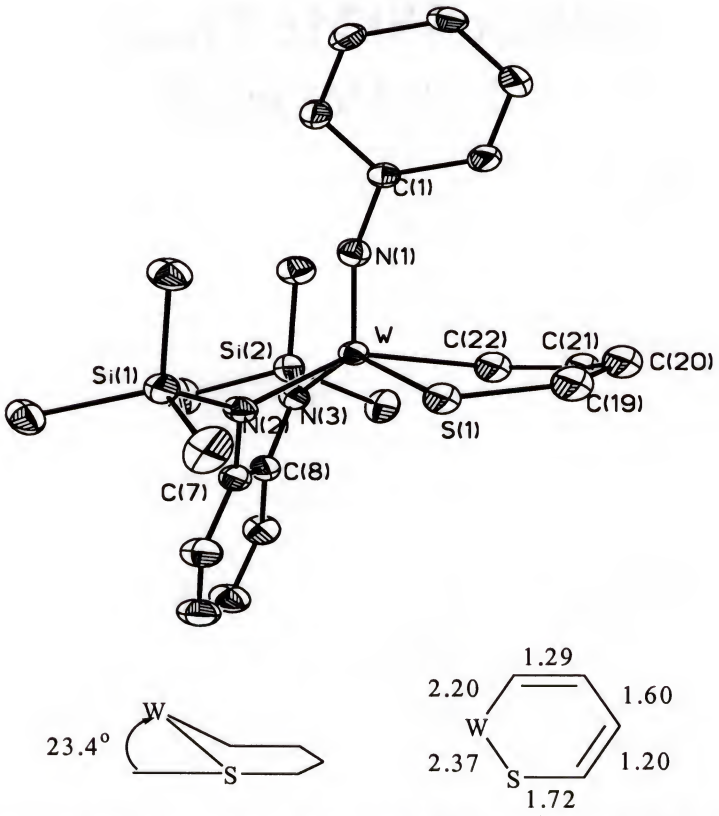

Figure 5-6. Molecular structure of $[(o\text{-}(Me_3SiN)_2C_6H_4)(NPh)W(SC_4H_4)]$ (**22**). Thermal ellipsoids are drawn at 40 % probability and the hydrogen atoms have been removed for clarity.

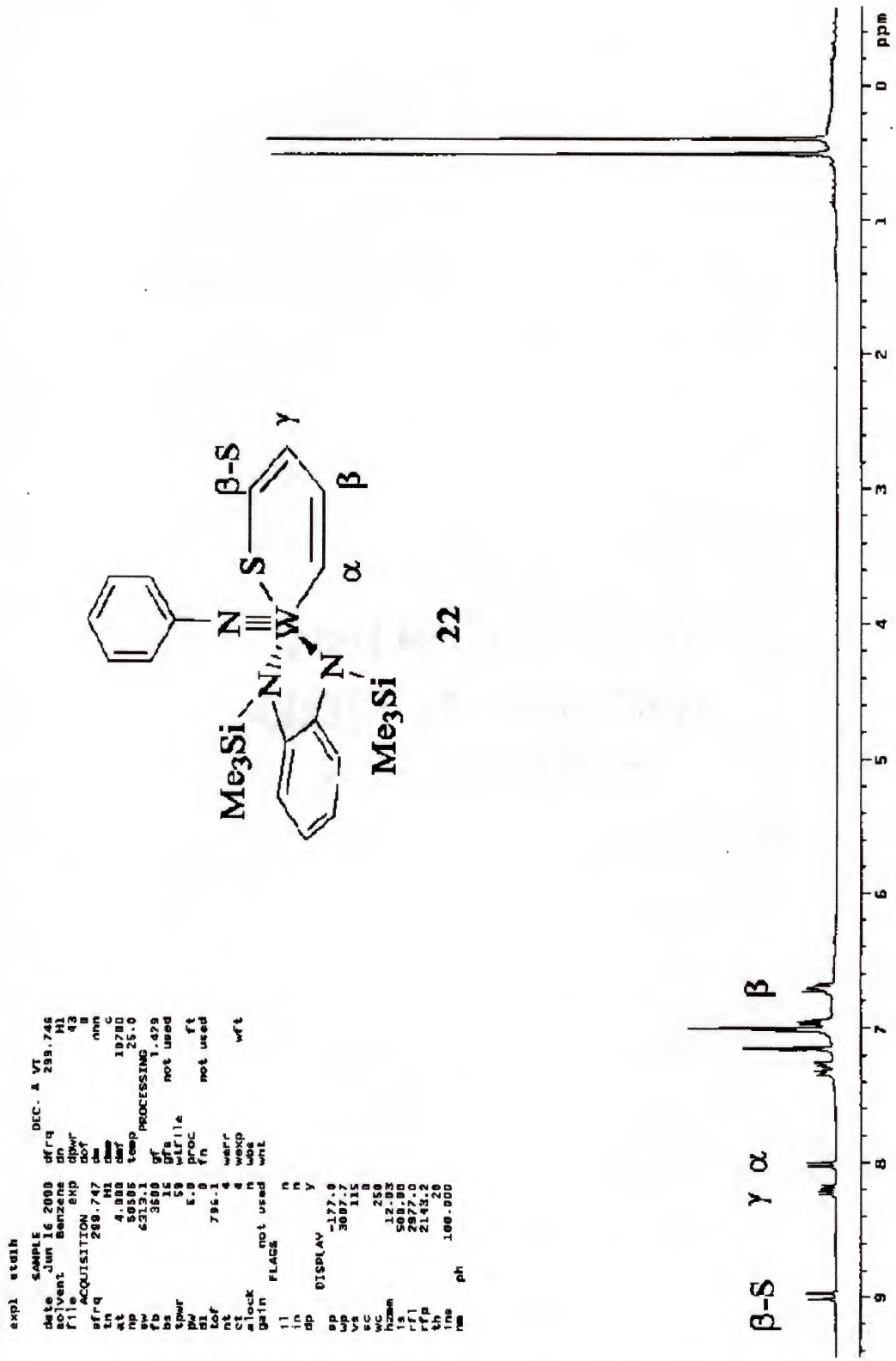

Figure 5-5. ^{1}H NMR spectrum of $[(o\text{-}(Me_3SiN)_2C_6H_4)(NPh)W(SC_4H_4)]$ (**22**)

The metallathiacycle six-membered ring of [(o-$(Me_3SiN)_2C_6H_4$)(NPh)W(SC_4H_4)] (**22**) is puckered slightly. The angle between the plane formed by W-S1-C22 and that formed by S1-C19-C20-C21-C22 was calculated to be 23.4°. This puckering of the metallathiacycle is comparable to the angles reported for $(C_5H_5)_2W(SC_4H_4)$ (23°)[152] and $(C_5Me_5)Rh(PMe_3)(SC_4H_4)$ (26°).[153,154] The observed nonplanarity of the metallathiacycle in **22** and the W and Rh complexes mentioned above is in agreement with the observed alternating bond lengths in the butadiene portion of the metallathiacycle. The localized nature of the bonding in the metallathiacycle of **22** differs from that found for $(C_5Me_5)Ir(SC_6H_8)$ and $[(triphos)Ir(SC_4H_4)]^+$, in which the bonding is believed to be delocalized based on the observed bond lengths and the presence of a planar metallathiacycle.[146,154-157]

2-Methylthiophene and Benzothiophene

Compound **8** also reacts with 2 equivalents of 2-methylthiophene and benzothiophene to yield the metallathiacycle complexes [(o-$(Me_3SiN)_2C_6H_4$)(NPh)W(SC_5H_6)] (**23**) and [(o-$(Me_3SiN)_2C_6H_4$)(NPh)W(SC_8H_6)] (**24**) respectively as a dark red solids in 80% isolated yield for **23** (Figure 5-7). Isolation of a pure sample of compound **24** has proved difficult because the complex slowly decomposes during the workup procedure. As determined by ^1H NMR spectroscopy, compound **24** is formed in *ca.* 50 % yield.

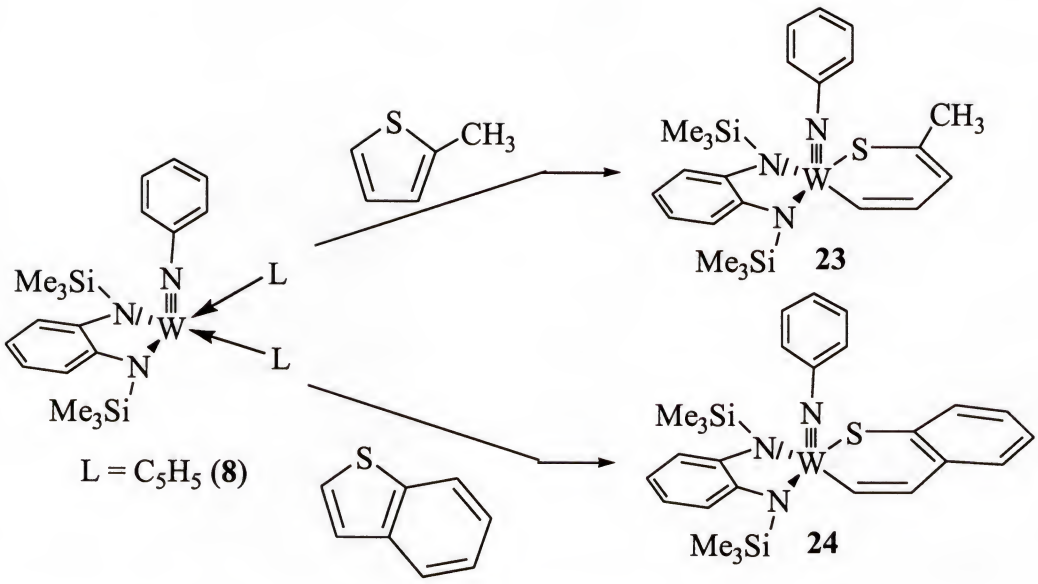

Figure 5-7. Synthesis of metallathiacycle complexes **23** and **24**.

The room temperature ^{1}H NMR spectra of compounds [(o-$(Me_3SiN)_2C_6H_4$)(NPh)W(SC_5H_6)] (**23**) and [(o-$(Me_3SiN)_2C_6H_4$)(NPh)W(SC_8H_6)] (**24**) are similar to the spectrum for compound **22**. Both compound **23** and **24** display two resonances that correspond to inequivalent Me_3Si groups (0.40, 0.51 ppm (**23**) and 0.37, 0.48 ppm (**24**)). For compound **23** the metallathiacyle protons resonate as a doublet (6.52 ppm, $^3J_{H-H}$ = 7 Hz) for the γ-CH proton, a doublet of doublets (8.21 ppm, $^3J_{H-H}$ = 7 and 13 Hz) for the β-CH proton and a doublet (8.89 ppm, $^3J_{H-H}$ = 13 Hz) corresponding to the α-CH proton. The CH_3 substituant appears as a singlet at 2.38 ppm. The metallathiacycle protons of compound **24** resonate as doublets at 8.52 ($^3J_{H-H}$ = 13.2 Hz) and 8.67 ppm ($^3J_{H-H}$ = 13.2 Hz) for the β-CH and α-CH protons respectively. A graphical representation of these assignments is shown in Figure 5-8. For compounds **23** and **24**, the chemical shifts, splitting patterns and coupling constants of the metallathiacycle protons are consistent with C-S bond activation of the C-S bond opposite the CH_3 group in 2-methylthiophene

and the phenyl substituant of benzothiophene. This selectivity results from a significant difference in the accessibility of the two C-S bonds. As explained in the following section, this selectivity is not observed when there is a substituant in the three position of thiophene.

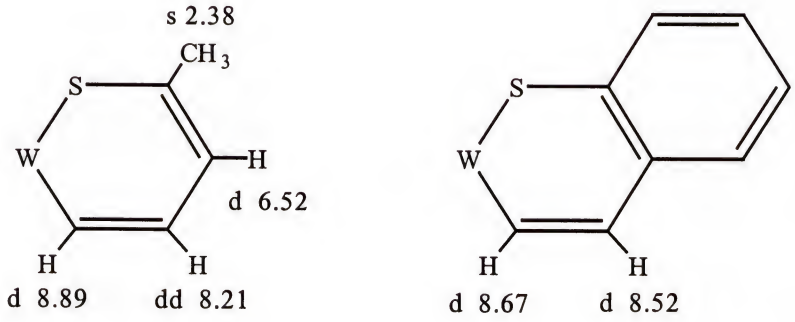

23 **24**

Figure 5-8. Metallathiacycle proton assignments for compounds **23** and **24**.

3-Methylthiophene

In contrast to the product selectivity observed for 2-methylthiophene and benzothiophene, reaction of $[W(NPh)(o\text{-}(Me_3SiN)_2C_6H_4)(C_5H_5N)_2]$ (**8**) with 2 equivalents of 3-methylthiophene generates a mixture of the two possible C-S bond activation products, $[(o\text{-}(Me_3SiN)_2C_6H_4)(NPh)W(SC_5H_6)]$ (**25a**) and (**25b**) (Figure 5-9). As determined by ^1H NMR spectroscopy, the products are formed in a 60:40 ratio with **25b** as the major component.

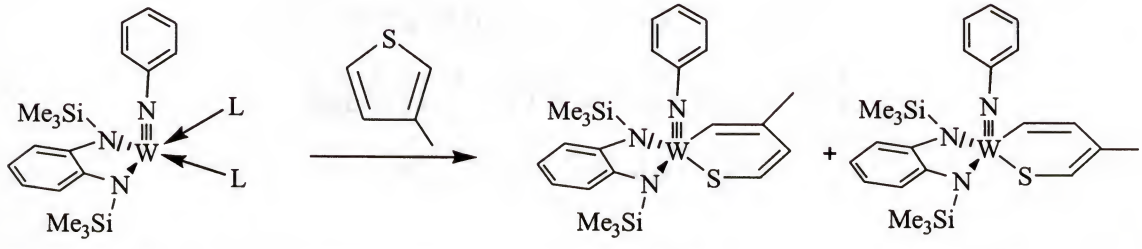

L = C_5H_5 (**8**) **25a** **25b**

Figure 5-9. Synthesis of metallathiacycles **25a** and **25b**.

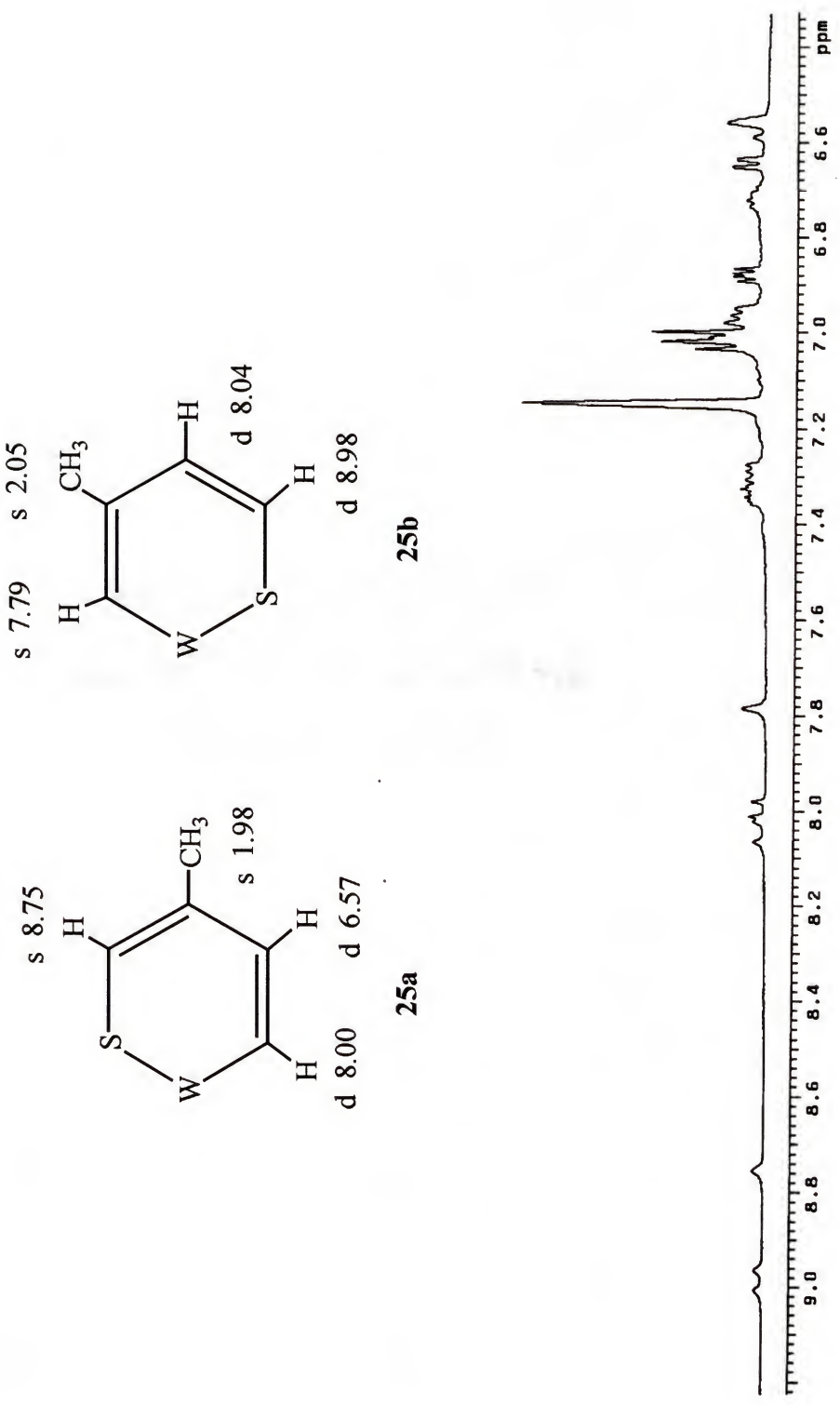

Figure 5-10. Proton assignment for compounds **25a** and **25b**.

Assignment of the metallathiacycle proton resonances for the two product isomers, **25a** and **25b**, was accomplished through a combination of ^{1}H NMR and ^{1}H COSY (proton-proton correlation spectroscopy). The ^{1}H COSY experiment revealed which hydrogens are on adjacent carbon atoms and the $^3J_{H-H}$ coupling calculated from the ^{1}H NMR spectrum confirmed the positioning of the hydrogens deduced from the ^{1}H COSY experiment. Figure 5-10 displays the aromatic region of the room temperature ^{1}H NMR spectrum and the proton assignment scheme for the metallathiacycle protons of compounds **25a** and **25b**. In addition to the aromatic resonances, two sets of resonances (0.43, 0.52 ppm (**25a**) and 0.42, 0.51 ppm (**25b**)) are observed for the inequivalent $SiMe_3$ groups. The CH_3 groups of **25a** and **25b** resonated as singlets at 1.98 and 2.05 ppm respectively.

The observed product selectivity in the reaction of [W(NPh)(o-$(Me_3SiN)_2C_6H_4)(C_5H_5N)_2$] (**8**) with 2-methylthiophene or benzothiophene as described in the previous section, arises from steric congestion on one side of the thiophene ring, whereby C-S bond activation opposite the substituant is preferred. For the reaction of 3-methylthiophene with **8**, both C-S bonds are accessible as demonstrated by the formation of both **25a** and **25b**.

Mechanistic Considerations

Thiophenes are known to interact with a metal center in a number of different modes, however, an η^1-S-bound thiophene[147-149] is believed to be a prerequisite for subsequent C-S bond activation. Although the initial interaction of thiophene and its derivatives with [W(NPh)(o-$(Me_3SiN)_2C_6H_4)(C_5H_5N)_2$] (**8**) has not been directly observed, the ability of **8** to accommodate additional ligands has been demonstrated, as

described in Chapter 3.[76] Compound **8** rapidly forms octahedral complexes with the addition ligands such as CO and PMe_3. For the reaction of the σ-donor ligand PMe_3 with **8**, the complex $[W(NPh)(o\text{-}(Me_3SiN)_2C_6H_4)(C_5H_5N)(PMe_3)_2$ is the preferred product, suggesting labilization of one of the pyridine ligands upon coordination of the first PMe_3 ligands. Although thiophenes are weaker donor ligands than PMe_3, under the thermolysis conditions for the reaction of thiophenes with **8,** labilization of a pyridine ligand would generate the open coordination site necessary for C-S bond activation to occur. The ability of the W(IV) metal center to facilitate oxidative addition chemistry was demonstrated by the reaction of **8** with olefins, Chapter 4. For example, when compound **8** was exposed to a positive pressure of ethylene, oxidative coupling of 2 ethylene molecules led to the formation of the metallacyclopentane complex $W(CH_2CH_2CH_2CH_2)(NPh)[o\text{-}(Me_3SiN)_2C_6H_4]$ (**20**). Therefore, even though no direct evidence for the mechanism of the formation of the metallathiacycles has been observed, based on the knowledge gained from the reactions of **8** with PMe_3 and olefins, the following mechanism is proposed. Initial coordination of thiophene, either S-bound or η^2-bound, followed by loss of pyridine would generate an unsaturated W(IV) intermediate. Subsequent C-S bond cleavage of the coordinated thiophene and loss of the remaining pyridine ligand generates the observed metallathiacycle complexes (Figure 5-11).

Conclusions

Due to the industrial importance of the HDS process, the use of organometallic modeling to gain a better understanding of this process is of great importance. Specifically, examples of metal-thiophene interactions for Group 6 metal complexes are

of interest because of their widespread use in the HDS process (MoS_2 and WS_2). In this chapter we have demonstrated that the chelate stabilized W(IV)L_2 complex [W(NPh)(o-$(Me_3SiN)_2C_6H_4)(C_5H_5N)_2$] (**8**) facilitates the C-S bond activation of both thiophene and substituted thiophenes to give the metallathiacycle complexes **22**, **23**, **24**, **25a** and **25b**. To our knowledge, this reactivity is the first example of thiophene C-S bond activation by a Group 6 metal complex in the +4 oxidation state. Previous reports involving C-S bond activation of thiophenes with Group 6 metals also suggest C-H bond activation as a competing process. For the reaction of **8** with thiophenes no evidence of such chemistry has been observed. In addition to its importance to the field of HDS modeling, this work also aids in our understanding of the properties and reactivity of the W(IV) fragment, [W(NPh)(o-$(Me_3SiN)_2C_6H_4)$].

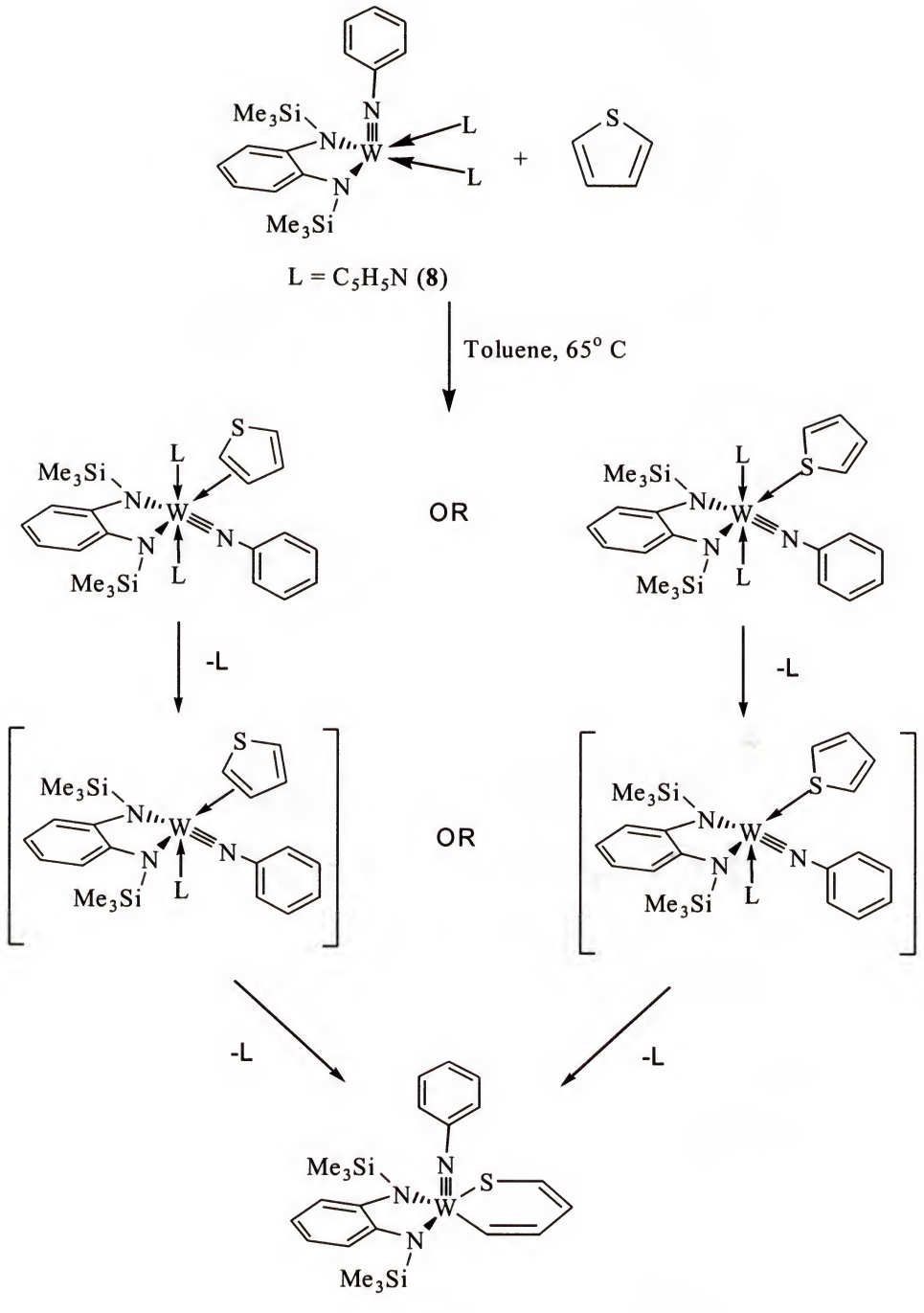

Figure 5-11. Proposed mechanism for the C-S bond activation of thiophenes.

CHAPTER 6
TUNGSTEN CATALYZED OLEFIN DIMERIZATION AND CODIMERIZATION

Introduction

The ability of transition metal compounds to carry out the facile and selective coupling or oligomerization of unsaturated organic substrates is a major feature of organometallic catalysis.[158] This area of research has seen the development of many different transition metal systems that facilitate the catalytic dimerization of 1-alkenes (α-olefins).[159-162] For early-transition metal complexes, two pathways have been identified for this class of reaction. The first involves metallacycle formation via oxidative coupling, followed by β-hydrogen transfer and reductive elimination, pathway A (Figure 6-1). The alternative pathway begins with hydrometallation of an alkene by a metal hydride to yield a metal alkyl intermediate. Migratory insertion of a second alkene into the M-alkyl bond followed by β-elimination results in the liberation of the newly formed dimer, pathway B (Figure 6-1).[163]

Pathway B (migratory insertion) is closely related to the mechanism of Ziegler-Natta polymerization.[164-166] The critical difference between polymerization and the related dimerization process is the rate of the β-elimination (chain transfer) step. For systems that give predominately dimerization products, this step is fast relative to subsequent migratory insertion of another alkene molecule. In polymerization systems, the rates are reversed, allowing chain propagation to dominate over chain transfer.

The alternative pathway (A), utilizes the propensity of low-valent, early-transition metals to form metallacyclopentane species through oxidative coupling of olefinic substrates. Although typically slow, to the point of being unobserved, β-hydrogen transfer from such metallacycles offers a possible pathway for the selective dimerization of olefins. A recent study by Rothwell, *et al.* demonstrated that titanacyclopentane rings exhibit the thermal stability that is typically associated with early-transition metal metallacyclopentanes.[167] However, at elevated temperatures these compounds act as catalysts for the slow dimerization of α-olefins. Several groups have expanded this reactivity to include the catalytic cyclization of acyclic dienes, which also believed to proceed through metallacyclic intermediates.[168-171]

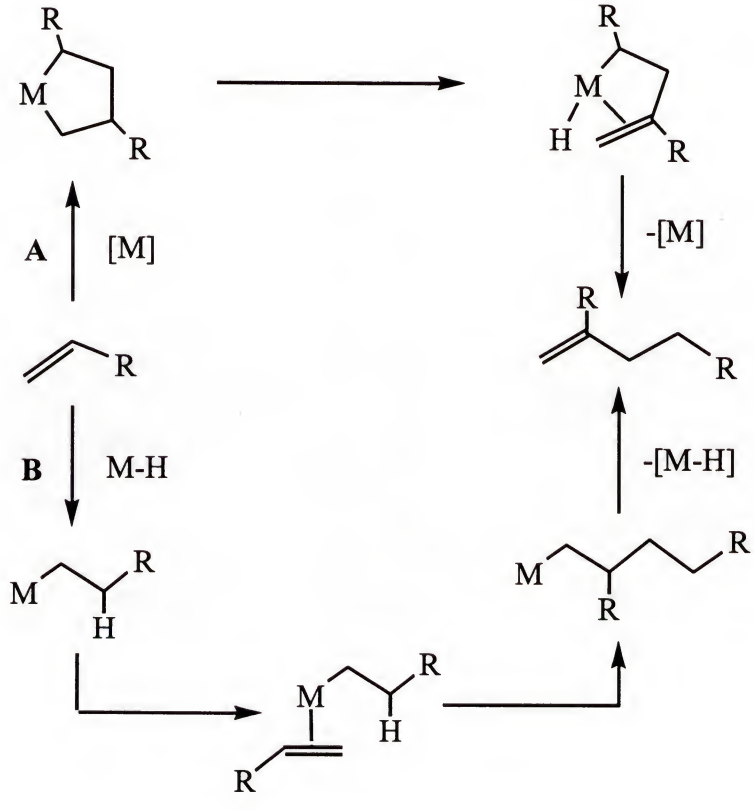

Figure 6-1. Mechanisms for the dimerization of 1-alkenes.

Group 6 metal complexes (tungsten and molybdenum) have long been known to be active homogeneous catalyst for the metathesis of cyclic and acyclic olefins.[172,173] It has been demonstrated that the active species in these reactions is a M(VI) alkylidene complex and that the metathesis reaction proceeds through a metallacyclobutane intermediate.[174] It is believed that the ancillary ligands of these complexes play an important role in the stabilization of the four membered metallacyclic intermediate and prevent intermolecular reactions.[175] Theoretical mechanistic studies have suggested that a spectator oxo ligand makes this metallacyclic formation favorable.[176] Imido ligands have also been used in metathesis systems, as demonstrated by the classical aniline/WCl_6/Al system, which is an efficient olefin metathesis catalyst.

In the seventies, Lawson and Menapace pointed out that the aniline/WCl_6/Al metathesis catalyst could be converted into an olefin dimerization catalyst simply by increasing the Al/W ratio to 5:1.[177-181] For example, a mixture of tungsten hexachloride, aniline (aniline:W, 2:1) and $EtAlCl_2$ (Al:W, 1-2) catalyzes the self-metathesis of propylene. As the amount of $EtAlCl_2$ was increased to Al/W = 3 both conversion and selectivity toward metathesis fell rapidly to zero. At this Al/W ratio and higher, conversion rose sharply with dimerization as the exclusive reaction, yielding a mixture of 2-methylpentene and 2,3-dimethylbutene (Figure 6-2).

More recently, Exxon revisited this system with the hope of developing an industrial process based on this reactivity.[182] The driving force for developing this chemistry was the desire to develop a catalyst that would convert propylene into 1-hexene, which is widely used as a comonomer in the olefin polymerization industry.

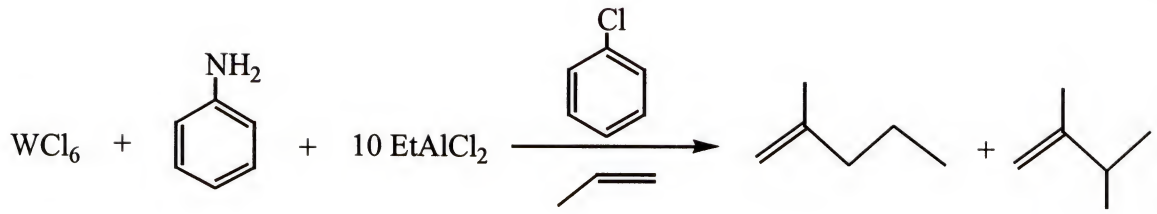

Figure 6-2. WCl_6/aniline catalyzed dimerization of propylene.

Even though the Exxon, aniline/WCl_6 system catalyzes the dimerization of alkenes, the selective formation of 1-hexene from propylene was not accomplished. From these studies it was also noted that the catalyst only facilitated dimerization of terminal olefins, ethylene through pentene. No activity was observed for larger α-olefins, internal or geminal olefins. In addition, the stability of the catalyst system was such that activity was observed for only short periods of time (30-60 min) before catalyst deactivation occurred.

The relative ease with which the W(IV)L_2 complexes, [W(NPh)(o-$(Me_3SiN)_2C_6H_4$)$(C_5H_5N)_2$] (**8**) and [W(NPh)(o-$(Me_3SiN)_2C_6H_4$)(p-$C_6H_7N)_2$] (**9**) facilitate the oxidative coupling of olefins to give metallacyclopentane species (Chapter 4) interested us in further exploitation of these facile reactions. The ultimate goal was to create a catalyst system for the dimerization of alkenes, which rivaled or exceeded the activity and selectivity of the previously reported dimerization catalysts. Doing so presented a significant challenge because the metallacyclopentane complexes display significant thermal and chemical stability. This stability was in part expected. Our studies of the W(IV) complexes have demonstrated the propensity of these complexes to be oxidized to W(VI) species that are significantly more stable, Chapters 4 and 5. Forcing the reverse, W(VI)-W(IV) that would make the olefin dimerization reaction catalytic is chemically and thermodynamically much more challenging. This chapter will

discuss our entry into the area of catalytic olefin dimerization. Included in this discussion are examples of two highly active catalysts systems, substrate and product selectivity and our ideas regarding the nature of the catalyst systems and their possible applications.

Metallacyclopentane Decomposition

Previous work from our group showed that the metallacyclopentane complex, $W(CH_2CH_2CH_2CH_2)(NPh)[o\text{-}(Me_3SiN)_2C_6H_4]$ (**20**), undergoes decomposition when heated in the presence of PMe_3 to yield the complex, $[o\text{-}(Me_3SiN)_2C_6H_4]W(NPh)(PMe_3)_2(C_2H_4)$ (**26**) (Figure 6-3).[32] Unfortunately, 1-butene was never observed as a product of this reaction. Instead this reactivity served to demonstrate a shift of the equilibrium between the metallacyclopentane and olefin complexes in the presence of σ-donor ligands. Although the formation of 1-butene from metallacyclopentanes has been reported for Ni(II),[183] Pd(II),[184] Pt(II),[185] Pt(IV),[186] Ta[187] and Ti,[184] it is worthwhile to note that thermolysis of **20** for extended periods of time results in complex decomposition instead of the desired β-hydrogen transfer reaction to yield 1-butene.

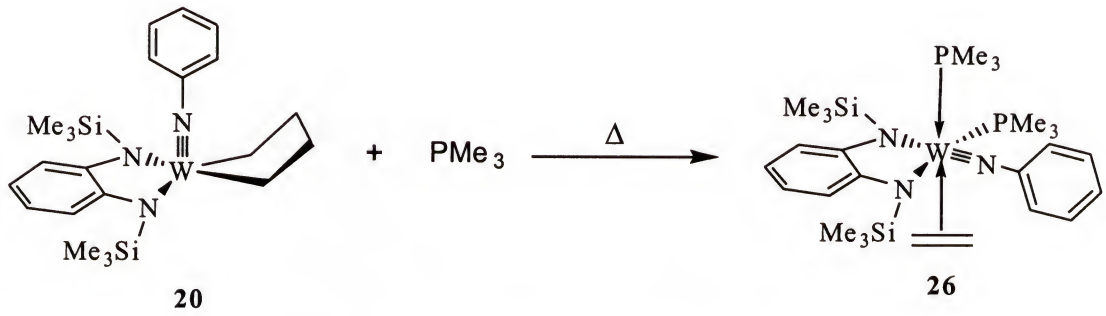

Figure 6-3. Formation of ethylene complex, **26** from metallacyclopentane, **20**.

During their examination of the aniline/W/Al system, researchers at Exxon observed the formation of metallacyclopentane complexes. Subsequent addition of Lewis acidic aluminum reagents to these metallacycles resulted in the liberation of alkenes.[182] These observations suggested that reagents such as $EtAlCl_2$ and Et_2AlCl could be applied to our metallacyclopentane system to facilitate decomposition through β-hydrogen transfer.

In a resealable NMR tube, 2 equivalents of $EtAlCl_2$ were added to a solution (C_6D_6) of $W(CH_2CH_2CH_2CH_2)(NPh)[o\text{-}(Me_3SiN)_2C_6H_4]$ (**20**) at room temperature. The room temperature ^1H NMR spectrum acquired after mixing the solution for 10 minutes displayed olefinic and aliphatic resonances consistent with the formation of 1-butene. Similar results were observed when either Et_2AlCl or $AlCl_3$ was added to the metallacyclopentane complex (Figure 6-4). The exact composition of the resulting metal complex has yet to be determined, but the presence of characteristic resonances for the diamide and imido ligand protons, suggests the metal fragment $W(NPh)[o\text{-}(Me_3SiN)_2C_6H_4]$ (**27**) remains intact.

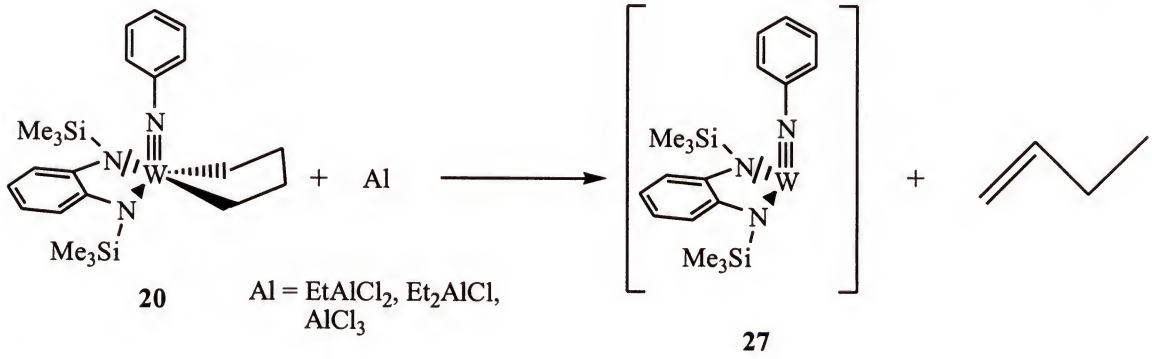

Figure 6-4. Lewis acid promoted metallacyclopentane decomposition.

Catalytic Ethylene Dimerization and Codimerization with Butene

Our desire to create an active olefin dimerization catalyst was realized by exposing a mixture of $W(CH_2CH_2CH_2CH_2)(NPh)[o\text{-}(Me_3SiN)_2C_6H_4]$ (**20**) and $EtAlCl_2$ to a positive pressure of ethylene. A Parr high-pressure reactor equipped with a magnetic stir bar and pressure gauge was charged with **20** (0.025 g, 0.042 mmol), toluene (50 mL) and 2 equivalents of $EtAlCl_2$ and heated at 70° C for 10 minutes to allow for catalyst aging. At this point, a positive pressure of ethylene (100 psi) was introduced to the reactor. Over a period of 15 min the total volume of ethylene was consumed as demonstrated by the rapid decrease in the observed pressure inside the reactor. Similar results were obtained when the initial ethylene pressure was varied from 100 – 500 psi. The products of the reaction were analyzed by gas chromatography on a Hewlett Packard 5890 gas chromatograph equipped with a 30 meter Supleco SPB-1 fused silica capillary column. A GC trace of the reaction solution revealed the presence of a four-component product mixture.

Invoking a mechanism that involves a metallacyclopentane intermediate we were able to generate a list of possible reaction products. Through this mechanism, initial dimerization of ethylene yields exclusively 1-butene. Subsequent codimerization of ethylene and 1-butene through a metallacyclic mechanism would yield a series of 5 different C_6 olefins (1-hexene, 2-hexene, 3-hexene, 3-methyl-1-pentene, 2-ethyl-1-butene) (Figure 6-5). The complexity of the theoretical product mixture is result of two possible metallacycles, one in which the ethyl substituant is on a α-carbon and the other with the ethyl group residing in a β-position.

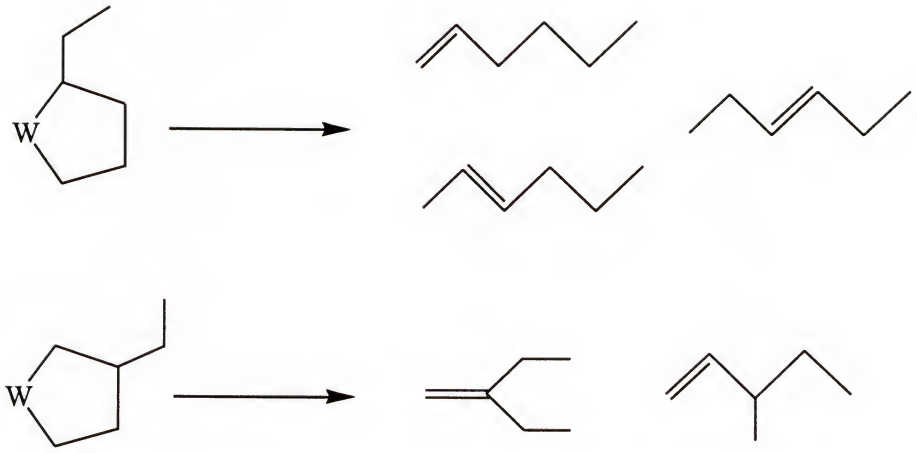

Figure 6-5. Theoretical product mixture based on a metallacycle mechanism.

Product Characterization

A combination of GC and ^{1}H NMR spectroscopy was utilized to determine the composition and relative yields of the ethylene dimerization reaction. By GC the product mixture contains four distinct products. By spiking the reaction mixture with aliquots of the known alkene standards, 1-butene, 3-methyl-1-pentene, 2-ethyl-1-butene and 1-hexene, the peaks in the GC trace were assigned as shown in (Figure 6-6). The relative abundances of the C_6 products were determined through integration values obtained from the GC trace to be 60% 2-ethyl-1-butene, 35% 3-methyl-1-pentene and 5% 1-hexene. However, this assignment only accounts for 3 of the 5 products expected from the metallacycle mechanism. The remaining two proposed products, 2-hexene and 3-hexene are generated from the same metallacycle as 1-hexene and would only be present in small amounts similar to 1-hexene. Spiking the reaction mixture with these standards caused an observed increase in the 3-methyl-1-pentene (2-hexene) and the 2-ethyl-1-butene (3-hexene) peaks respectively. From the integration values of the alkene region of the ^{1}H

NMR spectrum, the concentration of internal olefins (2-hexene, 3-hexene) was calculated to be *ca.* 3-4% as predicted by the proposed mechanism.

Confirmation of the components of the product mixture was made by a comparison of the ^{1}H NMR spectrum of a sample of the reaction mixture (Figure 6-7) to the spectra of pure samples of the proposed products. The spectrum of the reaction mixture contains resonances corresponding to terminal, internal and geminal olefins in addition to aliphatic resonances that are consistent with the proposed products. Also, the relative abundances of each product, as determined through integration of the NMR spectrum, are similar to the values obtained from the GC trace.

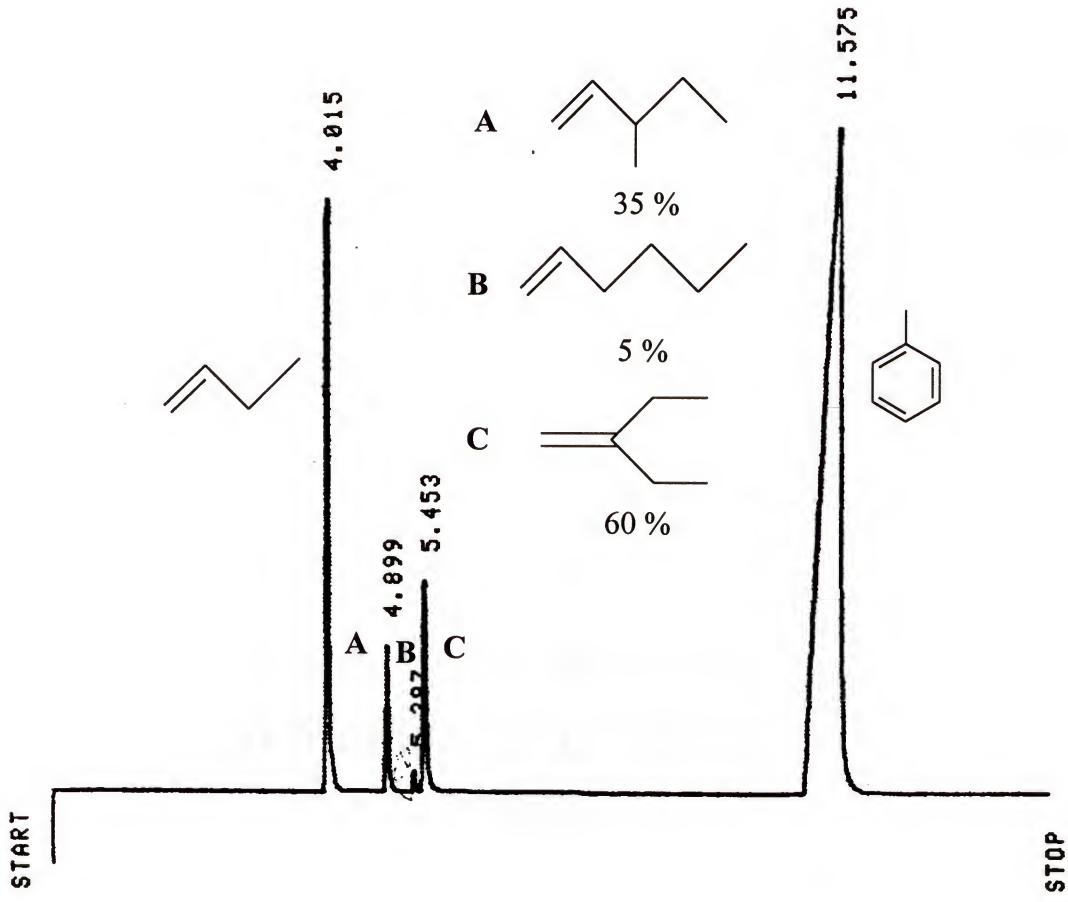

Figure 6-6. Ethylene dimerization/codimerization product mixture.

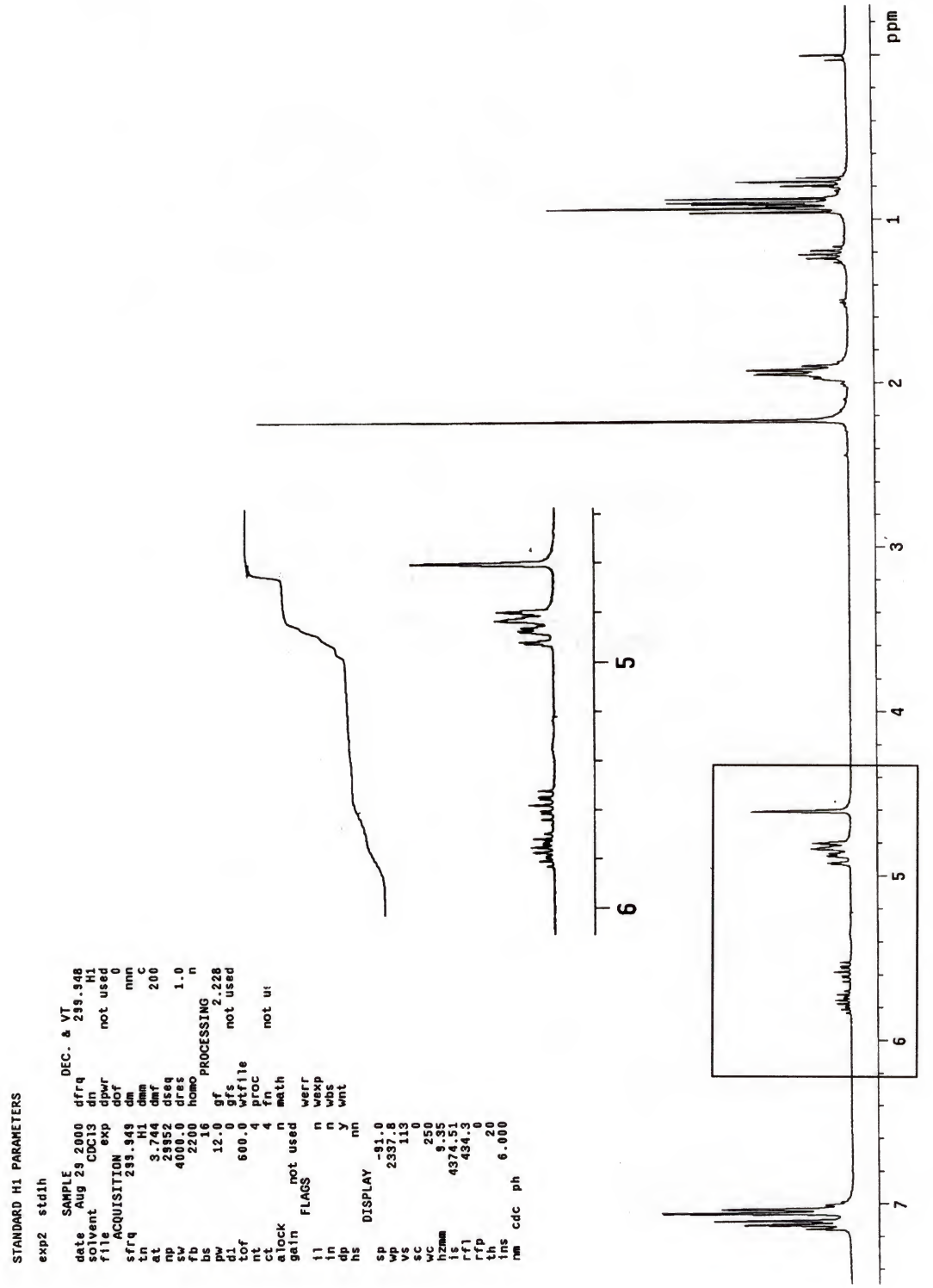

Figure 6-7. ^{1}H NMR spectrum of ethylene dimerization products.

For the catalytic reactions described above, the rate of ethylene consumption was variable as a result of inconsistencies in the effectiveness of the magnetic stir bar to maintain a constant mixing rate. Therefore, our understanding of the actual activity of the catalyst system towards the dimerization of ethylene was limited. In order to explore this variance, a similar dimerization experiment was conducted (0.04 mmol W, 2 eq. $EtAlCl_2$, 50 mL toluene, 70° C, 100 psi ethylene) in a reactor equipped with a mechanical stirring apparatus. The pressure inside the reactor was maintained at 100psi, with a continuous supply of ethylene from a gas burette. Ethylene uptake was monitored with a pressure transducer, which was attached to a recorder. Upon pressurizing the system with ethylene, the temperature inside the reactor rose sharply to 130° C over a period of 5 seconds.

The reaction temperature slowly decreased as the dimerization reaction proceeded. Figure 6-8 shows a plot of ethylene consumption in moles versus time for two successive charges of ethylene. The observed decrease in the rate of ethylene uptake between run 1 and run 2 is attributed catalyst decomposition, which occurs during the rapid temperature jump. Not only does this study demonstrate the exceptional reactivity of the catalyst system (**20**/$EtAlCl_2$), but it also confirms the inconsistencies in the rate of stirring when a magnetic stir bar is employed in the reactor.

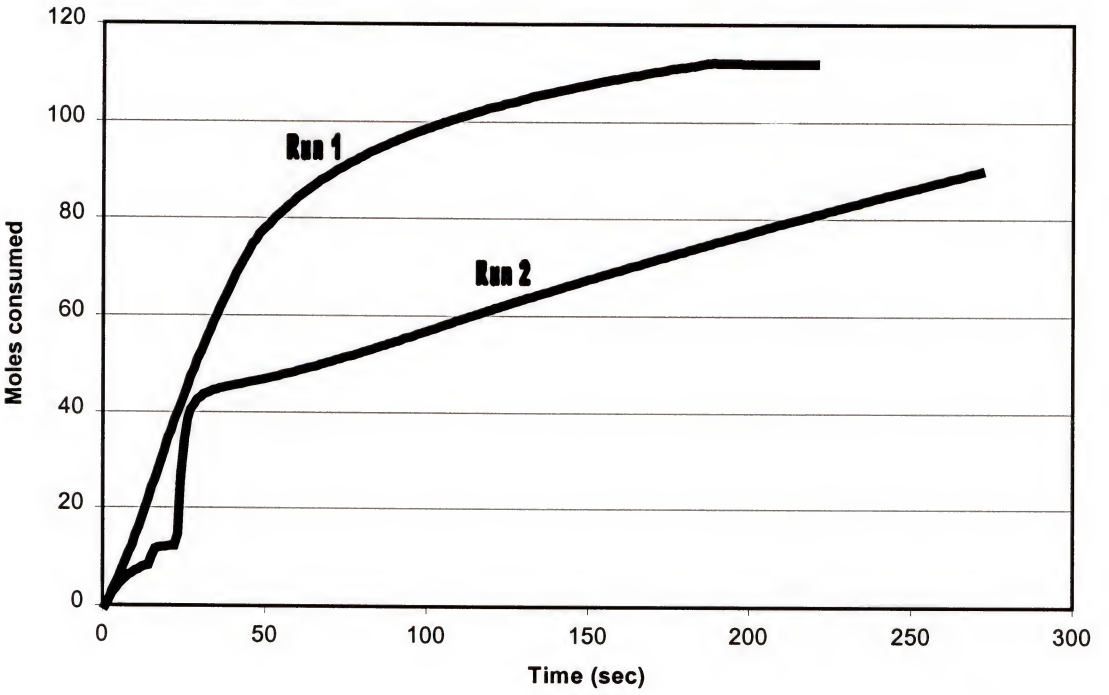

Figure 6-8. Plot of ethylene consumption vs. time.

W(NPh)[o-$(Me_3SiN)_2C_6H_4$]Cl_2 as a Catalyst Precursor

In light of the literature reports of utilizing (imido)WCl_4 as an olefin dimerization catalyst,[177-182] we decided to explore the catalytic activity of the dichloride complex, W(NPh)[o-$(Me_3SiN)_2C_6H_4$]Cl_2 (**28**). As was found for compound **20**, the dichloride complex is also active towards ethylene dimerization in the presence of a cocatalyst ($EtAlCl_2$). The activity observed for compound **28** in the dimerization/codimerization of ethylene was similar to that observed for **20**. Since this project is in its early stages a numerical comparison of the activity for two catalyst systems is pending. Of significance are the identical product mixtures and ratios that are generated by the different systems, suggesting a similar dimerization mechanism. The successful application of compound **28** as a dimerization catalyst combined with its ease of synthesis has made this the

catalyst of choice for our dimerization studies. In question at this point was the process by which these two different catalyst precursors are activated towards ethylene dimerization with the same cocatalyst ($EtAlCl_2$).

Activation of $W(CH_2CH_2CH_2CH_2)(NPh)[o\text{-}(Me_3SiN)_2C_6H_4$ (**20**)

Activation of compound **20** toward catalytic olefin dimerization and not olefin metathesis can be rationalized in a straightforward manner. We found that liberation of 1-butene from $W(CH_2CH_2CH_2CH_2)(NPh)[o\text{-}(Me_3SiN)_2C_6H_4]$ (**20**) only occurs in the presence of Lewis acids such as $EtAlCl_2$, Et_2AlCl or $AlCl_3$. For example, when **20** was thermolyzed in the presence of PMe_3, ethylene was liberated with formation of the olefin complex $[o\text{-}(Me_3SiN)_2C_6H_4]$ $W(NPh)(PMe_3)_2(C_2H_4)$ (**26**).[32] In addition, when exposed to an excess of ethylene or other olefins, compound **20** is indefinitely stable with no obseverable butene formation or metallacycle ring expansion. Therefore, it is suggested that the Al cocatalysts behave differently than PMe_3 in that they likely promote β-hydrogen transfer instead of metallacycle cycloreversion. Initially, alkyl abstraction leads to the formation of a bimetallic intermediate. Subsequent β-hydrogen abstraction produces a W-hydride complex that undergoes bimetallic reductive elimination to liberate 1-butene and form the W(IV) intermediate **27**. Compound **27** then rapidly facilitates oxidative coupling of two additional olefin molecules to complete the catalytic cycle (Figure 6-9).

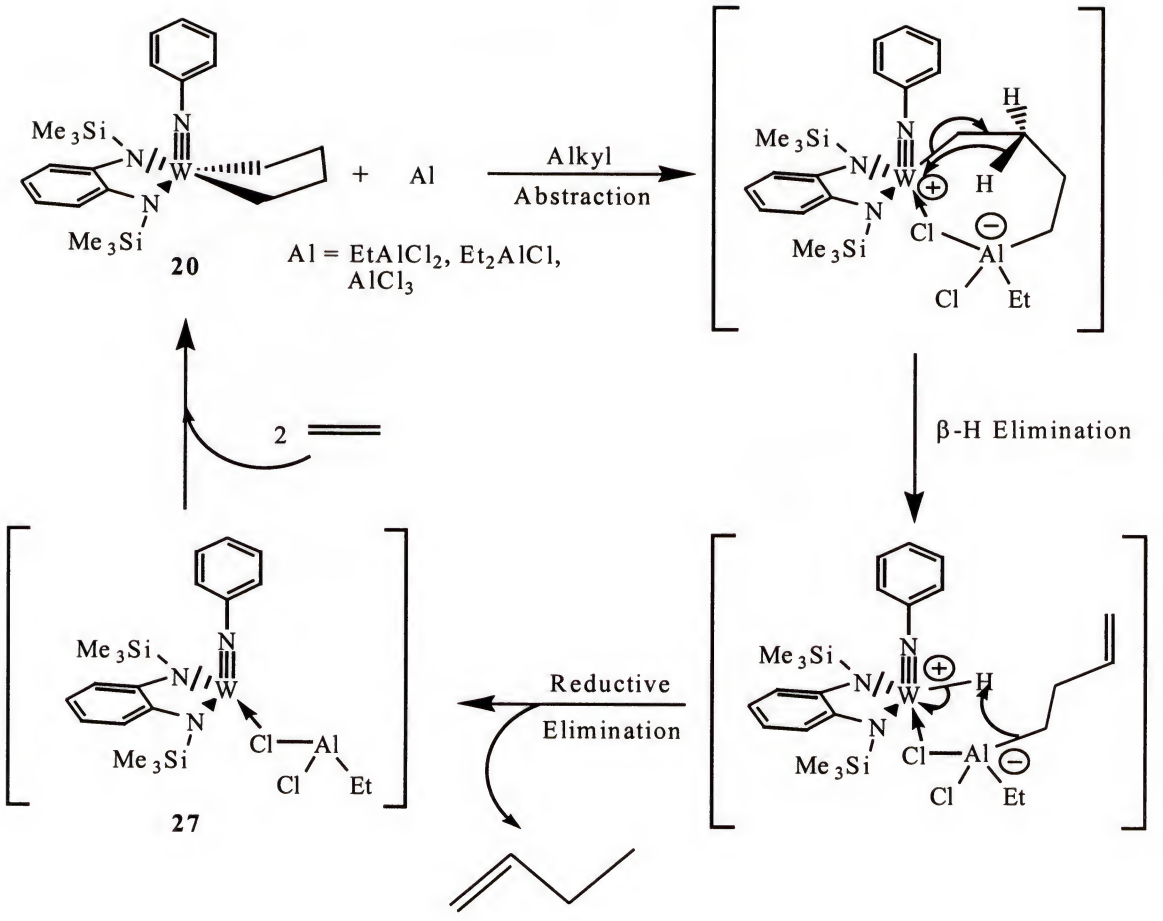

Figure 6-9. Aluminum promoted activation of metallacyclopentane, **20**.

Alkylidene Formation for the Aniline/W/Al System

Even though **20** and **28** yield similar dimerization products, due to their different composition, the process by which these complexes are activated must follow different pathways. To begin to understand the possible mechanism for the activation of **28** and why no metathesis was observed, it is necessary to examine more closely the chemistry involving the aniline/WCl_6/Al catalyst system.

Menapace[177] observed that when greater than four equivalents of $EtAlCl_2$ were used in conjunction with the WCl_6/aniline system only olefin dimerization occurred. At lower Al/W ratios, metathesis was found to be the predominating process. Hérisson and

Chauvin[188] suggested that the mechanism for olefin metathesis involves a metal-alkylidene bond (Figure 6-10). Numerous alkylidene complexes have since been synthesized. Alkylidene ligands are typically found on highly electropositive early-transition metals in complexes, which are formally electron deficient (fewer than 18 e^-).[1] Complexes of this type are capable of coordinating an olefin molecule to the electrophilic metal center of the alkylidene complex.[189] Subsequent formation of an intermediate metallacyclobutane followed by cycloreversion can give either the original alkylidene/olefin complex or a new alkylidene complex with the liberation of olefin (productive metathesis) (Figure 6-10).

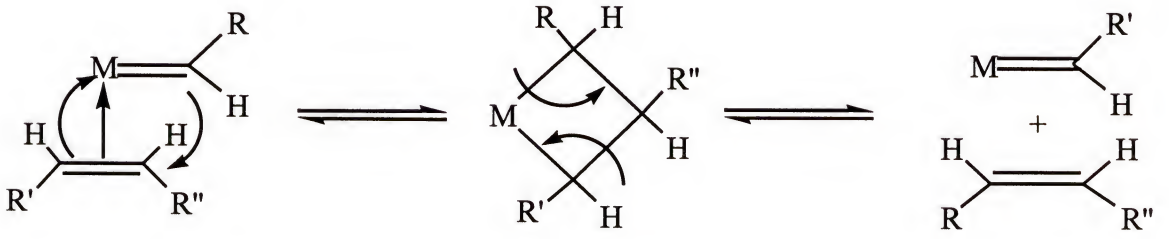

Figure 6-10. Chauvin mechanism for olefin metathesis, showing productive metathesis.

This mechanism has gained wide acceptance and seems quite plausible for the aniline/WCl_6/$EtAlCl_2$ metathesis catalyst, where initial formation of a tungsten ethylidene complex is easily rationalized by two different mechanisms (Figure 6-11). Mechanism A follows a pathway that includes di-alkylation of the (imido)WCl_4 complex with two equivalents of $EtAlCl_2$. Subsequent α-hydrogen abstraction yields the ethylidene species necessary for olefin metathesis. The other suggested mechanism, B, although more involved, generates the ethylidene complex through a series of steps that carry as much validity as those for mechanism A. In this case, mono-alkylation is suggested, followed by abstraction of the remaining chloride ligand with a second equivalent of $EtAlCl_2$.

Relief of the electron-deficient W cation is accomplished through loss of H^+ (scavenged by $EtAlCl_3^-$ present in the system) resulting in the formation of the W(VI) ethylidene complex. However, as suggested by Menapace, the presence of excess Lewis acid (more than 2 equivalents) in this system results in the destabilization of the ethylidene complex whereby the olefin dimerization process becomes dominant and metathesis is suppressed.

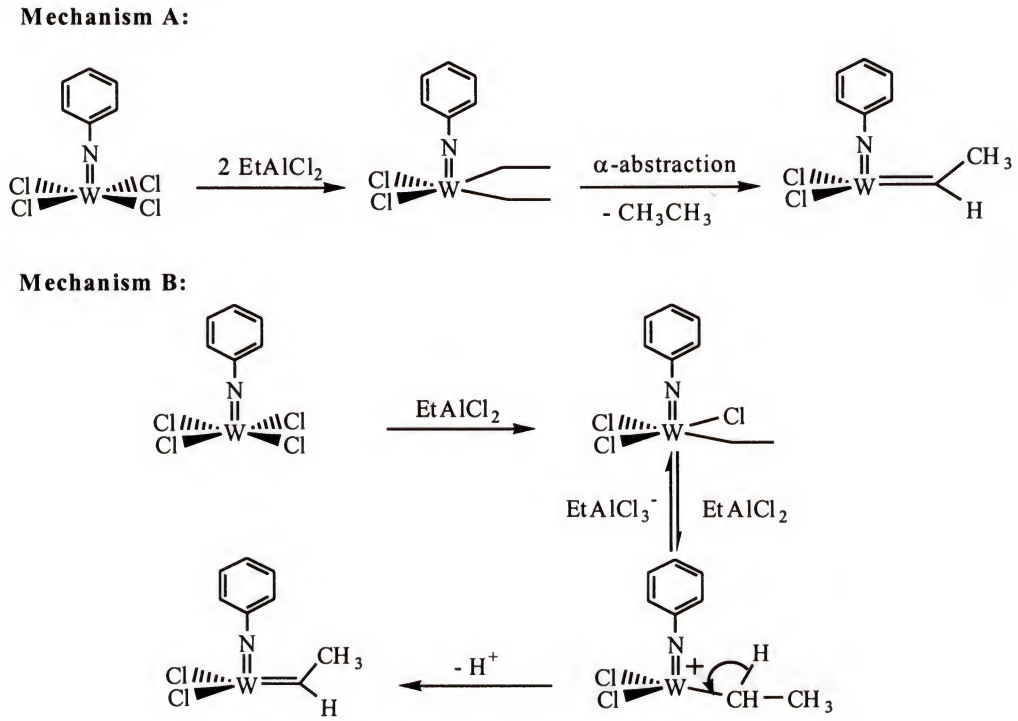

Figure 6-11. $EtAlCl_2$ promoted formation of a tungsten ethylidene.

Activation of W(NPh)[o-$(Me_3SiN)_2C_6H_4$]Cl_2 **28**

Regardless of the amount of $EtAlCl_2$, our catalyst system only promotes olefin dimerization. Pentene and propylene, the expected products of ethylene/butene metathesis are never observed. Even though compound **28** is a markedly different catalyst precursor than the metallacyclopentane complex **20**, it is our belief that the active species in both systems is the highly reactive W(IV) fragment, {W(NPh)[o-

$(Me_3SiN)_2C_6H_4]\}$ (**27**). With the numerous literature reports of the presence of alkylidene species in the aniline/W/$EtAlCl_2$ system it is necessary to explore possible activation processes for compound **28**/$EtAlCl_2$ that involve alkylidenes. However, it will become evident in this discussion that the actual catalyst activation most likely follows a mechanism that is void of alkylidene species.

Due to the similarities between the (imido)WCl_4 catalyst precursor and compound **28**, generation of an alkylidene from the reaction of **28** with $EtAlCl_2$ should follow one of the mechanisms presented in Figure 6-11. Mechanism A can be readily eliminated from consideration. Although the intermediate W(VI)-diethyl complex, W(NPh)[o-$(Me_3SiN)_2C_6H_4](CH_2CH_3)_2$ (**29**) has been prepared and well characterized,[31] the subsequent α-hydrogen abstraction step, necessary to form the ethylidene complex $W(CHCH_3)(NPh)[o\text{-}(Me_3SiN)_2C_6H_4]$ (**30**) is unlikely. For alkyl complexes containing both α- and β-hydrogens, β-abstraction usually occurs preferentially over the α-H processes.[190,191] Previously, our group had addressed this very question.

Several asymmetric dialkyl complexes were prepared to study how the steric bulk of the alkyl ligands affected the competition between the α- and β-processes.[33] Of significance to this work was the reaction of PMe_3 with W(NPh)[o-$(Me_3SiN)_2C_6H_4](CH_2CMe_3)(Et)$, (**31**), which yields exclusively β-abstraction products, including the ethylene complex, **26,** which is also formed through the reaction of **29** with PMe_3 (Figure 6-12). Competition between α- and β-abstraction was only observed for complexes with more sterically demanding ligands; hence β-abstraction would be the preferred decomposition pathway for the diethyl intermediate, **29** under the conditions of the dimerization reaction, ultimately forming metallacyclopentane **20** (Figure 6-12). The

necessity of steric bulk to facilitate α-abstraction in these dialkyl complexes was further demonstrated by reacting the dimethyl complex $W(NPh)[o\text{-}(Me_3SiN)_2C_6H_4](Me)_2$ with PMe_3. In contrast to the bulkier α-hydrogen containing dialkyl complexes that undergo α-abstraction, this reaction only yields the PMe_3 adduct, $W(NPh)[o\text{-}(Me_3SiN)_2C_6H_4](Me)_2(PMe_3)$.

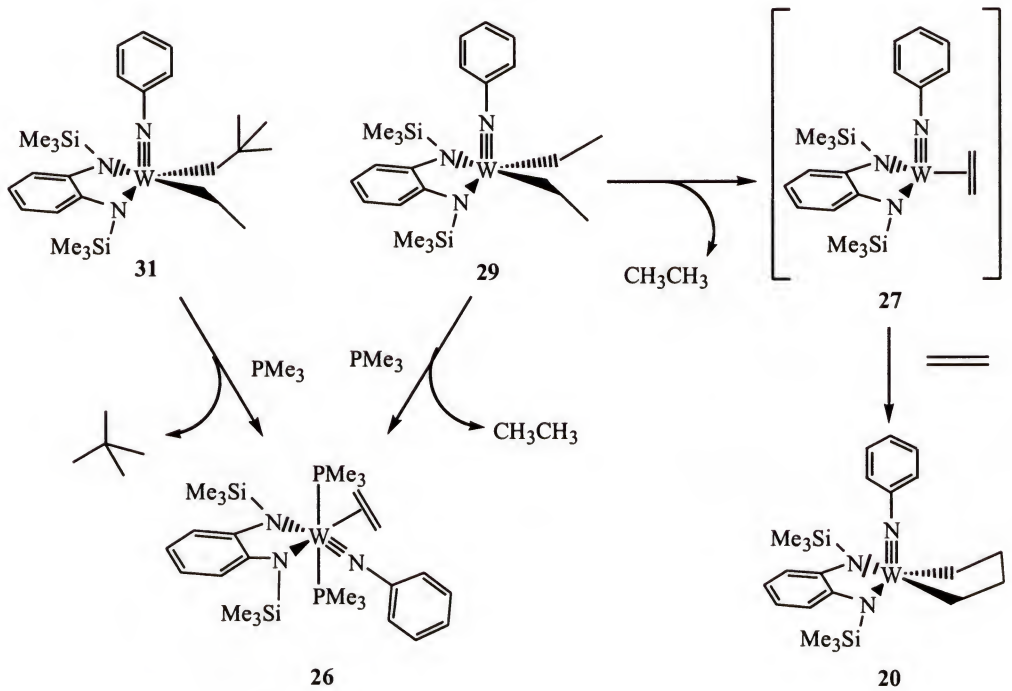

Figure 6-12. Preference for β-abstraction when ethyl ligands are present.

Another plausible alkylidene forming mechanism based on the reaction of $W(NPh)[o\text{-}(Me_3SiN)_2C_6H_4]Cl_2$ (**28**) with $EtAlCl_2$, is based on that proposed by Menapace, mechanism B (Figure 6-11). This pathway involves mono-alkylation of the W-dichloride with the first equivalent of $EtAlCl_2$ while the second equivalent acts as a chloride-abstracting agent to yield a W(VI)-alkyl cation (Figure 6-13). Expulsion of a proton to generate an ethylidene results in stabilization of the high-oxidation state metal center. Even though this is a rational mechanism for the formation of an ethylidene

species, the stability of such a complex is questionable. Several decomposition pathways have been demonstrated for these types of alkylidene species, supporting the proposed instability of this complex. Therefore, it is important here to mention the possible decomposition pathways for two reasons. First to demonstrate that the presence of an ethylidene species in the dimerization reactions is unlikely and secondly, if this complex was formed, each of the decomposition pathways ultimately lead to the formation of the W(IV) intermediate **27** that we believe is the active dimerization catalyst.

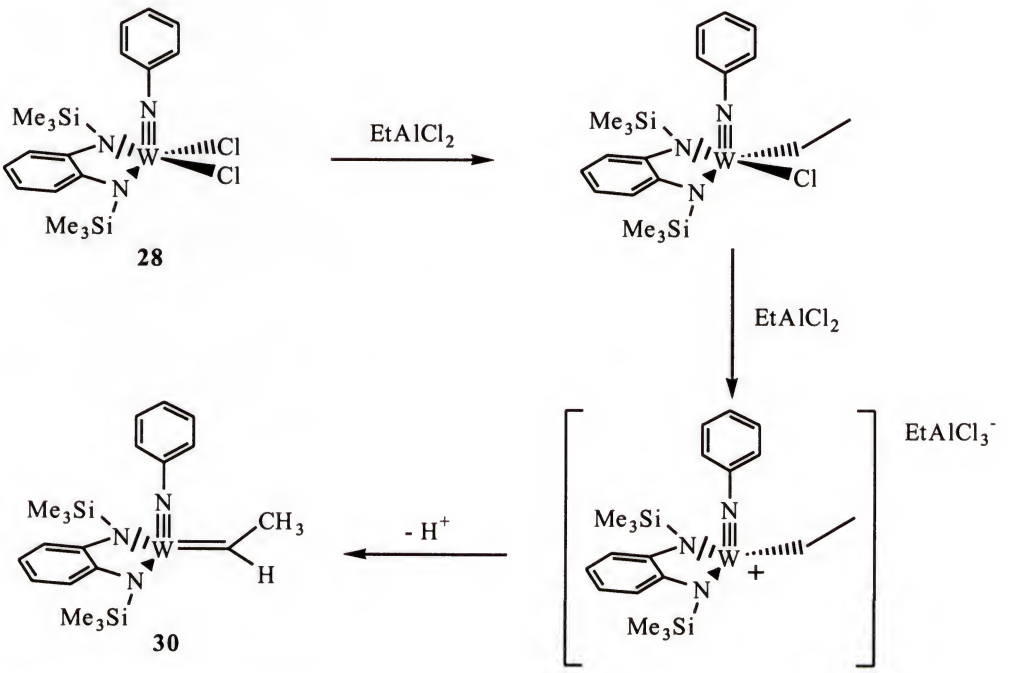

Figure 6-13. Proposed formation of W(VI)-ethylidene, **30**.

Alkylidene Decomposition

Recent work in our group has successfully used the reaction of W(NPh)[o-$(Me_3SiN)_2C_6H_4$]Cl_2 (**28**) with grignard reagents to prepare a wide range of W(VI) dialkyl complexes.[31] Our exploration of this class of d^0 dialkyl complexes led to the preparation of the alkylidene complex W($CHCMe_3$)(PMe_3)(NPh)[o-$(Me_3SiN)_2C_6H_4$] (**33**) via α-

abstraction when W(NPh)[o-$(Me_3SiN)_2C_6H_4$]$(CH_2CMe_3)_2$ (**32**) is thermolyzed in the presence of PMe_3 (Figure 6-14). Compound **33** has shown activity as a catalyst for the metathesis of terminal olefins, but competing decomposition processes drastically limit the catalyst's lifetime.[32] Further investigation of these decomposition reactions led to the characterization of the major decomposition product, the metallacyclopentane complex, **20** that we have now found to be a catalyst precursor for olefin dimerization. A combination of experimental results and the observation of key intermediates in the decomposition of **33** led to the proposal of two major pathways to rationalize the formation of **20** in the olefin metathesis reactions. Based on the similarities between **33** and the proposed ethylidene complex, **30**, it is our belief that the mechanism of decomposition displayed by **33** would also apply to **30**.

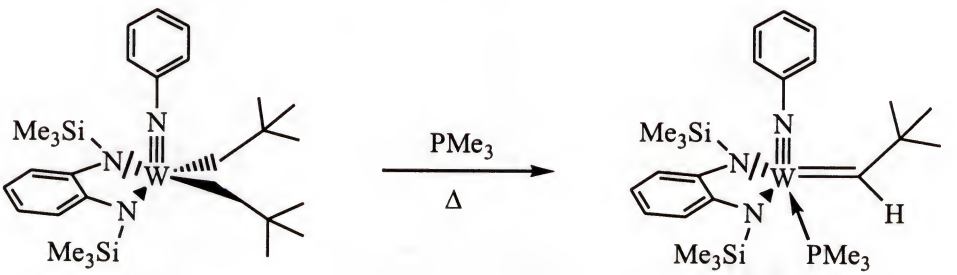

32 **33**

Figure 6-14. Synthesis of neopentylidene, **33**, via α-abstraction.

Ligand C-H Activation

Interestingly, attempts to isolate the base free neopentylidene analogous to compound **33** led instead to the reversible metallation of one of the Me_3Si groups of the o-$(Me_3SiN)_2C_6H_4$ ligand in the absence of PMe_3 (Figure 6-15). This served as the first of several observations that suggested instability of an alkylidene ligand in this type of complex.

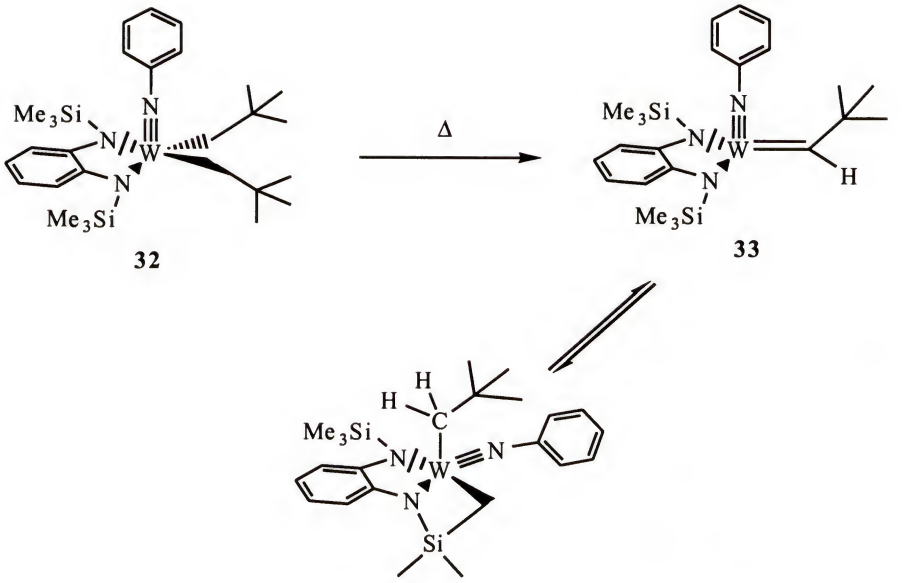

Figure 6-15. Ligand metallation as an alkylidene decomposition mechanism.

Application of this ligand metallation process to the W-ethylidene complex would result in the formation of a β-hydrogen containing W(VI)-alkyl complex **34** (Figure 6-16). The presence of β-hydrogens in **34** suggests the possibility for further decomposition. The ability of W(VI)-dialkyl complexes to undergo decomposition via β-hydrogen abstraction processes resulting in the formation of W(IV)-olefin complexes was previously demonstrated by our research group.[32,33] Invoking such a process for **34** results in the demetallation of the ligand and formation of an intermediate ethylene complex, which under the conditions of the dimerization reaction (ethylene pressure) would be rapidly scavenged by ethylene to give compound **20** (Figure 6-16). The presence of Lewis acid ($EtAlCl_2$) in the reaction mixture serves to enhance the rate of this β-abstraction process as suggested by the reaction of the metallacyclopentane, **20**, with $EtAlCl_2$.

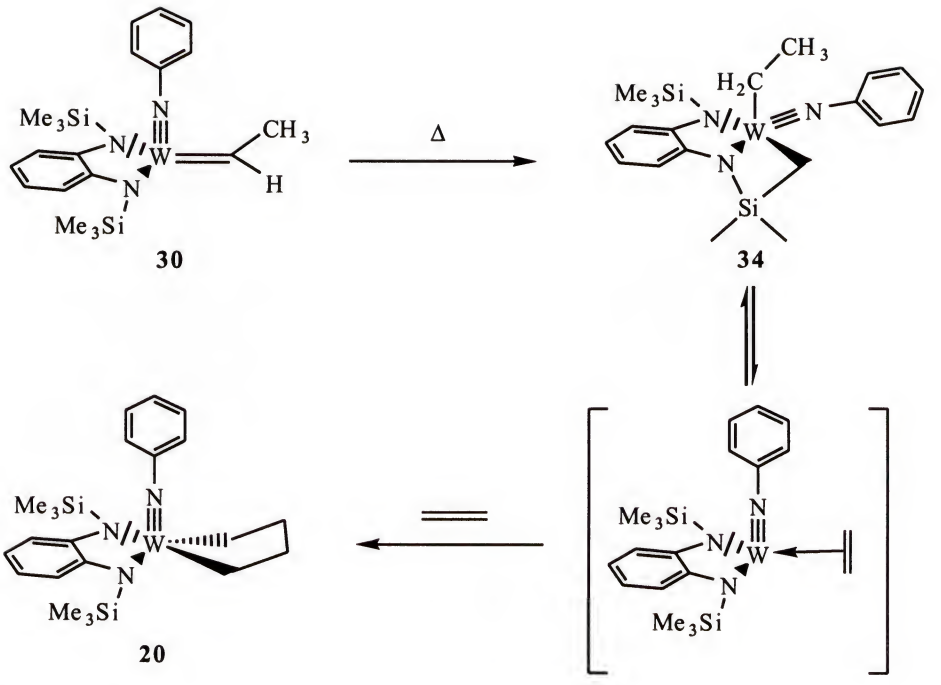

Figure 6-16. Metallacyclopentane formation via ligand metallation/β-abstraction.

Bimolecular Decomposition

The nature of the ethylene metathesis mechanism creates another possible decomposition pathway for the ethylidene complex, **30**. Productive metathesis of ethylene, promoted by **30** proceeds through a methyl-substituted metallacyclobutane intermediate, $W(CH_2(CH_3)CH_2CH_2)(NPh)[o\text{-}(Me_3SiN)_2C_6H_4]$ **35**. Rapid loss of propylene results in the formation of the methylidene complex, $W(CH_2)(NPh)[o\text{-}(Me_3SiN)_2C_6H_4]$ **36** (Figure 6-17). Since early-transition metal methylidene complexes of Ta, Mo and W are susceptible to bimolecular decomposition it is likely that **36** could follow a similar process.[32,129,192,193] This type of decomposition again yields $\{W(NPh)[o\text{-}(Me_3SiN)_2C_6H_4]\}$ (**27**), which is trapped by ethylene through oxidative coupling to form metallacyclopentane, **20**.

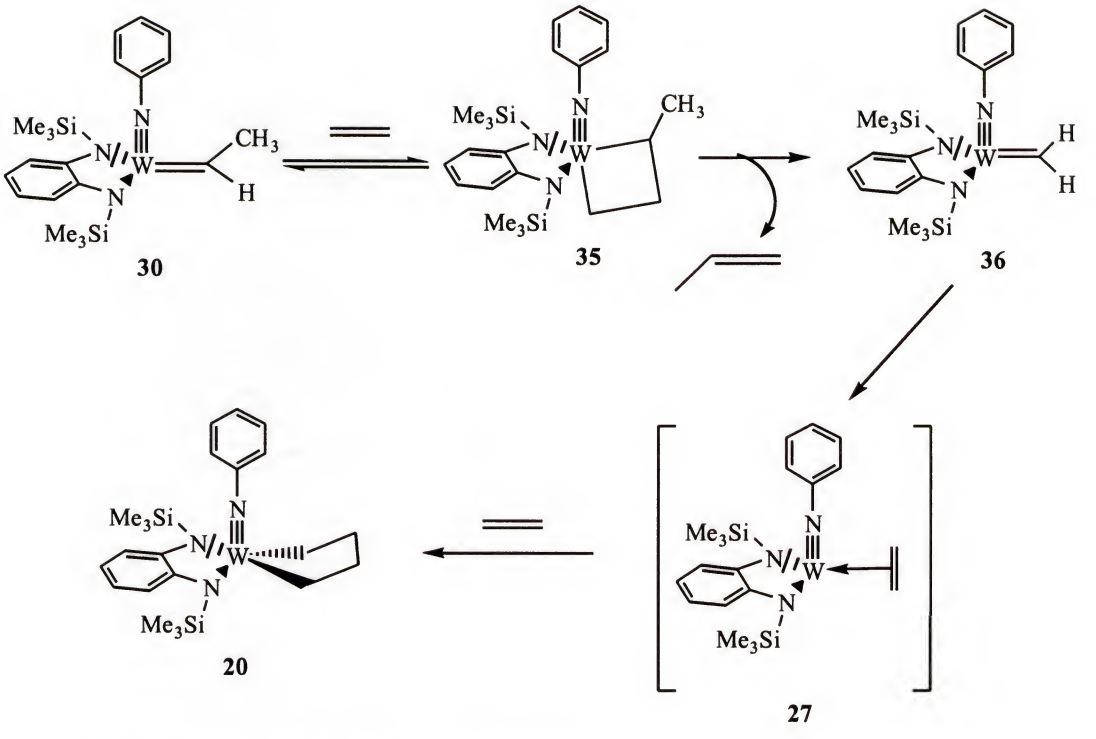

Figure 6-17. Bimolecular methylidene decomposition.

Ethylidene Rearrangement

Finally, direct decomposition of **30** is suggested as another way to rationalize the lack of olefin metathesis in the $WCL_2/EtAlCl_2$ olefin dimerization reaction. Several groups have demonstrated the inherent instability of early-transition metal ethylidene complexes.[194] This instability results from the relative ease with which ethylidene complexes containing β-hydrogens rearrange to the corresponding ethylene complex through a hydride migration mechanism. Figure 6-18 displays the application of this rearrangement to the ethylidene complex **30**, yielding an unsaturated W(IV) intermediate that rapidly incorporates another ethylene molecule to give **20**. As with the other alkylidene decomposition pathways explained above, the formation of **20** through ethylidene rearrangement allows olefin dimerization to predominate over metathesis.

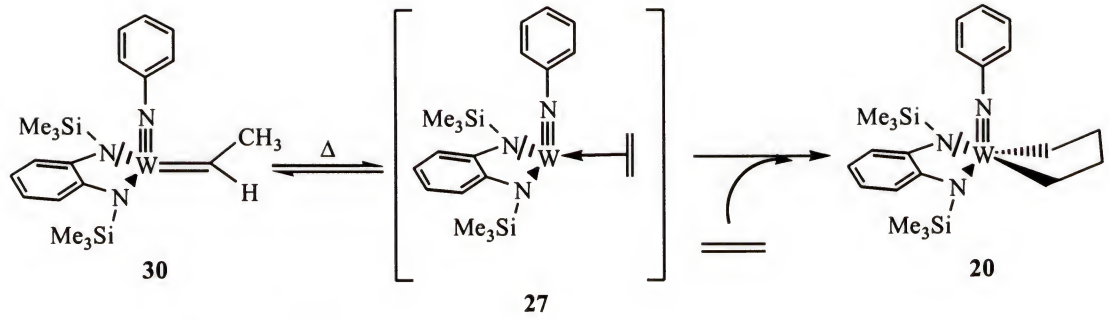

Figure 6-18. Ethylidene/olefin complex rearrangement to give **20**.

Proposed Activation of **28**

Although each of the alkylidene decomposition mechanisms described above acting either alone or collectively can account for the suppression of olefin metathesis in the WCl_2(**28**)/$EtAlCl_2$ dimerization system, we propose a more straightforward explanation to account for this. Our intimate understanding of the competition between α- and β-transfer processes for W(VI)-dialkyl complexes provides the basis for the following proposal. Initial dialkylation of **28** with $EtAlCl_2$ to give **29** represent the first step in the activation process that takes place during the period of catalyst aging prior to exposure of the catalyst system to ethylene. With our knowledge the β-hydrogen transfer chemistry of this type of complex in hand, formation of a W(IV)-ethylene intermediate via elimination of ethane marks the catalyst's entry into the catalytic cycle. Upon exposure to ethylene, the intermediate ethylene complex is rapidly trapped by an additional ethylene molecule through oxidative coupling to give **20**. To complete the catalytic cycle, $EtAlCl_2/AlCl_3$ facilitates decomposition of compound **20,** as presented in Figure 6-9, to liberate butene and reform the W(IV) intermediate (Figure 6-19). Formation of the observed C_6 products results from the build up of butene in the system,

which creates a competition between ethylene dimerization and ethylene/butene codimerization.

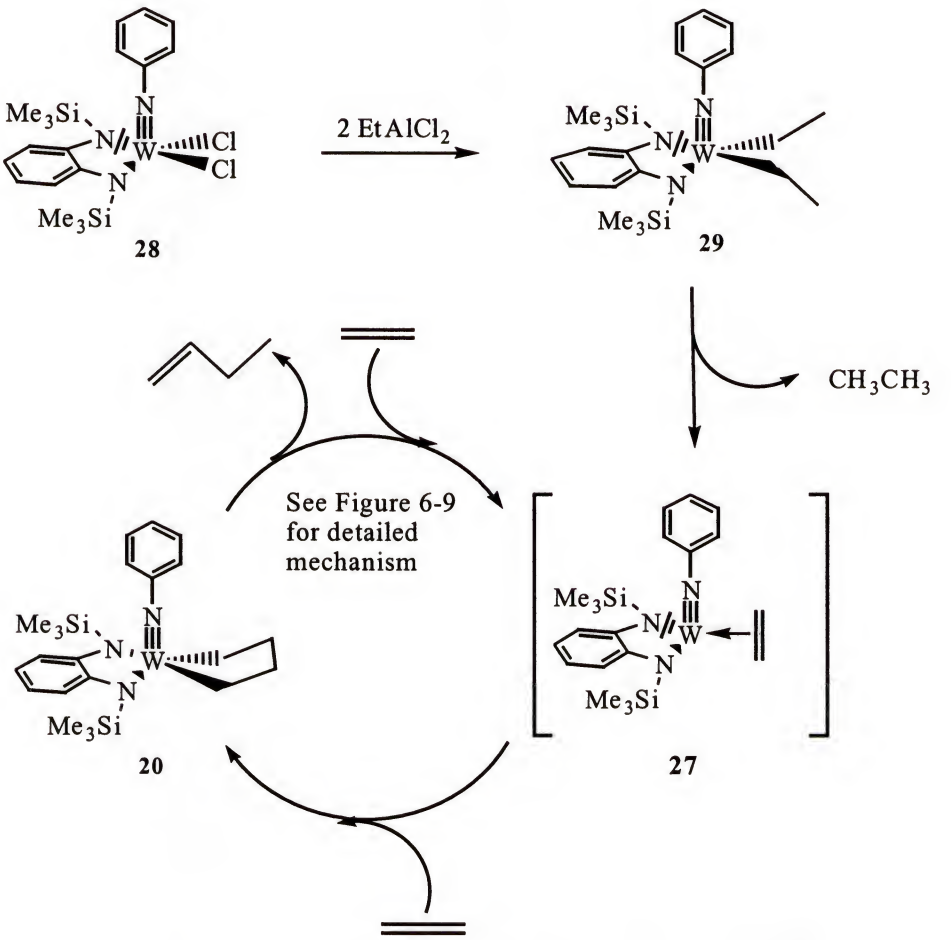

Figure 6-19. WCl_2 catalyzed ethylene dimerization and ethylene/butene codimerization.

Dimerization Substrate Selectivity

In order to begin to understand the scope of this catalyst system, some initial studies were performed with longer chain, cyclic, internal and geminal olefins as well as acyclic dienes. In contrast to other dimerization catalysts that typically are limited to short (C_2-C_5) terminal olefins as substrates, we have observed rapid dimerization of a wide variety of olefinic substrates with the $WCl_2/EtAlCl_2$ catalyst.

Straight-Chain α-Olefins

The first class of substrates examined was α-olefins of varying length. Typical reaction conditions for these experiments include; a toluene solution of W(NPh)[o-$(Me_3SiN)_2C_6H_4$]Cl_2 (**28**) and $EtAlCl_2$ (5-10 equivalents) that is aged (80-100°) for 10 minutes, followed by addition of the olefinic substrate. ^1H NMR spectroscopy and gas chromatography were used to analyze to resulting product mixtures. Table 6-1 contains a compilation of the reaction conditions and product characteristics for a series of straight-chain α-olefin substrates.

Table 6.1. Results from α-olefin dimerization as determined by NMR and GC.

Substrate	Rxn Temp	Product Size	# of Products	Type of Olefin
1-Pentene	80° C	C_{10}	4	Internal, geminal
1-Hexene	90° C	C_{12}	4	Internal, geminal
1-Octene	100° C	C_{16}	4	Internal, geminal
1-Decene	100° C	C_{20}	2, Broad	Internal, geminal
C_{14} α-olefin	100° C	C_{28}	Broad	Internal, geminal

Although exact rates have not been determined for these reactions, the amount of time required for the catalyst to completely consume the initial monomer is consistent throughout the range of substrates presented in Table 6-1. The slight temperature variance from pentene to C_{14} is necessary to obtain similar consumption rates. This small variability was attributed to a greater difficulty in the oxidative coupling of two olefin molecules as the size of the monomer was increased. Support for this argument was gained through the stoichiometric reactions between the $W(IV)L_2$ complex, [W(NPh)(o-$(Me_3SiN)_2C_6H_4)(C_5H_5N)_2$] (**8**) and the olefinic substrates to give the corresponding

W(VI)-metallacyclopentane complexes. It was found that for the larger olefins, slightly longer reaction times and higher temperatures were required to facilitate the formation of the metallacyclic species.

The observed product selectivity (number and type of olefin) for these reactions is consistent with the mechanism involving a metallacycle intermediate that was proposed for the dimerization/codimerization of ethylene and butene earlier in this chapter. In each case, the dimerization reaction resulted in the formation of four olefinic products, which by ^{1}H NMR spectroscopy were determined to be a mixture of internal and geminal olefins. A GC trace and the corresponding NMR spectrum for the dimerization of 1-pentene are presented in Figures 6-20 and 6-21 respectively as representative examples. For 1-decene and C_{14} broad peaks were observed in the corresponding GC traces as a result of the inability of the relatively short column (30 meters) to separate the higher molecular weight products.

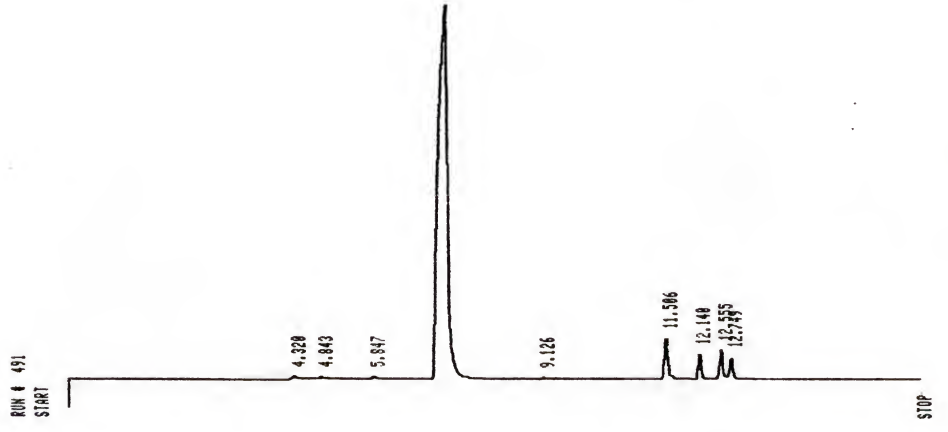

Figure 6-20. GC trace of the product mixture from the dimerization of 1-pentene.

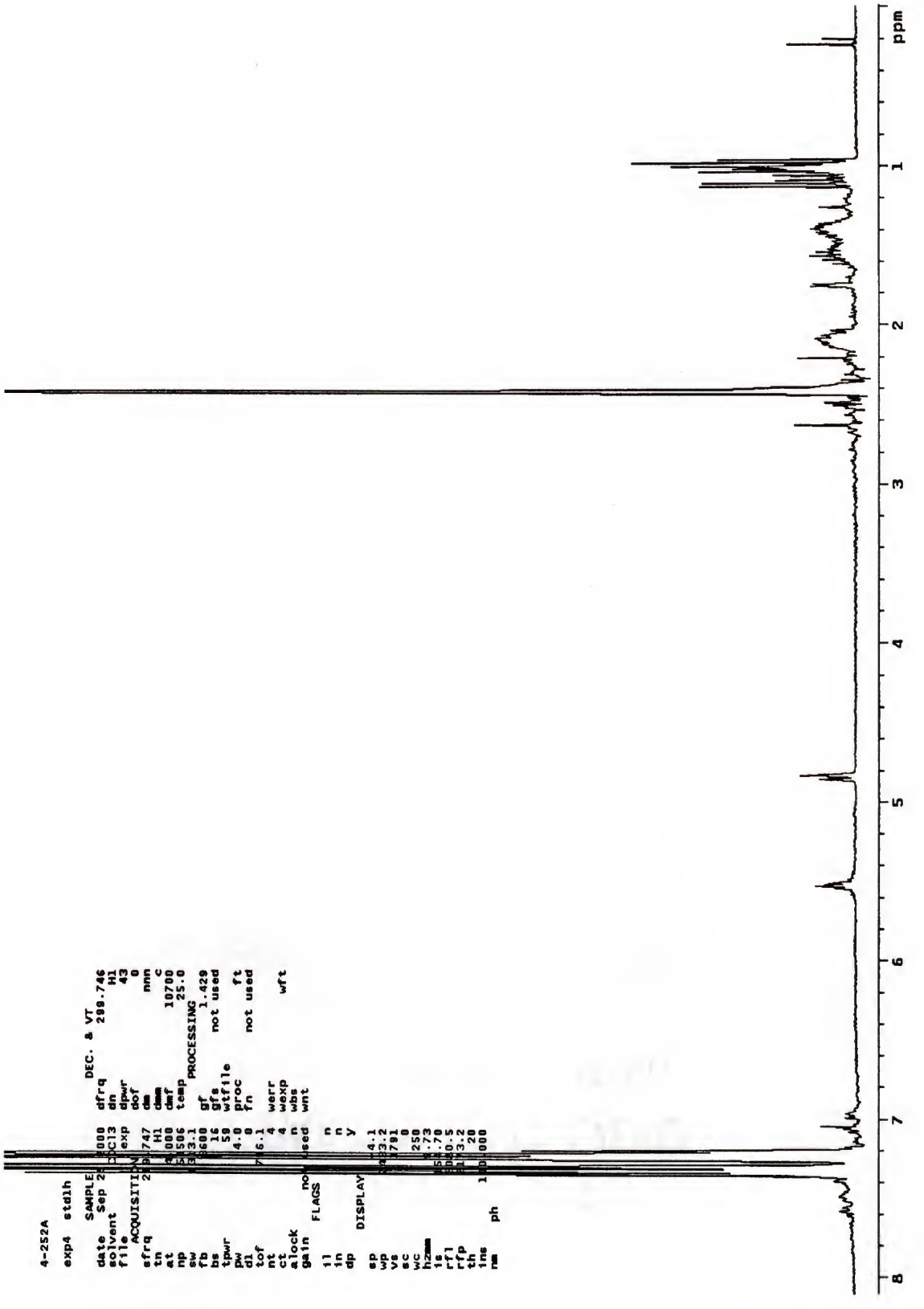

Figure 6-21. ^{1}H NMR spectrum of the pentene dimerization product mixture.

Cyclic Olefins and Dienes as Substrates

Our exploration of this chemistry has also produced results that suggest this catalyst system facilitates the dimerization of cyclic olefins and cyclization of acyclic dienes. Cyclohexene was dimerized in the presence of $WCl_2/EtAlCl_2$ to give a 90:10 mixture of two products. Once again, invoking a mechanism involving the formation of a metallacyclopentane intermediate predicts the observed number of products as shown in Figure 6-22. In addition, the ^1H NMR spectrum of the product mixture is consistent with the suggested exclusive formation of products containing internal carbon-carbon double bonds.

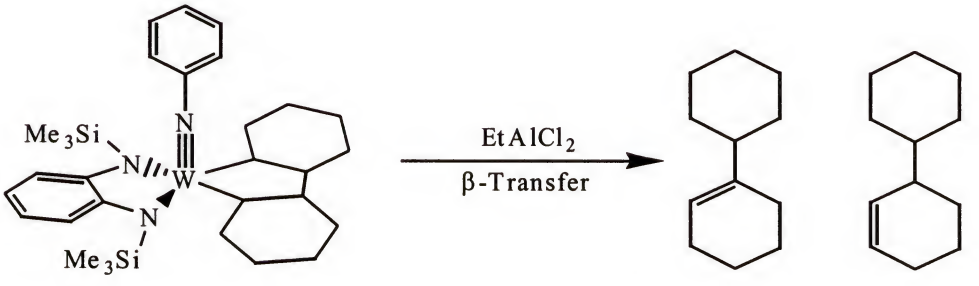

Figure 6-22. Proposed product distribution from the dimerization of cyclohexene.

Addition of excess 1,7-octadiene to a toluene solution containing an activated catalyst mixture produced different results from those observed for each of the other olefinic substrates that have been discussed. The GC trace of the resulting reaction solution displayed five product peaks, which because of their retention times were believed to be of the same molecular weight as the monomer. Subsequent GC analysis of the product mixture with the addition of a 1,7-octadiene spike confirmed this prediction. As expected, the retention times of the products and monomer were virtually identical. To explain this we propose that instead of dimerization, exposure of 1,7-octadiene to the

active dimerization catalyst results in cyclization to yield a series of cyclic olefins. Unfortunately, the exact nature of this product mixture has yet to be determined.

Alkene Oligomerization

The use of synthetic hydrocarbons in the formulation of lubricants, hydraulic fluids, engine oils and as functional fluids in general, has been receiving attention in recent years.[195] In the future, synthetic products will be used increasingly to supplement and replace petroleum-derived fluids. In addition, these synthetic fluids will provide consistently high quality products, which may not be attainable with petroleum-derived fluids due to the fluctuations in the availability and quality of future crude oil supplies.[196]

A large number of catalysts have been used to oligomerize olefins to useful hydrocarbons. In general, these catalysts fall into three categories; cationic, free radical and anionic.[197] Cationic catalysts, such as $AlCl_3$, were reported for the polymerization of olefins derived from the thermal cracking of wax as early as 1931.[198] Similarly, in 1951 Gulf oil described the use of $AlCl_3$ for the oligomerization of 1-octene. Free radical or peroxide initiators were patented by Socony Mobil in 1960.[199] The anionic or coordination complex catalysts include the ethylaluminumsesquichloride/titanium tetrachloride system first developed by Southern in 1961.[200]

We have found that not only is the WCl_2(**28**)/$EtAlCl_2$ system an excellent dimerization catalyst, but upon consumption of the initial monomer, the catalyst facilitates the subsequent dimerization of the product olefins. Although this behavior has been observed with the majority of the monomers described in this chapter, due to limited results regarding this process, this discussion will focus on the oligomerization of 1-hexene.

When a toluene solution of the activated catalyst system and 1-hexene is allowed to proceed, past the point where the majority of hexene has been consumed, new product peaks of greater molecular weight are observed in the GC trace. This suggests two things, first, the WCl_2 based catalyst system can also be applied as an oligomerization catalyst and secondly, that dimerization of internal and geminal olefins is possible. The later is suggested because initial dimerization of 1-hexene produces a mixture of C_{12} internal and geminal product olefins and to obtain these higher molecular weight oligomers requires dimerization of these products. To demonstrate this, dimerization experiments were run with 2-ethyl-1butene (geminal) and 2-hexene (internal) as monomers. At consumption rates comparable to that for linear α-olefins, $WCl_2/EtAlCl_2$ catalyses the dimerization of these substrates to give C_{12} products.

To more closely examine the oligomerization of 1-hexene, a reaction mixture of catalyst and monomer was monitored by GC over a 30-minute interval. The resulting GC traces suggested that upon formation of a significant amount of C_{12} products, subsequent codimerization of these products with 1-hexene results in the formation of several C_{18} products. Further progression of the reaction yielded the formation of what was believed to be C_{30} resulting from the codimerization of the C_{12} and C_{18} products as the amount of 1-hexene available for dimerization became minimal. In addition, a small fraction of products believed to be C_{24} was also observed, resulting from the codimerization of 1-hexene with the C_{18} products. The molecular weights that have been assigned to the products of this reaction are only suggested values based on the proposed mechanism that was discussed for the olefin dimerization reactions. Figure 6-23 displays a GC trace of

the 1-hexene oligomerization mixture as well as a series of equations to illustrate the possible origins of the proposed products.

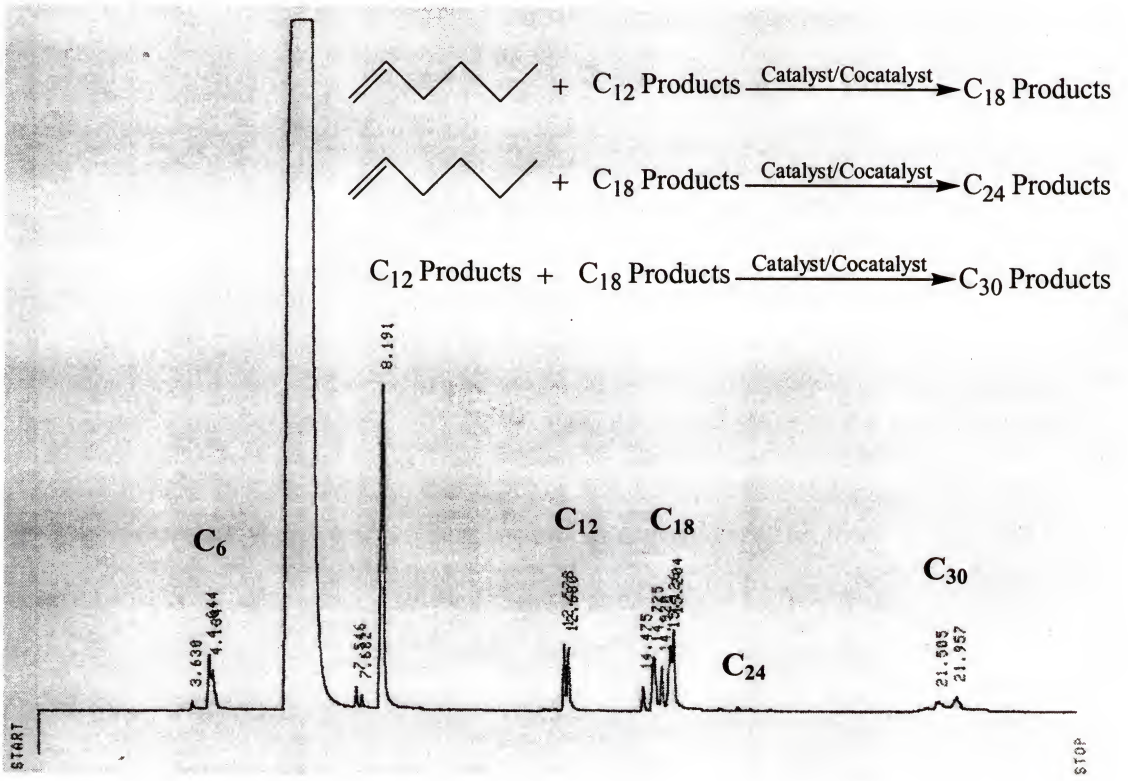

Figure 6-23. WCl_2 catalyzed oligomerization of 1-hexene.

To determine what type of higher oligomers this system was capable of producing, an identical reaction was allowed to proceed for 4 hours. Subsequent removal of the reaction solvent yielded a viscous, oily substance. ^{13}C NMR analysis of the oily product suggested the presence of a high degree of branching in the product olefins, based on the large number of aliphatic carbon resonances present in the spectrum (Figure 6-24). Although this is only an initial observation and much more research is necessary, the possible applications of this catalyst system in the field of highly branched synthetic lubricants are promising.

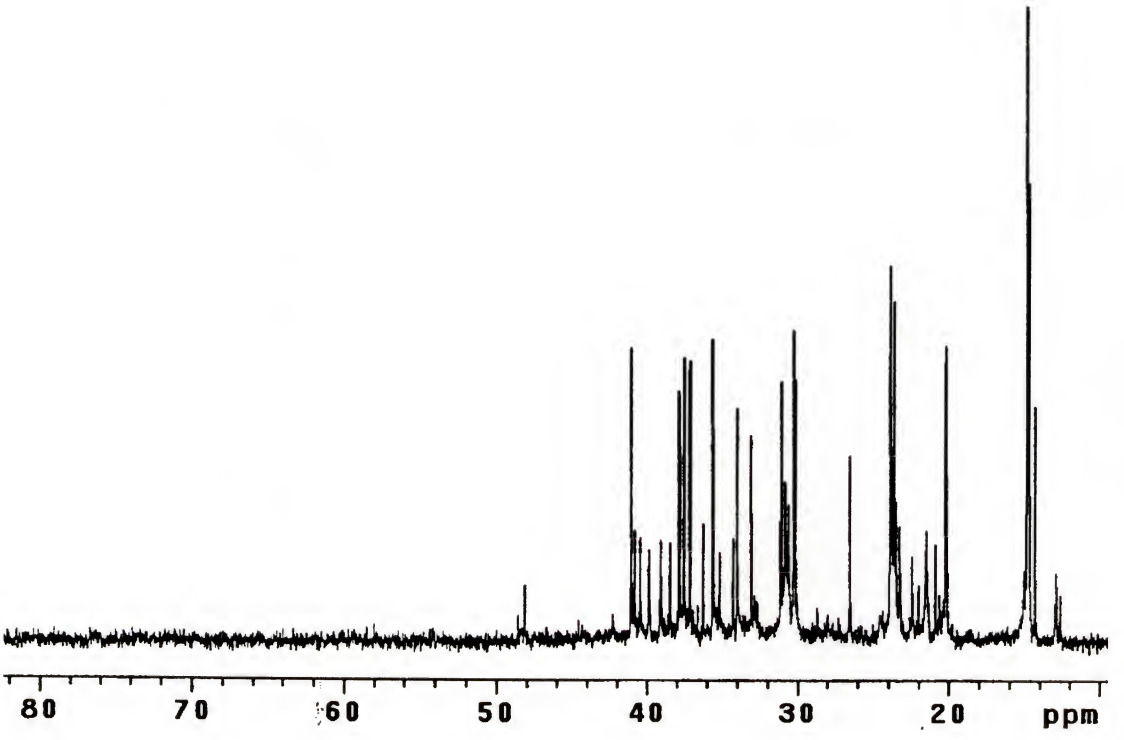

Figure 6-24. The aliphatic region of the ^{13}C NMR spectrum for hexene oligomerization.

Conclusions

In continuation of the oxidative coupling chemistry presented in Chapter 4 we have determined that when activated by Lewis acids, W(NPh)[o-$(Me_3SiN)_2C_6H_4$]Cl_2 (**28**) and W($CH_2CH_2CH_2CH_2$)(NPh)[o-$(Me_3SiN)_2C_6H_4$] (**20**) catalyze the dimerization of a series of olefinic substrates. We have proposed a mechanism to account for the formation of the six observed products from the codimerization of ethylene and butene. This mechanism was applied throughout this discussion to rationalize the similar results that were obtained with other substrates. This mechanism involves the oxidative coupling of two olefin molecules at an unsaturated W(IV) metal center yielding metallacyclic complexes. It is believed that the role of the Lewis acid is to promote

decomposition of the metallacycle through β-hydrogen transfer to yield the product alkenes and reform the intermediate W(IV) complex.

Although we have only just begun to explore this reactivity, several significant observations have been made. First, it has been demonstrated that these catalyst systems will promote the catalytic dimerization of a wide variety of olefinic substrates, including various straight-chain, internal, geminal and cyclic alkenes in addition to 1,7-octadiene. It has also been determined that oligomerization is facilitated upon consumption of the initial monomer and significant formation of product alkenes. The products formed as a result of the oligomerization of 1-hexene demonstrate a high degree of branching as determined by ^{13}C NMR spectroscopy. Therefore, this process may not only be useful in the generation of new organic molecules via dimerization, but also interest may lie in the ability of the catalyst system to generate highly branched oligomers that could have applications as synthetic lubricants.

CHAPTER 7
SUMMARY AND CONCLUSIONS

The research presented in this dissertation has taken a project that was focused on the chemistry of W(VI) complexes and opened many new areas of research involving a variety of both W(VI) and W(IV) chemistries. Even though the focus of this project was significantly changed by the work described in the previous chapters, a single observation can be singled out as the origin. When the bisphenethyl complex, **1** was exposed to a positive pressure of H_2 and the W(IV)-ethylbenzene complex was observed in the product mixture it became apparent that base free W(IV) compounds containing the W(NPh)(o-$(Me_3SiN)_2C_6H_4$) fragment could be synthesized. In the years since, we have developed a highly reactive source of W(IV) and a series of interesting and novel reactions that exploit the propensity of these complexes to achieve a W(VI) oxidation state whenever possible.

Through trial and error we were able to synthesize the W(IV)-arene complexes, W(NPh)(η^4-ethylbenzene)(o-$(Me_3SiN)_2C_6H_6$) (**3**) and W(NPh)(η^4-propylbenzene)(o-$(Me_3SiN)_2C_6H_6$) (**4**) via room temperature hydrogenolysis of the corresponding W(VI)-dialkyl complexes, **1** and **2**. Although these sources of W(IV) displayed only limited reactivity, they did allow the discovery of the highly reactive W(IV)L_2 series of complexes. Subsequently the synthesis of the compounds, W(NPh)(o-$(Me_3SiN)_2C_6H_4)(C_5H_5N)_2$ (**8**) and W(NPh)(o-$(Me_3SiN)_2C_6H_4)(p\text{-}C_6H_7N)_2$ (**9**) was accomplished in a much more efficient manner. Na^o reduction of the W(VI)Cl_2 complex

in the presence of pyridine or 4-picoline afforded these complexes in excellent yield. Some quite unique spectroscopic properties were observed for these complexes. At and even above room temperature the N-donor ligands were found to experience hindered rotation about the W-N bond due to a steric interaction between these ligands and the Me_3Si groups of the diamide ligand.

These results have also presented us with some structural and electronic features that have, until now, gone unnoticed in this system. Following the synthesis and characterization of the W(IV)-arene and W(IV)L_2 complexes we noticed a striking difference in the fold angle of the diamide ligand with respect to previously reported W(VI) complexes. The variability of the fold angle was attributed to the electronic configuration of the metal center (either d^0 or d^2). For d^0 W(VI) complexes, the ligand was significantly folded (*ca.* 50°) resulting from rotation of the N p_π orbitals to maximize overlap with the empty W d_{xy} orbital thereby increasing the overall stabilization of the complex. The opposite was observed for d^2 W(IV) complexes, such as W(NPh)(o-$(Me_3SiN)_2C_6H_4$)(p-$C_6H_7N)_2$ (**9**), where the ligand was flattened (fold angle = 5°) to avoid a destabilizing filled-filled interaction between these orbitals.

Throughout this dissertation this bonding model became a useful tool in understanding the properties of the complexes that were studied. It was found that in all cases, the observed fold angle of the ligand was in good agreement with other structural features of these complexes and has therefore become a means by which the oxidation state of the W metal center could be assessed. For example, the diphenylacetylene complex, **15** displays significant reduction of the acetylene moiety as determined by the W-C and C-C acetylene bond distances obtained from a crystallographic study. The

bonding model predicts that due to significant reduction of the acetylene ligand, the diamide ligand should have a fold angle similar to other W(VI) complexes. In agreement with this proposal, the observed fold angle for this complex was calculated to be 45°. Similar agreement between the W-ligand interaction and the fold angle of the diamide ligand was observed in each case present. Using these observations we were able to make predictions about subsequent reactions that seemed feasible given an understanding of the properties of the starting material. Table 7-1 summarizes the ligand fold angles for the five-coordinate or pseudo-five coordinate complexes discussed in this body of work.

Table 7-1. Summary of diamide ligand fold angles.

Compound	Ligand Fold Angle
$W(VI)R_2$	45-50°
W(IV)(propylbenzene) (**4**)	15°
W(VI) metallacyclopentene (**5**)	45°
$W(IV)(4\text{-picoline})_2$ (**9**)	5°
W(diphenylacetylene) (**15**)	45°
W(2,3-dimethylbutadiene) (**17**)	30°
W(VI) metallathiacycle (**22**)	42°

Time after time the reactions of the $W(IV)L_2$ complexes with various substrates yield products for which the W center had been oxidized from W(IV) to W(VI) making this the defining theme for this dissertation. With unsaturated substrates such as acetylene or butadiene, the metal center accomplished this through reduction of the substrate ligand to yield metallocyclopropene and metallacyclopentene complexes, respectively.

More conventional oxidation was observed for the reactions with thiophenes and olefins. With thiophenes, the W(IV)L_2 complex, W(NPh)(o-$(Me_3SiN)_2C_6H_4$)$(C_5H_5N)_2$ (**8**) achieved a W(VI) oxidation state through the oxidative addition of the carbon-sulfur bond giving a series of metallathiacycle complexes. Oxidation of the W(IV) center was also observed in the reactions of **8** or **9** with olefins, this time through oxidative coupling to give metallacyclopentane complexes. In the course of this research, many other examples that demonstrate the propensity of the W center in this system to achieve a W(VI) oxidation state were observed. Since these reactions represent only initial observations they have been omitted, however, this does not detract from the importance of these findings to the overall understanding of this system, instead it serves to strengthen it.

With the relative ease with which olefins were oxidatively coupled to give W(VI)-metallacyclopentane complexes, it was difficult not to wonder about promoting the reduction of these complexes to give new olefins and regenerate the active W(IV) center to create a catalytic process for the dimerization of olefins. Based on earlier results regarding the inherent stability of these complexes we realized that this would be daunting task.

The break we needed came in the way of a conversation with an individual (Dr. D. E. Hendricksen, Mobil) who had spent many years working in this area. With this advice we were able to facilitate the reverse process, W(VI)-W(IV), through the addition of a strong Lewis acid ($EtAlCl_2$) to the system. With this catalyst system we have been able to facilitate the dimerization and codimerization of a large number of alkenes having various structural features. The possible applications of this system are numerous and

should be a rich area of research for this group for some years. Finally, the development of this catalytic system serves as a satisfying culmination of many hours spent understanding the chemistry of these W(IV) systems.

CHAPTER 8
EXPERIMENTAL PROCEDURES

General Methods

Unless otherwise noted, all procedures were performed using standard Schlenk techniques or in a N_2-filled dry box. Diethyl ether (Et_2O), tetrahydrofuran (THF), pentane, hexanes and toluene were distilled from sodium benzophenone ketyl. After collection, all solvents were stored under argon and over activated molecular sieves. Glassware was oven dried prior to use. All NMR solvents were degassed (freeze-pump-thaw) and stored over activated molecular sieves in the dry box. Due to the sensitive nature of the majority of the complexes presented in this dissertation, all reagents were purified according to the corresponding literature procedures unless otherwise noted.

^{1}H, ^{13}C and ^{31}P NMR spectra were measured at 300MHz on a Varian Gemini 300, VXR 300 or Mercury 300 spectrometer with C_6D_6 and C_7D_8 as solvents. The chemical shifts in the ^{1}H and ^{13}C NMR spectra are reported in parts per million downfield from tetramethylsilane ($\delta = 0$ ppm) and were referenced to residual protons of benzene and toluene in the deuterated solvents. The chemical shifts in the ^{31}P NMR spectra are reported in parts per million and referenced to H_3PO_4 (0 ppm). Gas Chromatography was performed on a Hewlett-Packard 5960 GC instrument, equipped with a 30 m Supelco SPB-1 simulated distillation column. Mass spectrometry was performed by the UF Department of Chemistry Analytical Services.

Synthesis of W(NPh)($CH_2CH_2CH_2Ph$)$_2$(o-(Me_3SiN)$_2C_6H_4$) (**2**)

A diethyl ether solution of W(NPh)(o-(Me_3SiN)$_2C_6H_4$)Cl_2 (2.00g, 3.35mmol) was cooled to -78°C. Two equivalents of 1.95M $PhCH_2CH_2CH_2MgCl$ in Et_2O (3.44mL, 6.70mmol) were added dropwise via syringe. The reaction mixture was allowed to warm to room temperature and stir for 3 hours after which the solvent was removed and the resulting solid dried *in vacuo*. Extraction with pentane (3 X 20mL) followed by removal of the pentane *in vacuo* gave 1.74g (67%) of **2** an orange-brown oil. Mass Spec. Calcd. For ($C_{36}H_{49}N_3Si_2W$) $[M+H]^+$: 764.8121 m/e. Found (FAB): 764.3053 m/e. ^{1}H NMR (C_6D_6): δ 0.27 (s, 18H, $NSiMe_3$), 1.82 (m, 2H, $CH_2CH_2CH_2Ph$), 2.01 (m, 2H, $CH_2CH_2CH_2Ph$), 2.16 (m, 4H, $CH_2CH_2CH_2Ph$), 2.62 (m, 4H, $CH_2CH_2CH_2Ph$), 6.88 (t, 1H, p- W≡NC_6H_5), 7.02 (m, 2H, m-pdaC_6H_4), 7.13 (m, 12H, aromatic), 7.30 (d, 2H, aromatic), 7.35 (m, 2H, o-pdaC_6H_4). ^{13}C NMR (C_6D_6): δ 1.82 ($NSiMe_3$), 35.44 ($CH_2CH_2CH_2Ph$), 43.66 ($CH_2CH_2CH_2Ph$), 65.45 ($CH_2CH_2CH_2Ph$), aromatic: 122.68, 124.62, 125.53, 126.13, 128.81, 129.06, 129.36, 134.65, 143.65, 156.61.

Synthesis of W(NPh)(η^4-ethylbenzene)(o-(Me_3SiN)$_2C_6H_6$) (**3**)

A young's ampoule was charged with W(NPh)(CH_2CH_2Ph)$_2$(o-(Me_3SiN)$_2C_6H_4$) **1** (6.00g, 8.15mmol) and 200mL of toluene. The solution was frozen to allow for evacuation of the ampoule. After warming to room temperature the ampoule was pressurized to 34psi with H_2 and stirred for 7 days. During this time the reaction mixture slowly changed from a dark orange to dark purple color. Removal of the reaction solvent *in vacuo* followed by several washings of the resulting solid with cold $(Me_3Si)_2O$ gave 3.77g (73 %) of **3** as a light brown powder. Mass Spec. Calcd. For $C_{26}H_{37}N_3Si_2W$ $[M+H]^+$: 632.2079 m/e. Found (FAB) 632.2115 m/e. ^{1}H NMR (C_6D_6): δ 0.42 (s, 18H,

$NSiMe_3$), 0.55 (t, 3H, $C_6H_5CH_2CH_3$), 1.67 (q, 2H, $C_6H_5CH_2CH_3$), 4.27 (t, 1H, p-$C_6H_5CH_2CH_3$), 4.65 (d, 2H, o- $C_6H_5CH_2CH_3$), 4.73 (t, 2H, m- $C_6H_5CH_2CH_3$), 6.70 (m, 2H, o-pdaC_6H_4), 6.90 (m, 2H, m-pda), 6.91 (t, 1H, p-W≡NC_6H_5), 6.96 (d, 2H, o-W≡NC_6H_5) 7.10 (t, 2H, m- W≡NC_6H_5). ^{13}C NMR (C_6D_6): δ 4.12 ($NSiMe_3$), 12.30 ($C_6H_5CH_2CH_3$), 27.31 ($C_6H_5CH_2CH_3$), aromatic: 100.57, 101.97, 113.99, 116.63, 117.59, 120.73, 124.61, 129.09, 131.54, 155.35, 158.40.

Synthesis of W(NPh)(η^4-propylbenzene)(o-$(Me_3SiN)_2C_6H_6$) (**4**)

A toluene solution (100mL) of **3** (1.50g, 1.97mmol) was placed in a young's ampoule, frozen and then evacuated. After warming to room temperature the ampoule was charged with H_2 (34psi). The reaction mixture was allowed to stir for 4 days over which time the solution turned from orange to red-purple in color. Stripping off the toluene yielded a dark purple solid, which was dried *in vacuo* for 3 hours. Three washings with cold (0° C) $(Me_3Si)_2O$ (15 mL each) followed by drying *in vacuo* for 6 hours yielded 0.810g (64%) of **4** as a light brown solid. Anal. Calcd. For $[M+H]^+$ 646.2279 m/e. Found (FAB): 646.2271 m/e. ^{1}HNMR (C_6D_6): δ 0.42 (s, 18H, $NSiMe_3$), 0.64 (t, 3H, $C_6H_5CH_2CH_2CH_3$), 1.02 (m, 2H, $C_6H_5CH_2CH_2CH_3$), 1.64 (t, 2H, $C_6H_5CH_2CH_2CH_3$), 4.29 (t, 1H, p- $C_6H_5CH_2CH_2CH_3$), 4.68 (d, 2H, o- $C_6H_5CH_2CH_2CH_3$), 4.74 (t, 2H, m- $C_6H_5CH_2CH_2CH_3$), 6.69 (m, 2H, o-pdaC_6H_4), 6.91 (m, 2H, m-pdaC_6H_4), 6.92 (t, 1H, p-W≡NC_6H_5), 7.00 (d, 2H, o-W≡NC_6H_5), 7.12 (t, 2H, m-W≡NC_6H_5). ^{13}CNMR (C_6D_6): δ 4.53 ($NSiMe_3$), 13.97 ($C_6H_5CH_2CH_2CH_3$), 22.12 ($C_6H_5CH_2CH_2CH_3$), 36.72 ($C_6H_5CH_2CH_2CH_3$), aromatic: 101.52, 102.42, 114.42, 117.05, 117.99, 121.09, 125.01, 129.48, 130.93, 155.70, 158.81.

Synthesis of [o-$(Me_3SiN)_2C_6H_4$)(NPh)$WCH_2C(Ph)=C(Ph)CHPh$] (**5**)

A Young's ampoule was charged with **3** (0.135 g, 0.214 mmol), PhC≡CPh (0.038 g, 0.213 mmol) and toluene (30 mL). The mixture was stirred at 65° C for 18 hours, during which the solution turned red-brown in color. Removal of the reaction solvent *in vacuo* followed by recrystallization of the resulting solid from pentane at –78° C yielded 0.093g (54 %) of **5** as a dark, red-purple solid. Mass Spec. Calcd. For $[M+H]^+$ 807.8376 m/e. Found (FAB) 807.2662 m/e. ^{1}HNMR (C_6D_6): δ 0.24 (s, 9H, $NSiMe_3$), 0.31 (s, 9H, $NSiMe_3$), 2.58 (d, 1H, α-CH_2), 2.81 (d, 1H, α-CH_2), 4.77 (s, 1H, α-CH), 6.55 (m, 2H, aromatic), 6.76-7.16 (aromatic), 7.50 (m, 2H, aromatic). ^{13}CNMR (C_6D_6): δ 2.16 ($NSiMe_3$), 2.36 ($NSiMe_3$), 57.74 (α-CH_2), 73.72 (α-CH), 90.52 (β-C), aromatic: 121.30, 121.66, 122.01, 122.35, 124.28, 124.86, 125.94, 126.52, 127.21, 127.28, 127.81, 128.98, 130.43, 131.11, 132.30, 132.77, 140.67, 141.75, 145.85, 149.13, 150.13, 156.50.

Synthesis of [o-$(Me_3SiN)_2C_6H_4$)(NPh)$WCH_2C(Ph)=C(Ph)CHPh$] (**5**)

From W(NPh)[o-$(Me_3SiN)_2C_6H_6$](CH_2CH_2Ph)(Me) (**7**)

To a young's ampoule was added W(NPh)[o-$(Me_3SiN)_2C_6H_6$](CH_2CH_2Ph)(Me) (0.091 g, 0.141 mmol), PhC≡CPh (0.030 g, 0.168 mmol) and toluene (30 mL). The reaction mixture is stirred at 70° C for 21 hours, during which the solution becomes red-brown in color. Removal of the toluene and subsequent recrystallization from pentane produced 0.075 g (70 %) of **5** as a red-purple solid.

Synthesis of W(NPh)[o-$(Me_3SiN)_2C_6H_4$](CH_2CH_2Ph)Cl (**6**)

W(NPh)[o-$(Me_3SiN)_2C_6H_4$]Cl_2 (2.50 g, 4.19 mmol) was dissolved in Et_2O and cooled to -78° C. One equivalent of $PhCH_2CH_2MgCl$ (2.09 mL, 4.19 mmol) was added dropwise by syringe. The mixture was allowed to warm to room temperature and stir for 2 hrs, during which time the solution turned bright orange in color and a light brown precipitate formed. The reaction solvent was removed under reduced pressure and the resulting orange solid dried *in vacuo* for 1 hr. Subsequent extraction with several portions of cold pentane (0° C) followed by concentration and cooling of the filtrate (-78° C) produced bright orange crystals. The solid was collected via filtration and dried *in vacuo* to yield 1.67 g (60 %) of **(6)** as an orange crystalline solid. Anal. Calcd. For $C_{26}H_{36}N_3Si_2W$: C 46.89, H 5.45, N 6.31. Found: C 46.55, H 5.22, N 6.11. ^1H NMR (C_6D_6, 25° C): δ 0.26 (s, 9H, $Si(CH_3)_3$), 0.44 (s, 9H, $Si(CH_3)_3$), 2.19 (m, 1H, $C\underline{H}_2CH_2Ph$), 2.58 (m, 1H, CH_2CH_2Ph), 2.76 (m, 1H, CH_2CH_2Ph), 2.93 (m, 1H, CH_2CH_2Ph), 6.77 (t, 1H, p-$W{\equiv}NC_6H_5$), 6.94-7.33 (m, 13H, aromatic). ^{13}C NMR (C_6D_6, 25° C): δ 0.77 ($Si(CH_3)_3$), 1.56 ($Si(CH_3)_3$), 38.48 (CH_2CH_2Ph), 62.29 (CH_2CH_2Ph), aromatic: 121.37, 122.14, 124.05, 125.55, 126.03, 126.98, 127.35, 128.25, 128.31, 128.49, 132.36, 135.84, 148.36, 155.64.

Synthesis of W(NPh)[o-$(Me_3SiN)_2C_6H_4$](CH_2CH_2Ph)Me (**7**)

W(NPh)[o-$(Me_3SiN)_2C_6H_4$](CH_2CH_2Ph)Cl (**6**) (0.40 g, 0.60 mmol) was dissolved in Et_2O and cooled to -78° C. One equivalent of MeMgI (0.20 mL, 0.60 mmol) was added dropwise by syringe. The mixture was allowed to warm to room temperature and stir for 2 hrs, during which time the solution turned red-orange in color and a light brown precipitate formed. The reaction solvent was removed under reduced pressure and the

resulting orange solid dried *in vacuo* for 1 hr. Subsequent extraction with several portions of pentane followed by solvent removal and drying *in vacuo* yielded 0.30 g (77 %) of (**7**) as a orange-brown solid. Mass Spec. Calcd. For $C_{27}H_{40}N_3Si_2W$ $[M + H]^+$: 646.2279 m/e. Found (FAB): 646.2271 m/e. ^1H NMR (C_6D_6, 25° C): δ 0.30 (s, 18H, $Si(CH_3)_3$), 1.22 (s, 3H, CH_3), 2.20 (m, 1H, CH_2CH_2Ph), 2.48 (m, 2H, CH_2CH_2Ph), 2.82 (m, 1H, CH_2CH_2Ph), 6.86 (t, 1H, p-$W{\equiv}NC_6H_5$), 7.02-7.41 (m, 13H, aromatic).

Synthesis of $W(NPh)(o\text{-}(Me_3SiN)_2C_6H_4)(C_5H_5N)_2$ (**8**)

Pyridine (0.13 mL, 1.57 mmol) was added dropwise to a room temperature toluene solution of $W(NPh)(\eta^4\text{-propylbenzene})(o\text{-}(Me_3SiN)_2C_6H_6)$ (**4**) (0.51 g, 0.79 mmol). Upon addition of pyridine the solution became dark purple in color. The mixture was stirred for 1 hr at which time the solvent was stripped off and the resulting solid dried *in vacuo* for 1 hr. Subsequent washing with several portions of cold pentane (0° C), followed by drying the remaining solid *in vacuo*, yielded 0.39 g (73 %) of **8** as a dark purple solid. ^1H NMR (25° C, C_6D_6): δ 0.45 (s, 18H, $SiMe_3$), 4.97 (t, 2H, p-C_5H_5N), 5.71 (d, 2H, o-C_5H_5N), 6.28 (t, 4H, m-C_5H_5N), 6.90 (m, 1H, p-$W{\equiv}NC_6H_5$), 7.03 (m, 2H, o-pdaC_6H_4), 7.10-7.12 (m, 4H, o,m-$W{\equiv}NC_6H_5$), 7.41 (m, 2H, m-pdaC_6H_4), 7.82 (d, 2H, o-C_5H_5N). ^{13}C NMR (25° C, C_6D_6): δ 5.58 ($SiMe_3$), 118.64 (o-pdaC_6H_4), 118.66 (m-pdaC_6H_4), 121.62 (m-C_5H_5N), 122.17 (m-C_5H_5N), 124.23 (p-$W{\equiv}NC_6H_5$), 124.65 (o-$W{\equiv}NC_6H_5$), 127.75 (m-$W{\equiv}NC_6H_5$), 129.40 (p-C_5H_5N), 137.91 (o-C_5H_5N), 142.14 (o-C_5H_5N), 152.08 (pda C_6H_4), 158.76 ($W{\equiv}NC_6H_5$).

Synthesis of **8** From W(NPh)(o-$(Me_3SiN)_2C_6H_4$)Cl_2

To a dispersion of Na° (0.17 g, 7.24 mmol) in THF was added a THF solution of W(NPh)(o-$(Me_3SiN)_2C_6H_4$)Cl_2 (2.16 g, 3.62 mmol) and pyridine (0.88 mL, 10.09 mmol) at room temperature. The mixture was stirred for 30 min, during which time the solution changes from bright to dark purple in color. The solvent was removed under reduced pressure and the resulting solid extracted with toluene. Subsequent evaporation of the toluene and drying *in vacuo* gave 2.25 g (91 %) of **8**.

Synthesis of W(NPh)(o-$(Me_3SiN)_2C_6H_4$)(p-$C_6H_7N)_2$ (**9**)

4-Picoline (0.07 mL, 0.77 mmol) was added drop wise to a room temperature toluene solution of W(NPh)(η^4-propylbenzene)(o-$(Me_3SiN)_2C_6H_6$) (**4**) (0.25 g, 0.39 mmol). Upon addition of 4-picoline, the solution became dark purple in color. The mixture was stirred for 1 hr at which time the solvent was stripped off and the resulting solid dried *in vacuo* for 1 hr. Subsequent washing with several portions of cold pentane (0° C), followed by drying the remaining solid *in vacuo*, yielded 0.20 g (73 %) of **9** as a dark purple solid. ^{1}H NMR (C_6D_6, 25° C): δ 0.50 (s, 18H, $SiMe_3$), 2.37 (s, 3H, C_6H_7N), 5.78 (d, 2H, o-C_6H_7N), 6.28 (t, 4H, m-C_6H_7N), 6.93 (m, 1H, p-W≡NC_6H_5), 7.07 (m, 2H, o-pdaC_6H_4), 7.10-7.14 (m, 4H, o,m-W≡NC_6H_5), 7.48 (m, 2H, m-pdaC_6H_4), 7.88 (d, 2H, o-C_6H_7N). ^{13}C NMR (C_6D_6, 25° C): δ 5.79 ($SiMe_3$), 17.75 (p-CH_3(C_6H_7N)), aromatic: 118.51, 118.64, 123.84, 124.52, 126.52, 128.02, 128.89, 129.66, 138.31, 141.13, 142.26, 152.88, 159.29.

Synthesis of **9** From W(NPh)(o-$(Me_3SiN)_2C_6H_4$)Cl_2

To a dispersion of Na° (0.16 g, 7.24 mmol) in THF was added a THF solution of W(NPh)(o-$(Me_3SiN)_2C_6H_4$)Cl_2 (2.14 g, 3.62 mmol) and 4-picoline (0.88 mL, 10.09 mmol) at room temperature. The mixture was stirred for 30 min, during which time the solution changes from bright to dark purple in color. The solvent was removed under reduced pressure and the resulting solid extracted with toluene. Subsequent evaporation of the toluene and drying *in vacuo* gave 2.41 g (93 %) of **9**.

Synthesis of W(NPh)(o-$(Me_3SiN)_2C_6H_4$)$(C_9H_7N)_2$ (**10**)

Quinoline (0.09 mL, 0.77 mmol) was added drop wise to a room temperature toluene solution of W(NPh)(η^4-propylbenzene)(o-$(Me_3SiN)_2C_6H_6$) (**4**) (0.25 g, 0.39 mmol). Upon addition of quinoline, the solution became turquoise in color. The mixture was stirred for 1 hr at which time the solvent was stripped off and the resulting solid dried *in vacuo* for 1 hr. Subsequent washing with several portions of cold pentane (0° C), followed by drying the remaining solid *in vacuo*, yielded 0.19 g (63 %) of **10** as a black solid. ^{1}H NMR (25° C, C_6D_6): δ 0.38 (s, 18H, $SiMe_3$), 5.00 (d, 2H, C_9H_7N), 5.55 (d, 2H, C_9H_7N), 6.38 (m, 2H, C_9H_7N), 6.49 (m, 2H, C_9H_7N), 6.76 (m, 4H, C_9H_7N), 6.97 (m, 1H, p-W≡NC_6H_5), 7.05 (m, 2H, o-pdaC_6H_4), 7.25 (m, 2H, m-W≡NC_6H_5), 7.39 (m, 2H, m-pdaC_6H_4), 7.51 (d, 2H, o-W≡NC_6H_5), 8.91 (d, 2H, C_9H_7N). ^{13}C NMR (25° C, C_6D_6): δ 5.49 ($SiMe_3$), aromatic: 116.08, 118.64, 118.85, 125.05, 125.17, 125.33, 125.95, 126.40, 129.66, 129.81, 131.29, 135.48, 142.90, 150.20.

Synthesis of W(NPh)(o-$(Me_3SiN)_2C_6H_4$)Ph_2 (**11**)

W(NPh)(o-$(Me_3SiN)_2C_6H_4$)Cl_2 (1.0 g, 1.68 mmol) was dissolved in 50 mL of Et_2O and cooled to -78° C. Two equivalents of PhMgCl (1.12 mL, 3.36 mmol) was then added by syringe. The reaction was allowed to warm to room temperature and stir for 2 hours, during which time the solution became brown in color and a precipitate formed. The solvent was then removed under reduced pressure and the remaining brown-orange solid dried *in vacuo*. The solid was then extracted with pentane and filtered until the filtrate was clear. The solution was concentrated to 10 mL and cooled to -78° C for three hours. The resulting orange solid was isolated by filtration and dried *in vacuo* to yield 0.77 g (68 %) of **11** as an orange crystalline solid. ^{1}H NMR (25° C, C_6D_6): δ 0.12 (s, 18H, $SiMe_3$), 6.80-7.66 (m, 19H, aromatic). ^{13}C NMR (25° C, C_6D_6): δ 0.72 ($SiMe_3$), aromatic: 123.14, 124.93, 125.69, 125.80, 128.18, 129.09, 131.67, 136.71, 156.25, 196.30. Anal. Calc'd for $C_{32}H_{41}N_3Si_2W$: C, 54.31; H, 5.84; N, 5.94. Found: C, 53.98; H, 5.61; N, 5.69.

Synthesis of W(NPh)(o-$(Me_3SiN)_2C_6H_4$)$(C_5H_5N)_2$(CO) (**12a**)

An ampoule, fitted with a teflon valve was charged with W(NPh)(o-$(Me_3SiN)_2C_6H_4$)$(C_5H_5N)_2$ (**8**) (0.20 g, 0.29 mmol) and toluene (40 mL). The mixture was frozen in liq. N_2 and the flask evacuated. Upon warming to room temperature, the flask was charged with CO (20 psi). The solution immediately turned brown in color. After stirring at room temperature for 30 minutes, the reaction solvent was removed and the resulting solid was dried *in vacuo* for 3 hours to give 0.13 g (65 %) of **12a** as a dark brown crystalline solid. ^{1}H NMR (C_6D_6, 25° C): δ 0.35 (s, 9H, $SiMe_3$), 0.37 (s, 9H, $SiMe_3$), 6.26 (t, 4H, m-C_5H_5N), 6.46 (t, 2H, p-C_5H_5N), 6.65 (m, 2H, o-pdaC_6H_4), 6.86-

7.10 (m, 5H, aromatic), 7.29 (d, 2H, o-W≡NC$_6$H$_5$), 8.77 (d, 4H, m-C$_5$H$_5$N). ^{13}C NMR (C$_6$D$_6$, 25° C): δ 3.79 (SiMe$_3$), 4.20 (SiMe$_3$), aromatic: 115.62, 118.60, 119.16, 121.01, 124.02, 124.31, 125.03, 126.02, 129.63, 137.08, 149.73, 150.64, 154.03, 158.57, 281.05 (C≡O). IR ν_{CO} = 1889 cm^{-1}.

Synthesis of W(NPh)(o-(Me$_3$SiN)$_2$C$_6$H$_4$)(C$_6$H$_7$N)$_2$(CO) (**12b**)

Following the procedure used for the synthesis of **12a**, W(NPh)(o-(Me$_3$SiN)$_2$C$_6$H$_4$)(p-C$_6$H$_7$N)$_2$ (**9**) (0.75 g, 1.05 mmol) was exposed to a positive pressure (20 psi) of C≡O. Compound **12b** (0.58 g, 76 %) was isolated as a dark brown crystalline solid. ^{1}H NMR (C$_6$D$_6$, 25° C): δ 0.41 (s, 9H, SiMe$_3$), 0.45 (s, 9H, SiMe$_3$), 1.47 (s, 3H, C$_6$H$_7$N), 6.17 (d, 4H, C$_6$H$_7$N), 6.65 (m, 2H, o-pdaC$_6$H$_4$), 6.88 (t, 1H, p-W≡NC$_6$H$_5$), 6.94-7.13 (m, 6H, aromatic), 7.34 (d, 2H, o-W≡NC$_6$H$_5$), 8.77 (d, 4H, C$_6$H$_7$N). ^{13}C NMR (C$_6$D$_6$, 25° C): δ 3.89 (SiMe$_3$), 4.29 (SiMe$_3$), 20.44 (C$_6$H$_7$N), aromatic: 115.53, 118.62, 119.16, 121.00, 124.07, 124.91, 125.20, 126.02, 129.60, 138.22, 149.25, 149.95, 150.87, 153.64, 158.84 283.91 (C≡O). IR ν_{CO} = 1878 cm^{-1}.

Synthesis of W(NPh)(o-(Me$_3$SiN)$_2$C$_6$H$_4$)(C$_5$H$_5$N)(PMe$_3$)(CO) (**13a**)

W(NPh)(o-(Me$_3$SiN)$_2$C$_6$H$_4$)(C$_5$H$_5$N)$_2$(CO) (**12a**) (0.30 g, 0.42 mmol) was dissolved in pentane at room temperature and to the resulting solution was added PMe$_3$ (0.04 mL, 0.42 mmol). The solution was allowed to stir at room temperature for 30 min. The reaction solvent was removed and the resulting solid was dried *in vacuo* to give **13a** (0.22 g, 74 %) as a dark brown solid. ^{1}H NMR (C$_6$D$_6$, 25° C): δ 0.21 (s, 9H, SiMe$_3$), 0.30 (s, 9H, SiMe$_3$), 0.97 (d, 9H, PMe$_3$, ^{2}J$_{P-H}$ = 9.0 Hz), 6.38 (t, 2H, m-C$_5$H$_5$N), 6.80-7.12 (m, 8H, aromatic), 7.24 (d, 2H, o-W≡NC$_6$H$_5$), 8.70 (d, 2H, m-C$_5$H$_5$N). ^{13}C NMR

(C_6D_6, 25° C): δ 3.15 ($SiMe_3$), 3.70 ($SiMe_3$), 16.65 (PMe_3, $^1J_{P-C}$ = 28.4 Hz), aromatic: 114.98, 118.44, 118.52, 121.26, 122.99, 123.23, 123.82, 129.08, 137.20, 151.70, 271.50 (C≡O). ^{31}P NMR (C_6D_6, 25° C): δ -10.76 (PMe_3, $^1J_{W-P}$ = 188.8 Hz).

IR ν_{CO} = 1905 cm^{-1}.

Synthesis of W(NPh)(o-$(Me_3SiN)_2C_6H_4$)(C_6H_7N)(PMe_3)(CO) (**13b**)

Following the procedure used for the synthesis of **13a**, W(NPh)(o-$(Me_3SiN)_2C_6H_4$)(p-$C_6H_7N)_2$(CO) (**12a**) (0.25 g, 0.34 mmol) was reacted with PMe_3 (0.04 mL, 0.34 mmol) at room temperature. Compound **13b** (0.21 g, 87 %) was isolated as a dark-brown crystalline solid. ^1H NMR (C_6D_6, 25° C): δ 0.25 (s, 9H, $SiMe_3$), 0.34 (s, 9H, $SiMe_3$), 0.99 (d, 9H, PMe_3, $^2J_{P-H}$ = 9.3 Hz), 1.53 (s, 3H, C_6H_7N), 6.29 (d, 2H, C_6H_7N), 6.74-7.05 (m, 7H, aromatic), 7.26 (d, 2H, o-W≡NC_6H_5), 8.63 (d, 2H, C_6H_7N). ^{13}C NMR (C_6D_6, 25° C): δ 3.69 ($SiMe_3$), 4.25 ($SiMe_3$), 17.00 (PMe_3, $^1J_{P-C}$ = 27.9 Hz), 20.66 (C_6H_7N), aromatic: 115.42, 118.91, 119.00, 121.74, 123.52, 123.64, 124.96, 125.42, 129.56, 151.86, 158.79, 273.20 (C≡O). ^{31}P NMR (C_6D_6, 25° C): δ -10.71 (PMe_3, $^1J_{W-P}$ = 188.0 Hz). IR ν_{CO} = 1903 cm^{-1}.

Synthesis of W(NPh)(o-$(Me_3SiN)_2C_6H_4$)(C_5H_5N)(PMe_3)$_2$ (**14a**)

W(NPh)(o-$(Me_3SiN)_2C_6H_4$)($C_5H_5N)_2$ (**8**) (0.20 g, 0.29 mmol) was placed in a Schlenk tube and dissolved in toluene (40 mL). To this solution was added 2 eq. of PMe_3 (0.06 mL, 0.59 mmol) at room temperature. An immediate color change from purple to dark brown was observed. The mixture was stirred at room temperature for 30 minutes, at which time the reaction solvent was removed and the resulting brown solid was dried *in vacuo*. Compound **14a** (0.15 g, 67 %) was isolated as a dark brown crystalline solid.

^{1}H NMR (C_6D_6, 25° C): δ 0.13 (s, 9H, $SiMe_3$), 0.19 (s, 9H, $SiMe_3$), 1.10 (d, 9H, PMe_3, $^2J_{P-H}$ = 7.8 Hz), 1.43 (d, 9H, PMe_3, $^2J_{P-H}$ = 6.3 Hz), 6.40 (t, 1H, C_5H_5N), 6.51 (t, 1H, C_5H_5N), 6.70-7.10 (m, 8H, aromatic), 7.32 (d, 2H, o-W≡NC_6H_5), 8.52 (d, 1H, C_5H_5N), 8.79 (d, 1H, C_5H_5N). ^{13}C NMR (C_6D_6, 25° C): δ 4.16 ($SiMe_3$), 6.22 ($SiMe_3$), 22.39 (PMe_3, $^1J_{P-C}$ = 24.5 Hz), 26.26 (PMe_3, $^1J_{P-C}$ = 22.4 Hz), aromatic: 113.96, 118.66, 118.85, 121.56, 122.02, 125.07, 129.36, 136.40, 152.23, 153.59, 155.62, 160.24. ^{31}P NMR (C_6D_6, 25° C): δ -40.31 (PMe_3, $^1J_{W-P}$ = 157.9 Hz, $^2J_{P-P}$ = 10.0 Hz), -24.09 (PMe_3, $^1J_{W-P}$ = 190.0 Hz, $^2J_{P-P}$ = 10.0 Hz).

Synthesis of W(NPh)(o-$(Me_3SiN)_2C_6H_4$)(C_6H_7N)(PMe_3)$_2$ (**14b**)

Following the procedure used for the synthesis of **14a**, W(NPh)(o-$(Me_3SiN)_2C_6H_4$)(p-C_6H_7N)$_2$ (**9**) (0.20 g, 0.28 mmol) was reacted with PMe_3 (0.06 mL, 0.56 mmol). Compound **14b** (0.19 g, 86 %) was isolated as a dark brown crystalline solid. ^{1}H NMR (C_6D_6, 25° C): δ 0.17 (s, 9H, $SiMe_3$), 0.24 (s, 9H, $SiMe_3$), 1.11 (d, 9H, PMe_3, $^2J_{P-H}$ = 8.1 Hz), 1.46 (d, 9H, PMe_3, $^2J_{P-H}$ = 6.3 Hz), 1.83 (s, 3H, C_6H_7N), 6.24 (d, 1H, C_6H_7N), 6.69 (d, 1H, C_6H_7N), 6.76 (t, 1H, p-W≡NC_6H_5), 6.85-7.10 (m, 6H, aromatic), 8.51 (d, 1H, C_6H_7N), 8.72 (d, 1H, C_6H_7N). ^{13}C NMR (C_6D_6, 25° C): δ 4.20 ($SiMe_3$), 6.28 ($SiMe_3$), 20.14 (C_6H_7N), 22.72 (PMe_3, $^1J_{P-C}$ = 24.2 Hz), 26.25 (PMe_3, $^1J_{P-C}$ = 22.4 Hz), aromatic: 113.90, 118.64, 118.87, 121.50, 122.04, 125.11, 129.37, 152.137, 153.49, 155.79, 160.43. ^{31}P NMR (C_6D_6, 25° C): δ -39.93 (PMe_3, $^1J_{W-P}$ = 159.0 Hz, $^2J_{P-P}$ = 10.0 Hz), -24.09 (PMe_3, $^1J_{W-P}$ = 192.5 Hz, $^2J_{P-P}$ = 10.0 Hz).

Synthesis of W(NPh)(o-$(Me_3SiN)_2C_6H_4$)(PhC≡CPh) (**15**)

A Young's ampoule was charged with W(NPh)(o-$(Me_3SiN)_2C_6H_4$)$(C_5H_5N)_2$ (**8**) (0.50 g, 0.731 mmol) and diphenylacetylene (0.13 g, 0.731 mmol). The mixture was dissolved in toluene and heated at 55° C for 4 hrs, during which time the solution became yellow brown in color. Removal of the reaction solvent followed by extraction with pentane yielded a dark yellow solution from which the solvent was removed and the resulting solid dried *in vacuo* to yield 0.35 g (68%) of (**15**) as a dark brown solid. Mass Spec. Calcd. for $C_{32}H_{38}N_3Si_2W$ $[M + H]^+$: 704.2111 m/e. Found (FAB): 704.2114 m/e. ^1H NMR (C_6D_6, 25° C): δ 0.41 (s, 18H, Me_3Si), 6.81 (t, 1H, p-W≡NC_6H_5), 6.97 (m, 4H, o,m-W≡NC_6H_5), 7.11 (m, 5H, aromatic), 7.25 (m, 2H, o-pdaC_6H_4), 7.36 (m, 5H, aromatic) 7.51 (m, 2H, m-pdaC_6H_4). ^{13}C NMR (25° C, C_6D_6): δ 2.38 ($SiMe_3$), aromatic 123.33, 124.70, 125.67, 128.89, 129.01, 129.16, 129.61, 130.09, 132.32, 143.10, 198.54 (C≡C).

Reaction of **15** With H_2 to make **16**

In an NMR tube equipped with a Young valve, a small sample of **15** was dissolved in C_6D_6. The resulting solution was frozen and the NMR tube was evacuated. Upon warming to room temperature, the Tube was charged with 34 psi of H_2. After standing at room temperature for ~10 hours the solution has changed to an orange-brown color. The conversion of **15** to **16** was confirmed by ^1H NMR spectroscopy.

Synthesis of W(NPh)[o-$(Me_3SiN)_2C_6H_4$][η^4-$(CH_2=C(CH_3)C(CH_3)=CH_2)$] (**17**)

To a toluene solution of W(NPh)(o-$(Me_3SiN)_2C_6H_4$)$(C_5H_5N)_2$ (**8**) (1.00 g, 1.46 mmol) was added 2,3-dimethyl-1,3-butadiene (0.17 mL, 1.46 mmol). The mixture was

heated at 60° C for 20 hrs, during which time the solution became red-brown in color. Removal of the toluene under reduced pressure yield a brown sticky solid, which was extracted with several portions of pentane. The pentane was removed under reduced pressure and the resulting dark solid dried *in vacuo* for 3hrs to give 0.65 g (73%) of (**17**). Mass Spec. Calcd. for $C_{24}H_{38}N_3Si_2W$ $[M + H]^+$: 608.2114 m/e. Found: 608.2114 m/e. ^1H NMR (C_6D_6, 25° C) δ 0.37 (s, 18H, Me_3Si), 1.24 (s, 6H, diene-CH_3), 1.31 (d, 2H, α-CH_2, $J_{H,H'}$ = 8.5 Hz), 2.17 (d, 2H, α-CH_2, $J_{H,H'}$ = 8.5 Hz), 6.85 (m, 3H, aromatic), 7.12-7.20 (m, 4H, aromatic), 7.33 (d, 2H, aromatic). ^{13}C NMR (C_6D_6, 25° C) δ 2.45 (Me_3Si), 18.65 (butadiene CH_3), 50.53 (α-CH_2, $^1J_{C-H}$ = 143 Hz), 120.15 (β-C), aromatic: 120.48, 121.02, 125.33, 127.54, 128.78, 150.08.

Synthesis of W(NPh)[o-$(Me_3SiN)_2C_6H_4$](η^4-$(CH_2{=}CHCH{=}CH_2)$ (**18**)

W(NPh)(o-$(Me_3SiN)_2C_6H_4$)$(C_5H_5N)_2$ (**8**) (1.00 g, 1.46 mmol) was dissolved in toluene and placed in a Young's ampoule. The solution was then frozen and the flask evacuated. Upon warming to room temperature, the flask was charged with 1,3-butadiene (20 psi). The solution was stirred at room temperature for 45 min, during which time the color changed from purple to red-brown. Removal of the reaction solvent followed by drying the resulting solid *in vacuo* for 3 hrs yielded 0.80 g (93 %) of (**18**) as a dark brown solid. Mass Spec. Calcd. For $C_{22}H_{34}N_3Si_2W$ $[M + H]^+$: 580.1801 m/e. Found (FAB): 580.1801 m/e. ^1H NMR (C_6D_6, 25° C): δ 0.37 (s, 18H, Me_3Si), 4.59 (m, 2H, β-CH's, $^3J_{H\text{-}H(cis)}$ = 5.1 Hz, $^3J_{H\text{-}H(trans)}$ = 1.8 Hz), 6.86-7.13 (m, 9H, aromatic), 7.20 (d, 2H, α-CH_2), 7.32 (d, 2H, α-CH_2). ^{13}C NMR (C_6D_6, 25° C): δ 2.15 (Me_3Si), 43.83 (α-CH_2, $^1J_{C-H}$ = 149

Hz), 116.90 (β-CH, $^1J_{C-H}$ = 164 Hz), aromatic: 118.45, 121.94, 125.62, 127.36, 128.90, 129.66, 151.66.

Synthesis of W[OC(CH$_3$)$_2$CH$_2$C(CH$_3$)C(CH$_3$)CH$_2$](NPh)[o-(Me$_3$SiN)$_2$C$_6$H$_4$] (**19**)

W(NPh)(o-(Me$_3$SiN)$_2$C$_6$H$_4$)(C$_5$H$_5$N)$_2$ (**8**) (0.15 g, 0.25 mmol) was dissolved in toluene at room temperature. Acetone (0.02 mL, 0.25 mmol) was added and the resulting solution was stirred at room temperature for 5 hrs. During this time the solution changed from brown to red in color. Removal of the reaction solvent under reduced pressure yielded a red-brown solid that was washed with several portions of cold (0° C) pentane. The resulting solid was dried *in vacuo* to give 0.102 g (61%) as a dark red solid. ^{1}H NMR (C$_6$D$_6$, 25° C): δ 0.38 (s, 9H, SiMe$_3$), 0.48 (s, 9H, SiMe$_3$), 1.19 (s, 3H, C(CH$_3$)), 1.24 (d, 1H, γ-CH$_2$), 1.28, (s, 3H, C(CH$_3$)), 1.59 (s, 3H, C(CH$_3$)$_2$), 1.67 (s, 3H, C(CH$_3$)$_2$), 1.83 (d, 1H, γ-CH$_2$), 2.54 (d, 1H, α-CH$_2$), 3.02 (d, 1H, α-CH$_2$), 6.71-7.20 (m, 9H, aromatic).

Synthesis of W(CH$_2$CH$_2$CH$_2$CH$_2$)(NPh)[o-(Me$_3$SiN)$_2$C$_6$H$_4$] (**20**)

W(NPh)(o-(Me$_3$SiN)$_2$C$_6$H$_4$)(C$_5$H$_5$N)$_2$ (**8**) (0.535 g, 0.78 mmol) was placed in a Young's ampoule and dissolved in toluene. The sample was frozen and the flask evacuated. Upon warming to room temperature, the flask was pressurized with ethylene (20 psi). An immediate color change from purple to orange was observed. The reaction was stirred at room temperature for an additional 30 min, during which time the solution became yellow-brown in color. Removal of the reaction solvent *in vacuo* yielded a brown sticky solid. Subsequent extraction with several portions of pentane followed by solvent evaporation under reduced pressure yielded 0.300 g (66 %) of (**20**) as a yellow-

brown solid. Anal. Calcd. For $C_{22}H_{35}N_3Si_2W$: C 45.43, H 6.07, N 7.23. Found: C 45.19, H5.97, N 7.03. ^1H NMR (C_6D_6, 25° C): δ 0.28 (s, 18H, $NSiMe_3$), 1.54 (m, 2H, β-CH), 2.42 (m, 2H, β-CH'), 2.91 (m, 2H, α-CH), 2.93 (m, 2H, α-CH'), 6.86-7.44 (m, 9H, aromatic). ^{13}C NMR (C_6D_6, 25° C): δ 1.08 ($NSiMe_3$), 35.23 (β-C), 61.25 (α-C).

Synthesis of W(NPh)(o-$(Me_3SiN)_2C_6H_4$)($C_5H_5N)_2$(η^2-ethylene) (**21**)

A toluene solution of W(NPh)(o-$(Me_3SiN)_2C_6H_4$)$(C_6H_7N)_2$ (**9**) in a Young's ampoule was exposed to a positive pressure of ethylene at -78° C. An immediate color change from purple to orange-brown was observed upon addition of ethylene. The reaction flask was immediately evacuated to remove excess ethylene. Subsequent removal of the reaction solvent gave [W(NPh)(o-$(Me_3SiN)_2C_6H_4$)$(C_5H_5N)_2$(η^2-ethylene)] (**21**) as an extremely unstable orange-brown solid. The compound decomposes upon standing above 0° C. ^1H NMR (C_6D_6, 25° C): δ 0.34 (s, 9H, Me_3Si), 0.35 (s, 9H, Me_3Si), 1.51 (s, 6H, C_6H_7N), 3.10 (s, 4H, ethylene), 6.26 (d, 4H, m-C_6H_7N), 6.55-7.20 (m, 9H, aromatic), 8.89 (d, 4H, o-C_6H_7N). ^{13}C NMR (C_6D_6, 25° C): δ 3.78 (Me_3Si), 5.76 (Me_3Si), 20.60 (C_6H_7N), 61.32 (ethylene), aromatic: 115.24, 117.77, 117.86, 121.88, 123.92, 124.83, 126.03, 128.90, 129.53, 129.66, 153.66.

Synthesis of [o-$(Me_3SiN)_2C_6H_4$](NPh)W(SC_4H_4) (**22**)

A Young's ampoule was charged with W(NPh)(o-$(Me_3SiN)_2C_6H_4$)$(C_5H_5N)_2$ (**8**) (0.30 g, 0.44 mmol) and 50 mL of toluene. Thiophene (0.07 mL, 0.88 mmol) was added and the reaction heated at 65° C for 12 hrs, during which time the solution became red in color. The reaction solvent was stripped under reduced pressure and the resulting solid extracted with several portions of hexane. Subsequent drying of the red filtrate *in vacuo*

yielded 0.16 g (60 %) of **22** as a dark red solid. ^{1}H NMR (25° C, C_6D_6): δ 0.39 (s, 9H, Me_3Si), 0.50 (s, 9H, Me_3Si), 6.70 (dd, 1H, β-CH, $^{3}J_{H-H}$ = 6.6 and 9.0 Hz), 6.71 (t, 1H, p-W≡N(C_6H_5), 6.94-7.02 (m, 4H, aromatic), 7.30 (m, 2H, m- pdaC_6H_4), 8.01 (d, 1H, α-CH, $^{3}J_{H-H}$ = 9.0 Hz), 8.20 (dd, 1H, γ-CH, $^{3}J_{H-H}$ = 6.6 and 12.9 Hz), 9.00 (d, 1H, β-CH, $^{3}J_{H-H}$ = 12.9 Hz). ^{13}C NMR (25° C, C_6D_6): δ 1.81 (Me_3Si), 2.19 (Me_3Si), 121.47, 122.44, 124.58, 125.67, 126.15, 126.34, 131.97, 133.11, 137.28, 139.16, 140.53, 186.38.

Synthesis of [o-(Me_3SiN)$_2C_6H_4$](NPh)W(SC_5H_6) (**23**)

A Young's ampoule was charged with W(NPh)(o-(Me_3SiN)$_2C_6H_4$)(C_5H_5N)$_2$ (**8**) (0.50 g, 0.73 mmol) and 100 mL of toluene. 2-methylthiophene (0.14 mL, 1.46 mmol) was added and the reaction heated at 65° C for 9 hrs, during which time the solution became red in color. The reaction solvent was removed under reduced pressure and the resulting solid extracted with several portions of cyclohexane. Subsequent drying of the red filtrate *in vacuo* yielded 0.36 g (79 %) of **23** as a dark red solid. ^{1}H NMR (25° C, C_6D_6): δ 0.40 (s, 9H, Me_3Si), 0.51 (s, 9H, Me_3Si), 2.38 (s, 3H, CH_3), 6.30 (t, 1H, p-W≡NPh), 6.52 (d, 1H, γ-CH, $^{3}J_{H-H}$ = 7 Hz), 6.97-7.14 (m, 4H, aromatic), 7.28 (m, 2H, o-pda), 7.34 (m, 2H, m-pda), 8.21 (dd, 1H, β-CH, $^{3}J_{H-H}$ = 7 and 13 Hz) 8.89 (d, 1H, α-CH, $^{3}J_{H-H}$ = 13 Hz). ^{13}C NMR (25° C, C_6D_6): δ 1.85 (Me_3Si), 2.27 (Me_3Si), 30.43 (CH_3), 121.35, 122.46, 124.45, 125.52, 126.01, 126.21, 137.49, 140.71, 142.07, 144.98, 157.64, 184.81.

Synthesis of [o-$(Me_3SiN)_2C_6H_4$](NPh)W(SC_8H_6) (**24**)

A Young's ampoule was charged with W(NPh)(o-$(Me_3SiN)_2C_6H_4$)($C_5H_5N)_2$ (**8**) (0.30 g, 0.44 mmol) and 75 mL of toluene. Benzothiophene (0.12 g, 0.88 mmol) was added and the reaction heated at 65° C for 7 hrs, during which time the solution became red-brown in color. The reaction solvent was removed under reduced pressure. Attempts to extract the product led to decomposition. By ^{1}H NMR spectroscopy, the yield of compound **24** was calculated to be (50 %). ^{1}H NMR (25° C, C_6D_6): δ 0.37 (s, 9H, Me_3Si), 0.48 (s, 9H, Me_3Si), 6.56 (t, 1H, p-W≡NC_6H_5), 6.92-7.32 (m, 12H, aromatic), 8.52 (d, 1H, α-CH, $^3J_{H-H}$ = 13.2 Hz), 8.67 (d, 1H, β-CH, $^3J_{H-H}$ = 13.2 Hz).

Synthesis of [o-$(Me_3SiN)_2C_6H_4$](NPh)W(SC_5H_6) (**25a,b**)

A Young's ampoule was charged with W(NPh)(o-$(Me_3SiN)_2C_6H_4$)($C_5H_5N)_2$ (**8**) (0.50 g, 0.73 mmol) and 100 mL of toluene. 3-methylthiophene (0.14 mL, 1.46 mmol) was added and the reaction heated at 65° C for 8 hrs, during which time the solution became red-brown in color. The reaction solvent was removed under reduced pressure and the resulting solid extracted with several portions of pentane. Concentration of the red filtrate followed by cooling (-78° C) yielded 0.32 g (69 %) of **25a** and **25b** as a dark red solid. ^{1}H NMR (25° C, C_6D_6): **25a**, δ 0.43 (s, 9H, Me_3Si), 0.52 (s, 9H, Me_3Si), 1.98 (s, 3H, CH_3), 6.57 (d, 1H, β-CH, $^3J_{H-H}$ = 10 Hz), 8.00 (d, 1H, α-CH, $^3J_{H-H}$ = 10 Hz), 8.75 (s, 1H, S-CH), ^{13}C NMR (25° C, C_6D_6): δ 1.83 (Me_3Si), 2.23 (Me_3Si), 24.48. **25b**, 0.42 (s, 9H, Me_3Si), 0.51 (s, 9H, Me_3Si), 2.05 (s, 3H, CH_3), 7.79 (s, 1H, α–CH), 8.04 (d, 1H, α-CH, $^3J_{H-H}$ = 13 Hz), 8.98 (d, 1H, S-CH, $^3J_{H-H}$ = 13 Hz). ^{13}C NMR (25° C, C_6D_6): **25a,** δ 1.75 (Me_3Si), 1.90 (Me_3Si), 24.48 (CH_3), **25b,** δ 1.83 (Me_3Si), 2.23 (Me_3Si), 30.21

(CH_3). Aromatics for **25a** and **25b**: 120.98, 121.33, 121.40, 121.44, 122.33, 122.48, 124.34, 125.40, 125.48, 126.11, 126.17, 126.23, 126.26, 134.30, 135.19, 137.79, 137.87, 139.28, 141.08, 143.33, 148.08, 184.57, 186.82.

Reaction of $W(CH_2CH_2CH_2CH_2)(NPh)[o\text{-}(Me_3SiN)_2C_6H_4]$ (**20**) with $EtAlCl_2$

In a resealable NMR tube, $W(CH_2CH_2CH_2CH_2)(NPh)[o\text{-}(Me_3SiN)_2C_6H_4]$ (**20**) (0.02 g, 0.03 mmol) was dissolved in C_6D_6. 2 equivalents of $EtAlCl_2$ (0.038 mL, 0.06 mmol) were then added to the resulting solution and the NMR tube sealed. The sample was placed in the NMR probe and successive spectra were measured. Over time, the formation of 1-butene was observed as the major organic product from the Lewis acid assisted decomposition of **20**.

Ethylene Dimerization

Typical reaction conditions for the catalytic dimerization of ethylene are as follows. Inside the dry box, a Parr high pressure reactor was charged with toluene (50 mL), $W(NPh)(o\text{-}(Me_3SiN)_2C_6H_4)Cl_2$ (**28**) (0.050 g, 0.08 mmol) or $W(CH_2CH_2CH_2CH_2)(NPh)[o\text{-}(Me_3SiN)_2C_6H_4]$ (**20**) (0.046 g, 0.08 mmol) and $EtAlCl_2$ (3-15 equivalents). The reactor was then sealed and removed from the box imediately. The reactor was heated at 70° C for 10 minutes at which time the reactor was pressurized with ethylene (50-500 psi) drawn directly from the cylinder without further drying. The mixture was stirred room temperature until the added ethylene had been consumed. The resulting mixture was analyzed by Gas Chromatography and NMR spectroscopy as described in Chapter 6.

Hexene Dimerization

Inside the dry box an ampoule equipped with a resealable valve was charged with toluene (50 mL), W(NPh)(o-$(Me_3SiN)_2C_6H_4$)Cl_2 (**28**) (0.050 g, 0.08 mmol) or W($CH_2CH_2CH_2CH_2$)(NPh)[o-$(Me_3SiN)_2C_6H_4$] (**20**) (0.046 g, 0.08 mmol) and $EtAlCl_2$ (3-15 equivalents). The ampoule was then sealed and removed from the box immediately. Upon heating (90° C) the reaction vessel in an oil bath for 10 minutes to allow for catalyst aging, excess 1-hexene was added to the solution containg the activated catalyst. Aliquots were taken at predetermined intervals using a syringe. The aliquots were then analyzed by Gas Chromatography, ^1H NMR and ^{13}C NMR spectroscopies.

Additional Dimerization Experiments

For the dimerization studies of 1-pentene, 1-octene, 1-decene, C_{14} α-olefin, cyclohexene and 1,7-octadiene, a similar procedure to that described for the dimerization of 1-hexene was utilized. The only variation in these experiments was the reaction temperature. A list of reaction temperatures corresponding to the substrates listed above was presented in Table 6.1 and should be refered to for exact reaction conditions for these dimerization experiments.

Crystallographic Studies

X-ray Data Collection and Structure Refinement for Compounds **4** and **5**.

Data for **4** and **5** were collected at 173 K on a Siemens SMART PLATFORM equipped with A CCD area detector and a graphite monochromator utilizing MoK_α radiation (λ = 0.71073 Å). Cell parameters for each structure were refined using up to 8192 reflections and a hemisphere of data (1381 frames) was collected using the ω-scan

method (0.3° frame width). The first 50 frames were remeasured at the end of data collection to monitor instrument and crystal stability (maximum correction on I was < 1 %). Absorption corrections by integration were applied based on measured indexed crystal faces.

The structures of **4** and **5** were solved by the Direct Methods in *SHELXTL5,*[201] and refined using full-matrix least squares. The non-H atoms were treated anisotropically, whereas the hydrogen atoms were calculated in ideal positions and were riding on their respective carbon atoms. For **4**, the C7 phenyl ring was found to be disordered and was refined in two parts. Their site occupation factors were dependently refined to 0.66(1) for the major part, and consequently 0.34(1) for the minor part. For **5**, there are two chemically equivalent but crystallographically independent complexes in the asymmetric unit. A total of 301 parameters of **4** were refined in the final cycle of refinement using 4221 reflections with $I > 2\sigma(I)$ to yield R_1 and wR_2 of 3.71% and 5.53%, respectively. For **5,** a total of 841 parameters were refined in the final cycle of refinement using 13192 reflections with $I > 2\sigma(I)$ to yield R_1 and wR_2 of 3.28% and 6.16%, respectively. Refinement of **4** and **5** was done using F^2. The final atomic coordinates, bond lengths and angles for the non-hydrogen atoms of **4** and **5** are given in Tables B.1-B.5 and B.6-B.10 of Appendix B.

X-ray Data Collection and Structure Refinement for Compounds **9** and **12a**.

Data for **9** and **12a** were collected at 173 K on a Siemens SMART PLATFORM equipped with A CCD area detector and a graphite monochromator utilizing $MoK\alpha$ radiation ($\lambda = 0.71073$ Å). Cell parameters were refined using up to 8192 reflections. A hemisphere of data (1381 frames) was collected using the ω-scan method (0.3° frame

width). The first 50 frames were remeasured at the end of data collection to monitor instrument and crystal stability (maximum correction on I was < 1 %). Absorption corrections by integration were applied based on measured indexed crystal faces.

The structures were solved by the Direct Methods in *SHELXTL5*,{Sheldrick 1986 #1} and refined using full-matrix least squares. The non-H atoms were treated anisotropically, whereas the hydrogen atoms were calculated in ideal positions and were riding on their respective carbon atoms. For compound **9,** the N1 imido and the N5 methylpyridyl ligands are slightly disordered in their planes but could not be resolved. This is evidenced by the larger than normal and elongated thermal ellipsoids of their atoms. A total of 351 parameters were refined in the final cycle of refinement using 6092 reflections with $I > 2\sigma(I)$ to yield R_1 and wR_2 of 2.48% and 5.63%, respectively. Refinement was done using F^2. For compound **12a** the asymmetric unit consists of one complex and a half diethyl ether disordered over a center of inversion (1/2 ether in the asymmetric unit). The ether was refined in two parts and their occupancy was fixed at 50% due to symmetry. A total of 369 parameters were refined in the final cycle of refinement using 6907 reflections with $I > 2\sigma(I)$ to yield R_1 and wR_2 of 3.07% and 7.48%, respectively. Refinement was done using F^2. The final atomic coordinates, bond lengths and angles for the non-hydrogen atoms of **9** and **12a** are given in Tables B.11-B.15 and B.16-B.20 of Appendix B.

X-ray Data Collection and Structure Refinement for Compound **14a**.

Data were collected at 173 K on a Siemens SMART PLATFORM equipped with A CCD area detector and a graphite monochromator utilizing MoK_α radiation (λ = 0.71073 Å). Cell parameters were refined using up to 8192 reflections. A hemisphere of

data (1381 frames) was collected using the ω-scan method (0.3° frame width). The first 50 frames were remeasured at the end of data collection to monitor instrument and crystal stability (maximum correction on I was < 1 %). Absorption corrections by integration were applied based on measured indexed crystal faces.

The structure was solved by the Direct Methods in *SHELXTL5,* and refined using full-matrix least squares. The non-H atoms were treated anisotropically, whereas the hydrogen atoms were calculated in ideal positions and were riding on their respective carbon atoms. A heavily disordered pentane molecule was observed in the lattice and could not be resolved. Thus program PLATON/SQUEEZE was used to remove its intensity contribution to the reflection data and the structure was solved and refined without the solvent molecule. A total of 697 parameters were refined in the final cycle of refinement using 13661 reflections with $I > 2\sigma(I)$ to yield R_1 and wR_2 of 4.28% and 9.03%, respectively. Refinement was done using F^2. The final atomic coordinates, bond lengths and angles for the non-hydrogen atoms of **14a** are given in Tables B.21-B.25 of Appendix B.

X-ray Data Collection and Structure Refinement for Compound **15**.

Data for **15** were collected at 173 K on a Siemens SMART PLATFORM equipped with A CCD area detector and a graphite monochromator utilizing MoK_α radiation ($\lambda = 0.71073$ Å). Cell parameters were refined using up to 8192 reflections. A hemisphere of data (1381 frames) was collected using the ω-scan method (0.3° frame width). The first 50 frames were remeasured at the end of data collection to monitor instrument and crystal stability (maximum correction on I was < 1 %). Absorption corrections by integration were applied based on measured indexed crystal faces.

The structure was solved by the Direct Methods in *SHELXTL5,* and refined using full-matrix least squares. The non-H atoms were treated anisotropically, whereas the hydrogen atoms were calculated in ideal positions and were riding on their respective carbon atoms. The N1 imido and the N5 methylpyridyl ligands are slightly disordered in their planes but could not be resolved. This is evidenced by the larger than normal and elongated thermal ellipsoids of their atoms. A total of 349 parameters were refined in the final cycle of refinement using 6182 reflections with $I > 2\sigma(I)$ to yield R_1 and wR_2 of 2.08% and 4.87%, respectively. Refinement was done using F^2. The final atomic coordinates, bond lengths and angles for the non-hydrogen atoms of **15** are given in Tables B.26-B.30 of Appendix B.

X-ray Data Collection and Structure Refinement for Compound **17.**

Data were collected at 173 K on a Siemens SMART PLATFORM equipped with A CCD area detector and a graphite monochromator utilizing $MoK\alpha$ radiation (λ = 0.71073 Å). Cell parameters were refined using up to 8192 reflections. A hemisphere of data (1381 frames) was collected using the ω-scan method (0.3° frame width). The first 50 frames were remeasured at the end of data collection to monitor instrument and crystal stability (maximum correction on I was < 1 %). Absorption corrections by integration were applied based on measured indexed crystal faces.

The structure was solved by the Direct Methods in *SHELXTL5,* and refined using full-matrix least squares. The non-H atoms were treated anisotropically, whereas the methyl hydrogen atoms were calculated in ideal positions and were riding on their respective carbon atoms. The asymmetric unit consisted of two W complexes. A total of 589 parameters were refined in the final cycle of refinement using 19003 reflections with

$I > 2\sigma(I)$ to yield R_1 and wR_2 of 3.00% and 6.55%, respectively. Refinement was done using F^2. The final atomic coordinates, bond lengths and angles for the non-hydrogen atoms of **17** are given in Tables B.31-B.35 of Appendix B.

X-ray Data Collection and Structure Refinement for Compound **19**.

Data were collected at 173 K on a Siemens SMART PLATFORM equipped with A CCD area detector and a graphite monochromator utilizing MoK_α radiation ($\lambda = 0.71073$ Å). Cell parameters were refined using up to 8192 reflections. A hemisphere of data (1381 frames) was collected using the ω-scan method (0.3° frame width). The first 50 frames were remeasured at the end of data collection to monitor instrument and crystal stability (maximum correction on I was < 1 %). Absorption corrections by integration were applied based on measured indexed crystal faces.

The structure was solved by the Direct Methods in *SHELXTL5,* and refined using full-matrix least squares. The non-H atoms were treated anisotropically, whereas the hydrogen atoms were calculated in ideal positions and were riding on their respective carbon atoms, excpet the C29 proton which was obtained from a Difference Fourrier map and refined freely. A total of 367 parameters were refined in the final cycle of refinement using 4634 reflections with $I > 2\sigma(I)$ to yield R_1 and wR_2 of 5.59% and 9.23%, respectively. Refinement was done using F^2. The final atomic coordinates, bond lengths and angles for the non-hydrogen atoms of **19** are given in Tables B.36-B.40 of Appendix B.

X-ray Data Collection and Structure Refinement for Compound **22**.

Data for **22** were collected at 173 K on a Siemens SMART PLATFORM equipped with A CCD area detector and a graphite monochromator utilizing MoK_α radiation ($\lambda = 0.71073$ Å). Cell parameters were refined using up to 8192 reflections. A hemisphere of data (1381 frames) was collected using the ω-scan method (0.3° frame width). The first 50 frames were remeasured at the end of data collection to monitor instrument and crystal stability (maximum correction on I was < 1 %). Absorption corrections by integration were applied based on measured indexed crystal faces.

The structure was solved by the Direct Methods in *SHELXTL5,* and refined using full-matrix least squares. The non-H atoms, except the disorder, were treated anisotropically, whereas the methyl hydrogen atoms were calculated in ideal positions and were riding on their respective carbon atoms. The S1-C22 is found to be disordered by a 180° rotation and was refined in two parts. The major part represented by the S1-C22 chain and the minor part by S1'-C22'. Their site occupation factors were dependently refined to 0.55(1) for the major part and, consequently, 0.45(1) for the minor part. All atoms of the disorder were refined with isotropic thermal parameters. The W-S1 and W-S1' bonds were constrained to be equivalent during refinement. Similarly, W-C22 and W-C22' were also constrained to remain equivalent. A total of 264 parameters were refined in the final cycle of refinement using 5106 reflections with $I > 2\sigma(I)$ to yield R_1 and wR_2 of 2.64% and 6.48%, respectively. Refinement was done using F^2. The final atomic coordinates, bond lengths and angles for the non-hydrogen atoms of **22** are given in Tables B.41-B.44 of Appendix B.

APPENDIX A
NUCLEAR MAGNETIC RESONANCE SPECTRA

Figure A-1. Proton NMR of $W(NPh)(CH_2CH_2CH_2Ph)_2(o\text{-}(Me_3SiN)_2C_6H_4)$ (**2**) in C_6D_6.

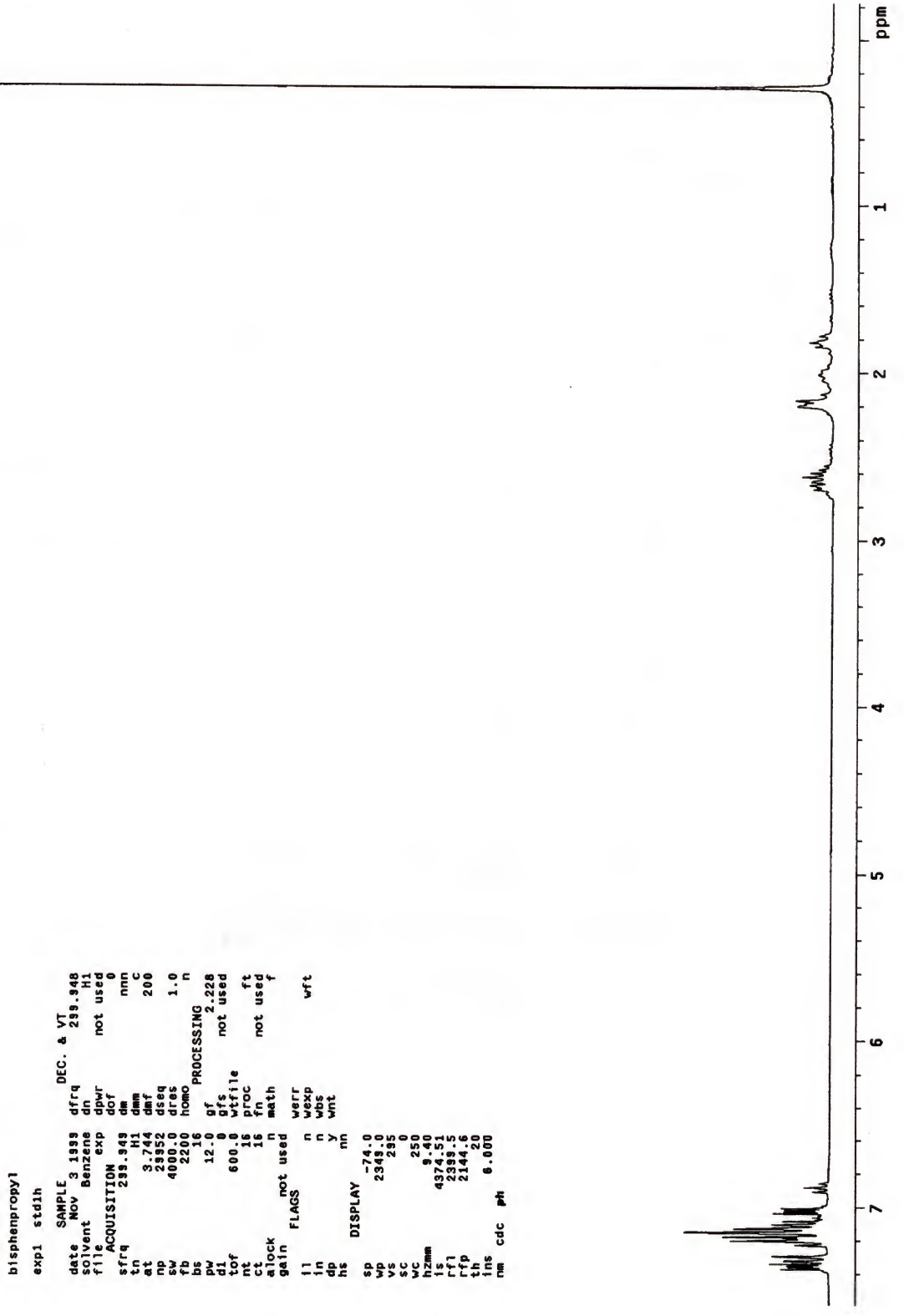

Figure A-2. Carbon NMR of $W(NPh)(CH_2CH_2CH_2Ph)_2(o\text{-}(Me_3SiN)_2C_6H_4)$ (**2**) in C_6D_6.

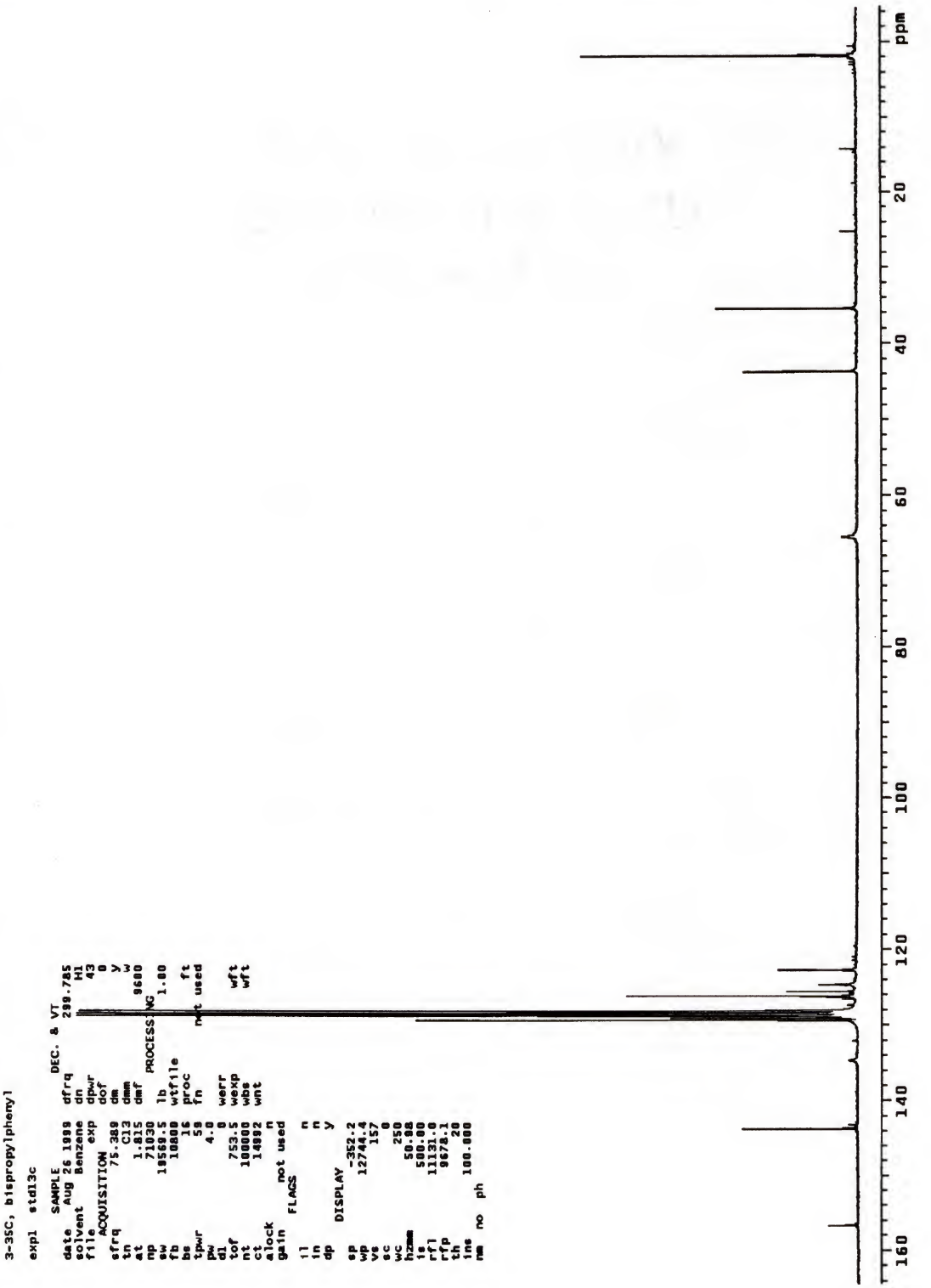

Figure A-3. Proton NMR of W(NPh)[o-$(Me_3SiN)_2C_6H_4$](η^4-ethylbenzene) (**3**) in C_6D_6.

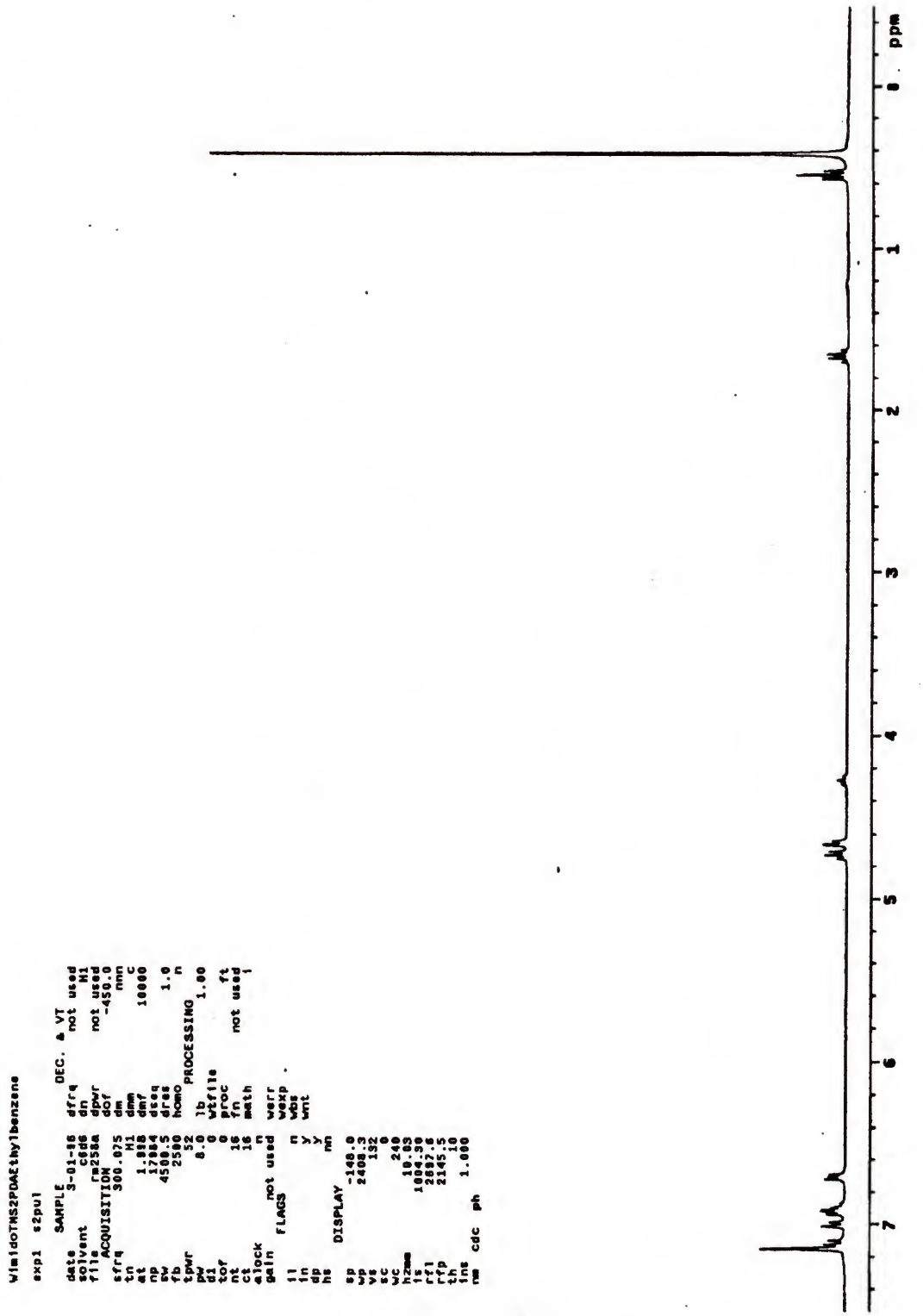

Figure A-4. Carbon NMR of W(NPh)[o-$(Me_3SiN)_2C_6H_4$](η^4-ethylbenzene) (**3**) in C_6D_6.

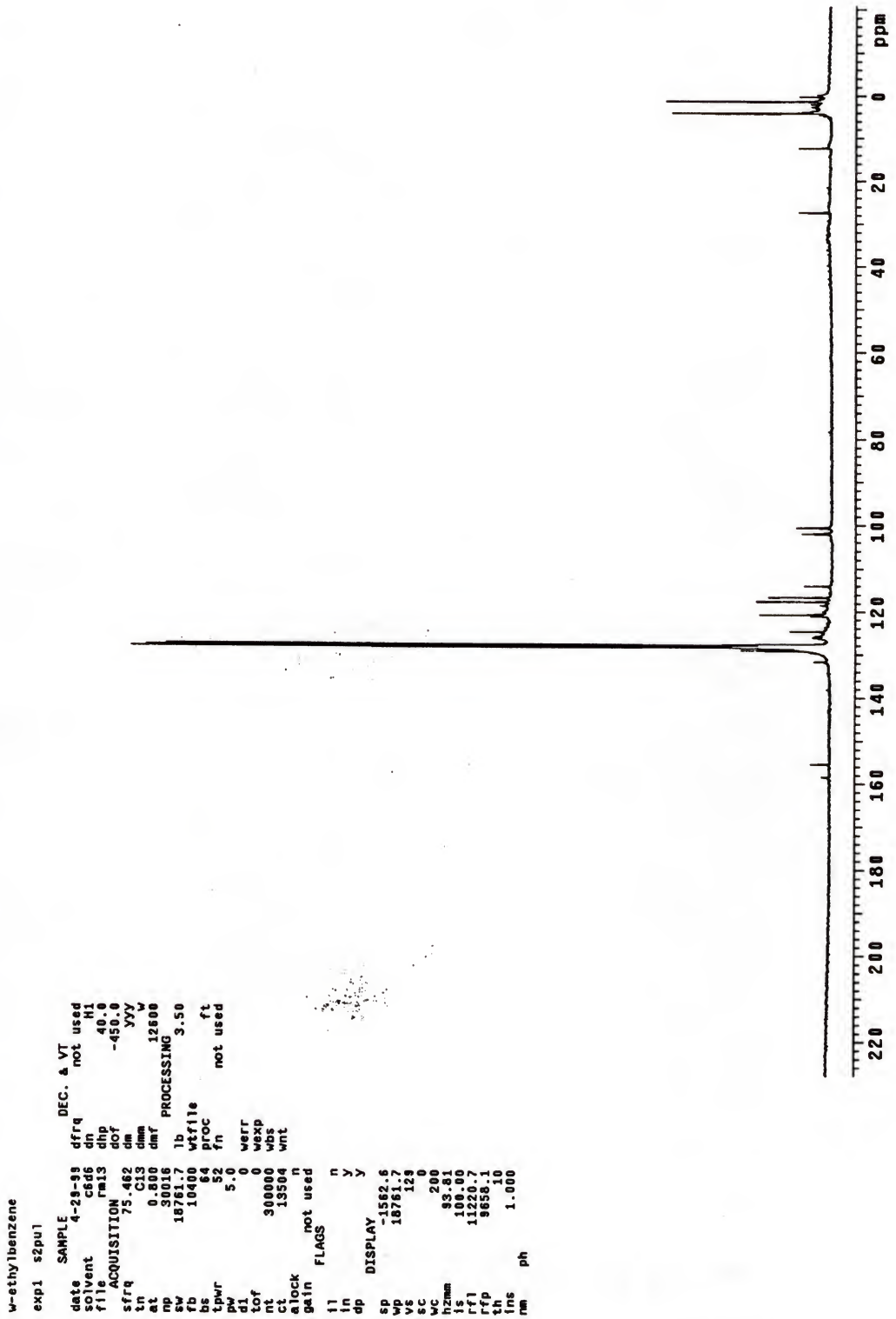

Figure A-5. Proton NMR of W(NPh)[o-$(Me_3SiN)_2C_6H_4$](η^4-propylbenzene) (**4**) in C_6D_6.

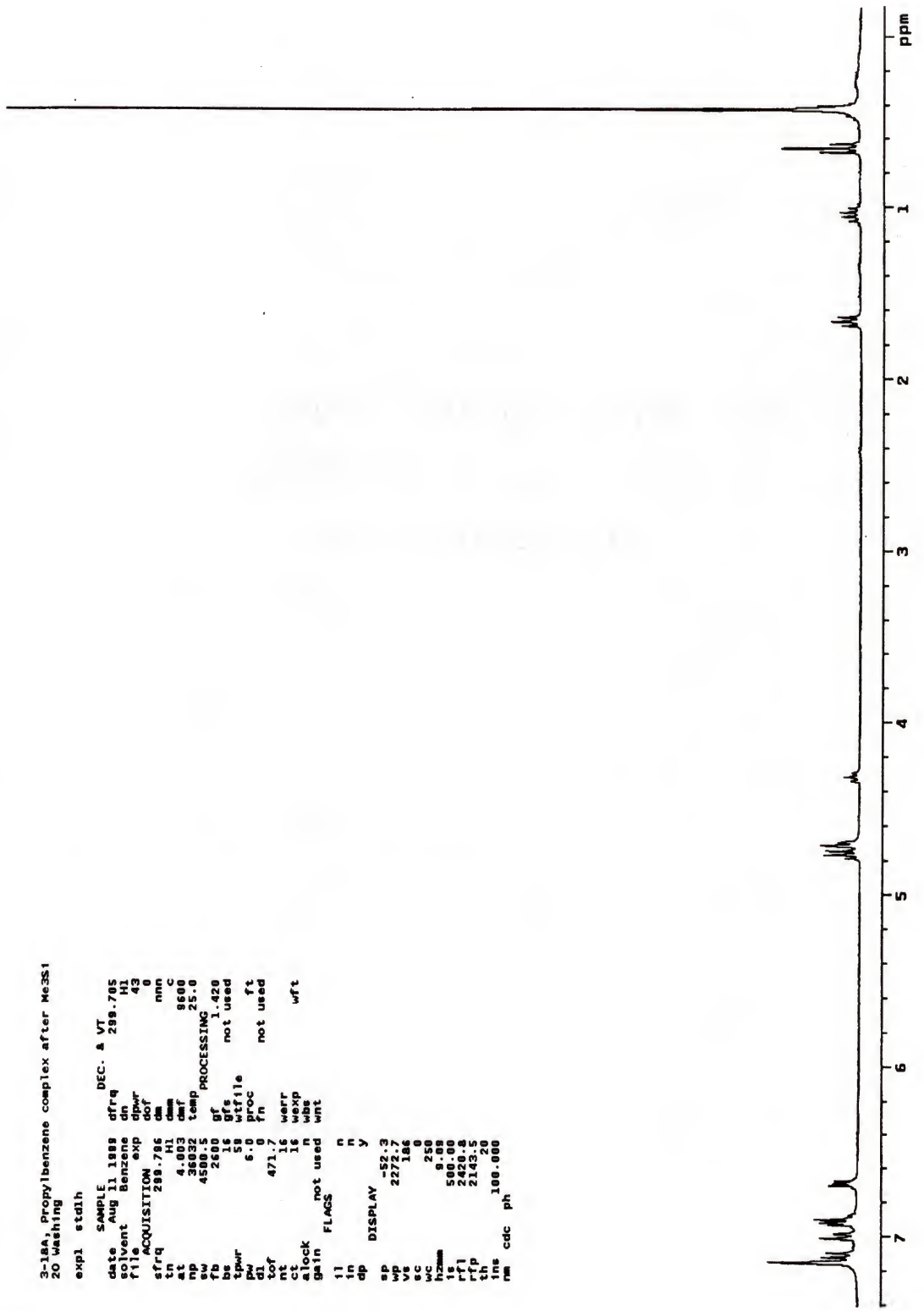

Figure A-6. Carbon NMR of W(NPh)[o-$(Me_3SiN)_2C_6H_4$](η^4-propylbenzene) (**4**) in C_6D_6.

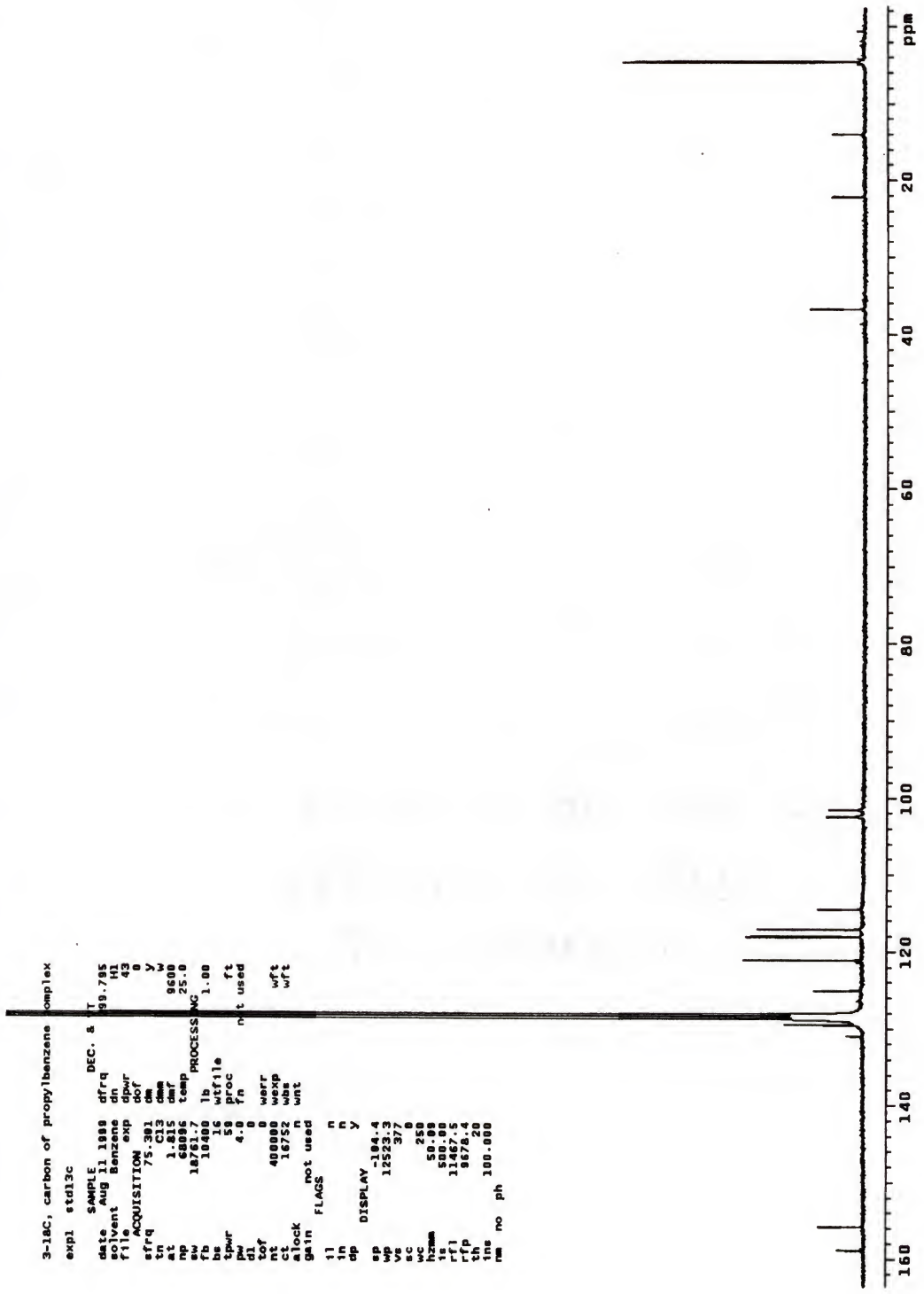

Figure A-7. Proton NMR of [o-$(Me_3SiN)_2C_6H_4$)(NPh)$WCH_2C(Ph)=C(Ph)CHPh$] (**5**) in C_6D_6.

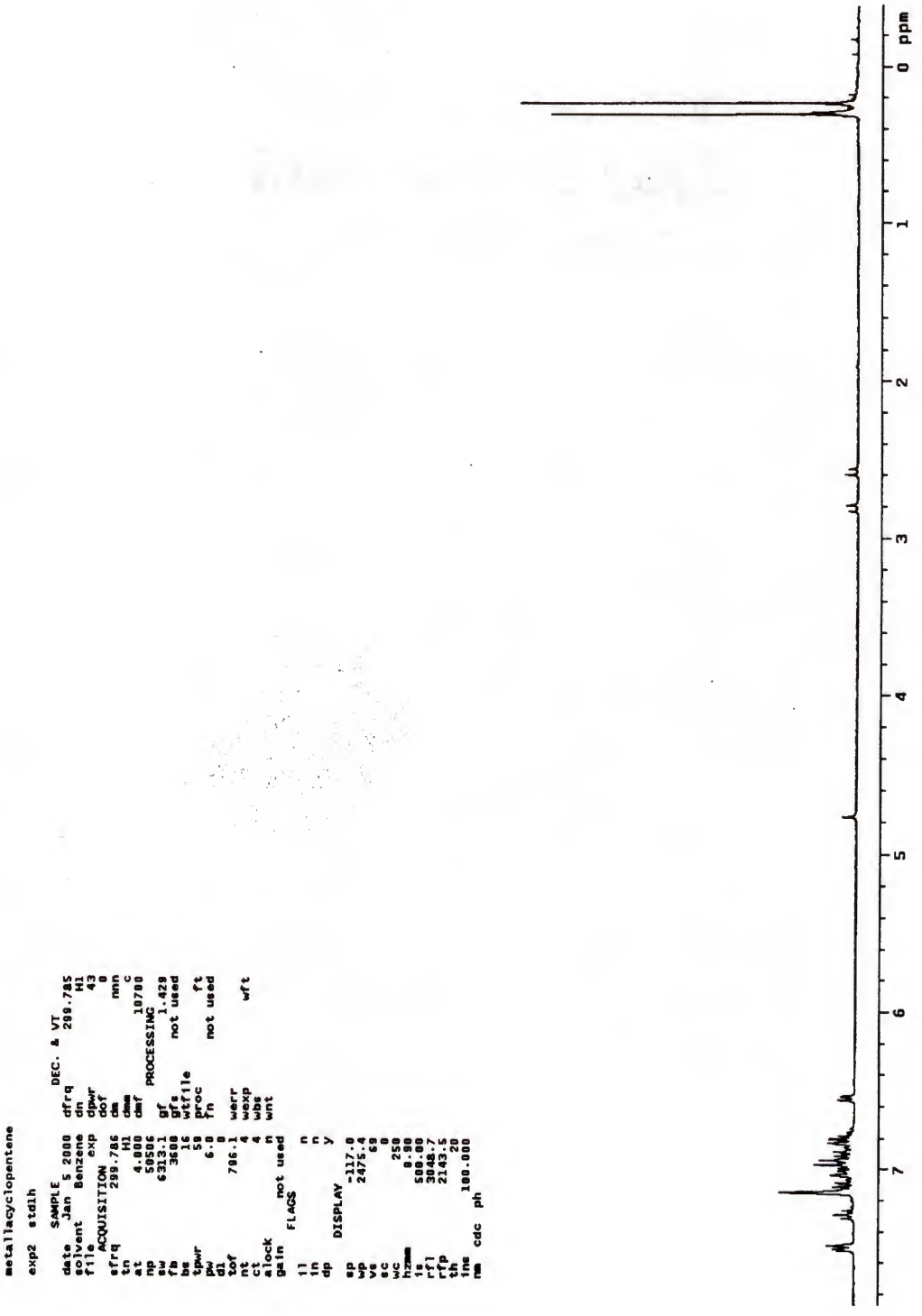

Figure A-8. Carbon NMR of [o-$(Me_3SiN)_2C_6H_4$)(NPh)$\overline{WCH_2C(Ph)=C(Ph)CHPh}$] (**5**) in C_6D_6.

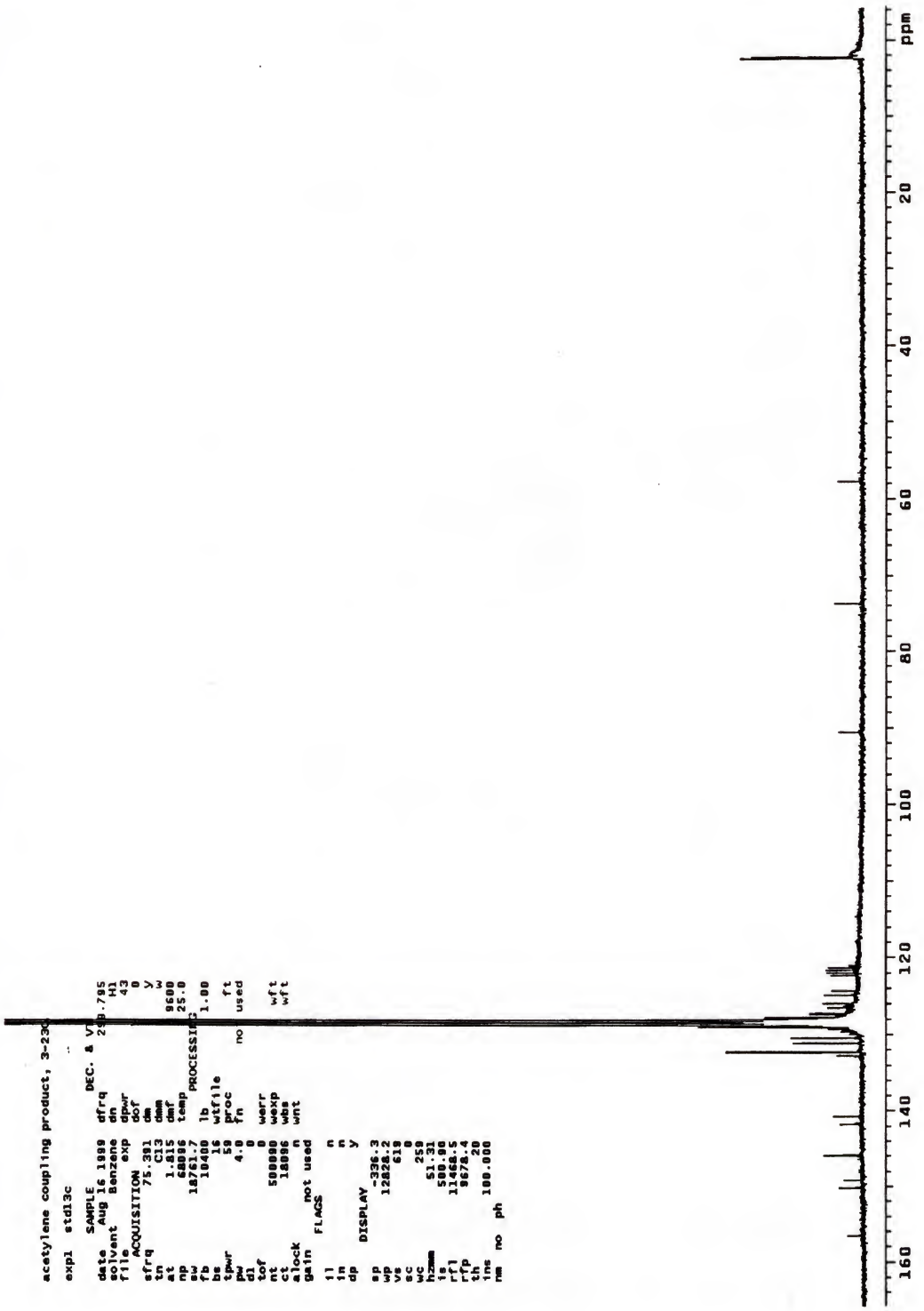

Figure A-9. Proton NMR of W(NPh)[o-$(Me_3SiN)_2C_6H_4$](CH_2CH_2Ph)(Cl) (**6**) in C_6D_6.

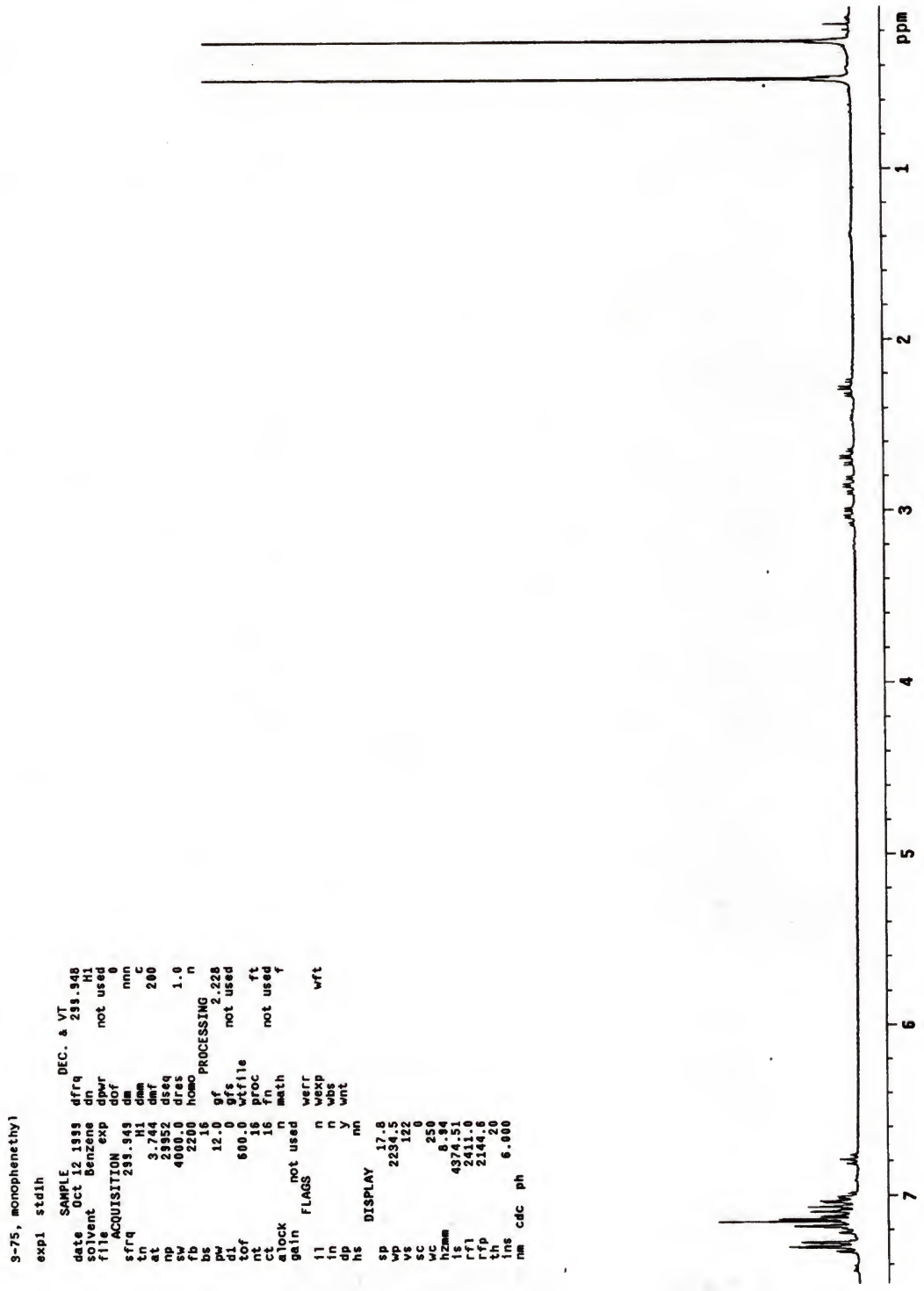

Figure A-10. Proton NMR of W(NPh)[o-$(Me_3SiN)_2C_6H_4$](CH_2CH_2Ph)(Me) (**7**) in C_6D_6.

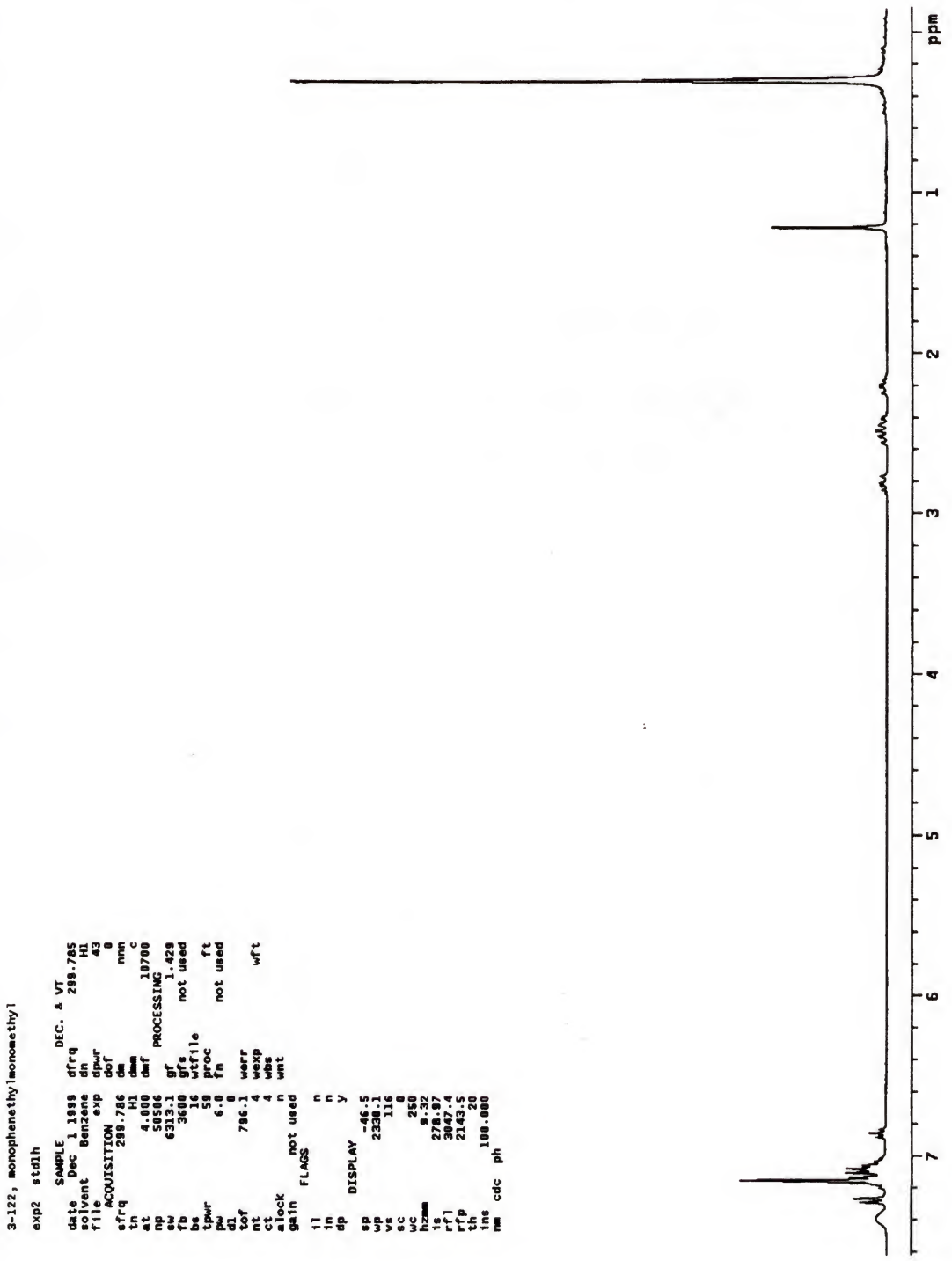

Figure A-11. Proton NMR of W(NPh)(o-$(Me_3SiN)_2C_6H_4$)$(C_5H_5N)_2$ (**8**) in C_6D_6.

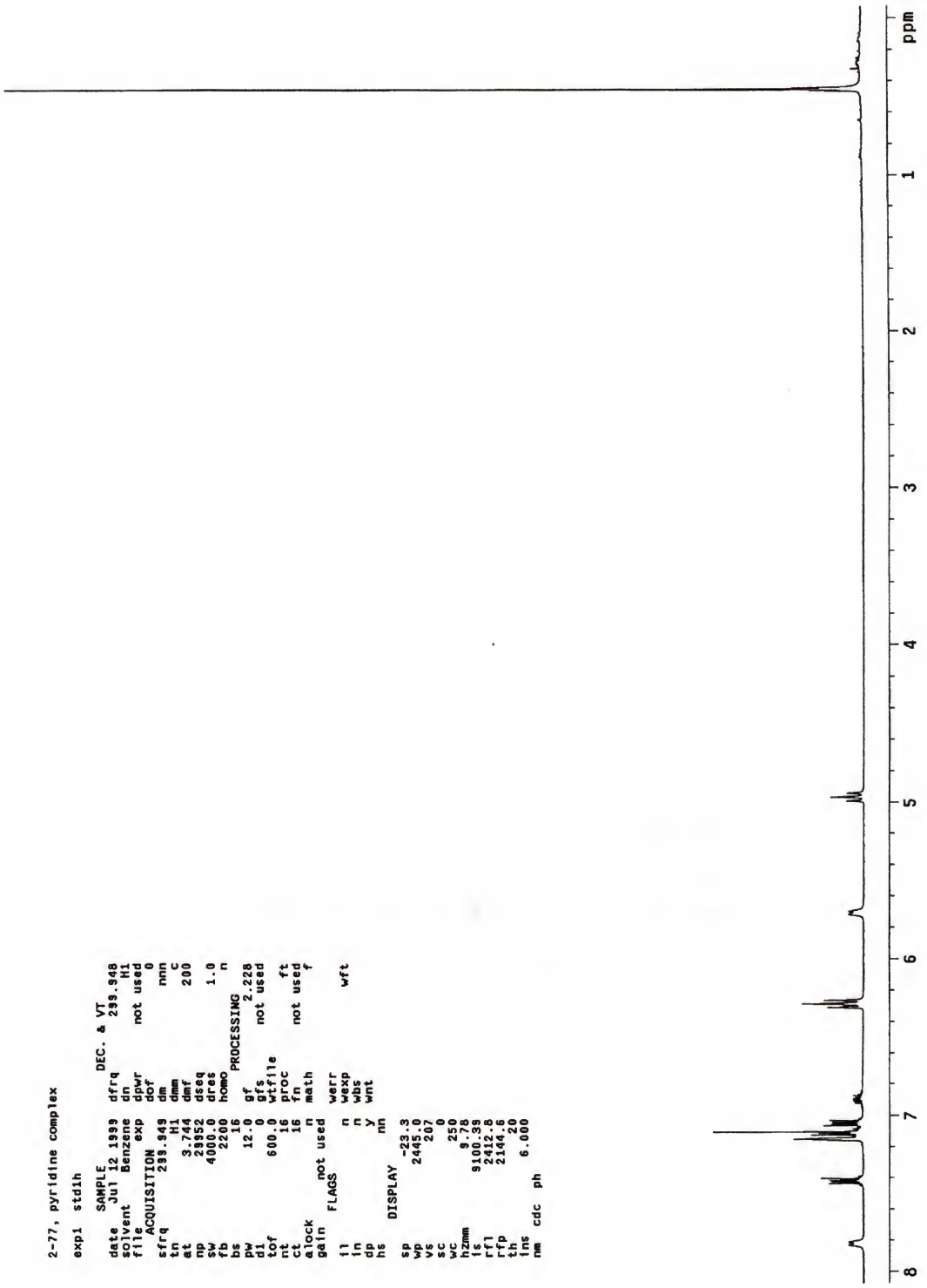

Figure A-12. Carbon NMR of W(NPh)(o-$(Me_3SiN)_2C_6H_4$)$(C_5H_5N)_2$ (**8**) in C_6D_6.

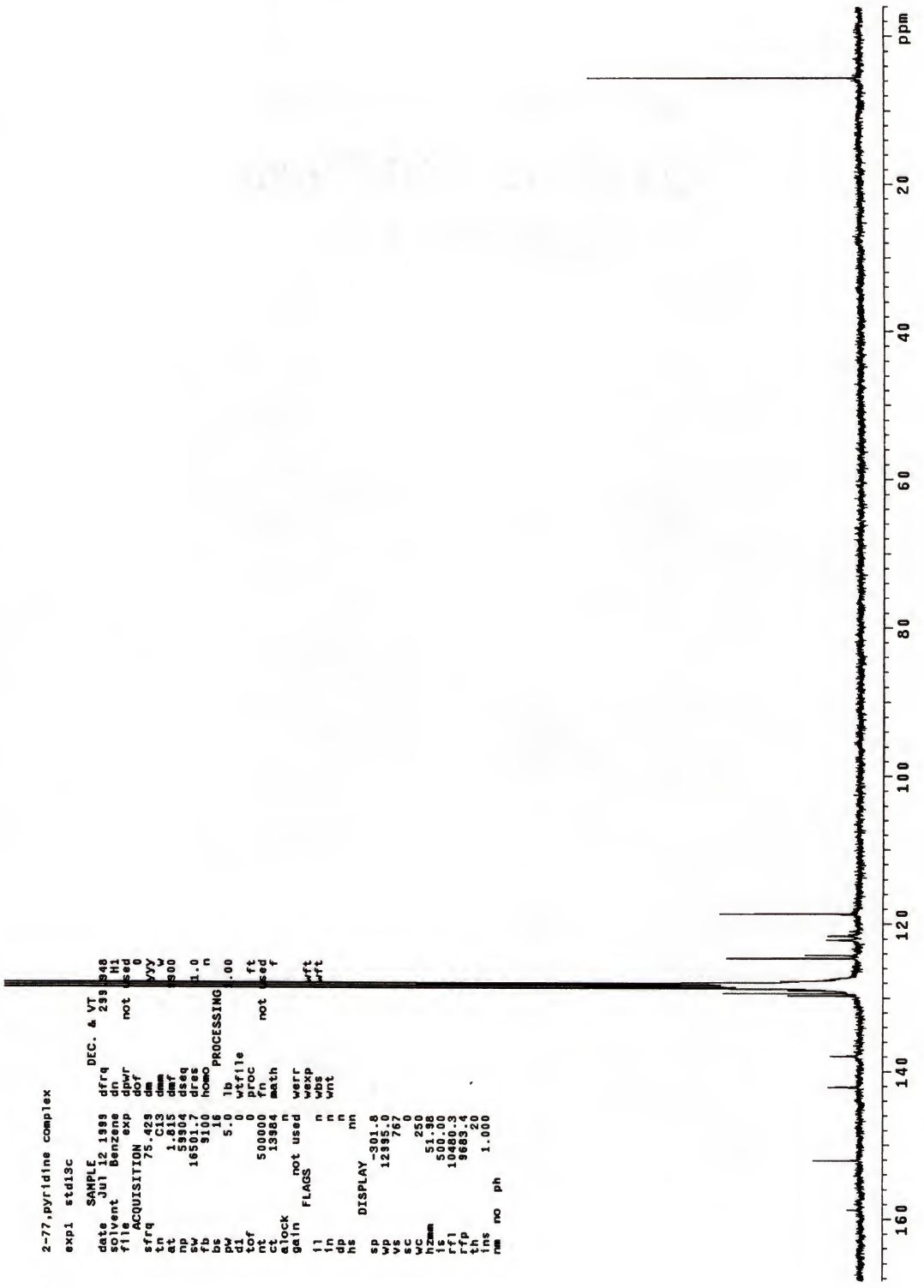

Figure A-13. Proton NMR of W(NPh)(o-$(Me_3SiN)_2C_6H_4$)(p-$C_6H_7N)_2$ (**9**) in C_6D_6.

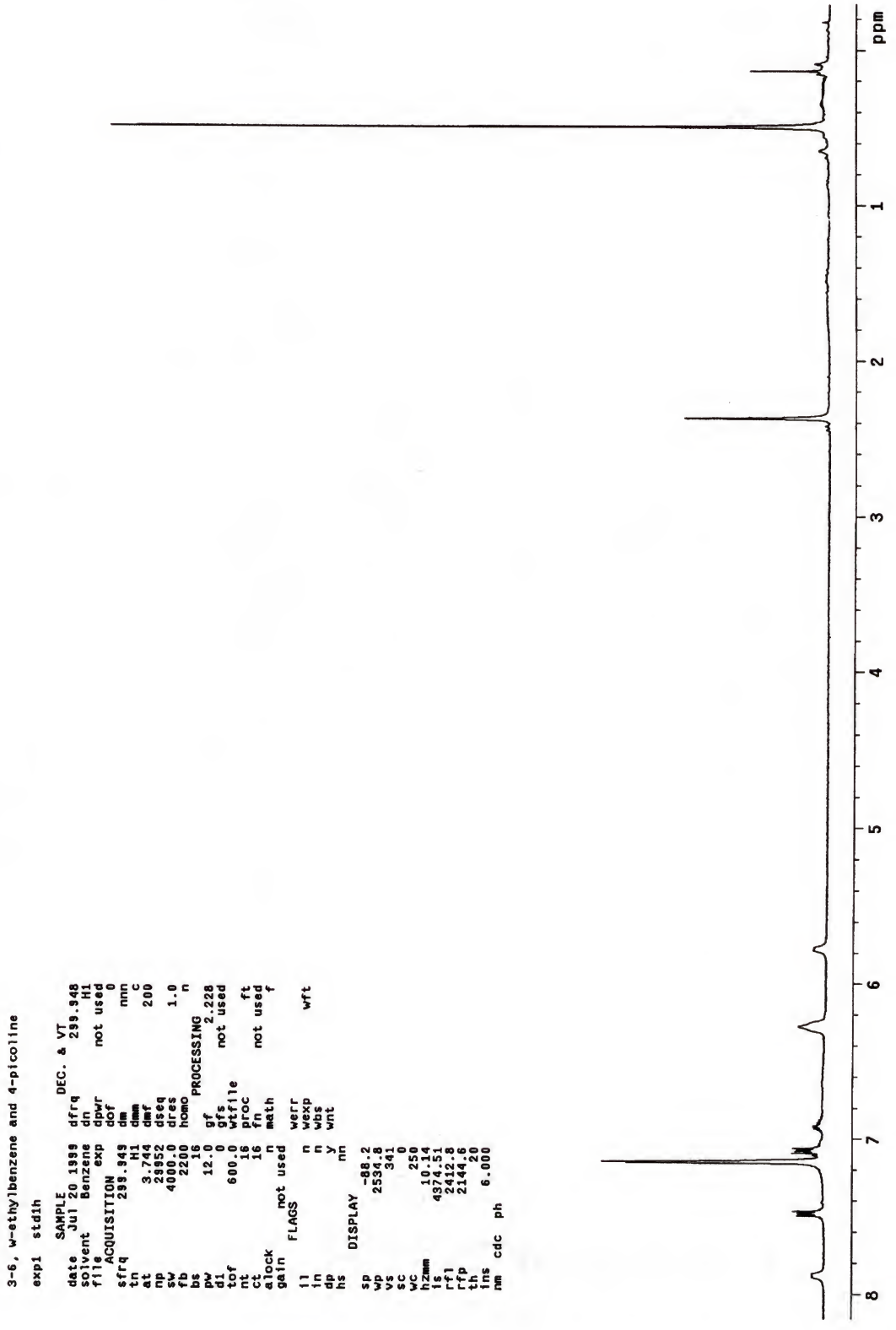

Figure A-14. Carbon NMR of W(NPh)(o-$(Me_3SiN)_2C_6H_4$)(p-$C_6H_7N)_2$ (**9**) in C_6D_6.

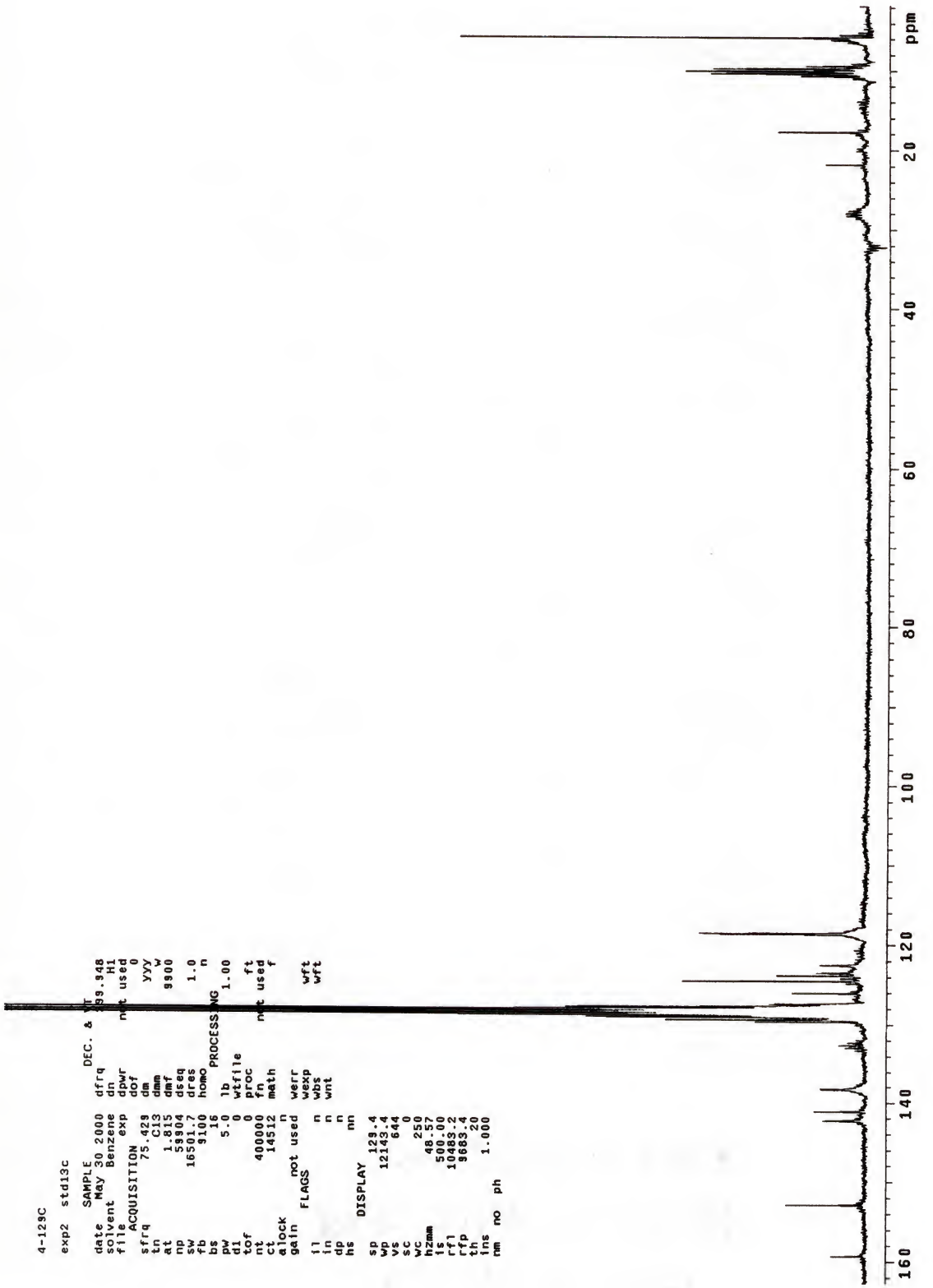

Figure A-15. Proton NMR of W(NPh)(o-$(Me_3SiN)_2C_6H_4$)(C_9H_7N)$_2$ (**10**) in C_6D_6.

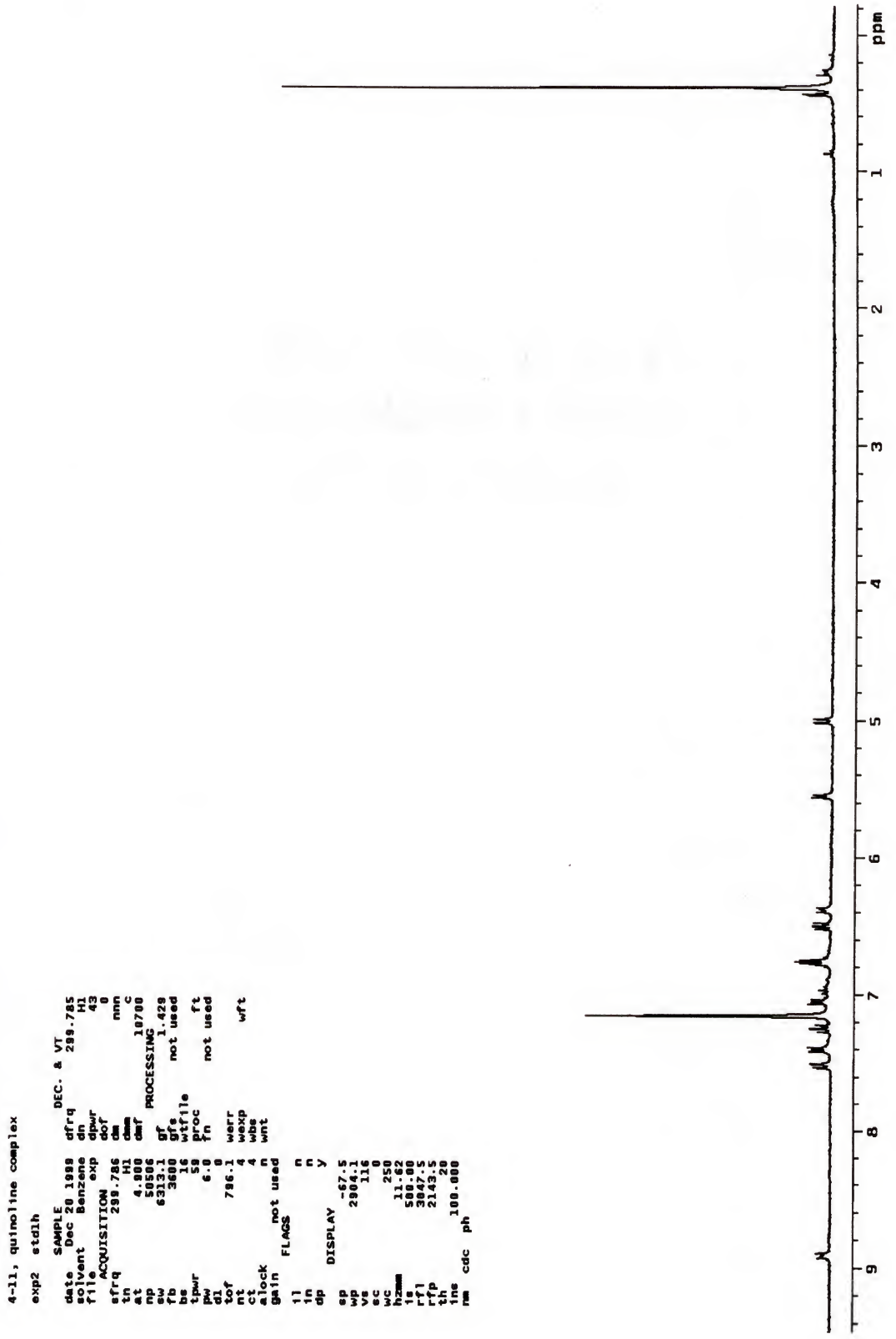

Figure A-16. Carbon NMR of W(NPh)(o-$(Me_3SiN)_2C_6H_4$)$(C_9H_7N)_2$ (**10**) in C_6D_6.

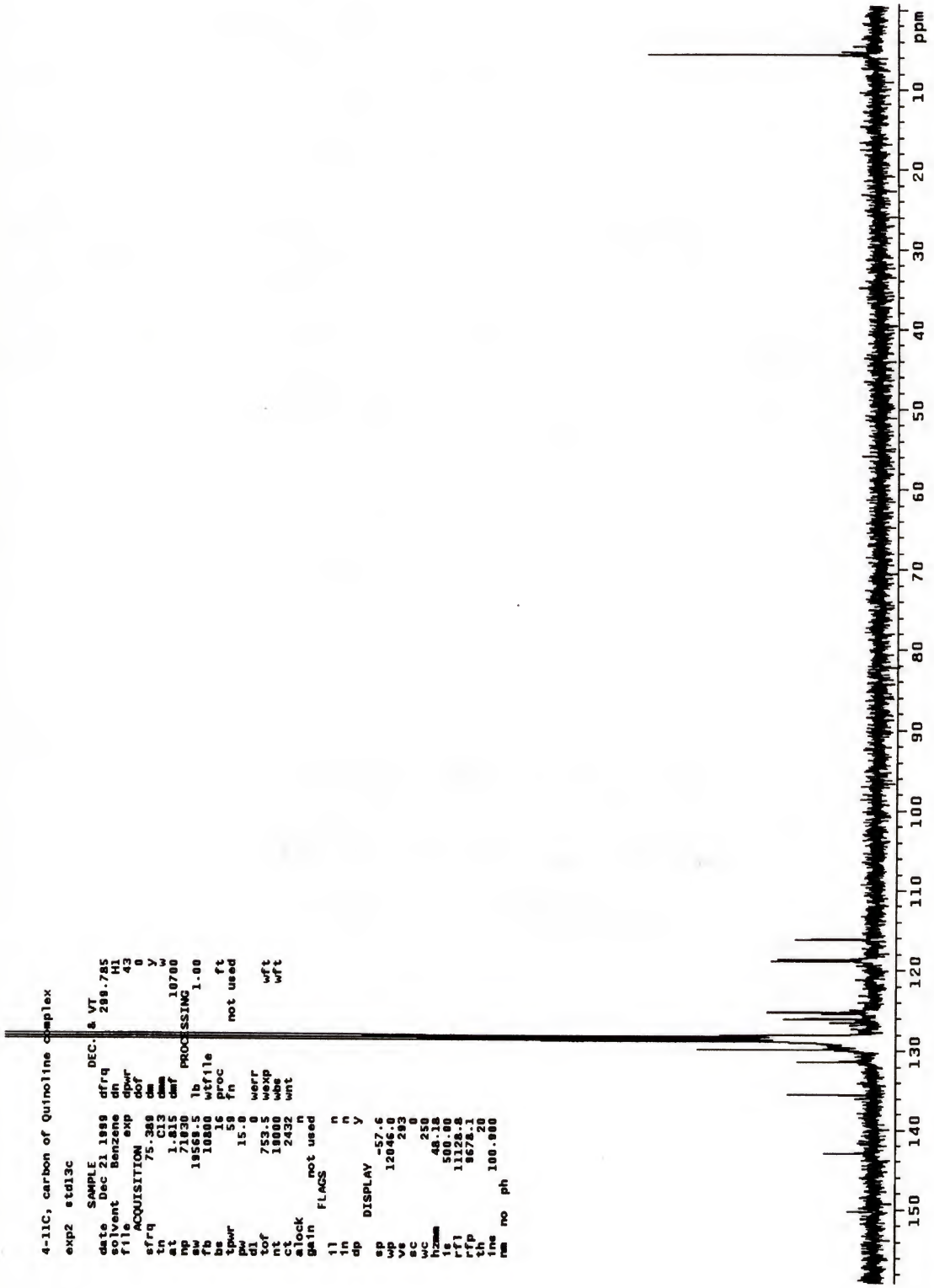

Figure A-17. Proton NMR of [W(NPh)(o-$(Me_3SiN)_2C_6H_4$)(C_5H_5N)$_2$(CO)] (**12a**) in C_6D_6.

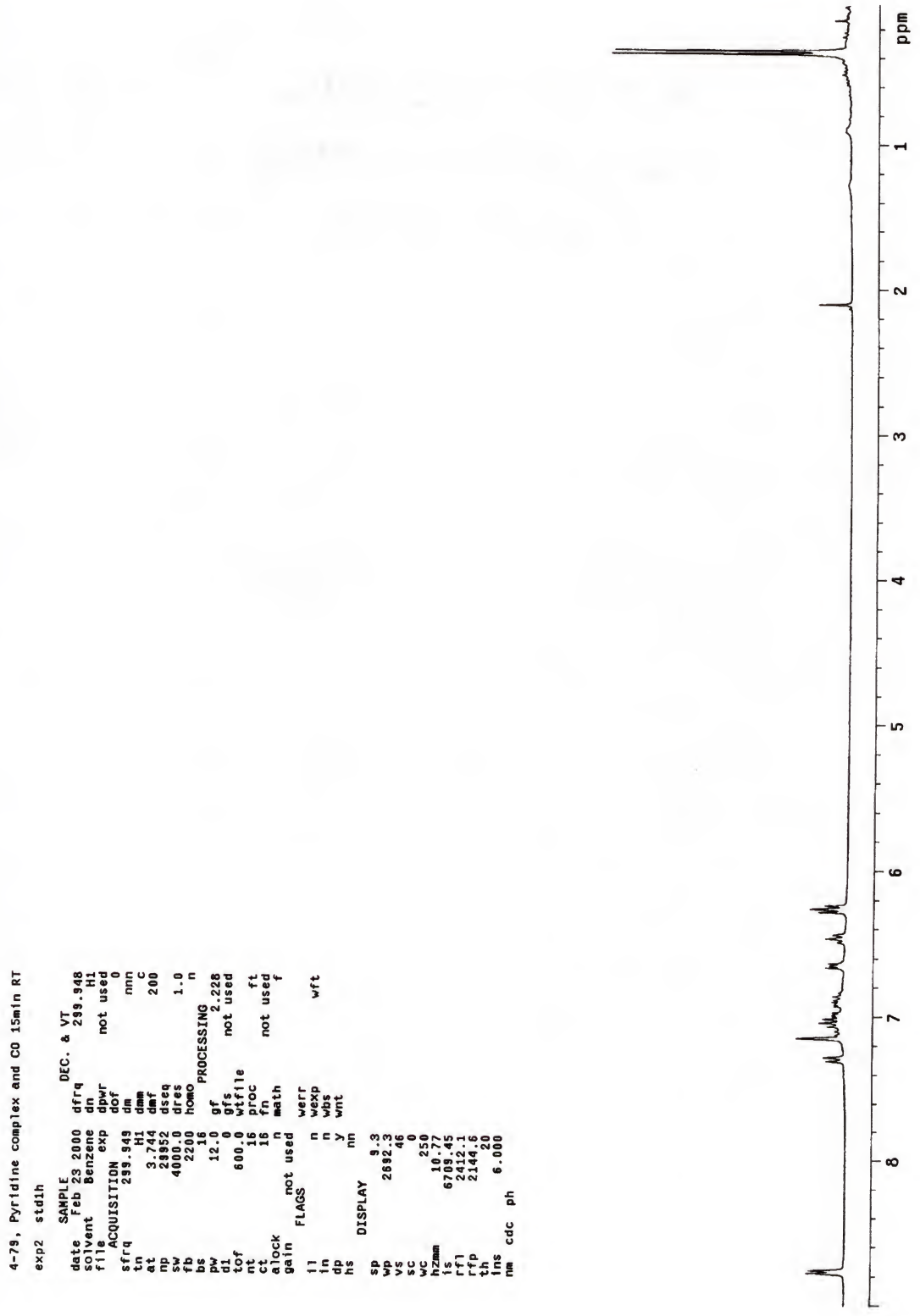

Figure A-18. Carbon NMR of W(NPh)(o-$(Me_3SiN)_2C_6H_4$)$(C_5H_5N)_2$(CO) (**12a**) in C_6D_6.

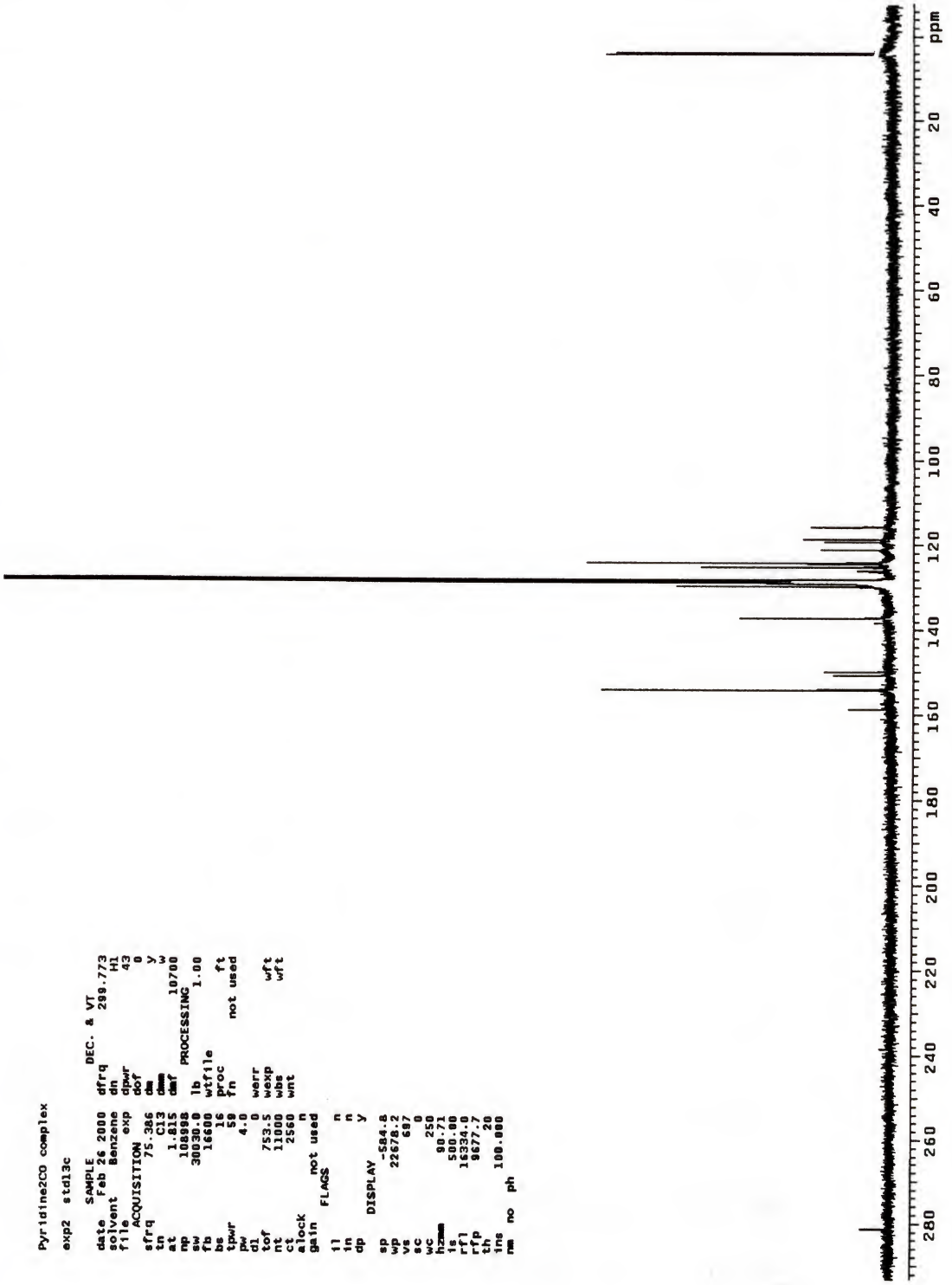

Figure A-19. Proton NMR of W(NPh)(o-$(Me_3SiN)_2C_6H_4$)$(C_6H_7N)_2$(CO) (**12b**) in C_6D_6.

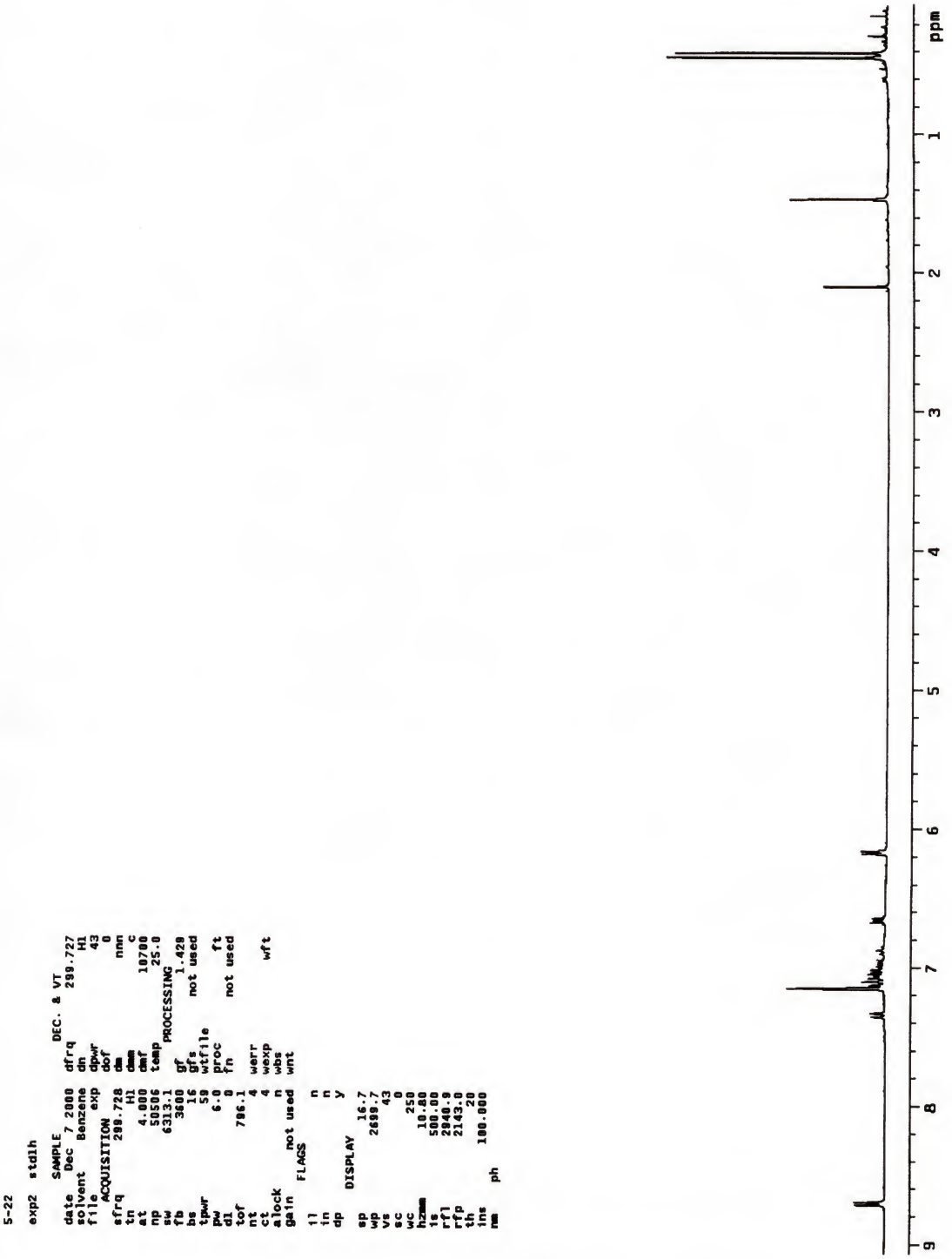

Figure A-20. Carbon NMR of W(NPh)(o-$(Me_3SiN)_2C_6H_4$)$(C_6H_7N)_2$(CO) (**12b**) in C_6D_6.

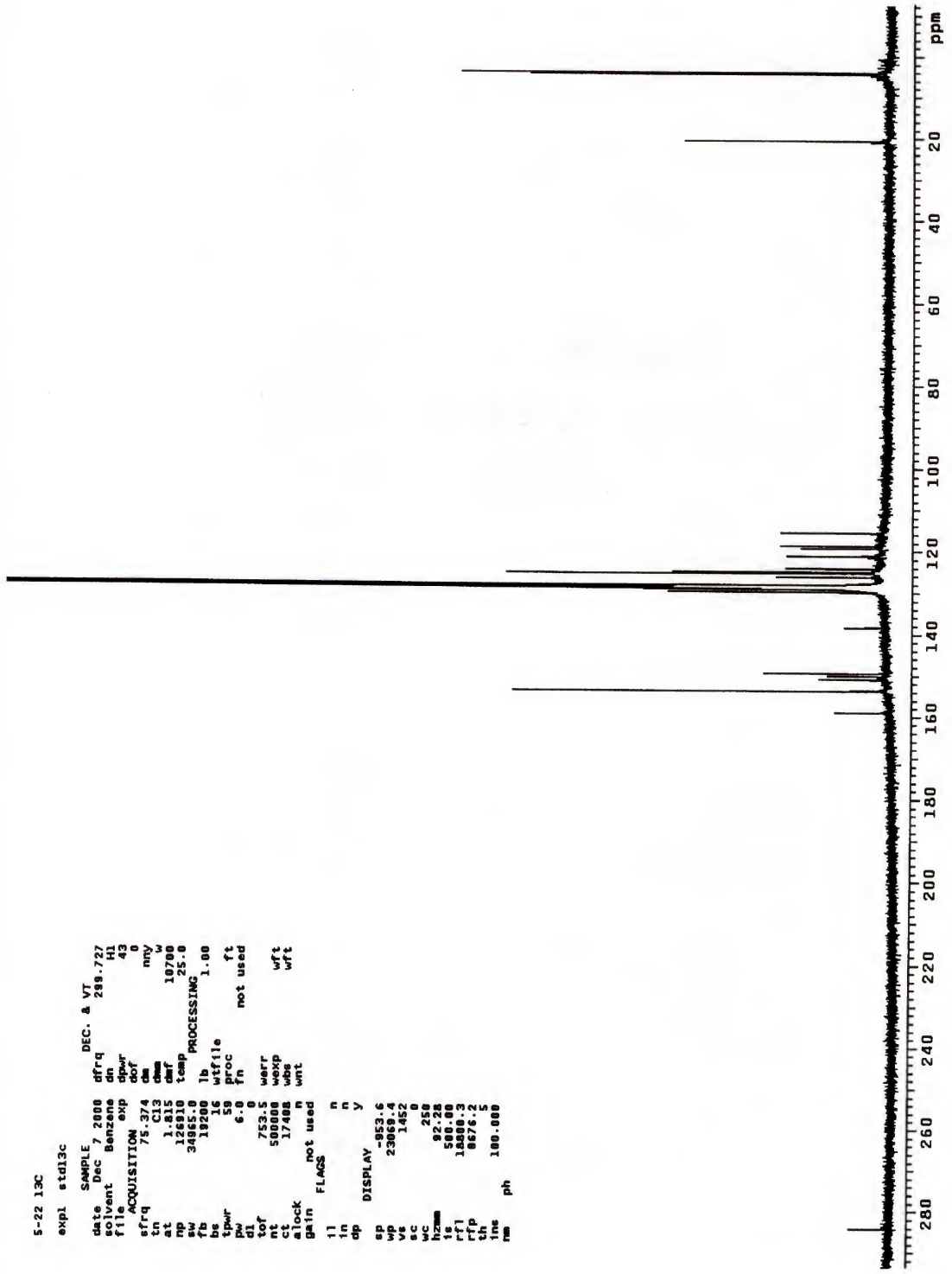

Figure A-21. Proton NMR of W(NPh)(o-$(Me_3SiN)_2C_6H_4$)(C_5H_5N)(PMe_3)(CO) (**13a**) in C_6D_6.

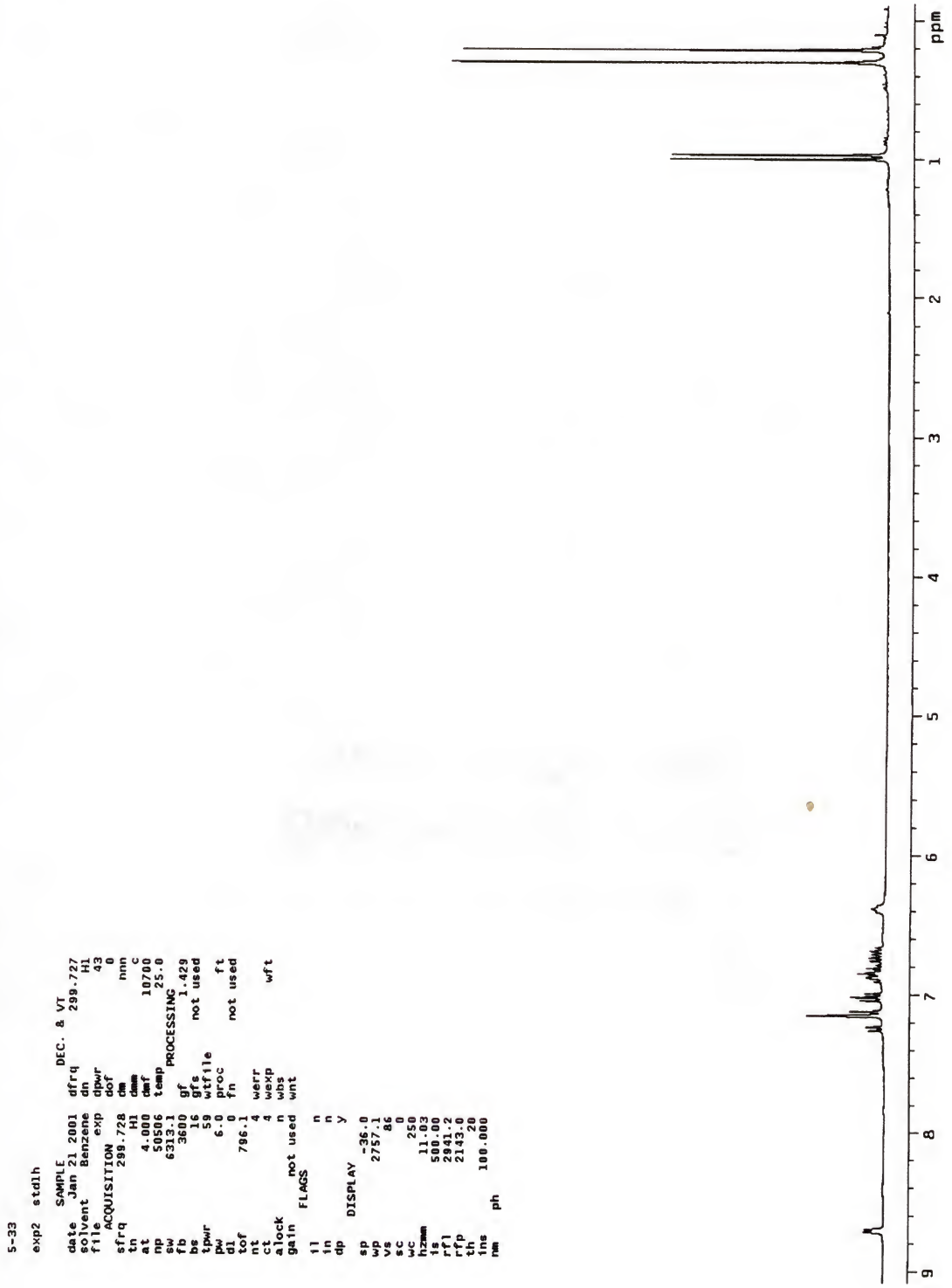

Figure A-22. Carbon NMR of W(NPh)(o-$(Me_3SiN)_2C_6H_4$)(C_5H_5N)(PMe_3)(CO) (**13a**) in C_6D_6.

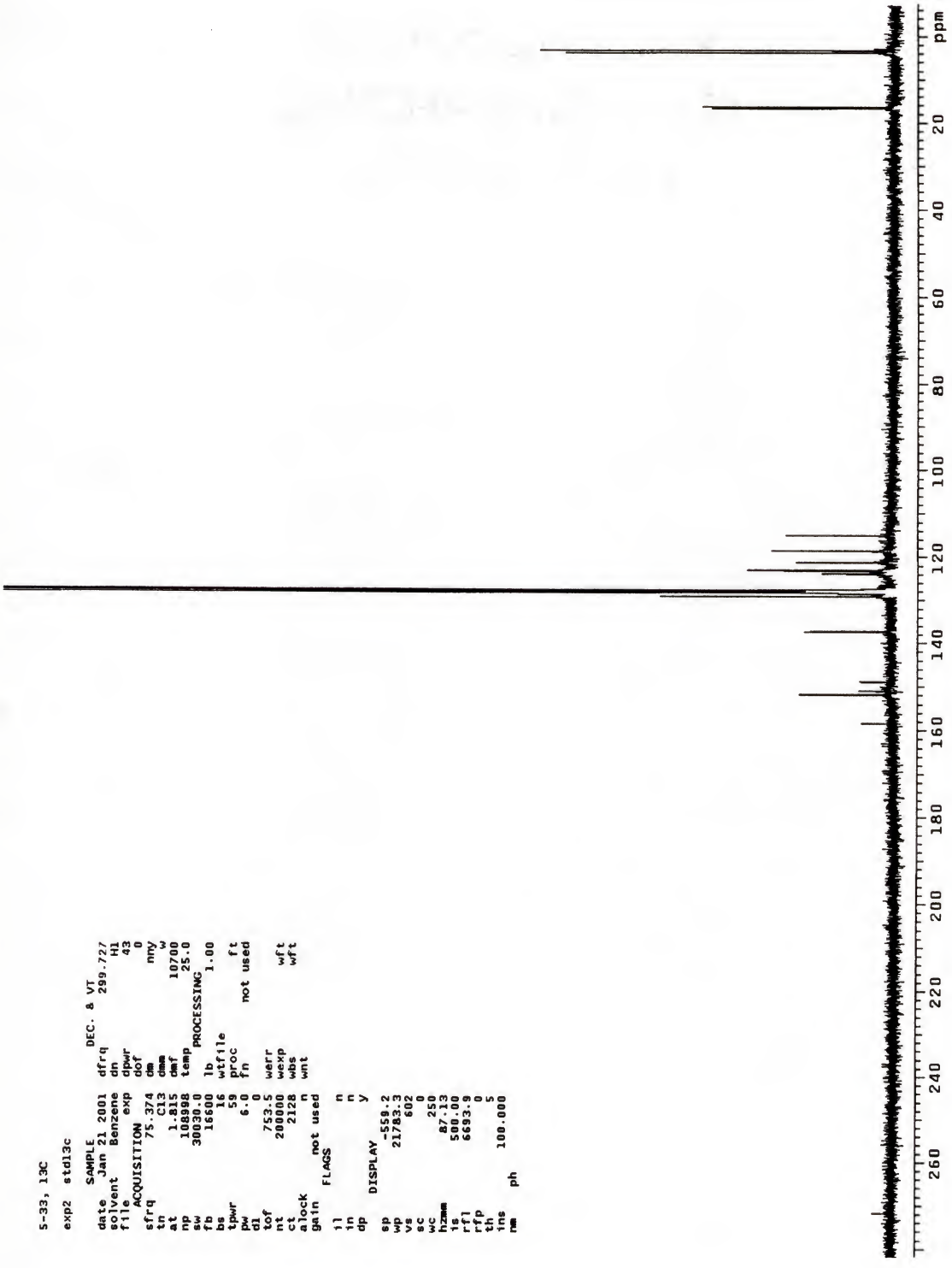

Figure A-23. Phosphorous NMR of W(NPh)(o-$(Me_3SiN)_2C_6H_4$)(C_5H_5N)(PMe_3)(CO) (**13a**) in C_6D_6.

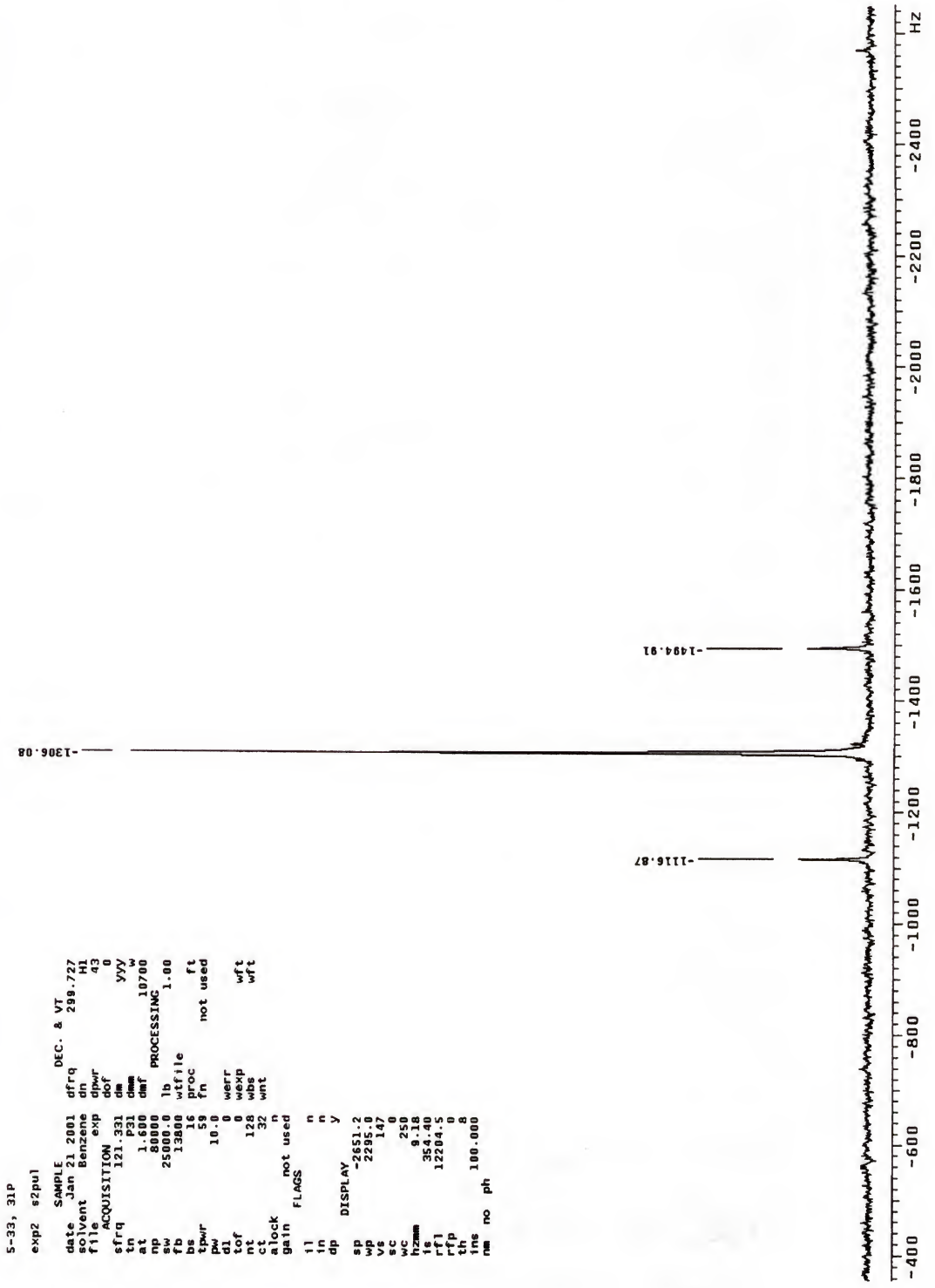

Figure A-24. Proton NMR of W(NPh)(o-$(Me_3SiN)_2C_6H_4$)(C_6H_7N)(PMe_3)(CO) (**13b**) in C_6D_6.

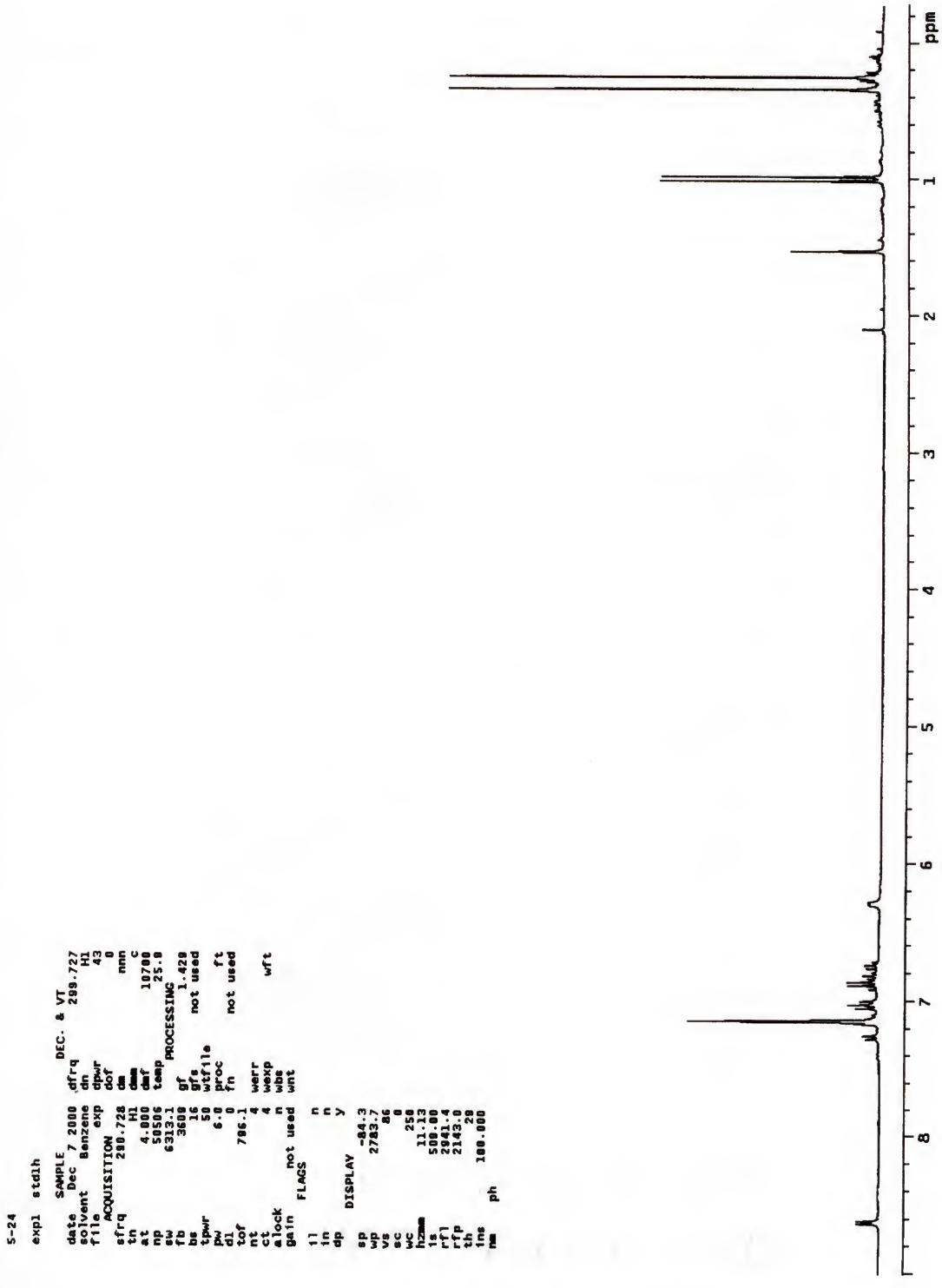

Figure A-25. Carbon NMR of W(NPh)(o-$(Me_3SiN)_2C_6H_4$)(C_6H_7N)(PMe_3)(CO) (**13b**) in C_6D_6.

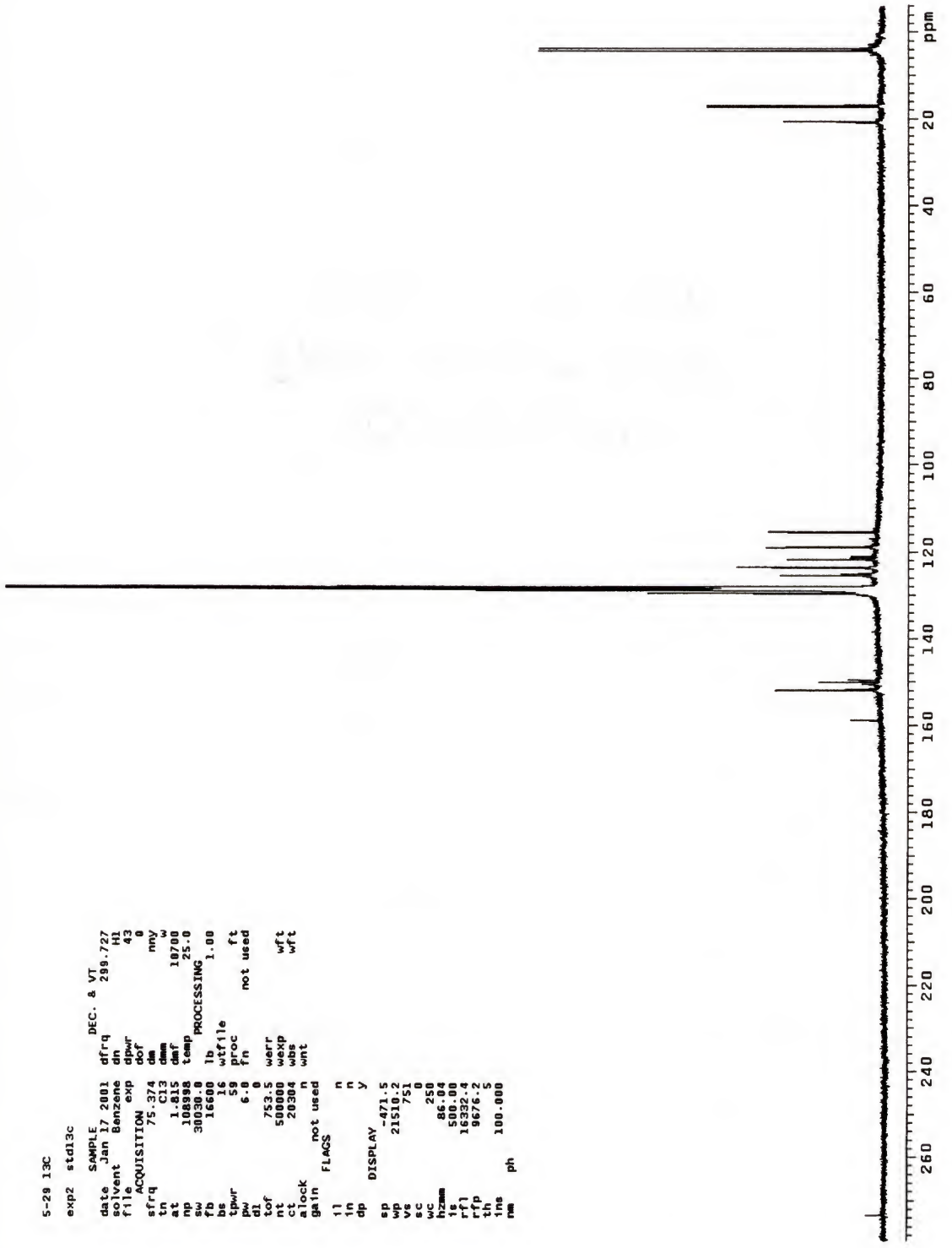

Figure A-26. Phosphorous NMR of W(NPh)(o-$(Me_3SiN)_2C_6H_4$)(C_6H_7N)(PMe_3)(CO) (**13b**) in C_6D_6.

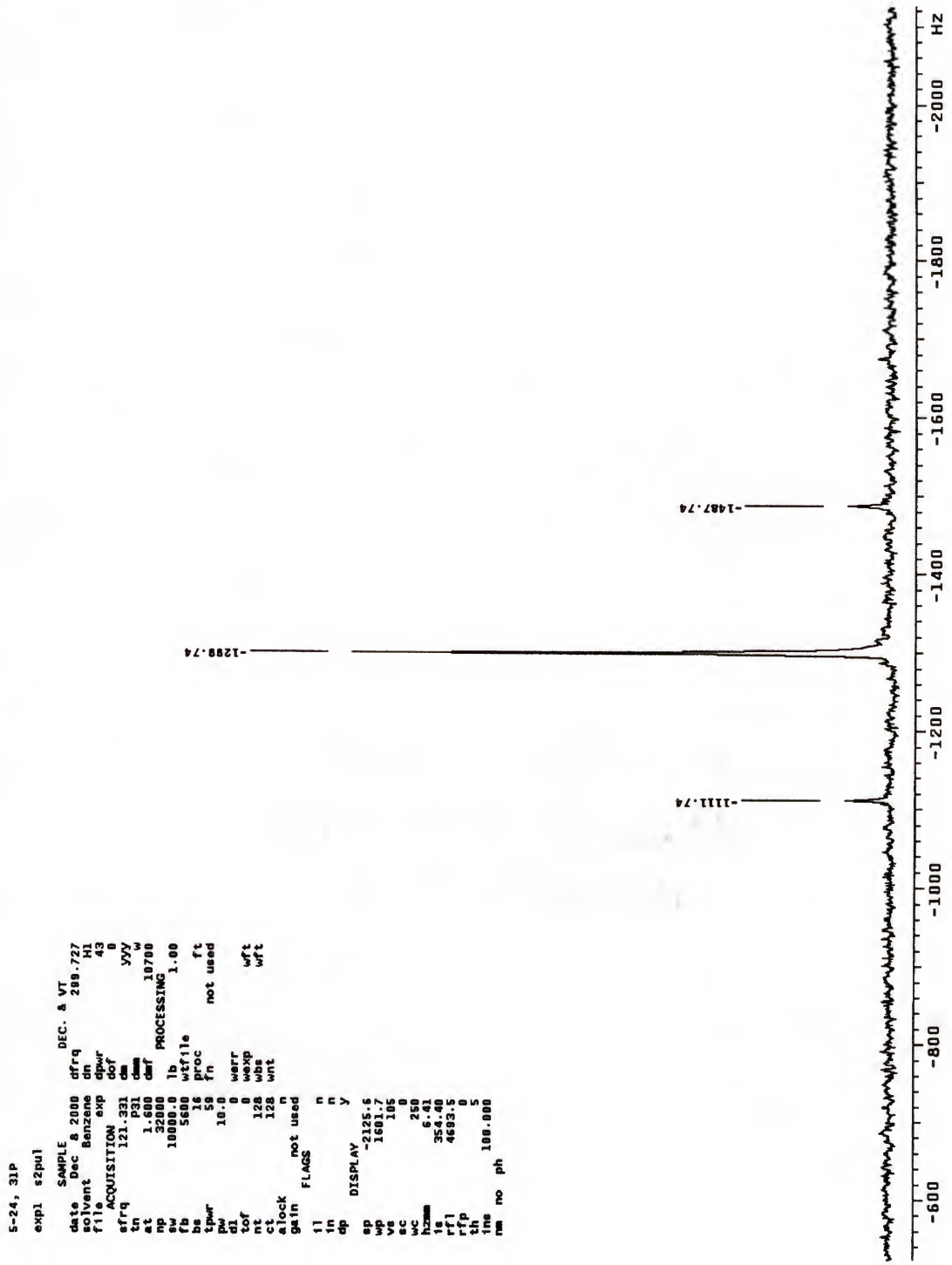

Figure A-27. Proton NMR of W(NPh)(o-$(Me_3SiN)_2C_6H_4$)(C_5H_5N)(PMe_3)$_2$ (**14a**) in C_6D_6.

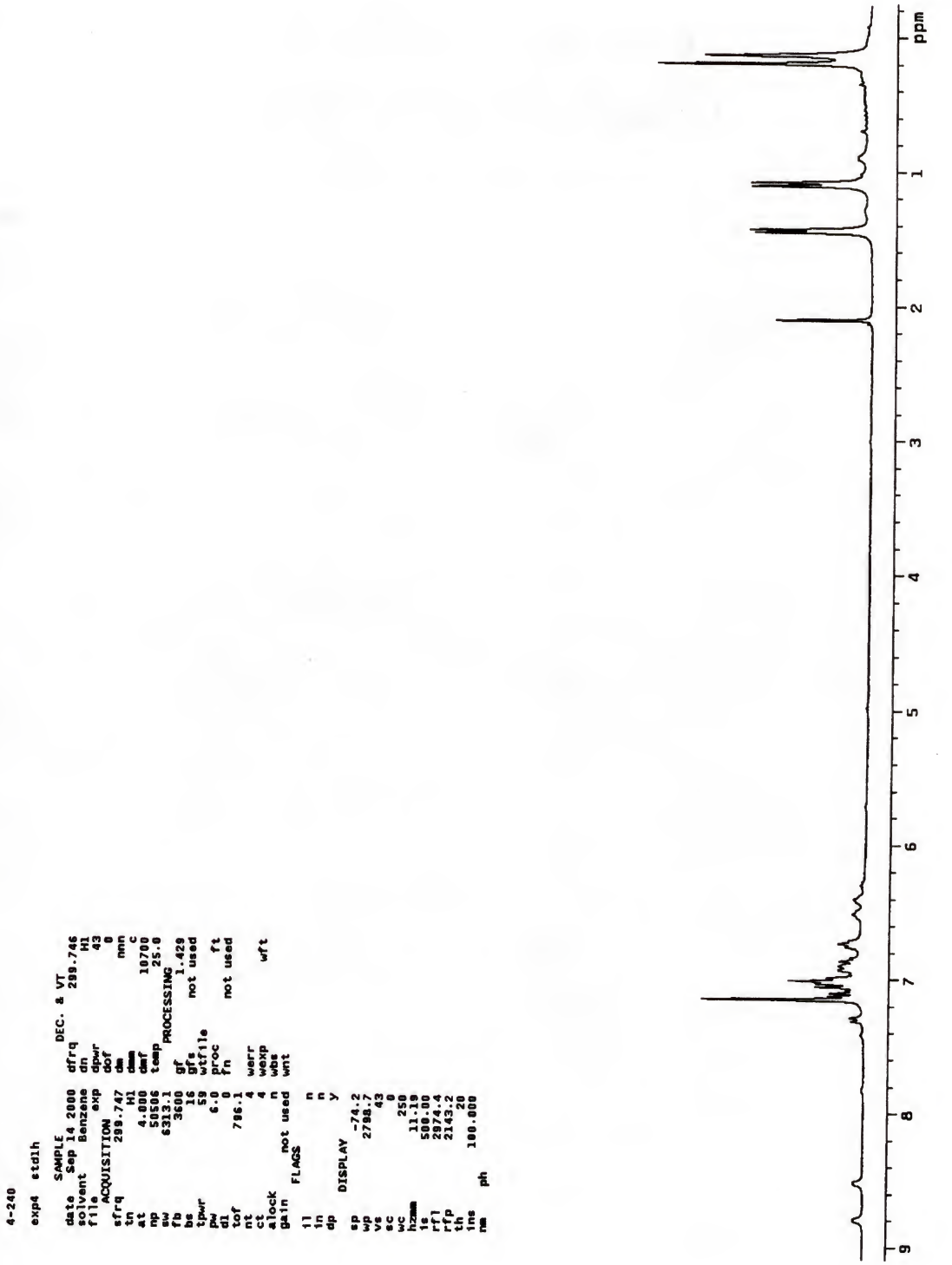

Figure A-28. Carbon NMR of W(NPh)(o-$(Me_3SiN)_2C_6H_4$)(C_5H_5N)$(PMe_3)_2$ (**14a**) in C_6D_6.

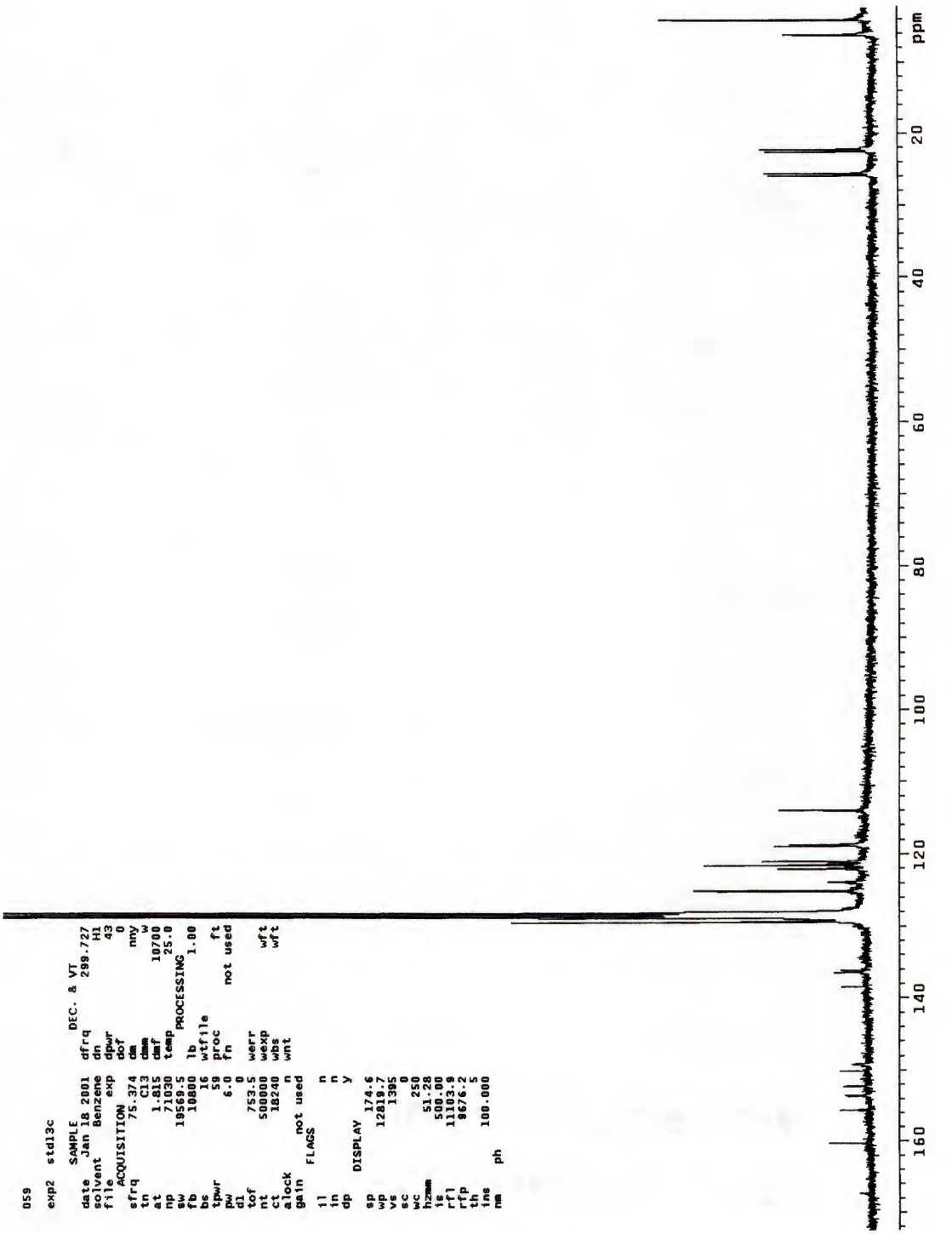

Figure A-29. Phosphorous NMR of W(NPh)(o-$(Me_3SiN)_2C_6H_4$)(C_5H_5N)$(PMe_3)_2$ (**14a**) in C_6D_6.

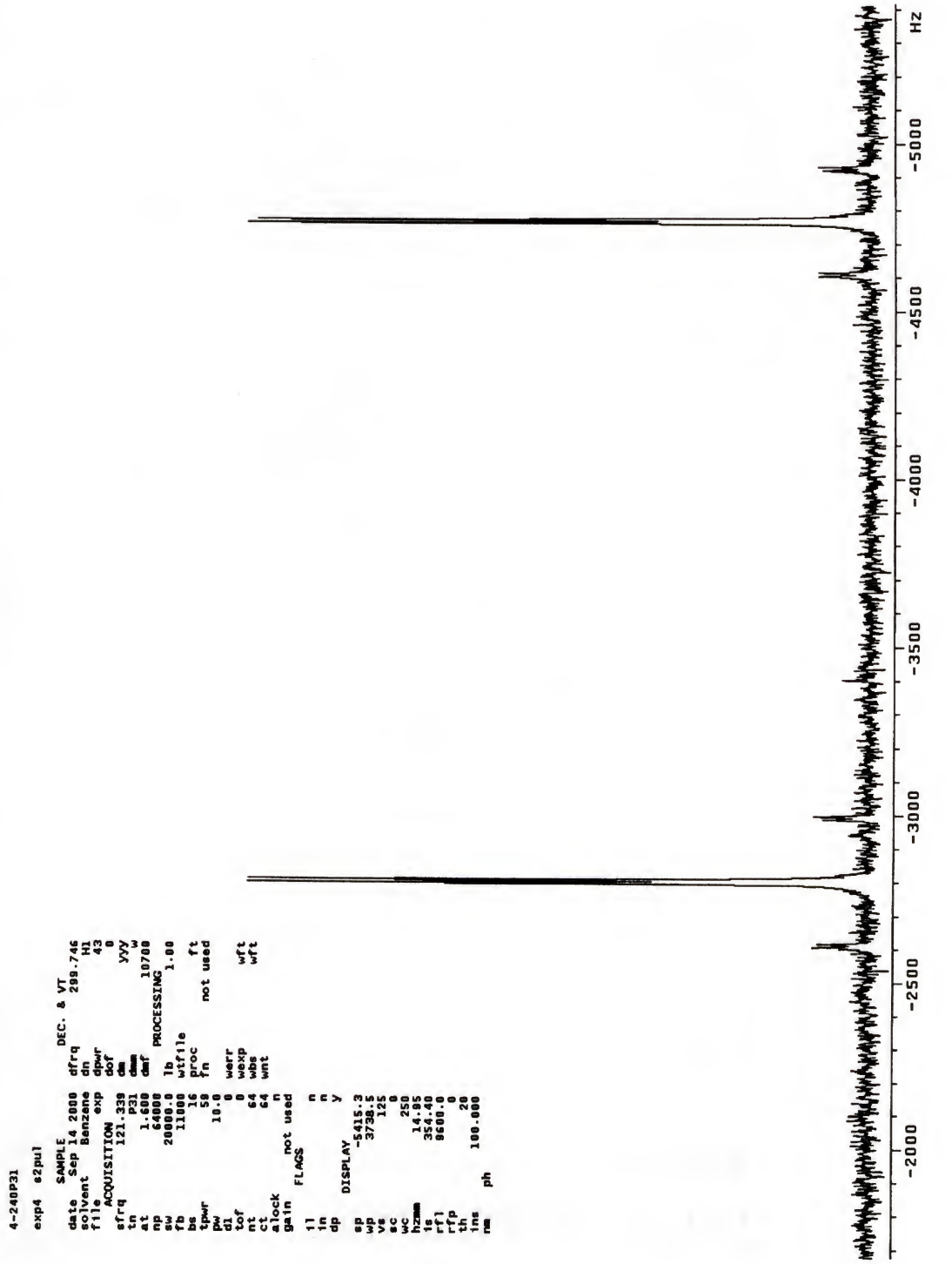

Figure A-30. Proton NMR of W(NPh)(o-$(Me_3SiN)_2C_6H_4$)(C_6H_7N)(PMe_3)$_2$ (**14b**) in C_6D_6.

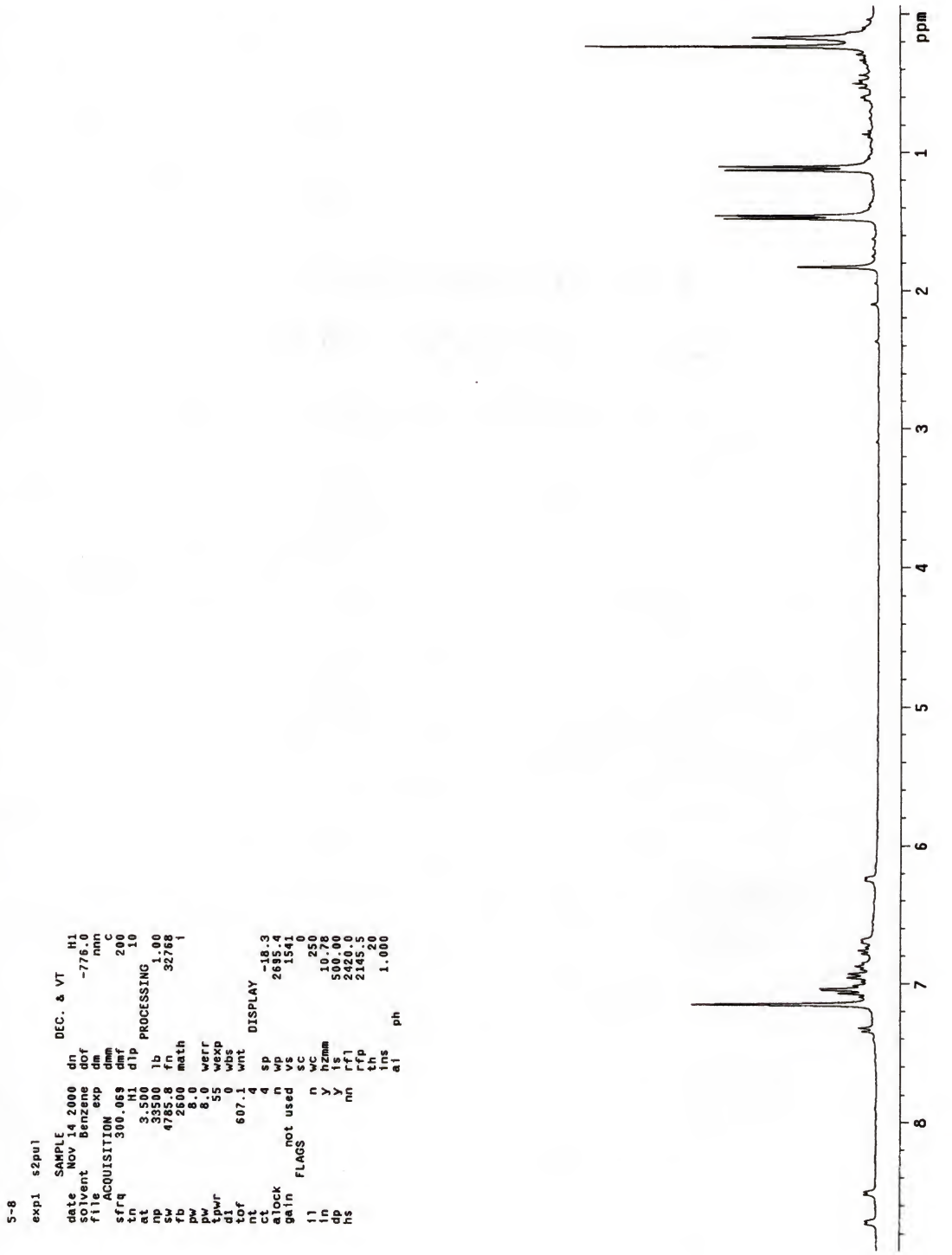

Figure A-31. Carbon NMR of W(NPh)(o-$(Me_3SiN)_2C_6H_4$)(C_6H_7N)$(PMe_3)_2$ (**14b**) in C_6D_6.

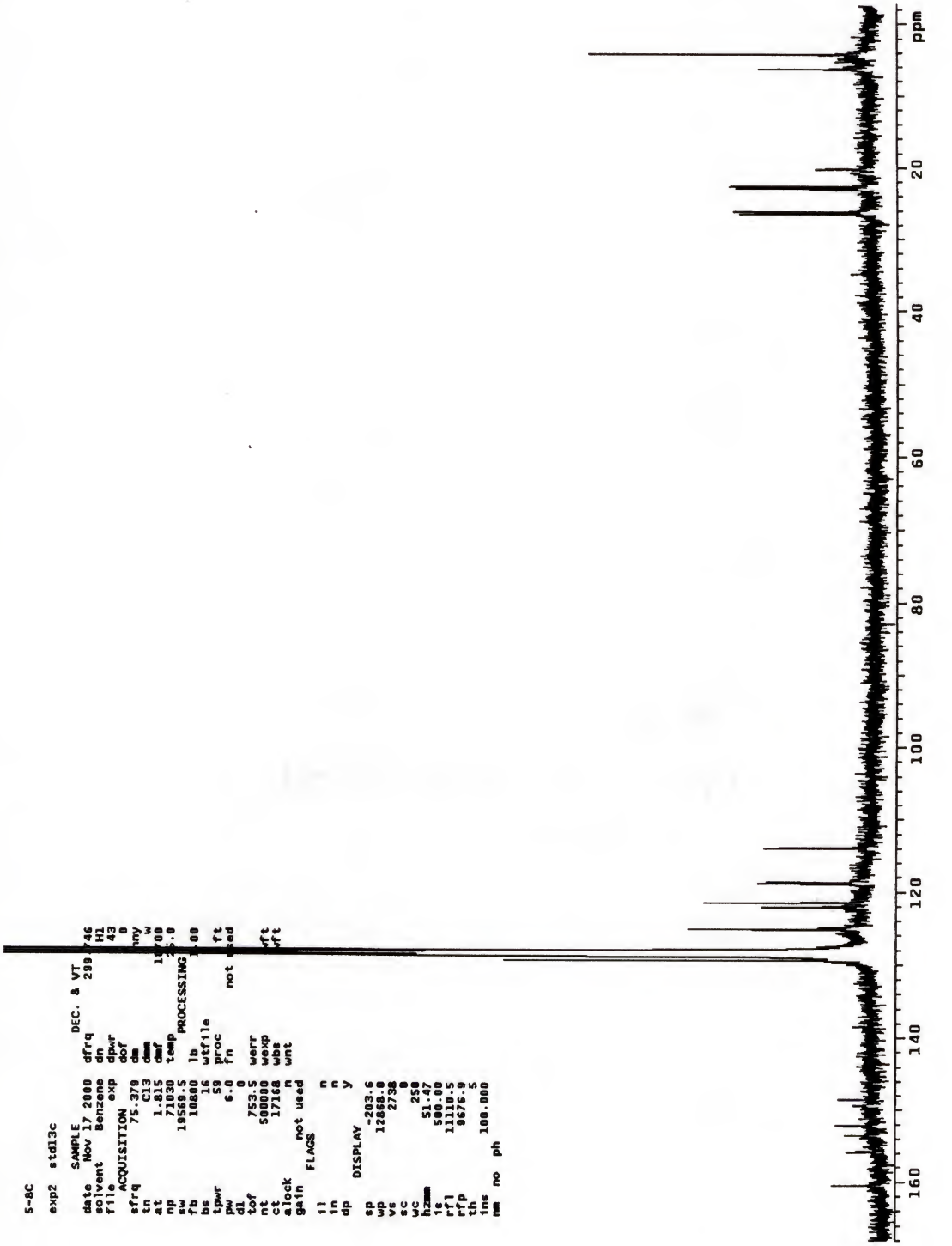

Figure A-32. Phosphorous NMR of W(NPh)(o-$(Me_3SiN)_2C_6H_4$)(C_6H_7N)(PMe_3)$_2$ (**14b**) in C_6D_6.

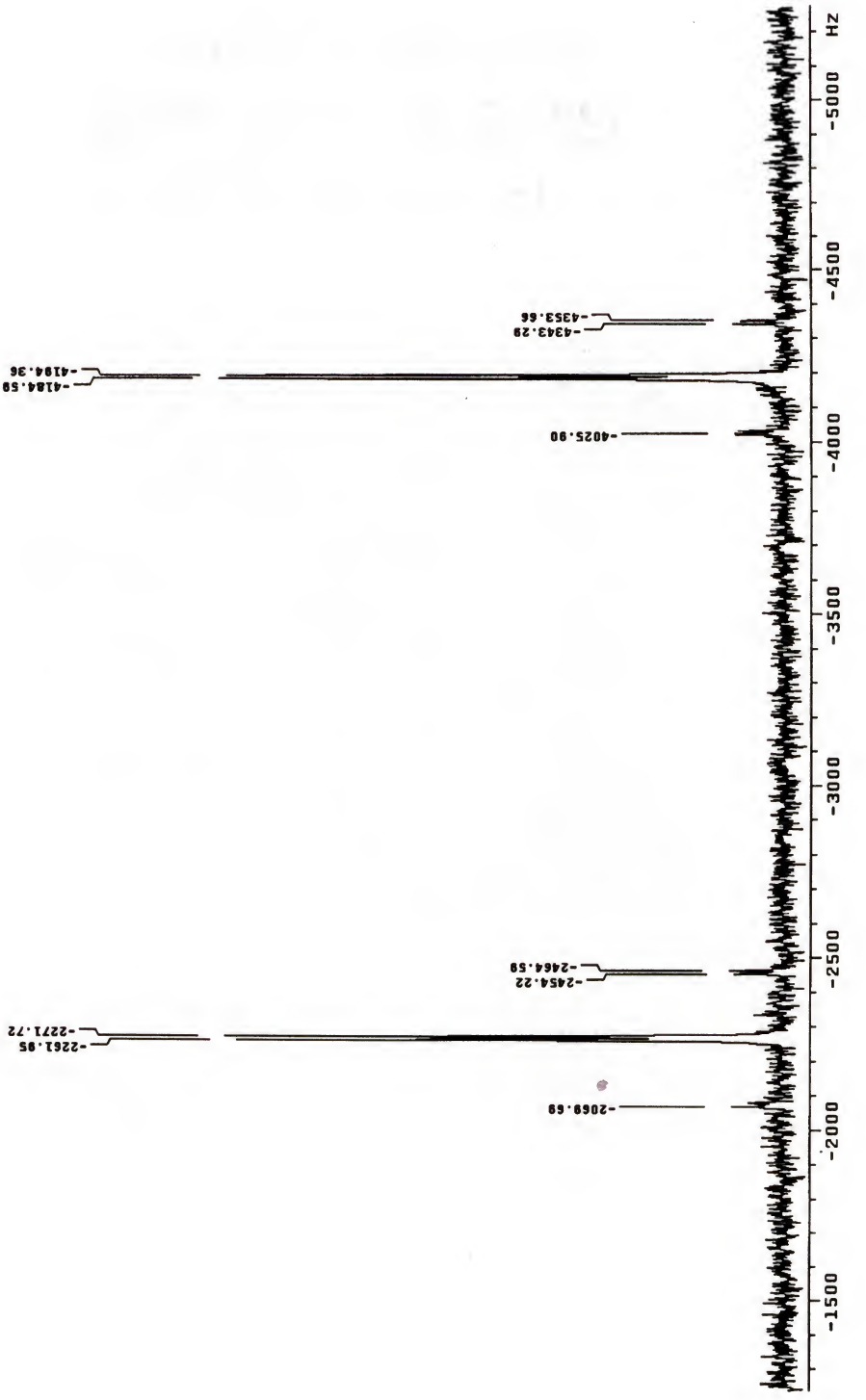

Figure A-33. Proton NMR of W(NPh)(o-$(Me_3SiN)_2C_6H_4$)(PhC≡CPh) (**15**) in C_6D_6.

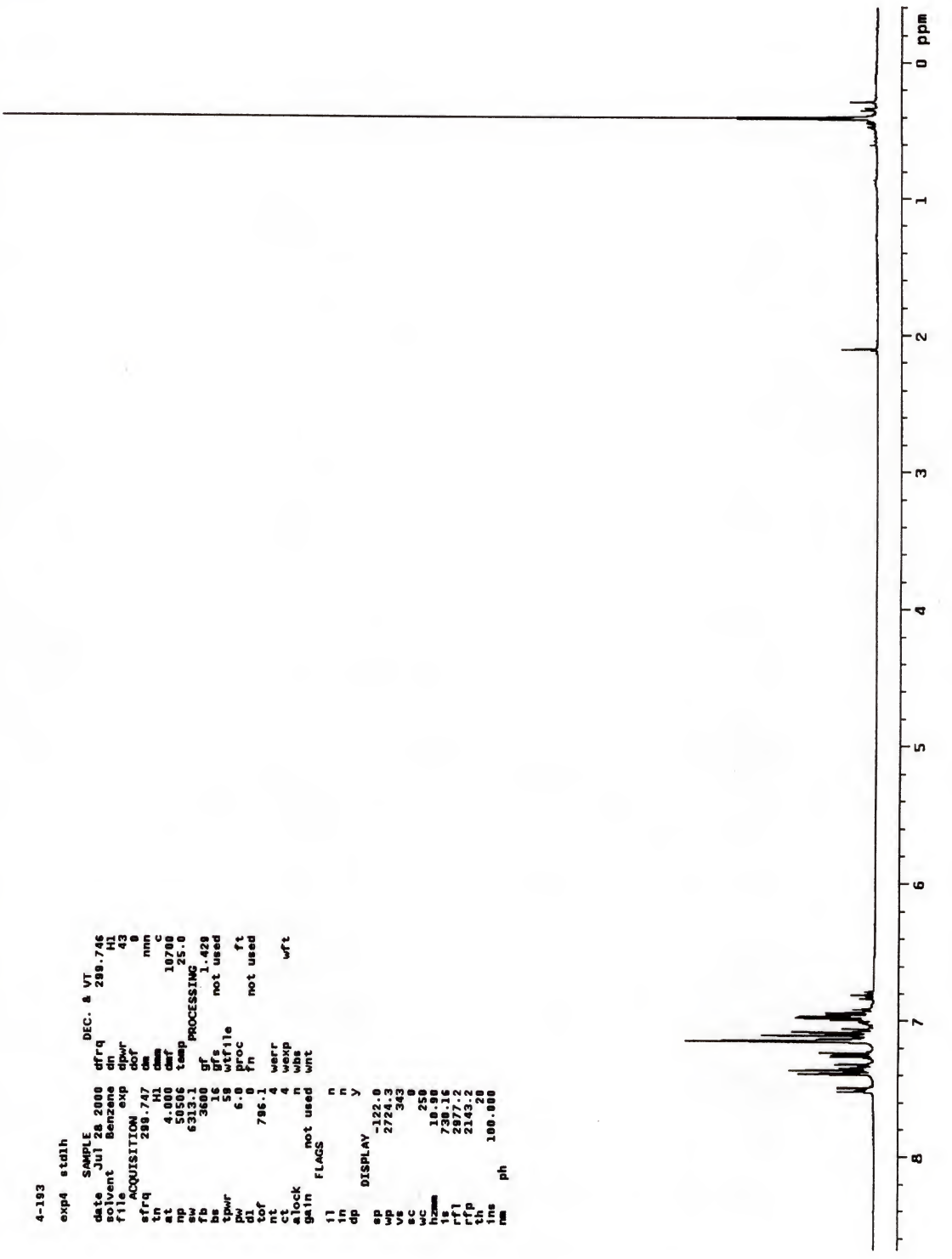

Figure A.34. Carbon NMR of W(NPh)(o-$(Me_3SiN)_2C_6H_4$)(PhC≡CPh) (**15**) in C_6D_6.

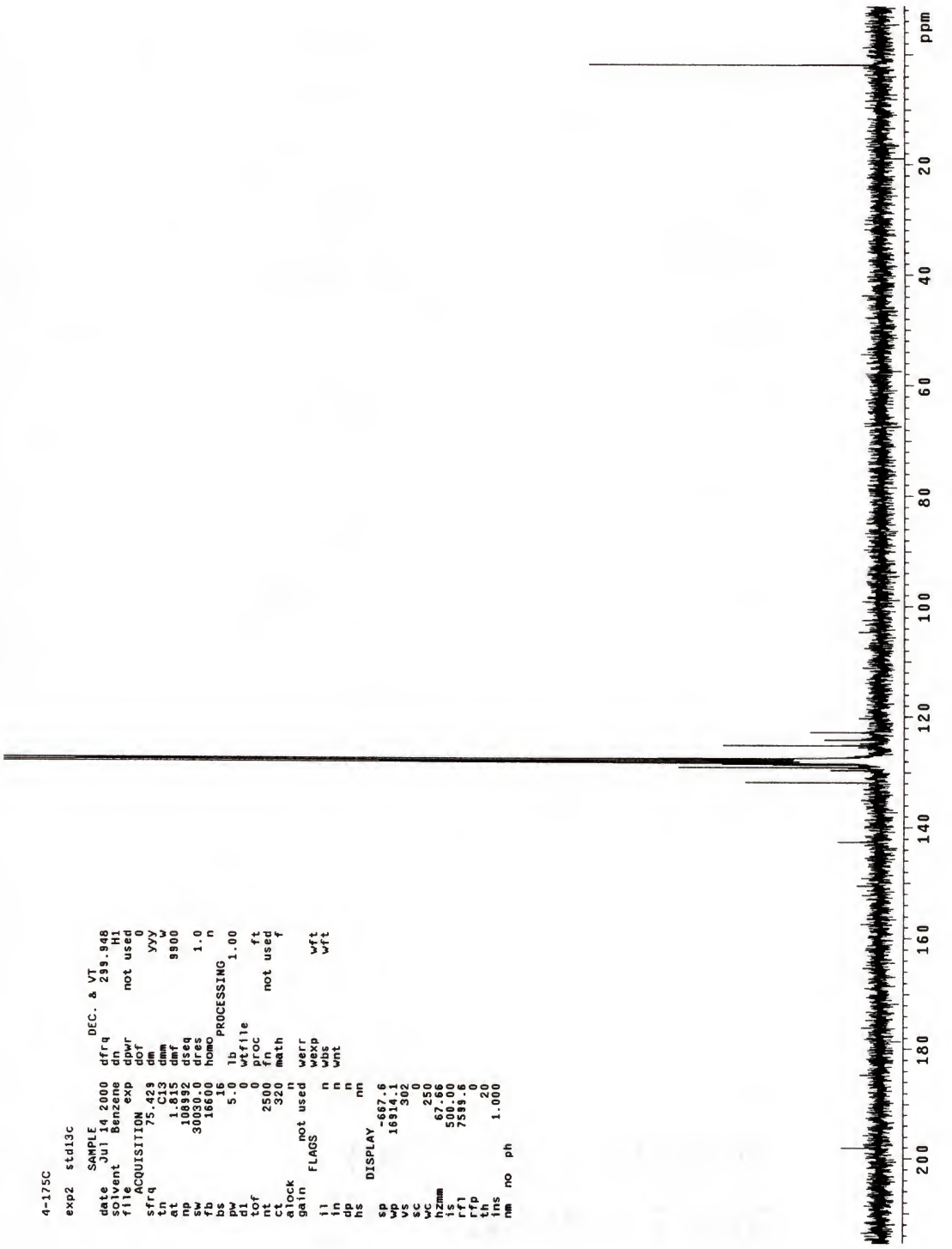

Figure A-35. Proton NMR of W(NPh)[o-$(Me_3SiN)_2C_6H_4$][η^4-$(CH_2=C(CH_3)C(CH_3)=CH_2)$] (**17**) in C_6D_6.

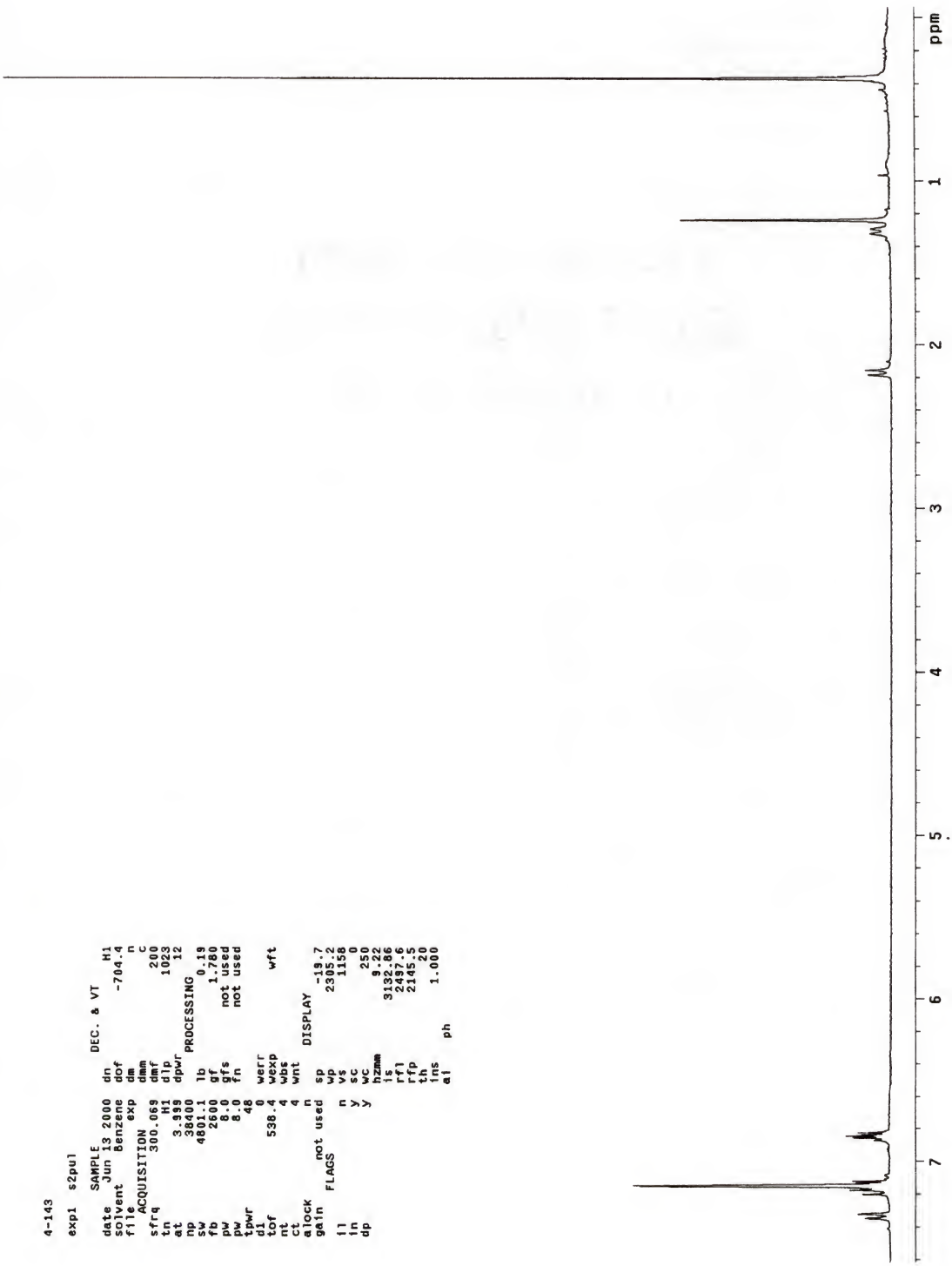

Figure A-36. Carbon NMR of W(NPh)[o-$(Me_3SiN)_2C_6H_4$][η^4-$(CH_2=C(CH_3)C(CH_3)=CH_2)$] (**17**) in C_6D_6.

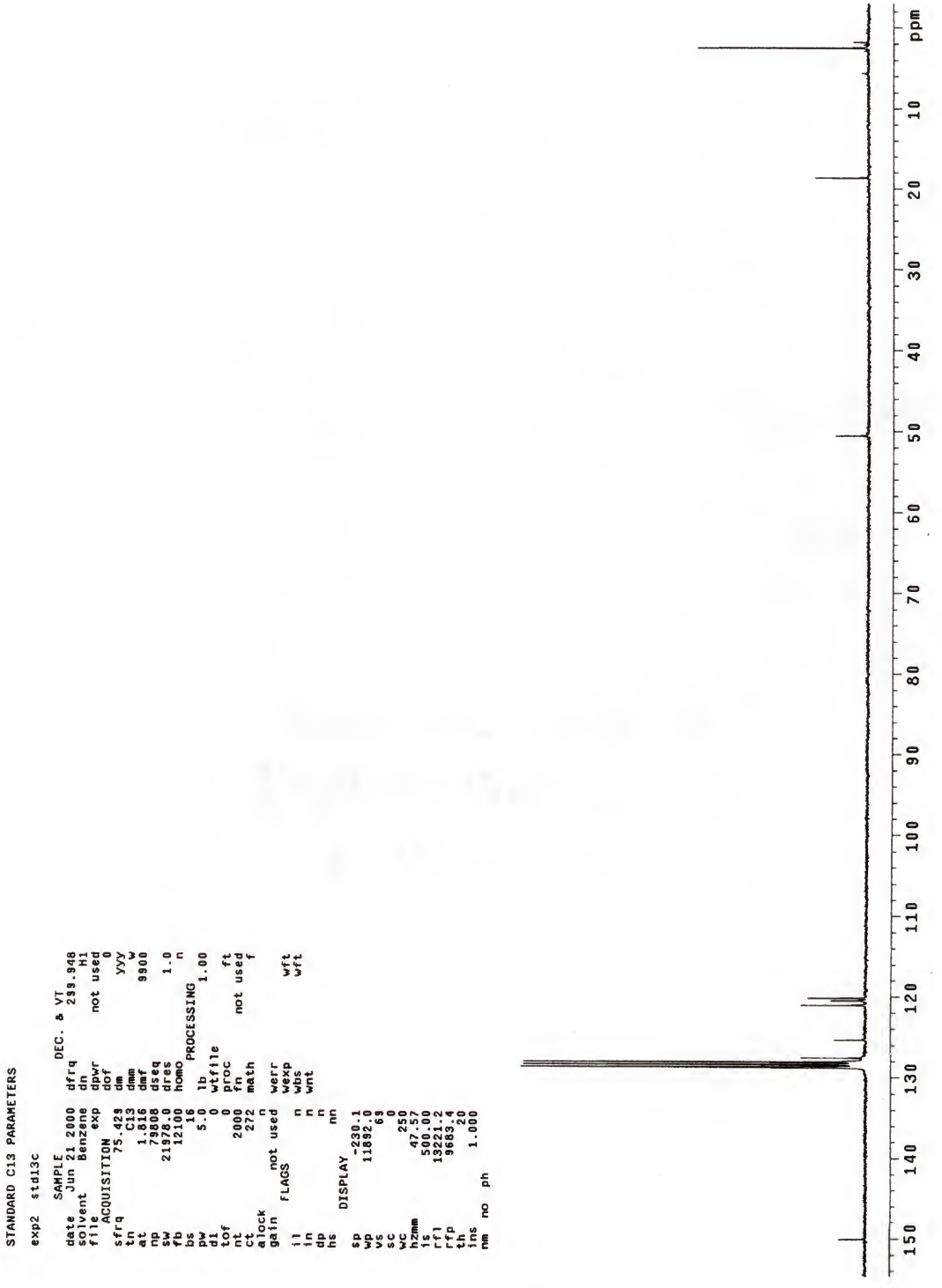

Figure A-37. Proton NMR of W(NPh)[o-$(Me_3SiN)_2C_6H_4$](η^4-$(CH_2{=}CHCH{=}CH_2)$ (**18**) in C_6D_6.

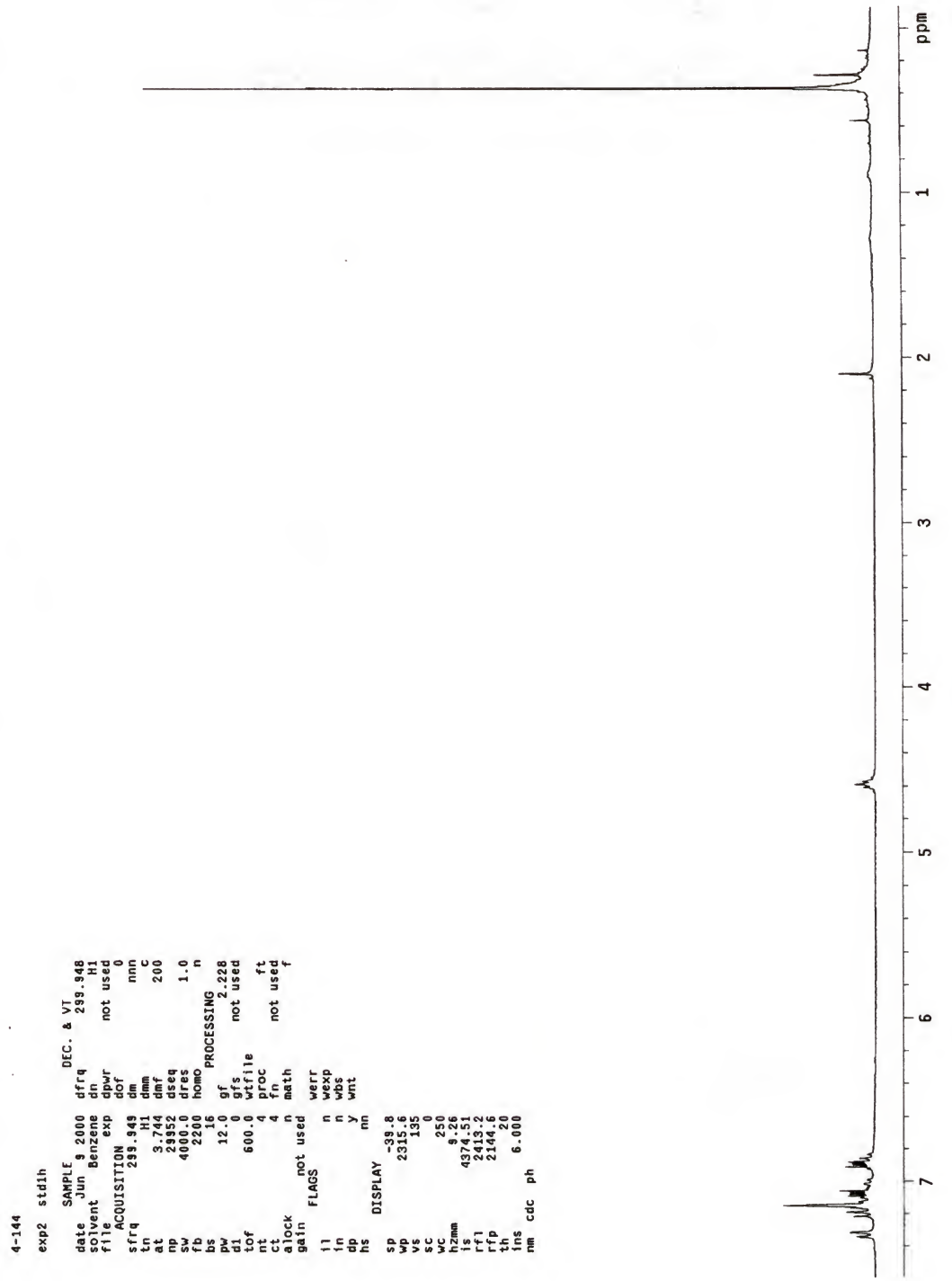

Figure A-38. Carbon NMR of W(NPh)[o-$(Me_3SiN)_2C_6H_4$](η^4-$(CH_2{=}CHCH{=}CH_2)$ (**18**) in C_6D_6.

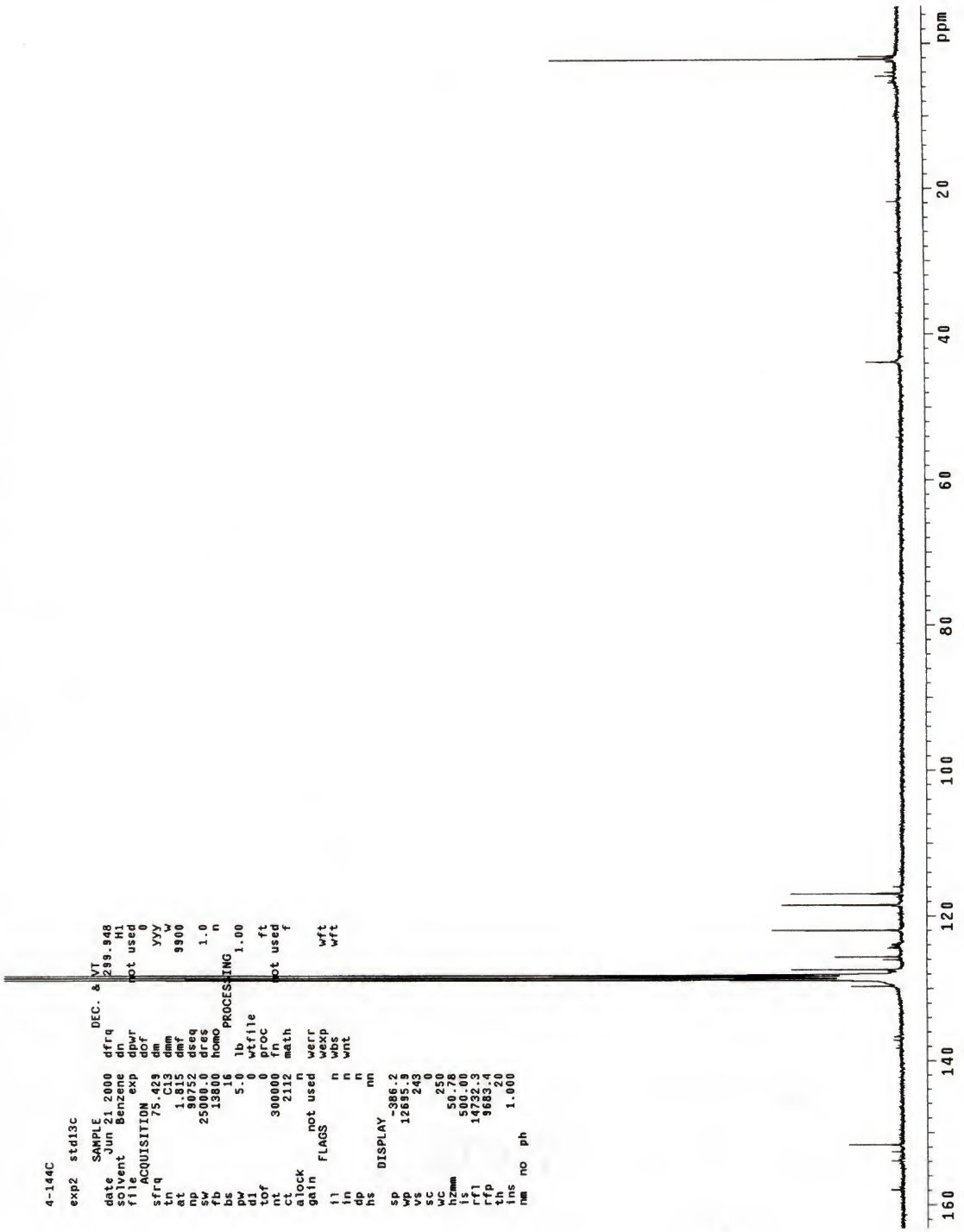

Figure A-39. Proton NMR of $W(CH_2CH_2CH_2CH_2)(NPh)[o\text{-}(Me_3SiN)_2C_6H_4]$ (**20**) in C_6D_6.

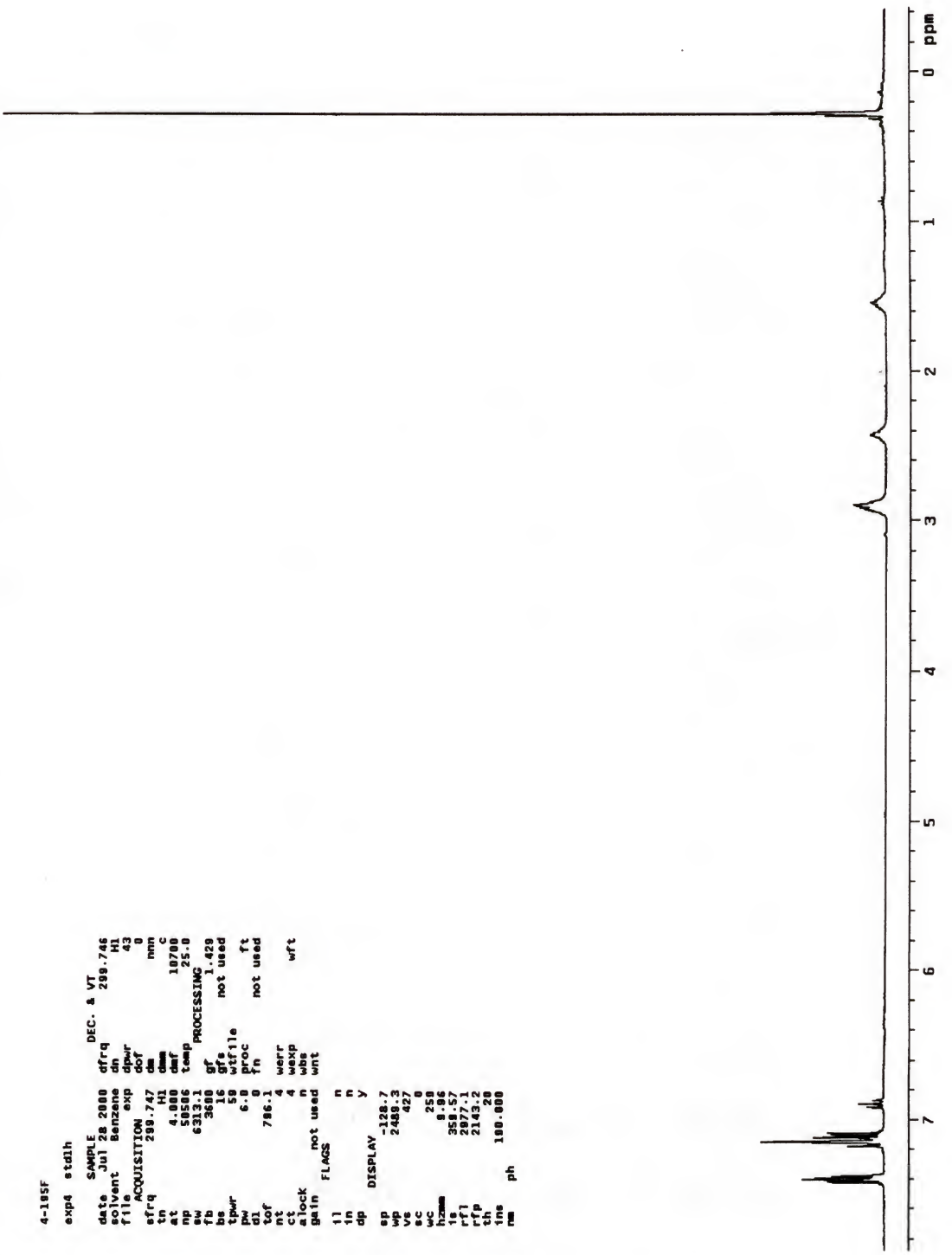

Figure A-40. Proton NMR of W(NPh)(o-$(Me_3SiN)_2C_6H_4$)$(C_5H_5N)_2$(η^2-ethylene) (**21**) in C_6D_6.

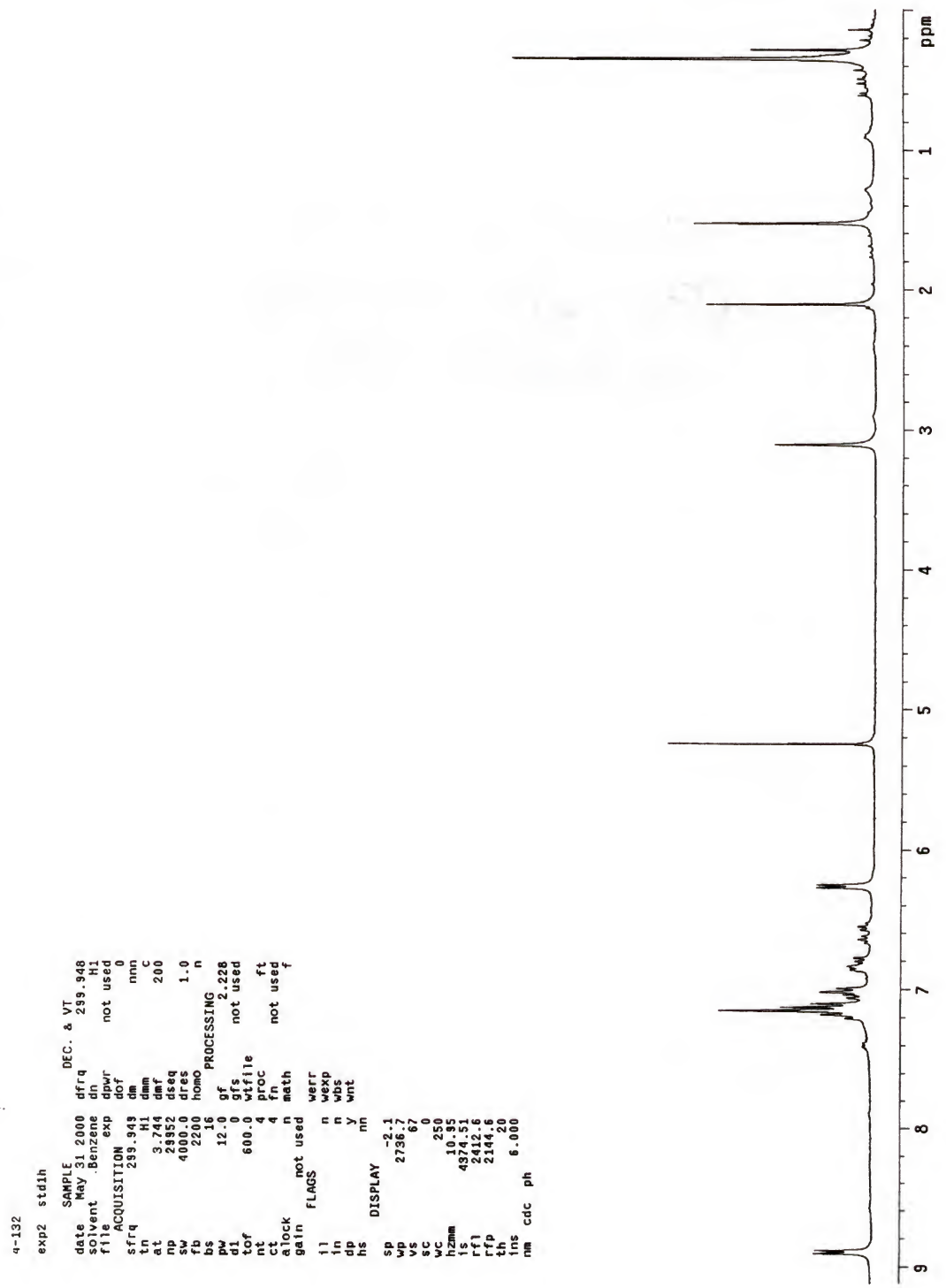

Figure A-41. Carbon NMR of W(NPh)(o-$(Me_3SiN)_2C_6H_4$)$(C_5H_5N)_2$(η^2-ethylene) (**21**) in C_6D_6.

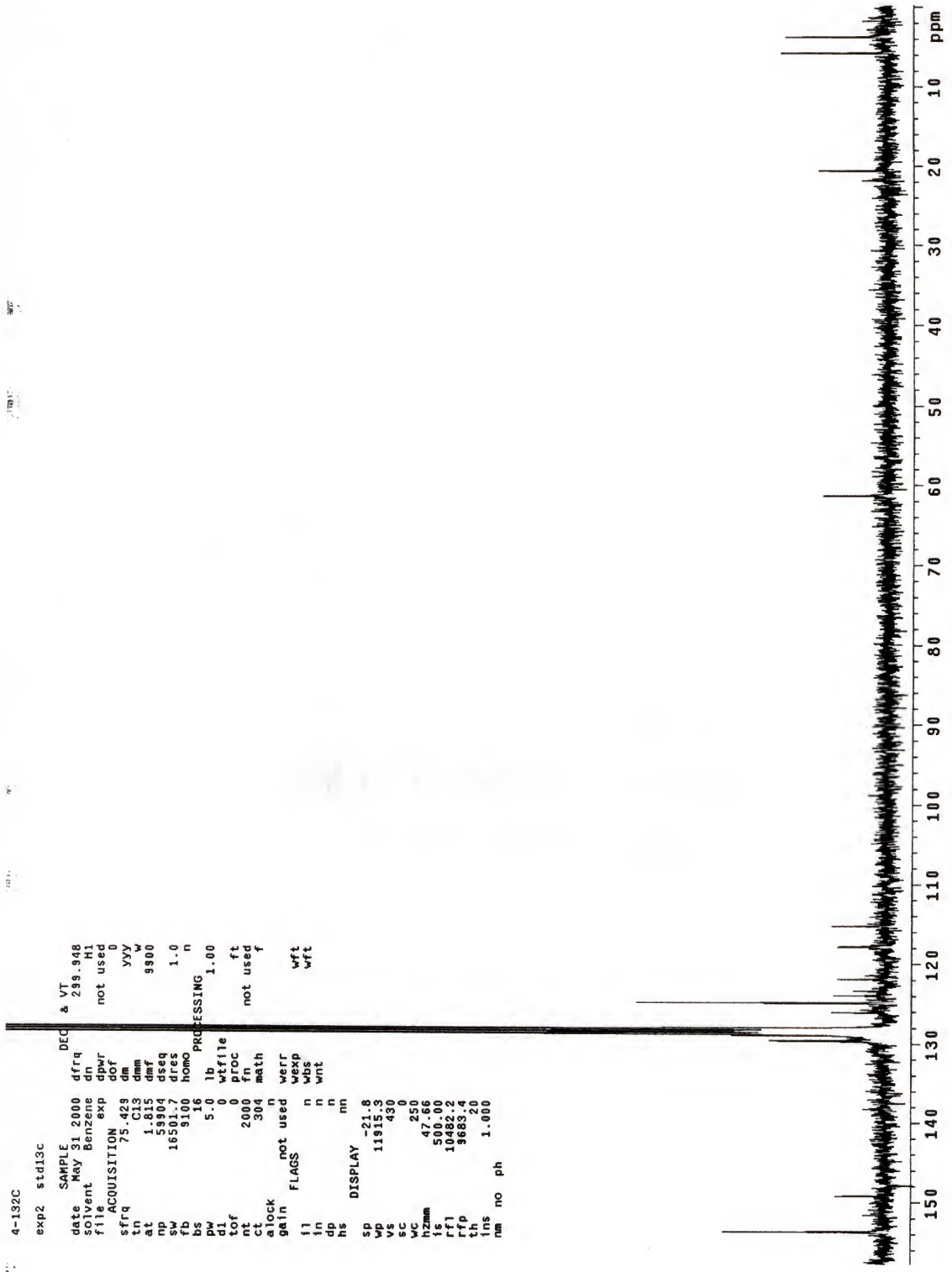

Figure A-42. Proton NMR of [o-$(Me_3SiN)_2C_6H_4$](NPh)W(SC_4H_4) (**22**) in C_6D_6.

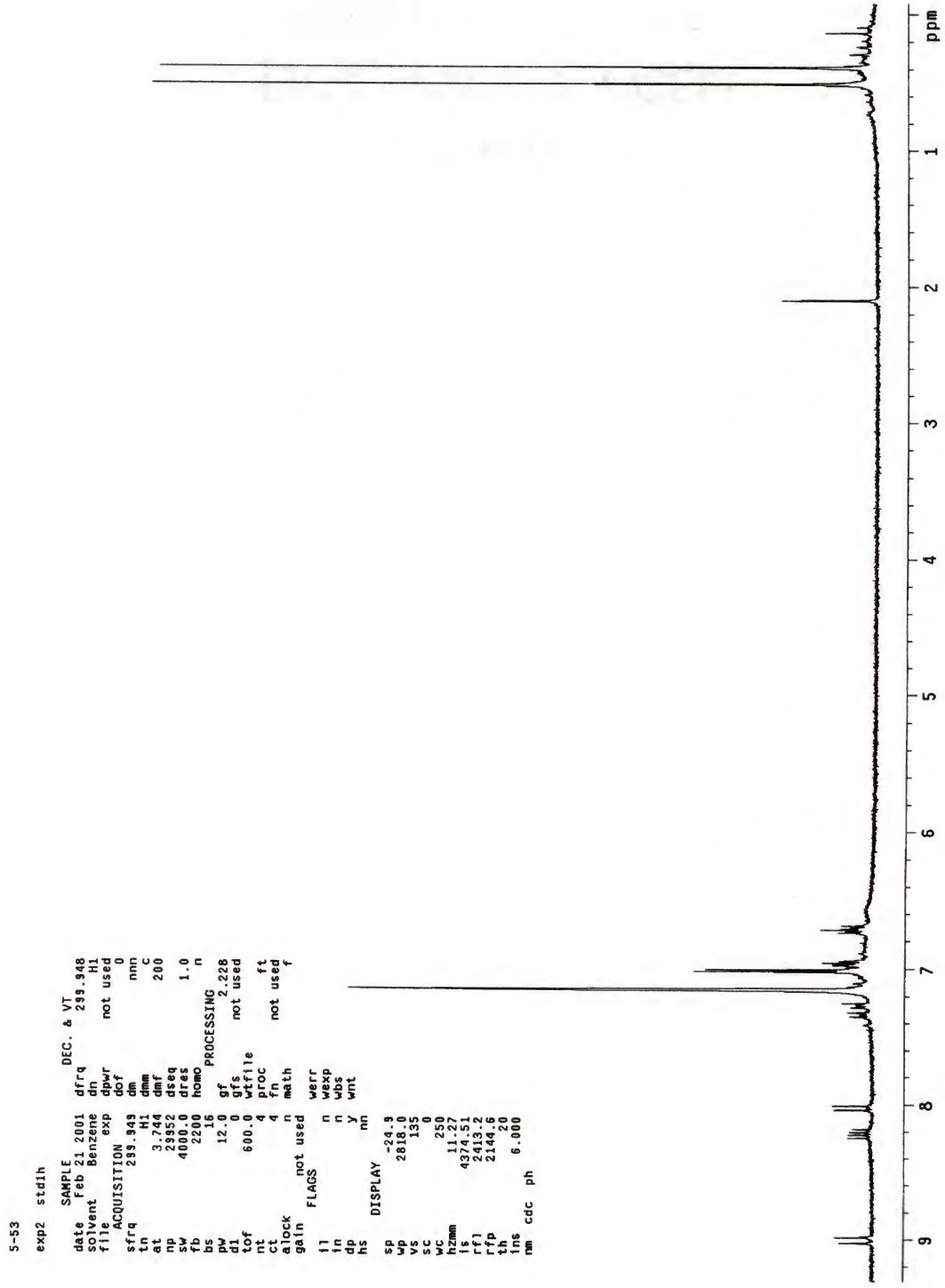

Figure A-43. Carbon NMR of [o-$(Me_3SiN)_2C_6H_4$](NPh)W(SC_4H_4) (**22**) in C_6D_6.

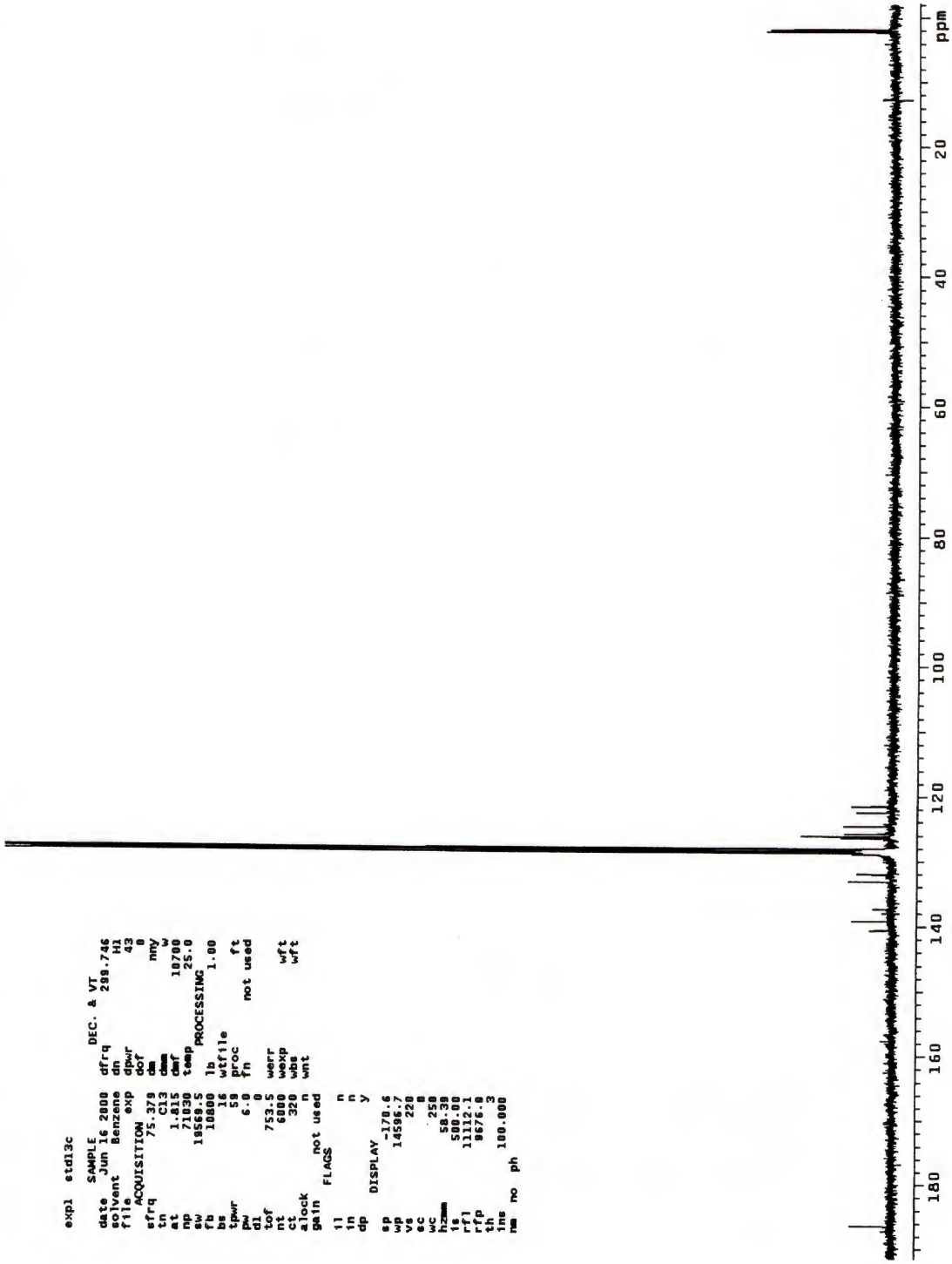

Figure A-44. Proton NMR of [o-$(Me_3SiN)_2C_6H_4$](NPh)W(SC_5H_6) (**23**) in C_6D_6.

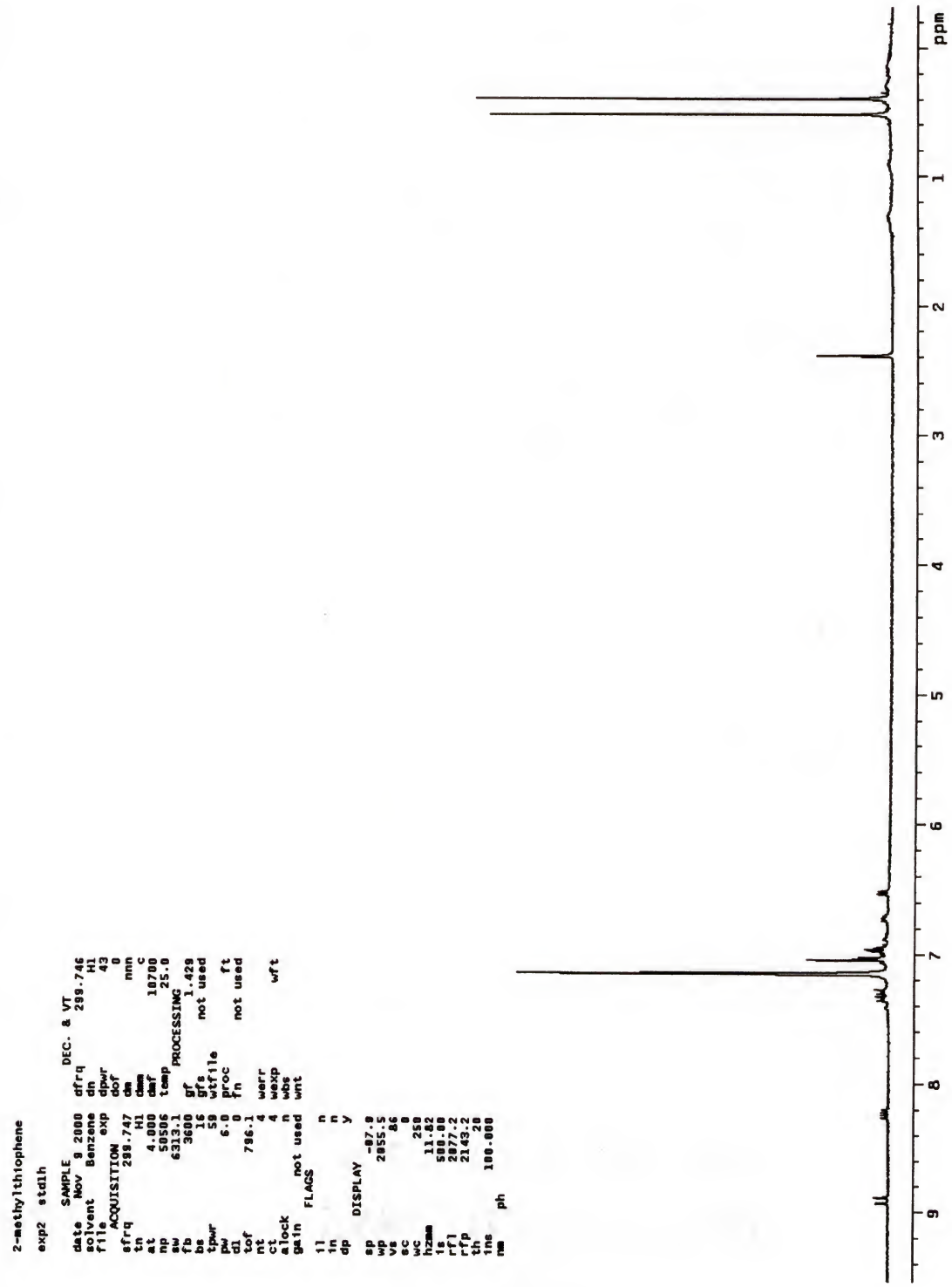

Figure A-45. Carbon NMR of [o-$(Me_3SiN)_2C_6H_4$](NPh)W(SC_5H_6) (**23**) in C_6D_6.

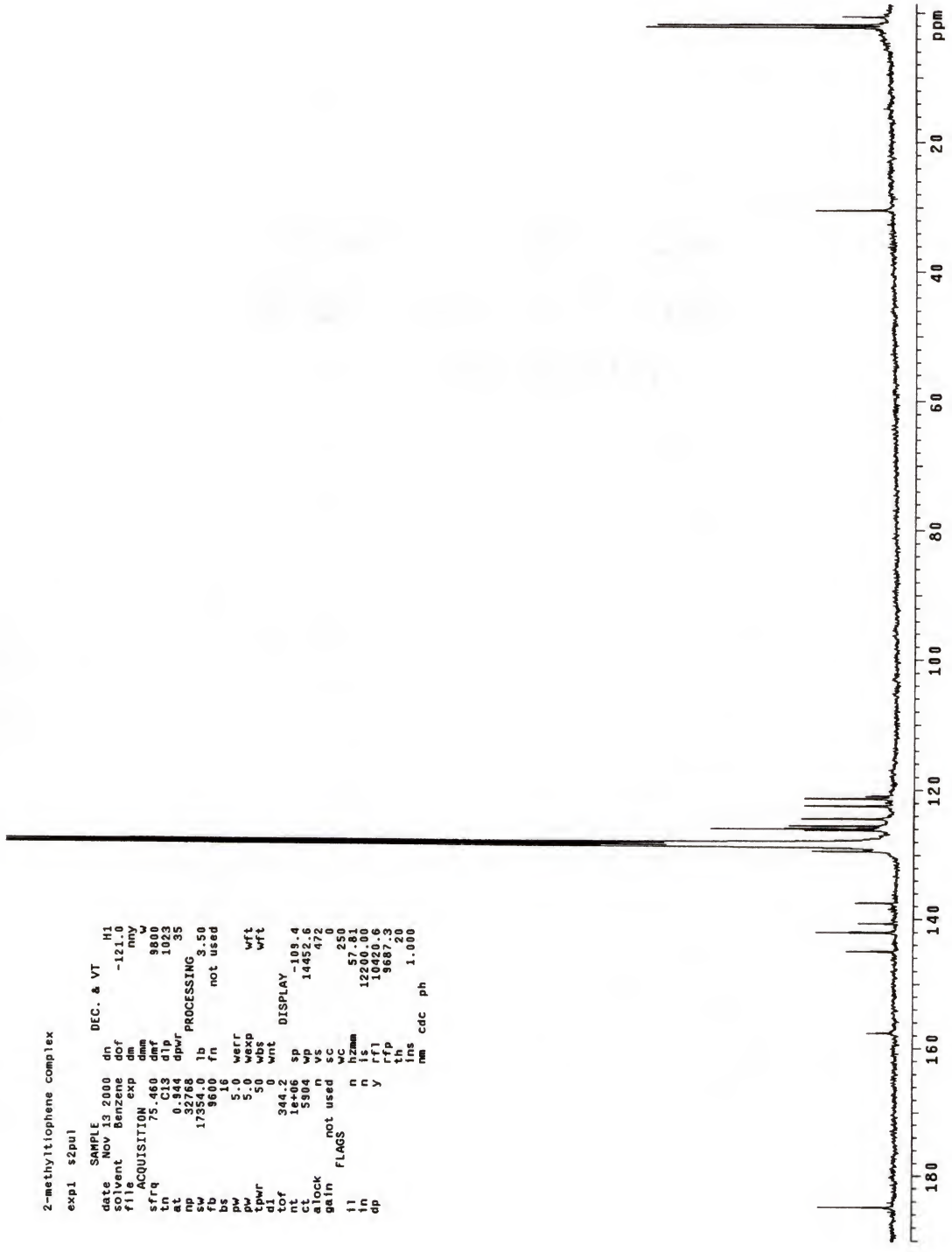

Figure A-46. Proton NMR of [o-$(Me_3SiN)_2C_6H_4$](NPh)W(SC_8H_6) (**24**) in C_6D_6.

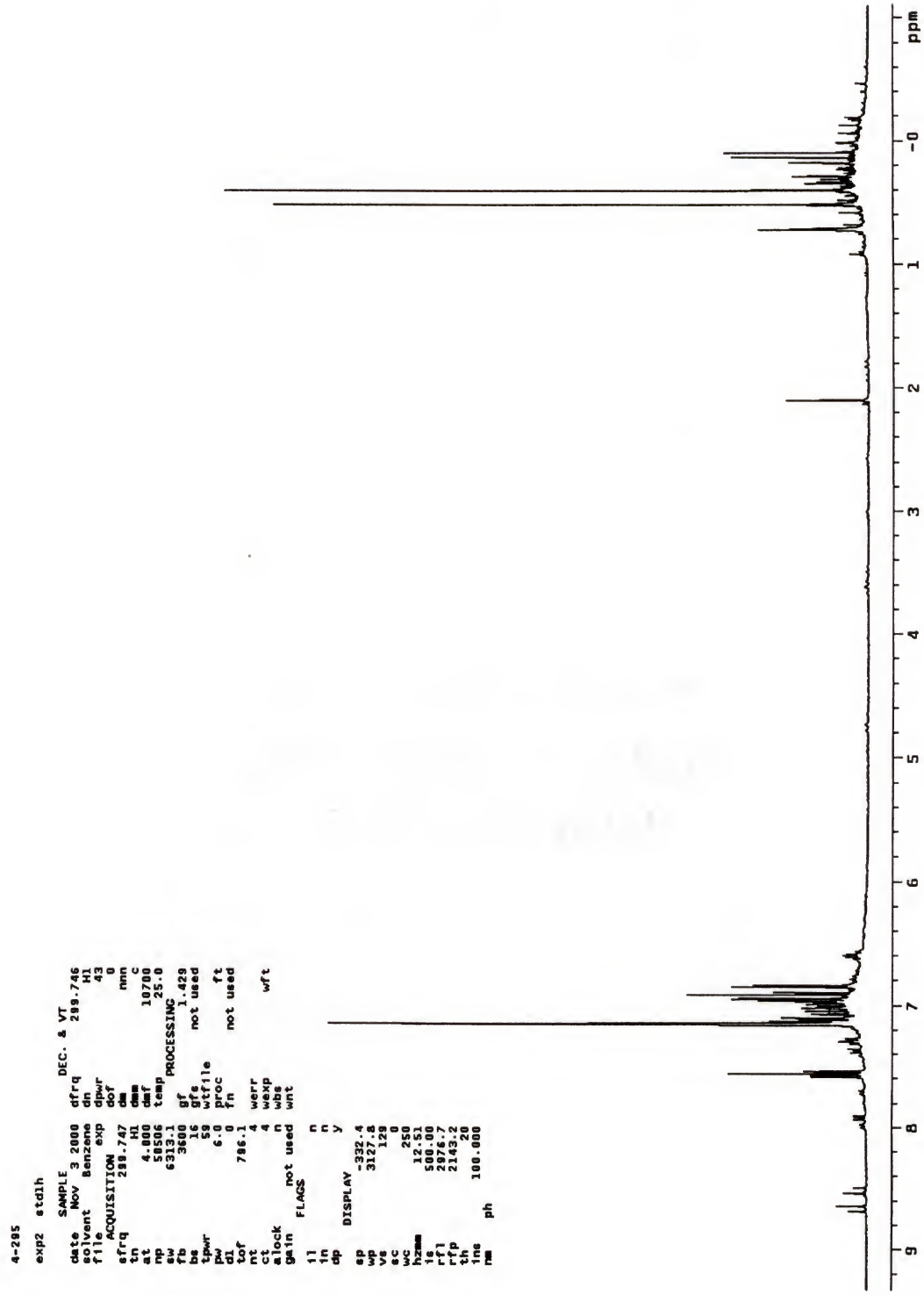

Figure A-47. Proton NMR of [o-$(Me_3SiN)_2C_6H_4$](NPh)W(SC_5H_6) (**25a,b**) in C_6D_6.

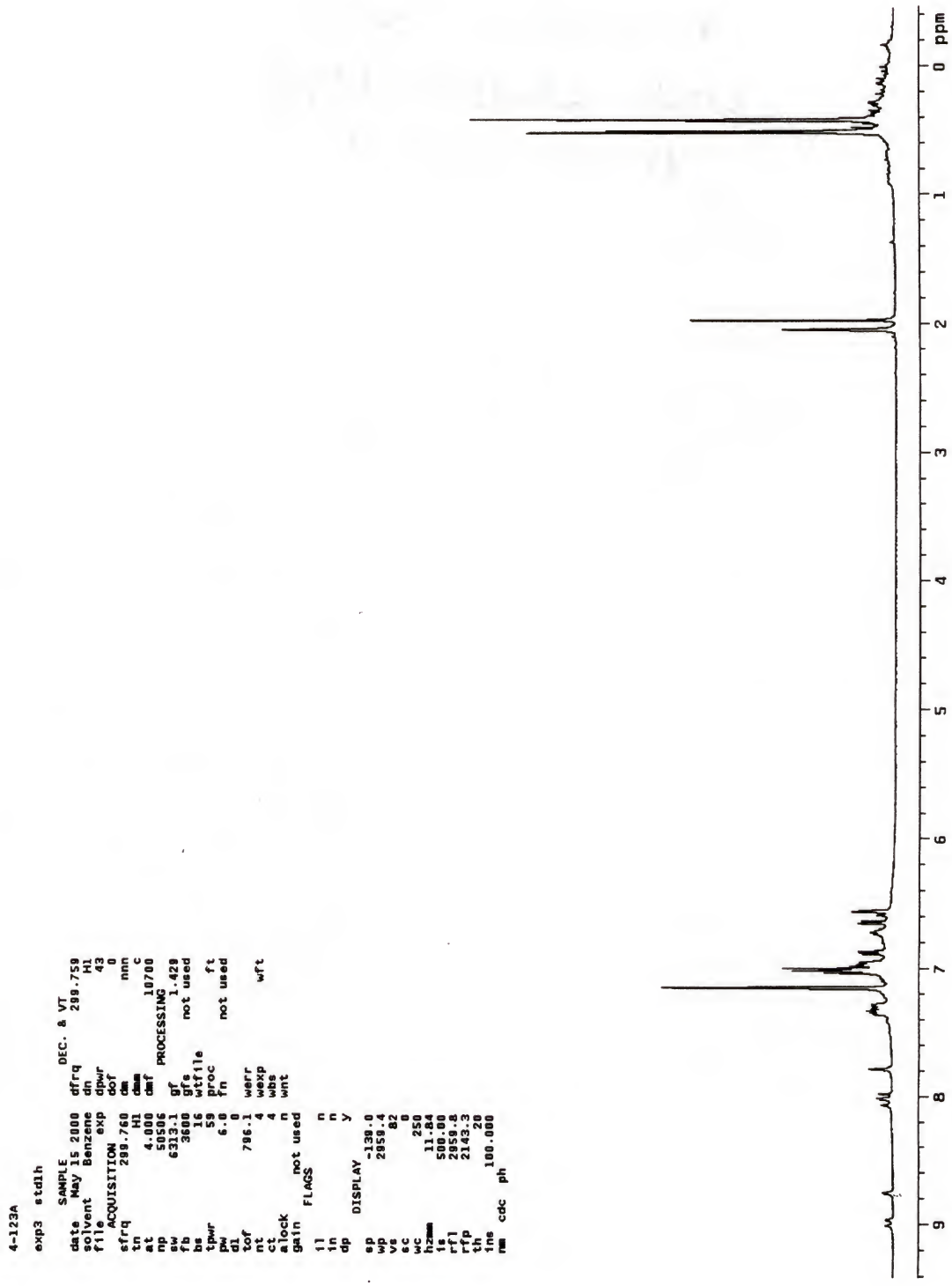

Figure A-48. Carbon NMR of [o-$(Me_3SiN)_2C_6H_4$](NPh)W(SC_5H_6) (**25a,b**) in C_6D_6.

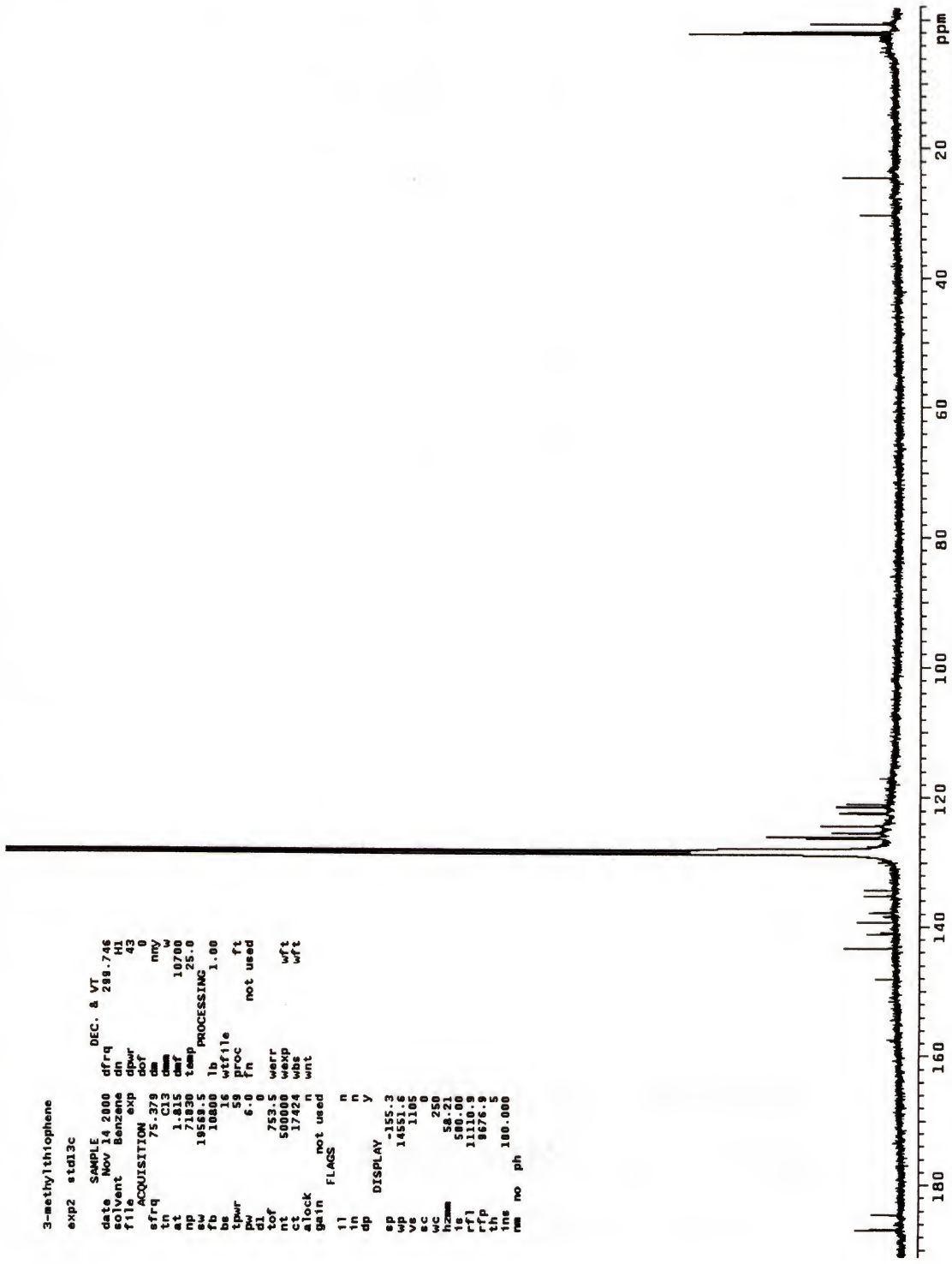

APPENDIX B
TABLES OF CRYSTALLOGRAPHIC DATA

Table B-1. Crystal data and structure refinement for **4**.

Empirical formula	C27 H39 N3 Si2 W	
Formula weight	645.64	
Temperature	173(2) K	
Wavelength	0.71073 Å	
Crystal system	Monoclinic	
Space group	P2(1)/n	
Unit cell dimensions	a = 12.1874(5) Å	α= 90°.
	b = 15.6037(7) Å	β= 94.317(1)°.
	c = 14.5968(6) Å	γ = 90°.
Volume	2768.0(2) $Å^3$	
Z	4	
Density (calculated)	1.549 Mg/m^3	
Absorption coefficient	4.279 mm^{-1}	
F(000)	1296	
Crystal size	0.16 x 0.10 x 0.02 mm^3	
Theta range for data collection	1.91 to 27.50°.	
Index ranges	-15≤h≤13, -20≤k≤15, -18≤l≤18	
Reflections collected	20021	
Independent reflections	6319 [R(int) = 0.0666]	
Completeness to theta = 27.50°	99.5 %	
Absorption correction	Integration	
Max. and min. transmission	0.9153 and 0.5992	
Refinement method	Full-matrix least-squares on F^2	
Data / restraints / parameters	6319 / 0 / 301	
Goodness-of-fit on F^2	0.961	
Final R indices [I>2sigma(I)]	R1 = 0.0371, wR2 = 0.0553 [4221]	
R indices (all data)	R1 = 0.0798, wR2 = 0.0642	
Extinction coefficient	0.00025(5)	
Largest diff. peak and hole	0.648 and -0.725 $e.Å^{-3}$	

$R1 = \Sigma(||F_o| - |F_c||) / \Sigma|F_o|$

$wR2 = [\Sigma[w(F_o^2 - F_c^2)^2] / \Sigma[w(F_o^2)^2]]^{1/2}$

$S = [\Sigma[w(F_o^2 - F_c^2)^2] / (n-p)]^{1/2}$ $w = 1/[\sigma^2(F_o^2)+(0.0370*p)^2+0.31*p]$, $p = [\max(F_o^2,0)+ 2* F_c^2]/3$

Table B-2. Atomic coordinates (x 10^4) and equivalent isotropic displacement parameters ($Å^2$x 10^3)for **4**. U(eq) is defined as one third of the trace of the orthogonalized U^{ij} tensor.

	x	y	z	U(eq)
W	1921(1)	-8141(1)	12379(1)	23(1)
Si1	4436(1)	-8744(1)	13243(1)	26(1)
Si2	-220(1)	-9481(1)	11993(1)	24(1)
N1	2345(3)	-8344(3)	11272(3)	28(1)
N2	3003(3)	-8868(2)	13202(3)	21(1)
N3	989(3)	-9198(2)	12645(3)	21(1)
C1	1791(4)	-7298(3)	13850(4)	27(1)
C2	734(4)	-7464(3)	13505(4)	29(1)
C3	413(4)	-7335(3)	12531(4)	32(1)
C4	1090(4)	-6800(4)	12029(4)	37(1)
C5	2148(4)	-6625(3)	12363(4)	38(2)
C6	2575(4)	-7000(3)	13213(4)	30(1)
C1'	2235(4)	-7507(4)	14816(4)	32(1)
C2'	1506(4)	-8010(4)	15415(3)	34(1)
C3'	2121(4)	-8235(4)	16333(4)	46(2)
C7	2787(9)	-8839(8)	10586(7)	26(3)
C8	2944(7)	-8463(8)	9709(7)	34(2)
C9	3393(8)	-8941(9)	9016(7)	43(3)
C10	3684(8)	-9765(8)	9217(9)	45(3)
C11	3554(8)	-10154(7)	10072(8)	46(3)
C12	3079(8)	-9686(7)	10722(8)	36(3)
C7'	2697(16)	-8626(14)	10472(14)	19(5)
C8'	2780(13)	-8052(13)	9732(11)	25(4)
C9'	3125(15)	-8439(15)	8927(14)	48(6)
C10'	3465(15)	-9328(17)	8972(14)	35(6)
C11'	3430(20)	-9896(18)	9630(20)	67(8)
C12'	2961(17)	-9479(17)	10423(17)	48(6)
C13	5134(4)	-9809(3)	13159(4)	32(1)
C14	5017(4)	-8199(4)	14314(4)	41(1)
C15	4861(4)	-8114(4)	12239(4)	42(1)
C16	2506(4)	-9509(3)	13703(3)	22(1)
C17	2977(4)	-9949(3)	14466(3)	25(1)
C18	2384(4)	-10535(3)	14933(3)	29(1)
C19	1289(4)	-10702(3)	14640(3)	30(1)
C20	805(4)	-10274(3)	13881(3)	26(1)
C21	1389(3)	-9682(3)	13403(3)	18(1)
C22	-321(4)	-8921(4)	10859(3)	33(1)
C23	-191(4)	-10647(3)	11714(4)	36(1)
C24	-1478(4)	-9222(4)	12600(4)	36(1)

Table B-3. Bond lengths [Å] and angles [°] for **4**.

W-N1	1.762(4)
W-N3	2.056(4)
W-N2	2.057(4)
W-C3	2.251(5)
W-C6	2.267(5)
W-C4	2.363(5)
W-C5	2.382(5)
W-C2	2.503(5)
W-C1	2.533(5)
Si1-N2	1.753(4)
Si1-C15	1.869(5)
Si1-C14	1.872(5)
Si1-C13	1.876(5)
Si2-N3	1.750(4)
Si2-C23	1.866(6)
Si2-C22	1.867(5)
Si2-C24	1.873(5)
N1-C7'	1.35(2)
N1-C7	1.405(12)
N2-C16	1.404(6)
N3-C21	1.398(5)
C1-C2	1.371(6)
C1-C6	1.459(7)
C1-C1'	1.507(7)
C2-C3	1.459(7)
C3-C4	1.416(7)
C4-C5	1.372(7)
C5-C6	1.434(7)
C1'-C2'	1.513(7)
C2'-C3'	1.527(7)
C7-C12	1.379(16)
C7-C8	1.434(14)
C8-C9	1.400(14)
C9-C10	1.360(15)
C10-C11	1.406(16)
C11-C12	1.361(14)
C7'-C12'	1.37(3)
C7'-C8'	1.41(3)
C8'-C9'	1.41(3)
C9'-C10'	1.45(3)
C10'-C11'	1.31(3)
C11'-C12'	1.48(3)
C16-C17	1.394(6)
C16-C21	1.424(6)
C17-C18	1.378(7)
C18-C19	1.394(6)
C19-C20	1.387(6)
C20-C21	1.386(6)
N1-W-N3	103.44(16)
N1-W-N2	102.50(16)
N3-W-N2	77.66(14)
N1-W-C3	119.28(19)

Table B-3—continued.

N3-W-C3	87.89(18)
N2-W-C3	137.97(18)
N1-W-C6	121.20(18)
N3-W-C6	134.90(17)
N2-W-C6	86.29(17)
C3-W-C6	76.44(18)
N1-W-C4	96.40(18)
N3-W-C4	121.15(17)
N2-W-C4	149.34(18)
C3-W-C4	35.63(18)
C6-W-C4	63.21(19)
N1-W-C5	97.33(19)
N3-W-C5	149.88(17)
N2-W-C5	118.93(17)
C3-W-C5	62.78(19)
C6-W-C5	35.83(18)
C4-W-C5	33.61(18)
N1-W-C2	154.42(17)
N3-W-C2	81.98(16)
N2-W-C2	103.08(15)
C3-W-C2	35.25(17)
C6-W-C2	60.90(17)
C4-W-C2	60.60(18)
C5-W-C2	70.16(18)
N1-W-C1	155.83(17)
N3-W-C1	100.72(16)
N2-W-C1	82.52(15)
C3-W-C1	61.50(18)
C6-W-C1	34.85(16)
C4-W-C1	70.79(18)
C5-W-C1	60.50(18)
C2-W-C1	31.60(15)
N2-Si1-C15	111.4(2)
N2-Si1-C14	113.1(2)
C15-Si1-C14	107.9(3)
N2-Si1-C13	110.8(2)
C15-Si1-C13	105.1(3)
C14-Si1-C13	108.2(2)
N3-Si2-C23	109.6(2)
N3-Si2-C22	111.1(2)
C23-Si2-C22	105.3(2)
N3-Si2-C24	112.0(2)
C23-Si2-C24	110.1(2)
C22-Si2-C24	108.5(2)
C7'-N1-C7	15.9(10)
C7'-N1-W	171.0(10)
C7-N1-W	155.2(6)
C16-N2-Si1	121.9(3)
C16-N2-W	114.5(3)
Si1-N2-W	123.5(2)
C21-N3-Si2	121.6(3)
C21-N3-W	114.7(3)
Si2-N3-W	123.7(2)

Table B-3—continued.

C2-C1-C6	117.9(5)
C2-C1-C1'	124.4(5)
C6-C1-C1'	117.2(4)
C2-C1-W	73.0(3)
C6-C1-W	62.6(3)
C1'-C1-W	129.8(3)
C1-C2-C3	120.5(5)
C1-C2-W	75.4(3)
C3-C2-W	62.9(3)
C4-C3-C2	117.5(5)
C4-C3-W	76.5(3)
C2-C3-W	81.8(3)
C5-C4-C3	120.1(5)
C5-C4-W	74.0(3)
C3-C4-W	67.9(3)
C4-C5-C6	119.8(5)
C4-C5-W	72.4(3)
C6-C5-W	67.7(3)
C5-C6-C1	117.9(4)
C5-C6-W	76.5(3)
C1-C6-W	82.6(3)
C1-C1'-C2'	117.8(4)
C1'-C2'-C3'	110.8(4)
C12-C7-N1	122.2(9)
C12-C7-C8	118.1(11)
N1-C7-C8	119.7(10)
C9-C8-C7	120.8(10)
C10-C9-C8	117.2(10)
C9-C10-C11	123.7(10)
C12-C11-C10	118.0(11)
C11-C12-C7	122.1(11)
N1-C7'-C12'	117.0(18)
N1-C7'-C8'	120.1(16)
C12'-C7'-C8'	122.9(19)
C7'-C8'-C9'	114.1(18)
C8'-C9'-C10'	118.3(18)
C11'-C10'-C9'	131(2)
C10'-C11'-C12'	108(2)
C7'-C12'-C11'	125(2)
C17-C16-N2	126.8(4)
C17-C16-C21	118.6(4)
N2-C16-C21	114.5(4)
C18-C17-C16	121.5(4)
C17-C18-C19	119.9(5)
C20-C19-C18	119.6(5)
C21-C20-C19	121.3(4)
C20-C21-N3	126.7(4)
C20-C21-C16	119.1(4)
N3-C21-C16	114.2(4)

Symmetry transformations used to generate equivalent atoms:

Table B-4. Anisotropic displacement parameters ($Å^2 x\ 10^3$) for **4**. The anisotropic displacement factor exponent takes the form: $-2\pi^2[\ h^2\ a^{*2}U^{11} + ... + 2\ h\ k\ a^*\ b^*\ U^{12}\ ]$

	U^{11}	U^{22}	U^{33}	U^{23}	U^{13}	U^{12}
W	24(1)	20(1)	24(1)	2(1)	2(1)	1(1)
Si1	20(1)	25(1)	32(1)	-2(1)	2(1)	-2(1)
Si2	21(1)	28(1)	22(1)	0(1)	-1(1)	2(1)
N1	27(2)	30(3)	26(2)	3(2)	3(2)	-2(2)
N2	19(2)	18(2)	26(2)	2(2)	3(2)	2(2)
N3	20(2)	23(2)	20(2)	0(2)	-2(2)	-1(2)
C1	30(3)	16(3)	35(3)	-7(2)	5(2)	2(2)
C2	30(3)	24(3)	32(3)	-4(2)	4(2)	6(2)
C3	29(3)	27(3)	38(3)	-2(3)	-4(2)	4(2)
C4	49(3)	25(3)	37(3)	7(3)	0(3)	8(3)
C5	44(4)	21(3)	51(4)	7(3)	10(3)	3(2)
C6	29(3)	20(3)	42(3)	-5(3)	5(2)	4(2)
C1'	25(3)	38(3)	33(3)	-9(3)	4(2)	-6(2)
C2'	32(3)	42(4)	29(3)	-8(3)	6(2)	-1(3)
C3'	48(3)	55(4)	34(3)	-5(3)	9(3)	1(3)
C13	25(3)	31(3)	42(3)	3(3)	9(2)	-1(2)
C14	23(3)	43(4)	55(4)	-17(3)	-7(2)	1(3)
C15	30(3)	41(3)	57(4)	8(4)	16(2)	-7(3)
C16	24(3)	17(3)	25(3)	-4(2)	5(2)	-1(2)
C17	14(2)	35(3)	26(3)	2(2)	-1(2)	3(2)
C18	28(3)	31(3)	28(3)	11(3)	3(2)	4(2)
C19	30(3)	35(3)	25(3)	8(3)	3(2)	-7(3)
C20	22(3)	27(3)	31(3)	2(2)	6(2)	-5(2)
C21	19(2)	15(3)	19(2)	-1(2)	4(2)	4(2)
C22	31(3)	39(3)	28(3)	3(3)	-5(2)	2(3)
C23	36(3)	35(3)	37(3)	1(3)	1(2)	-3(3)
C24	21(3)	51(4)	36(3)	3(3)	4(2)	0(3)

Table B-5. Hydrogen coordinates (x 10^4) and isotropic displacement parameters ($Å^2$x 10^3) for **4**.

	x	y	z	U(eq)
H2A	207	-7664	13903	34
H3A	-226	-7599	12245	38
H4A	810	-6563	11459	45
H5A	2596	-6255	12033	46
H6A	3346	-7053	13357	36
H1'A	2427	-6960	15132	38
H1'B	2928	-7832	14778	38
H2'A	1261	-8544	15094	41
H2'B	845	-7668	15524	41
H3'1	2767	-8584	16225	68
H3'2	1633	-8557	16711	68
H3'3	2358	-7706	16653	68
H8A	2742	-7883	9597	40
H9A	3490	-8700	8430	51
H10A	3992	-10097	8755	54
H11A	3790	-10725	10191	56
H12A	2943	-9952	11288	43
H8'A	2617	-7459	9772	30
H9'A	3133	-8124	8371	57
H10B	3760	-9535	8430	42
H11B	3674	-10474	9608	80
H12B	2828	-9828	10936	57
H13A	5102	-10119	13740	48
H13B	5905	-9721	13033	48
H13C	4761	-10144	12660	48
H14A	4749	-7607	14323	61
H14B	5822	-8199	14329	61
H14C	4784	-8506	14852	61
H15A	4612	-8409	11668	63
H15B	5664	-8061	12279	63
H15C	4529	-7542	12245	63
H17A	3723	-9841	14668	30
H18A	2720	-10825	15453	35
H19A	878	-11108	14958	36
H20A	58	-10388	13686	31
H22A	-438	-8307	10953	50
H22B	-940	-9157	10471	50
H22C	363	-9007	10557	50
H23A	445	-10770	11363	54
H23B	-869	-10804	11349	54
H23C	-134	-10980	12285	54
H24A	-1525	-9610	13123	54
H24B	-2134	-9291	12175	54
H24C	-1435	-8629	12821	54

Table B-6. Crystal data and structure refinement for **5**.

Empirical formula	C40 H46 N3 Si2 W	
Formula weight	808.83	
Temperature	173(2) K	
Wavelength	0.71073 Å	
Crystal system	Monoclinic	
Space group	P2(1)/n	
Unit cell dimensions	a = 18.4684(8) Å	α= 90°.
	b = 20.4038(9) Å	β= 109.780(1)°.
	c = 20.9892(9) Å	γ = 90°.
Volume	7442.6(6) $Å^3$	
Z	8	
Density (calculated)	1.444 Mg/m^3	
Absorption coefficient	3.200 mm^{-1}	
F(000)	3272	
Crystal size	0.20 x 0.19 x 0.18 mm^3	
Theta range for data collection	1.62 to 27.50°.	
Index ranges	-23≤h≤18, -26≤k≤25, -22≤l≤27	
Reflections collected	51240	
Independent reflections	19090 [R(int) = 0.0452]	
Completeness to theta = 27.50°	99.7 %	
Absorption correction	Empirical	
Maximum and minimum transmission	0.643 and 0.547	
Refinement method	Full-matrix least-squares on F^2	
Data / restraints / parameters	17049 / 0 / 841	
Goodness-of-fit on F^2	1.072	
Final R indices [I>2sigma(I)]	R1 = 0.0328, wR2 = 0.0616 [13192]	
R indices (all data)	R1 = 0.0548, wR2 = 0.0705	
Largest diff. peak and hole	1.438 and -1.003 $e.Å^{-3}$	

Table B-7. Atomic coordinates (x 10^4) and equivalent isotropic displacement parameters ($Å^2$x 10^3) for **5**. U(eq) is defined as one third of the trace of the orthogonalized U^{ij} tensor.

	x	y	z	U(eq)
W	3259(1)	9238(1)	279(1)	26(1)
C1	3691(2)	9667(2)	-463(2)	30(1)
C2	2884(2)	9871(2)	-855(2)	28(1)
C3	2323(2)	9411(2)	-940(2)	27(1)
C4	2578(2)	8741(2)	-666(2)	33(1)
C5	2740(2)	10544(2)	-1152(2)	32(1)
C6	2921(3)	11106(2)	-757(2)	41(1)
C7	2801(3)	11722(2)	-1060(2)	50(1)
C8	2518(3)	11781(2)	-1748(3)	57(1)
C9	2348(3)	11232(3)	-2144(3)	61(1)
C10	2456(3)	10615(2)	-1848(2)	49(1)
C11	1486(2)	9545(2)	-1261(2)	28(1)
C12	1128(2)	10101(2)	-1126(2)	35(1)
C13	343(2)	10198(2)	-1441(3)	46(1)
C14	-88(3)	9753(2)	-1907(2)	50(1)
C15	257(2)	9198(2)	-2050(2)	42(1)
C16	1034(2)	9087(2)	-1725(2)	33(1)
C18	2990(2)	8323(2)	-1031(2)	38(1)
C19	3113(3)	8517(2)	-1615(2)	48(1)
C20	3494(3)	8116(3)	-1936(3)	68(2)
C21	3743(3)	7505(3)	-1683(4)	84(2)
C22	3620(3)	7295(3)	-1101(4)	84(2)
C23	3239(3)	7699(2)	-771(3)	60(1)
N1	3936(2)	8649(2)	705(2)	31(1)
C24	4465(2)	8192(2)	1082(2)	30(1)
C25	4956(2)	7875(2)	803(2)	38(1)
C26	5497(3)	7442(2)	1196(2)	50(1)
C27	5553(3)	7324(2)	1856(2)	50(1)
C28	5063(3)	7624(2)	2128(2)	46(1)
C29	4517(2)	8062(2)	1745(2)	37(1)
Si1	1781(1)	8642(1)	738(1)	35(1)
C30	2343(3)	7873(2)	814(2)	46(1)
C31	834(3)	8539(2)	47(3)	54(1)
C32	1639(3)	8799(2)	1563(2)	46(1)
N2	2304(2)	9295(1)	553(2)	29(1)
C33	2122(2)	9950(2)	624(2)	26(1)
C34	1406(2)	10182(2)	625(2)	31(1)
C35	1307(2)	10835(2)	743(2)	37(1)
C36	1922(2)	11275(2)	851(2)	37(1)
C37	2619(2)	11065(2)	850(2)	32(1)
C38	2741(2)	10397(2)	742(2)	28(1)
N3	3442(2)	10115(1)	772(2)	27(1)
Si2	4346(1)	10476(1)	1215(1)	31(1)
C39	5101(2)	9826(2)	1423(2)	42(1)
C40	4602(2)	11140(2)	720(2)	37(1)
C41	4329(3)	10829(3)	2030(2)	54(1)
W'	2932(1)	9151(1)	4497(1)	27(1)
C1'	3985(2)	9503(2)	5250(2)	35(1)

Table B-7—continued.

C2'	3497(2)	9759(2)	5629(2)	31(1)
C3'	2955(2)	9332(2)	5709(2)	28(1)
C4'	2937(2)	8657(2)	5432(2)	29(1)
C5'	3589(2)	10443(2)	5885(2)	37(1)
C6'	3626(3)	10962(2)	5466(2)	51(1)
C7'	3679(3)	11605(2)	5697(3)	71(2)
C8'	3702(3)	11736(3)	6342(3)	74(2)
C9'	3703(3)	11227(3)	6773(3)	67(2)
C10'	3641(3)	10583(2)	6546(2)	49(1)
C11'	2354(2)	9514(2)	6005(2)	31(1)
C12'	1932(2)	10090(2)	5864(2)	35(1)
C13'	1386(3)	10228(2)	6157(2)	46(1)
C14'	1254(3)	9786(2)	6612(2)	47(1)
C15'	1657(3)	9214(2)	6760(2)	45(1)
C16'	2201(2)	9071(2)	6457(2)	35(1)
C18'	3567(2)	8178(2)	5780(2)	31(1)
C19'	4116(2)	8295(2)	6409(2)	42(1)
C20'	4654(3)	7817(2)	6730(2)	50(1)
C21'	4648(3)	7214(2)	6432(2)	51(1)
C22'	4113(3)	7093(2)	5806(2)	48(1)
C23'	3579(2)	7566(2)	5480(2)	39(1)
N1'	3210(2)	8534(2)	4050(2)	33(1)
C24'	3394(2)	8042(2)	3671(2)	32(1)
C25'	4114(2)	7747(2)	3891(2)	39(1)
C26'	4282(3)	7258(2)	3506(2)	44(1)
C27'	3741(3)	7058(2)	2909(2)	47(1)
C28'	3024(3)	7348(2)	2686(2)	50(1)
C29'	2851(3)	7842(2)	3064(2)	42(1)
Si1'	1043(1)	8676(1)	4050(1)	35(1)
C30'	1460(3)	7851(2)	4014(3)	52(1)
C31'	593(3)	8640(2)	4720(2)	51(1)
C32'	326(3)	8866(2)	3202(2)	50(1)
N2'	1770(2)	9277(1)	4238(2)	29(1)
C33'	1588(2)	9944(2)	4178(2)	28(1)
C34'	902(2)	10225(2)	4201(2)	35(1)
C35'	768(2)	10884(2)	4105(2)	40(1)
C36'	1319(3)	11293(2)	3991(2)	43(1)
C37'	1997(2)	11033(2)	3972(2)	38(1)
C38'	2149(2)	10356(2)	4057(2)	31(1)
N3'	2791(2)	10029(1)	4020(2)	30(1)
Si2'	3276(1)	10295(1)	3461(1)	35(1)
C39'	3974(3)	9656(2)	3419(3)	61(2)
C40'	3846(3)	11065(2)	3758(3)	54(1)
C41'	2525(3)	10426(3)	2620(2)	56(1)

Table B-8. Bond lengths [Å] and angles [°] for **5**.

W-N1	1.745(3)
W-N2	2.034(3)
W-N3	2.037(3)
W-C1	2.162(4)
W-C4	2.204(4)
W-C3	2.582(3)
W-C2	2.589(4)
C1-C2	1.497(5)
C2-C3	1.364(5)
C2-C5	1.494(5)
C3-C11	1.488(5)
C3-C4	1.495(5)
C4-C18	1.512(5)
C5-C10	1.384(6)
C5-C6	1.388(6)
C6-C7	1.392(6)
C7-C8	1.364(7)
C8-C9	1.367(7)
C9-C10	1.388(6)
C11-C12	1.390(5)
C11-C16	1.403(5)
C12-C13	1.389(6)
C13-C14	1.374(6)
C14-C15	1.381(6)
C15-C16	1.384(6)
C18-C19	1.381(6)
C18-C23	1.400(6)
C19-C20	1.393(6)
C20-C21	1.371(9)
C21-C22	1.383(10)
C22-C23	1.408(8)
N1-C24	1.389(4)
C24-C29	1.389(6)
C24-C25	1.392(5)
C25-C26	1.379(6)
C26-C27	1.375(7)
C27-C28	1.367(7)
C28-C29	1.382(6)
Si1-N2	1.765(3)
Si1-C30	1.859(4)
Si1-C32	1.865(5)
Si1-C31	1.867(4)
N2-C33	1.399(4)
C33-C34	1.405(5)
C33-C38	1.417(5)
C34-C35	1.380(5)
C35-C36	1.403(6)
C36-C37	1.358(6)
C37-C38	1.413(5)
C38-N3	1.398(5)
N3-Si2	1.774(3)
Si2-C40	1.863(4)
Si2-C41	1.865(4)

Table B-8—continued.

Si2-C39	1.867(4)
W'-N1'	1.747(3)
W'-N3'	2.027(3)
W'-N2'	2.044(3)
W'-C1'	2.171(4)
W'-C4'	2.203(4)
W'-C3'	2.556(4)
W'-C2'	2.568(4)
C1'-C2'	1.484(6)
C2'-C3'	1.380(5)
C2'-C5'	1.485(5)
C3'-C11'	1.490(5)
C3'-C4'	1.491(5)
C4'-C18'	1.505(5)
C5'-C10'	1.388(6)
C5'-C6'	1.392(6)
C6'-C7'	1.390(6)
C7'-C8'	1.367(8)
C8'-C9'	1.377(8)
C9'-C10'	1.389(7)
C11'-C12'	1.385(5)
C11'-C16'	1.407(5)
C12'-C13'	1.378(6)
C13'-C14'	1.393(7)
C14'-C15'	1.363(6)
C15'-C16'	1.391(6)
C18'-C19'	1.386(6)
C18'-C23'	1.402(5)
C19'-C20'	1.392(6)
C20'-C21'	1.378(6)
C21'-C22'	1.372(6)
C22'-C23'	1.385(6)
N1'-C24'	1.392(5)
C24'-C29'	1.390(6)
C24'-C25'	1.390(6)
C25'-C26'	1.383(6)
C26'-C27'	1.375(6)
C27'-C28'	1.380(7)
C28'-C29'	1.385(6)
Si1'-N2'	1.761(3)
Si1'-C31'	1.863(5)
Si1'-C30'	1.863(5)
Si1'-C32'	1.864(4)
N2'-C33'	1.399(5)
C33'-C34'	1.406(5)
C33'-C38'	1.421(5)
C34'-C35'	1.370(5)
C35'-C36'	1.397(6)
C36'-C37'	1.373(6)
C37'-C38'	1.409(5)
C38'-N3'	1.386(5)
N3'-Si2'	1.784(3)
Si2'-C39'	1.857(5)
Si2'-C41'	1.857(5)

Table B-8—continued.

Si2'-C40'	1.876(5)
N1-W-N2	115.76(14)
N1-W-N3	112.17(13)
N2-W-N3	79.43(12)
N1-W-C1	105.79(15)
N2-W-C1	138.31(13)
N3-W-C1	88.40(13)
N1-W-C4	103.65(14)
N2-W-C4	89.75(14)
N3-W-C4	143.83(13)
C1-W-C4	76.97(15)
N1-W-C3	136.40(13)
N2-W-C3	85.34(12)
N3-W-C3	108.90(12)
C1-W-C3	61.09(13)
C4-W-C3	35.29(12)
N1-W-C2	137.40(14)
N2-W-C2	104.08(12)
N3-W-C2	88.61(12)
C1-W-C2	35.31(12)
C4-W-C2	60.51(13)
C3-W-C2	30.58(11)
C2-C1-W	88.1(2)
C3-C2-C5	123.9(3)
C3-C2-C1	116.8(3)
C5-C2-C1	119.2(3)
C3-C2-W	74.4(2)
C5-C2-W	142.8(3)
C1-C2-W	56.56(19)
C2-C3-C11	123.9(3)
C2-C3-C4	117.0(3)
C11-C3-C4	119.1(3)
C2-C3-W	75.0(2)
C11-C3-W	135.9(2)
C4-C3-W	58.41(18)
C3-C4-C18	117.9(3)
C3-C4-W	86.3(2)
C18-C4-W	118.9(3)
C10-C5-C6	118.2(4)
C10-C5-C2	119.1(4)
C6-C5-C2	122.6(4)
C5-C6-C7	120.3(4)
C8-C7-C6	120.5(4)
C7-C8-C9	119.8(4)
C8-C9-C10	120.3(5)
C5-C10-C9	120.8(4)
C12-C11-C16	118.2(4)
C12-C11-C3	123.4(3)
C16-C11-C3	118.4(3)
C13-C12-C11	120.8(4)
C14-C13-C12	120.3(4)
C13-C14-C15	119.8(4)
C14-C15-C16	120.3(4)
C15-C16-C11	120.5(4)

Table B-8—continued.

C19-C18-C23	118.4(4)
C19-C18-C4	123.4(4)
C23-C18-C4	118.2(4)
C18-C19-C20	121.6(5)
C21-C20-C19	120.3(6)
C20-C21-C22	119.4(5)
C21-C22-C23	120.7(6)
C18-C23-C22	119.6(6)
C24-N1-W	176.2(3)
N1-C24-C29	119.7(4)
N1-C24-C25	120.4(4)
C29-C24-C25	119.9(4)
C26-C25-C24	119.3(4)
C27-C26-C25	120.5(4)
C28-C27-C26	120.5(4)
C27-C28-C29	120.2(4)
C28-C29-C24	119.7(4)
N2-Si1-C30	108.99(18)
N2-Si1-C32	109.50(19)
C30-Si1-C32	108.3(2)
N2-Si1-C31	110.63(18)
C30-Si1-C31	108.7(2)
C32-Si1-C31	110.6(2)
C33-N2-Si1	121.9(3)
C33-N2-W	110.4(2)
Si1-N2-W	127.60(17)
N2-C33-C34	125.6(3)
N2-C33-C38	115.1(3)
C34-C33-C38	119.2(3)
C35-C34-C33	120.4(4)
C34-C35-C36	119.9(4)
C37-C36-C35	120.9(4)
C36-C37-C38	120.5(4)
N3-C38-C37	125.9(3)
N3-C38-C33	115.0(3)
C37-C38-C33	119.1(3)
C38-N3-Si2	123.0(2)
C38-N3-W	110.3(2)
Si2-N3-W	126.61(16)
N3-Si2-C40	112.42(17)
N3-Si2-C41	109.66(19)
C40-Si2-C41	108.5(2)
N3-Si2-C39	108.87(17)
C40-Si2-C39	109.64(19)
C41-Si2-C39	107.6(2)
N1'-W'-N3'	112.55(14)
N1'-W'-N2'	114.82(14)
N3'-W'-N2'	79.02(12)
N1'-W'-C1'	106.02(15)
N3'-W'-C1'	90.04(14)
N2'-W'-C1'	138.88(14)
N1'-W'-C4'	103.63(14)
N3'-W'-C4'	143.69(13)
N2'-W'-C4'	88.97(13)

Table B-8—continued.

C1'-W'-C4'	76.74(15)
N1'-W'-C3'	136.87(13)
N3'-W'-C3'	108.64(12)
N2'-W'-C3'	84.77(12)
C1'-W'-C3'	61.25(14)
C4'-W'-C3'	35.55(12)
N1'-W'-C2'	138.05(14)
N3'-W'-C2'	88.50(12)
N2'-W'-C2'	104.31(12)
C1'-W'-C2'	35.25(14)
C4'-W'-C2'	61.26(13)
C3'-W'-C2'	31.24(12)
C2'-C1'-W'	87.1(2)
C3'-C2'-C1'	116.1(3)
C3'-C2'-C5'	123.2(4)
C1'-C2'-C5'	120.6(3)
C3'-C2'-W'	73.9(2)
C1'-C2'-W'	57.6(2)
C5'-C2'-W'	138.6(3)
C2'-C3'-C11'	124.6(3)
C2'-C3'-C4'	117.2(3)
C11'-C3'-C4'	118.1(3)
C2'-C3'-W'	74.8(2)
C11'-C3'-W'	133.4(2)
C4'-C3'-W'	59.20(19)
C3'-C4'-C18'	119.9(3)
C3'-C4'-W'	85.3(2)
C18'-C4'-W'	119.9(3)
C10'-C5'-C6'	118.2(4)
C10'-C5'-C2'	121.1(4)
C6'-C5'-C2'	120.7(4)
C7'-C6'-C5'	120.8(5)
C8'-C7'-C6'	120.2(5)
C7'-C8'-C9'	119.8(5)
C8'-C9'-C10'	120.4(5)
C5'-C10'-C9'	120.5(5)
C12'-C11'-C16'	117.6(4)
C12'-C11'-C3'	124.5(4)
C16'-C11'-C3'	118.0(3)
C13'-C12'-C11'	121.4(4)
C12'-C13'-C14'	119.9(4)
C15'-C14'-C13'	120.1(4)
C14'-C15'-C16'	120.0(4)
C15'-C16'-C11'	120.9(4)
C19'-C18'-C23'	117.6(4)
C19'-C18'-C4'	123.2(4)
C23'-C18'-C4'	119.1(4)
C18'-C19'-C20'	120.9(4)
C21'-C20'-C19'	120.7(4)
C22'-C21'-C20'	119.2(4)
C21'-C22'-C23'	120.6(4)
C22'-C23'-C18'	121.1(4)
C24'-N1'-W'	177.2(3)
C29'-C24'-C25'	119.3(4)

Table B-8—continued.

C29'-C24'-N1'	119.7(4)
C25'-C24'-N1'	121.0(4)
C26'-C25'-C24'	119.8(4)
C27'-C26'-C25'	120.7(4)
C26'-C27'-C28'	119.9(4)
C27'-C28'-C29'	120.0(4)
C28'-C29'-C24'	120.2(4)
N2'-Si1'-C31'	111.05(19)
N2'-Si1'-C30'	110.08(19)
C31'-Si1'-C30'	106.9(2)
N2'-Si1'-C32'	108.15(18)
C31'-Si1'-C32'	112.0(2)
C30'-Si1'-C32'	108.6(2)
C33'-N2'-Si1'	121.0(3)
C33'-N2'-W'	110.2(2)
Si1'-N2'-W'	128.66(17)
N2'-C33'-C34'	125.9(3)
N2'-C33'-C38'	115.1(3)
C34'-C33'-C38'	119.0(3)
C35'-C34'-C33'	121.0(4)
C34'-C35'-C36'	120.4(4)
C37'-C36'-C35'	119.8(4)
C36'-C37'-C38'	121.4(4)
N3'-C38'-C37'	127.0(4)
N3'-C38'-C33'	114.6(3)
C37'-C38'-C33'	118.5(4)
C38'-N3'-Si2'	121.4(3)
C38'-N3'-W'	111.5(2)
Si2'-N3'-W'	125.79(17)
N3'-Si2'-C39'	109.16(18)
N3'-Si2'-C41'	106.8(2)
C39'-Si2'-C41'	111.3(3)
N3'-Si2'-C40'	112.7(2)
C39'-Si2'-C40'	106.4(2)
C41'-Si2'-C40'	110.5(2)

Symmetry transformations used to generate equivalent atoms:

Table B-9. Anisotropic displacement parameters ($Å^2 x\ 10^3$) for **5**. The anisotropic displacement factor exponent takes the form: $-2\pi^2[\ h^2\ a^{*2}U^{11} + ... + 2\ h\ k\ a^*\ b^*\ U^{12}\ ]$

	U^{11}	U^{22}	U^{33}	U^{23}	U^{13}	U^{12}
W	24(1)	23(1)	28(1)	-1(1)	5(1)	3(1)
C1	28(2)	31(2)	32(2)	-3(2)	10(2)	4(2)
C2	27(2)	33(2)	22(2)	1(2)	7(2)	3(2)
C3	30(2)	29(2)	20(2)	-5(1)	7(2)	6(1)
C4	30(2)	26(2)	38(2)	-3(2)	6(2)	3(2)
C5	26(2)	37(2)	33(2)	-1(2)	10(2)	-4(2)
C6	50(3)	38(2)	35(2)	2(2)	14(2)	-2(2)
C7	63(3)	37(2)	50(3)	-2(2)	17(3)	-6(2)
C8	65(3)	44(3)	53(3)	20(2)	7(3)	-4(2)
C9	80(4)	54(3)	38(3)	13(2)	5(3)	-4(3)
C10	66(3)	43(3)	32(2)	2(2)	7(2)	-9(2)
C11	30(2)	26(2)	26(2)	2(1)	8(2)	0(2)
C12	31(2)	32(2)	39(2)	-1(2)	7(2)	4(2)
C13	29(2)	38(2)	69(3)	5(2)	13(2)	7(2)
C14	27(2)	55(3)	59(3)	16(2)	3(2)	0(2)
C15	32(2)	49(3)	40(2)	2(2)	4(2)	-14(2)
C16	33(2)	36(2)	30(2)	-2(2)	9(2)	-4(2)
C18	31(2)	34(2)	40(2)	-15(2)	-3(2)	6(2)
C19	44(3)	58(3)	36(2)	-19(2)	6(2)	9(2)
C20	49(3)	93(4)	54(3)	-39(3)	9(3)	12(3)
C21	45(3)	96(5)	91(5)	-62(4)	-3(3)	23(3)
C22	64(4)	46(3)	109(5)	-37(3)	-13(4)	28(3)
C23	57(3)	38(3)	68(3)	-15(2)	1(3)	12(2)
N1	27(2)	29(2)	32(2)	0(1)	3(1)	4(1)
C24	27(2)	24(2)	36(2)	0(2)	5(2)	1(1)
C25	40(2)	38(2)	34(2)	3(2)	12(2)	8(2)
C26	44(3)	45(3)	57(3)	-4(2)	13(2)	14(2)
C27	45(3)	38(2)	52(3)	14(2)	-3(2)	11(2)
C28	43(3)	47(3)	39(2)	12(2)	4(2)	-4(2)
C29	33(2)	41(2)	36(2)	1(2)	10(2)	-1(2)
Si1	27(1)	31(1)	43(1)	6(1)	6(1)	-5(1)
C30	46(3)	30(2)	56(3)	6(2)	8(2)	-7(2)
C31	34(3)	54(3)	62(3)	7(2)	2(2)	-15(2)
C32	43(3)	52(3)	44(3)	14(2)	17(2)	0(2)
N2	24(2)	28(2)	33(2)	1(1)	5(1)	-1(1)
C33	29(2)	27(2)	22(2)	2(1)	8(2)	2(1)
C34	25(2)	37(2)	29(2)	2(2)	6(2)	0(2)
C35	32(2)	42(2)	36(2)	3(2)	11(2)	12(2)
C36	43(2)	30(2)	38(2)	1(2)	16(2)	7(2)
C37	39(2)	26(2)	35(2)	-2(2)	16(2)	-2(2)
C38	28(2)	31(2)	23(2)	-1(1)	8(2)	2(2)
N3	23(2)	27(2)	29(2)	-4(1)	8(1)	-2(1)
Si2	29(1)	33(1)	30(1)	-3(1)	9(1)	-6(1)
C39	29(2)	44(2)	45(3)	9(2)	4(2)	-6(2)
C40	35(2)	35(2)	44(2)	1(2)	16(2)	-4(2)
C41	58(3)	70(3)	34(2)	-13(2)	15(2)	-16(3)
W'	27(1)	24(1)	31(1)	5(1)	9(1)	2(1)
C1'	26(2)	33(2)	44(2)	7(2)	11(2)	-2(2)
C2'	27(2)	31(2)	31(2)	2(2)	2(2)	1(2)

Table B-9—continued.

C3'	28(2)	28(2)	26(2)	4(1)	4(2)	3(1)
C4'	32(2)	26(2)	30(2)	3(2)	10(2)	1(2)
C5'	31(2)	32(2)	40(2)	-1(2)	3(2)	-5(2)
C6'	58(3)	37(2)	44(3)	5(2)	-2(2)	-11(2)
C7'	87(4)	35(3)	60(4)	2(2)	-13(3)	-17(3)
C8'	82(4)	36(3)	75(4)	-20(3)	-10(3)	-7(3)
C9'	76(4)	57(3)	58(3)	-21(3)	9(3)	-15(3)
C10'	49(3)	46(3)	44(3)	-6(2)	7(2)	-14(2)
C11'	29(2)	29(2)	33(2)	-6(2)	8(2)	-5(2)
C12'	34(2)	36(2)	34(2)	-3(2)	8(2)	0(2)
C13'	38(3)	47(3)	51(3)	-8(2)	11(2)	8(2)
C14'	40(3)	58(3)	45(3)	-15(2)	17(2)	-4(2)
C15'	47(3)	52(3)	41(2)	-6(2)	21(2)	-13(2)
C16'	36(2)	35(2)	32(2)	1(2)	9(2)	-4(2)
C18'	37(2)	28(2)	30(2)	6(2)	14(2)	2(2)
C19'	42(3)	33(2)	41(2)	-1(2)	0(2)	2(2)
C20'	47(3)	45(3)	43(3)	3(2)	-5(2)	5(2)
C21'	50(3)	44(3)	53(3)	12(2)	11(2)	17(2)
C22'	57(3)	31(2)	52(3)	2(2)	15(2)	11(2)
C23'	44(2)	32(2)	36(2)	3(2)	8(2)	4(2)
N1'	36(2)	29(2)	34(2)	7(1)	12(2)	5(1)
C24'	37(2)	28(2)	30(2)	7(2)	12(2)	1(2)
C25'	36(2)	42(2)	42(2)	4(2)	18(2)	2(2)
C26'	40(2)	46(3)	56(3)	10(2)	28(2)	12(2)
C27'	57(3)	42(2)	50(3)	-2(2)	31(2)	4(2)
C28'	60(3)	53(3)	35(2)	0(2)	14(2)	5(2)
C29'	47(3)	42(2)	32(2)	7(2)	7(2)	11(2)
Si1'	33(1)	30(1)	38(1)	5(1)	7(1)	-8(1)
C30'	54(3)	34(2)	67(3)	0(2)	19(3)	-10(2)
C31'	43(3)	57(3)	50(3)	10(2)	12(2)	-13(2)
C32'	53(3)	46(3)	40(3)	4(2)	2(2)	-12(2)
N2'	31(2)	25(2)	30(2)	6(1)	9(1)	-1(1)
C33'	28(2)	30(2)	25(2)	2(1)	5(2)	0(2)
C34'	28(2)	34(2)	42(2)	5(2)	9(2)	-1(2)
C35'	30(2)	42(2)	47(3)	2(2)	10(2)	9(2)
C36'	44(3)	28(2)	54(3)	3(2)	13(2)	4(2)
C37'	39(2)	27(2)	51(3)	5(2)	18(2)	-3(2)
C38'	27(2)	28(2)	35(2)	4(2)	7(2)	-1(2)
N3'	27(2)	26(2)	38(2)	7(1)	13(1)	2(1)
Si2'	32(1)	34(1)	42(1)	10(1)	14(1)	1(1)
C39'	66(3)	50(3)	90(4)	28(3)	56(3)	17(2)
C40'	47(3)	50(3)	69(3)	5(2)	26(3)	-12(2)
C41'	52(3)	70(3)	43(3)	10(2)	13(2)	1(3)

Table B-10. Hydrogen coordinates (x 10^4) and isotropic displacement parameters ($Å^2$x 10^3) for **5**.

	x	y	z	U(eq)
H1A	4048	10038	-288	36
H1B	3908	9344	-701	36
H4A	2141	8493	-602	39
H6A	3128	11070	-278	49
H7A	2917	12105	-786	60
H8A	2439	12203	-1951	69
H9A	2156	11273	-2623	73
H10A	2334	10236	-2128	59
H12A	1424	10418	-814	42
H13A	104	10575	-1334	55
H14A	-622	9827	-2129	60
H15A	-41	8892	-2374	51
H16A	1263	8698	-1816	40
H19A	2935	8935	-1803	58
H20A	3582	8266	-2332	81
H21A	3996	7229	-1905	101
H22A	3795	6874	-922	100
H23A	3152	7549	-375	71
H25A	4918	7956	347	45
H26A	5834	7224	1010	60
H27A	5934	7031	2125	60
H28A	5098	7532	2581	55
H29A	4180	8273	1935	45
H30A	2437	7789	389	69
H30B	2052	7506	910	69
H30C	2836	7916	1184	69
H31A	524	8936	14	80
H31B	562	8162	148	80
H31C	919	8465	-384	80
H32A	2140	8869	1915	69
H32B	1385	8421	1683	69
H32C	1318	9190	1524	69
H34A	986	9886	543	37
H35A	824	10988	750	44
H36A	1849	11726	926	44
H37A	3028	11370	923	39
H39A	5001	9507	1731	62
H39B	5608	10026	1640	62
H39C	5092	9605	1006	62
H40A	4634	10958	298	56
H40B	5099	11329	987	56
H40C	4205	11481	613	56
H41A	3991	11214	1937	81
H41B	4851	10959	2308	81
H41C	4136	10500	2273	81
H1'A	4344	9151	5488	42
H1'B	4253	9847	5082	42
H4'A	2424	8452	5361	35

Table B-10—continued.

H6'A	3614	10876	5018	62
H7'A	3700	11955	5405	85
H8'A	3716	12176	6492	89
H9'A	3746	11316	7229	80
H10B	3635	10235	6845	58
H12B	2022	10396	5558	42
H13B	1100	10624	6050	55
H14B	881	9884	6819	56
H15B	1566	8913	7070	54
H16B	2474	8667	6556	43
H19B	4125	8706	6624	50
H20B	5030	7908	7158	60
H21B	5008	6886	6657	61
H22B	4110	6681	5594	57
H23B	3215	7475	5046	46
H25B	4491	7880	4305	46
H26B	4776	7059	3656	53
H27B	3861	6720	2649	56
H28B	2650	7210	2274	60
H29B	2359	8044	2908	51
H30D	1793	7873	3737	78
H30E	1044	7537	3812	78
H30F	1762	7709	4473	78
H31D	993	8679	5166	77
H31E	324	8221	4691	77
H31F	225	9001	4657	77
H32D	116	9305	3209	75
H32E	-92	8543	3093	75
H32F	577	8847	2859	75
H34B	526	9953	4284	42
H35B	298	11064	4116	49
H36B	1225	11751	3928	51
H37B	2371	11315	3900	46
H39D	4291	9529	3879	92
H39E	4304	9830	3179	92
H39F	3694	9272	3177	92
H40D	3498	11424	3765	80
H40E	4124	11175	3448	80
H40F	4216	10997	4214	80
H41D	2189	10041	2500	83
H41E	2771	10492	2278	83
H41F	2219	10814	2638	83

Table B-11. Crystal data and structure refinement for **9**.

Empirical formula	C30 H41 N5 Si2 W	
Formula weight	711.71	
Temperature	173(2) K	
Wavelength	0.71073 Å	
Crystal system	Monoclinic	
Space group	P2(1)/c	
Unit cell dimensions	a = 13.6142(7) Å	α= 90°.
	b = 12.7895(6) Å	β= 101.720(1)°.
	c = 19.054(1) Å	γ = 90°.
Volume	3248.4(3) $Å^3$	
Z	4	
Density (calculated)	1.455 Mg/m^3	
Absorption coefficient	3.656 mm^{-1}	
F(000)	1432	
Crystal size	0.30 x 0.18 x 0.06 mm^3	
Theta range for data collection	1.93 to 27.50°.	
Index ranges	-17=h=16, -16=k=14, -24=l=23	
Reflections collected	22571	
Independent reflections	7453 [R(int) = 0.0352]	
Completeness to theta = 27.50°	99.9 %	
Absorption correction	Integration	
Max. and min. transmission	0.8168 and 0.4250	
Refinement method	Full-matrix least-squares on F^2	
Data / restraints / parameters	7453 / 0 / 351	
Goodness-of-fit on F^2	1.034	
Final R indices [I>2sigma(I)]	R1 = 0.0248, wR2 = 0.0563 [6092]	
R indices (all data)	R1 = 0.0366, wR2 = 0.0626	
Largest diff. peak and hole	1.375 and -0.720 $e.Å^{-3}$	

$R1 = \Sigma(||F_o| - |F_c||) / \Sigma|F_o|$

$wR2 = [\Sigma[w(F_o^2 - F_c^2)^2] / \Sigma[w(F_o^2)^2]]^{1/2}$

$S = [\Sigma[w(F_o^2 - F_c^2)^2] / (n-p)]^{1/2}$

$w= 1/[\sigma^2(F_o^2)+(0.0370*p)^2+0.31*p]$, $p = [\max(F_o^2,0)+ 2* F_c^2]/3$

Table B-12. Atomic coordinates (x 10^4) and equivalent isotropic displacement parameters ($Å^2$x 10^3) for **9**. U(eq) is defined as one third of the trace of the orthogonalized U^{ij} tensor.

	x	y	z	U(eq)
W	3030(1)	7668(1)	1877(1)	34(1)
Si1	791(1)	6554(1)	1204(1)	48(1)
Si2	4876(1)	8095(1)	959(1)	35(1)
N1	2520(2)	8920(2)	1919(2)	42(1)
N2	2067(2)	6705(2)	1189(1)	39(1)
N3	3860(2)	7339(2)	1112(1)	33(1)
N4	4380(2)	7785(2)	2644(1)	36(1)
N5	2615(2)	6872(3)	2725(1)	44(1)
C1	1999(3)	9861(3)	1839(2)	44(1)
C2	2169(3)	10609(3)	2378(2)	61(1)
C3	1647(4)	11542(4)	2291(3)	82(2)
C4	958(4)	11745(4)	1695(4)	90(2)
C5	764(4)	11006(5)	1162(3)	92(2)
C6	1273(4)	10065(4)	1222(2)	67(1)
C7	2456(2)	6273(2)	619(2)	37(1)
C8	3435(2)	6595(2)	590(2)	33(1)
C9	3919(3)	6143(2)	87(2)	38(1)
C10	3429(3)	5422(3)	-409(2)	47(1)
C11	2455(3)	5144(3)	-401(2)	54(1)
C12	1971(3)	5557(3)	115(2)	49(1)
C13	19(3)	6989(4)	329(2)	64(1)
C14	394(3)	7409(4)	1887(2)	68(1)
C15	471(3)	5174(4)	1397(2)	69(1)
C16	4698(3)	8514(3)	-3(2)	51(1)
C17	4988(3)	9331(3)	1483(2)	56(1)
C18	6098(3)	7381(3)	1205(2)	55(1)
C19	4630(3)	8612(3)	3098(2)	44(1)
C20	5495(3)	8652(3)	3620(2)	49(1)
C21	6167(3)	7822(3)	3713(2)	47(1)
C22	5900(3)	6969(3)	3266(2)	45(1)
C23	5030(2)	6967(3)	2759(2)	40(1)
C24	7121(3)	7845(4)	4275(2)	69(1)
C25	2397(3)	7369(4)	3315(2)	65(1)
C26	2168(4)	6846(6)	3883(2)	92(2)
C27	2176(4)	5761(7)	3900(3)	108(3)
C28	2413(3)	5262(5)	3322(3)	89(2)
C29	2635(3)	5814(3)	2750(2)	58(1)
C30	1954(5)	5160(8)	4543(4)	179(4)

Table B-13. Bond lengths [Å] and angles [°] for **9**.

W-N1	1.753(3)
W-N3	2.060(2)
W-N2	2.062(3)
W-N5	2.083(3)
W-N4	2.109(3)
Si1-N2	1.754(3)
Si1-C14	1.863(4)
Si1-C13	1.865(4)
Si1-C15	1.872(4)
Si2-N3	1.761(3)
Si2-C17	1.858(4)
Si2-C18	1.872(4)
Si2-C16	1.877(4)
N1-C1	1.390(4)
N2-C7	1.413(4)
N3-C8	1.413(4)
N4-C23	1.359(4)
N4-C19	1.365(4)
N5-C29	1.354(5)
N5-C25	1.376(5)
C1-C2	1.389(5)
C1-C6	1.398(5)
C2-C3	1.381(6)
C3-C4	1.343(8)
C4-C5	1.373(8)
C5-C6	1.383(7)
C7-C12	1.393(4)
C7-C8	1.407(4)
C8-C9	1.394(4)
C9-C10	1.390(5)
C10-C11	1.376(5)
C11-C12	1.392(5)
C19-C20	1.378(5)
C20-C21	1.390(5)
C21-C22	1.385(5)
C21-C24	1.506(5)
C22-C23	1.369(5)
C25-C26	1.362(6)
C26-C27	1.389(9)
C27-C28	1.366(9)
C27-C30	1.527(7)
C28-C29	1.382(5)
N1-W-N3	119.86(11)
N1-W-N2	111.59(12)
N3-W-N2	78.34(10)
N1-W-N5	103.81(12)
N3-W-N5	136.30(11)
N2-W-N5	87.91(10)
N1-W-N4	101.58(12)
N3-W-N4	88.80(10)
N2-W-N4	146.60(10)
N5-W-N4	80.33(10)
N2-Si1-C14	112.04(16)

Table B-13—continued.

N2-Si1-C13	109.50(17)
C14-Si1-C13	105.0(2)
N2-Si1-C15	112.21(18)
C14-Si1-C15	107.6(2)
C13-Si1-C15	110.2(2)
N3-Si2-C17	111.07(14)
N3-Si2-C18	112.27(15)
C17-Si2-C18	107.94(19)
N3-Si2-C16	111.62(15)
C17-Si2-C16	105.18(18)
C18-Si2-C16	108.44(18)
C1-N1-W	169.7(3)
C7-N2-Si1	119.7(2)
C7-N2-W	115.66(19)
Si1-N2-W	124.03(14)
C8-N3-Si2	118.4(2)
C8-N3-W	115.54(19)
Si2-N3-W	124.58(13)
C23-N4-C19	115.1(3)
C23-N4-W	120.3(2)
C19-N4-W	124.4(2)
C29-N5-C25	116.0(3)
C29-N5-W	120.6(2)
C25-N5-W	123.1(3)
C2-C1-N1	120.7(3)
C2-C1-C6	118.5(4)
N1-C1-C6	120.8(3)
C3-C2-C1	120.1(4)
C4-C3-C2	121.5(5)
C3-C4-C5	119.3(5)
C4-C5-C6	121.3(5)
C5-C6-C1	119.3(5)
C12-C7-C8	119.0(3)
C12-C7-N2	126.1(3)
C8-C7-N2	114.9(3)
C9-C8-C7	119.3(3)
C9-C8-N3	125.5(3)
C7-C8-N3	115.1(3)
C10-C9-C8	120.9(3)
C11-C10-C9	119.6(3)
C10-C11-C12	120.4(3)
C11-C12-C7	120.7(3)
N4-C19-C20	123.5(3)
C19-C20-C21	120.5(3)
C22-C21-C20	116.0(3)
C22-C21-C24	122.2(4)
C20-C21-C24	121.7(3)
C23-C22-C21	121.1(3)
N4-C23-C22	123.6(3)
C26-C25-N5	123.0(5)
C25-C26-C27	120.5(5)
C28-C27-C26	116.8(5)
C28-C27-C30	121.9(8)
C26-C27-C30	121.3(7)

Table B-13—continued.

C27-C28-C29	121.5(6)
N5-C29-C28	122.2(5)

Symmetry transformations used to generate equivalent atoms:

Table B-14. Anisotropic displacement parameters ($Å^2 x\ 10^3$) for **9**. The anisotropic displacement factor exponent takes the form: $-2\pi^2[\ h^2\ a^{*2}U^{11} + ... + 2\ h\ k\ a^*\ b^*\ U^{12}\ ]$

	U^{11}	U^{22}	U^{33}	U^{23}	U^{13}	U^{12}
W	31(1)	42(1)	28(1)	-3(1)	6(1)	-5(1)
Si1	36(1)	69(1)	38(1)	3(1)	3(1)	-15(1)
Si2	34(1)	35(1)	36(1)	0(1)	9(1)	-4(1)
N1	37(2)	52(2)	39(2)	-5(1)	9(1)	-2(1)
N2	37(2)	51(2)	29(1)	-1(1)	5(1)	-10(1)
N3	35(1)	35(1)	30(1)	-3(1)	8(1)	-6(1)
N4	34(1)	45(2)	30(1)	-7(1)	8(1)	-5(1)
N5	33(2)	68(2)	29(1)	4(1)	2(1)	-7(1)
C1	37(2)	52(2)	47(2)	2(2)	17(2)	2(2)
C2	46(2)	65(3)	75(3)	-17(2)	17(2)	9(2)
C3	59(3)	73(3)	122(5)	-22(3)	34(3)	13(2)
C4	77(4)	68(3)	139(5)	22(3)	55(4)	25(3)
C5	91(4)	104(4)	82(4)	43(3)	21(3)	36(3)
C6	82(3)	74(3)	46(2)	9(2)	14(2)	15(2)
C7	41(2)	41(2)	28(2)	1(1)	4(1)	-7(1)
C8	41(2)	31(2)	27(2)	2(1)	4(1)	-3(1)
C9	47(2)	36(2)	33(2)	2(1)	10(1)	-3(1)
C10	63(2)	45(2)	35(2)	-5(2)	16(2)	-5(2)
C11	70(3)	51(2)	37(2)	-12(2)	4(2)	-15(2)
C12	49(2)	56(2)	41(2)	-7(2)	7(2)	-17(2)
C13	51(2)	82(3)	54(2)	5(2)	-4(2)	-6(2)
C14	36(2)	113(4)	57(3)	-11(2)	15(2)	-10(2)
C15	52(2)	91(3)	61(3)	13(2)	2(2)	-32(2)
C16	60(2)	48(2)	46(2)	7(2)	11(2)	-9(2)
C17	64(3)	46(2)	64(2)	-15(2)	26(2)	-20(2)
C18	39(2)	60(2)	64(3)	7(2)	9(2)	4(2)
C19	43(2)	51(2)	38(2)	-11(2)	9(2)	-2(2)
C20	46(2)	65(2)	37(2)	-19(2)	10(2)	-10(2)
C21	36(2)	73(2)	32(2)	-7(2)	9(1)	-6(2)
C22	38(2)	54(2)	41(2)	0(2)	7(2)	1(2)
C23	41(2)	43(2)	35(2)	-3(1)	7(1)	-2(1)
C24	46(2)	107(4)	49(2)	-16(2)	-3(2)	-5(2)
C25	47(2)	113(4)	35(2)	-10(2)	7(2)	-14(2)
C26	52(3)	193(6)	34(2)	10(3)	13(2)	-8(4)
C27	48(3)	207(8)	71(4)	71(5)	14(2)	-2(4)
C28	50(3)	119(4)	94(4)	67(3)	7(3)	3(3)
C29	39(2)	76(3)	56(2)	22(2)	1(2)	-3(2)
C30	110(5)	327(12)	110(5)	134(7)	46(4)	13(7)

Table B-15. Hydrogen coordinates (x 10^4) and isotropic displacement parameters ($Å^2$x 10^3) for **9**.

	x	y	z	U(eq)
H2A	2645	10479	2808	74
H3A	1779	12052	2660	99
H4A	609	12392	1643	108
H5A	269	11145	743	110
H6A	1132	9562	848	81
H9A	4593	6330	83	46
H10A	3764	5122	-752	56
H11A	2110	4669	-749	64
H12A	1304	5347	122	59
H13A	123	7738	265	96
H13B	-692	6858	325	96
H13C	220	6599	-61	96
H14A	614	7099	2364	102
H14B	-338	7475	1780	102
H14C	698	8102	1877	102
H15A	725	4699	1072	104
H15B	-259	5101	1327	104
H15C	779	5000	1894	104
H16A	4697	7897	-308	77
H16B	5246	8982	-61	77
H16C	4056	8882	-142	77
H17A	4318	9620	1470	84
H17B	5389	9835	1274	84
H17C	5316	9188	1980	84
H18A	6242	7230	1720	82
H18B	6636	7816	1089	82
H18C	6057	6724	936	82
H19A	4185	9192	3052	53
H20A	5632	9252	3918	59
H22A	6329	6376	3313	54
H23A	4872	6360	2471	48
H24A	6957	7942	4748	103
H24B	7544	8424	4176	103
H24C	7481	7184	4266	103
H25A	2406	8112	3327	78
H26A	2001	7226	4271	111
H28A	2426	4519	3314	106
H29A	2807	5438	2362	70
H30A	2308	4488	4586	269
H30B	1231	5037	4476	269
H30C	2183	5570	4981	269

Table B-16. Crystal data and structure refinement for **12a**.

Empirical formula	C31 H42 N5 O1.50 Si2 W	
Formula weight	748.73	
Temperature	173(2) K	
Wavelength	0.71073 Å	
Crystal system	Triclinic	
Space group	P-1	
Unit cell dimensions	a = 10.0740(7) Å	α= 69.341(1)°.
	b = 12.0912(9) Å	β= 78.022(1)°.
	c = 15.336(1) Å	γ = 76.008(1)°.
Volume	1680.6(2) $Å^3$	
Z	2	
Density (calculated)	1.480 Mg/m^3	
Absorption coefficient	3.540 mm^{-1}	
F(000)	754	
Crystal size	0.39 x 0.32 x 0.02 mm^3	
Theta range for data collection	1.83 to 27.50°.	
Index ranges	$-13 \le h \le 12$, $-15 \le k \le 8$, $-19 \le l \le 18$	
Reflections collected	11730	
Independent reflections	7565 [R(int) = 0.0399]	
Completeness to theta = 27.50°	98.1 %	
Absorption correction	Integration	
Max. and min. transmission	0.9287 and 0.3380	
Refinement method	Full-matrix least-squares on F^2	
Data / restraints / parameters	7565 / 0 / 369	
Goodness-of-fit on F^2	1.061	
Final R indices [I>2sigma(I)]	R1 = 0.0307, wR2 = 0.0748 [6907]	
R indices (all data)	R1 = 0.0359, wR2 = 0.0801	
Largest diff. peak and hole	1.330 and -1.534 $e.Å^{-3}$	

$R1 = \Sigma(||F_o| - |F_c||) / \Sigma|F_o|$

$wR2 = [\Sigma[w(F_o^2 - F_c^2)^2] / \Sigma[w(F_o^2)^2]]^{1/2}$

$S = [\Sigma[w(F_o^2 - F_c^2)^2] / (n-p)]^{1/2}$

$w = 1/[\sigma^2(F_o^2)+(0.0370*p)^2+0.31*p]$, $p = [\max(F_o^2,0)+ 2* F_c^2]/3$

Table B-17. Atomic coordinates (x 10^4) and equivalent isotropic displacement parameters ($Å^2$x 10^3) for **12a**. U(eq) is defined as one third of the trace of the orthogonalized U^{ij} tensor.

	x	y	z	U(eq)
W	1891(1)	2857(1)	2893(1)	26(1)
Si1	-402(1)	5525(1)	2056(1)	40(1)
Si2	4015(1)	2662(1)	4500(1)	32(1)
O1	3706(4)	273(3)	3550(3)	53(1)
N1	1007(4)	2143(3)	2407(2)	32(1)
N2	1152(3)	4757(3)	2459(2)	28(1)
N3	3142(3)	3451(3)	3520(2)	27(1)
N4	351(3)	2687(3)	4162(2)	29(1)
N5	3431(4)	3241(3)	1616(2)	32(1)
C1	515(4)	1413(4)	2081(3)	35(1)
C2	1328(6)	893(5)	1425(4)	50(1)
C3	825(7)	148(5)	1104(4)	64(2)
C4	-478(7)	-86(6)	1437(4)	65(2)
C5	-1309(7)	416(7)	2095(5)	72(2)
C6	-822(6)	1164(6)	2418(4)	56(1)
C7	2154(4)	5360(4)	2483(3)	27(1)
C8	3259(4)	4651(3)	3014(2)	26(1)
C9	4362(4)	5180(4)	2984(3)	33(1)
C10	4362(4)	6395(4)	2516(3)	36(1)
C11	3252(4)	7106(4)	2055(3)	37(1)
C12	2162(4)	6595(4)	2044(3)	33(1)
C13	-1290(6)	6644(5)	2678(5)	59(1)
C14	-1577(5)	4447(6)	2284(5)	68(2)
C15	-184(7)	6312(6)	751(4)	66(2)
C16	4186(6)	3648(5)	5159(3)	51(1)
C17	3056(5)	1507(4)	5386(3)	44(1)
C18	5796(5)	1909(5)	4134(4)	49(1)
C19	-269(5)	1730(4)	4550(3)	38(1)
C20	-1228(5)	1589(5)	5345(4)	53(1)
C21	-1577(6)	2456(6)	5779(4)	60(2)
C22	-946(6)	3444(5)	5387(4)	54(1)
C23	-8(5)	3533(4)	4583(3)	41(1)
C24	3027(6)	3583(5)	758(3)	47(1)
C25	3944(7)	3742(7)	-50(4)	69(2)
C26	5327(7)	3562(7)	-16(4)	74(2)
C27	5760(6)	3231(6)	860(4)	59(1)
C28	4785(5)	3075(5)	1653(3)	43(1)
C29	3020(4)	1229(4)	3358(3)	33(1)
O2	4635(12)	-63(11)	309(8)	82(3)
C30	5820(20)	-710(20)	860(14)	95(6)
C31	5384(19)	-475(16)	1785(13)	90(5)
C32	5000(20)	129(18)	572(13)	91(5)
C33	5920(30)	-450(20)	1179(19)	119(8)

Table B-18. Bond lengths [Å] and angles [°] for **12a**.

W-N1	1.787(3)
W-C29	1.985(4)
W-N3	2.112(3)
W-N2	2.139(3)
W-N4	2.203(3)
W-N5	2.215(3)
Si1-N2	1.729(3)
Si1-C14	1.865(6)
Si1-C13	1.873(6)
Si1-C15	1.879(6)
Si2-N3	1.753(3)
Si2-C16	1.869(5)
Si2-C17	1.870(5)
Si2-C18	1.875(5)
O1-C29	1.165(5)
N1-C1	1.379(5)
N2-C7	1.393(5)
N3-C8	1.405(5)
N4-C23	1.336(5)
N4-C19	1.339(5)
N5-C28	1.340(6)
N5-C24	1.350(6)
C1-C2	1.391(6)
C1-C6	1.404(7)
C2-C3	1.395(7)
C3-C4	1.365(9)
C4-C5	1.387(9)
C5-C6	1.390(8)
C7-C12	1.406(6)
C7-C8	1.436(5)
C8-C9	1.396(5)
C9-C10	1.389(6)
C10-C11	1.387(6)
C11-C12	1.389(6)
C19-C20	1.376(6)
C20-C21	1.372(8)
C21-C22	1.376(8)
C22-C23	1.377(6)
C24-C25	1.367(7)
C25-C26	1.367(10)
C26-C27	1.390(9)
C27-C28	1.382(6)
O2-C32#1	1.35(2)
O2-C30	1.50(2)
C30-C31	1.50(3)
C32-C33	1.34(3)
N1-W-C29	84.62(16)
N1-W-N3	171.39(14)
C29-W-N3	86.83(15)
N1-W-N2	110.34(14)
C29-W-N2	164.10(14)
N3-W-N2	78.08(12)

Table B-18—continued.

N1-W-N4	92.67(14)
C29-W-N4	96.07(14)
N3-W-N4	89.23(12)
N2-W-N4	88.77(12)
N1-W-N5	92.18(14)
C29-W-N5	88.85(15)
N3-W-N5	86.63(12)
N2-W-N5	85.34(13)
N4-W-N5	173.39(12)
N2-Si1-C14	109.8(2)
N2-Si1-C13	111.3(2)
C14-Si1-C13	107.4(3)
N2-Si1-C15	112.2(2)
C14-Si1-C15	106.5(3)
C13-Si1-C15	109.5(3)
N3-Si2-C16	112.9(2)
N3-Si2-C17	111.48(19)
C16-Si2-C17	104.5(2)
N3-Si2-C18	110.6(2)
C16-Si2-C18	107.7(3)
C17-Si2-C18	109.3(2)
C1-N1-W	169.5(3)
C7-N2-Si1	121.6(3)
C7-N2-W	110.5(2)
Si1-N2-W	127.77(19)
C8-N3-Si2	120.3(3)
C8-N3-W	110.2(2)
Si2-N3-W	129.53(18)
C23-N4-C19	116.7(4)
C23-N4-W	121.7(3)
C19-N4-W	121.7(3)
C28-N5-C24	117.4(4)
C28-N5-W	122.7(3)
C24-N5-W	119.8(3)
N1-C1-C2	121.3(4)
N1-C1-C6	120.3(4)
C2-C1-C6	118.4(4)
C1-C2-C3	120.9(5)
C4-C3-C2	120.2(6)
C3-C4-C5	120.2(5)
C4-C5-C6	120.3(6)
C5-C6-C1	120.1(5)
N2-C7-C12	125.8(4)
N2-C7-C8	116.5(3)
C12-C7-C8	117.7(4)
C9-C8-N3	125.0(4)
C9-C8-C7	118.9(4)
N3-C8-C7	116.1(3)
C10-C9-C8	121.6(4)
C11-C10-C9	119.7(4)
C10-C11-C12	119.9(4)
C11-C12-C7	121.7(4)
N4-C19-C20	123.3(4)
C21-C20-C19	119.5(5)

Table B-18—continued.

C20-C21-C22	117.7(4)
C21-C22-C23	119.6(5)
N4-C23-C22	123.1(5)
N5-C24-C25	122.4(5)
C26-C25-C24	120.4(5)
C25-C26-C27	118.0(5)
C28-C27-C26	119.0(5)
N5-C28-C27	122.8(5)
O1-C29-W	174.0(4)
C32#1-O2-C30	109.0(12)
C31-C30-O2	105.1(15)
C33-C32-O2#1	117.2(19)

Symmetry transformations used to generate equivalent atoms:
#1 -x+1,-y,-z

Table B-19. Anisotropic displacement parameters ($Å^2 x\ 10^3$) for **12a**. The anisotropic displacement factor exponent takes the form: $-2\pi^2[\ h^2\ a^{*2}U^{11} + ... + 2\ h\ k\ a^*\ b^*\ U^{12}\ ]$

	U^{11}	U^{22}	U^{33}	U^{23}	U^{13}	U^{12}
W	23(1)	30(1)	27(1)	-12(1)	-2(1)	-7(1)
Si1	28(1)	40(1)	49(1)	-6(1)	-14(1)	-4(1)
Si2	31(1)	34(1)	31(1)	-6(1)	-9(1)	-8(1)
O1	49(2)	34(2)	72(2)	-16(2)	-7(2)	-4(2)
N1	34(2)	29(2)	33(2)	-11(1)	-2(1)	-8(1)
N2	24(2)	32(2)	29(2)	-8(1)	-6(1)	-4(1)
N3	24(2)	27(2)	31(2)	-9(1)	-4(1)	-7(1)
N4	25(2)	32(2)	33(2)	-14(1)	-2(1)	-6(1)
N5	36(2)	35(2)	30(2)	-14(1)	0(1)	-11(1)
C1	36(2)	35(2)	38(2)	-13(2)	-7(2)	-8(2)
C2	55(3)	49(3)	56(3)	-26(2)	2(2)	-22(2)
C3	88(5)	55(3)	66(4)	-35(3)	-14(3)	-16(3)
C4	92(5)	57(3)	71(4)	-26(3)	-31(3)	-32(3)
C5	64(4)	87(5)	87(5)	-37(4)	-13(3)	-40(3)
C6	45(3)	76(4)	64(3)	-35(3)	-1(2)	-27(3)
C7	25(2)	32(2)	23(2)	-9(2)	0(1)	-6(1)
C8	26(2)	31(2)	23(2)	-12(2)	-2(1)	-5(1)
C9	28(2)	40(2)	32(2)	-12(2)	-3(2)	-11(2)
C10	37(2)	41(2)	35(2)	-12(2)	0(2)	-20(2)
C11	43(2)	33(2)	32(2)	-8(2)	-1(2)	-13(2)
C12	33(2)	33(2)	28(2)	-6(2)	-2(2)	-5(2)
C13	40(3)	50(3)	75(4)	-20(3)	-3(2)	10(2)
C14	34(3)	59(3)	106(5)	-8(3)	-36(3)	-4(2)
C15	73(4)	68(4)	59(3)	-7(3)	-39(3)	-9(3)
C16	67(3)	58(3)	37(2)	-16(2)	-12(2)	-23(3)
C17	47(3)	44(3)	36(2)	-3(2)	-10(2)	-12(2)
C18	29(2)	48(3)	59(3)	-7(2)	-13(2)	0(2)
C19	41(2)	40(2)	38(2)	-14(2)	1(2)	-18(2)
C20	47(3)	65(3)	46(3)	-13(2)	10(2)	-30(3)
C21	45(3)	93(5)	42(3)	-30(3)	16(2)	-23(3)
C22	58(3)	66(3)	47(3)	-36(3)	10(2)	-13(3)
C23	43(2)	41(2)	44(2)	-22(2)	5(2)	-11(2)
C24	52(3)	64(3)	33(2)	-18(2)	-4(2)	-23(2)
C25	84(4)	106(5)	31(2)	-27(3)	9(3)	-50(4)
C26	76(4)	107(5)	46(3)	-39(3)	28(3)	-42(4)
C27	45(3)	79(4)	55(3)	-32(3)	16(2)	-20(3)
C28	36(2)	54(3)	39(2)	-20(2)	4(2)	-10(2)
C29	31(2)	33(2)	38(2)	-14(2)	0(2)	-12(2)

Table B-20. Hydrogen coordinates (x 10^4) and isotropic displacement parameters ($Å^2$x 10^3) for **12a**.

	x	y	z	U(eq)
H2A	2238	1048	1191	60
H3A	1391	-198	654	77
H4A	-817	-594	1217	78
H5A	-2214	249	2327	86
H6A	-1396	1506	2869	68
H9A	5132	4697	3291	39
H10A	5118	6739	2513	43
H11A	3238	7941	1746	44
H12A	1403	7093	1733	40
H13A	-1558	6218	3343	88
H13B	-2115	7123	2390	88
H13C	-661	7175	2626	88
H14A	-1208	3925	1892	102
H14B	-2495	4895	2131	102
H14C	-1648	3956	2948	102
H15A	424	6895	597	99
H15B	-1087	6731	552	99
H15C	224	5719	424	99
H16A	5005	4015	4870	76
H16B	4281	3165	5815	76
H16C	3363	4280	5137	76
H17A	2161	1907	5627	66
H17B	3594	1052	5907	66
H17C	2911	957	5089	66
H18A	5733	1320	3847	73
H18B	6280	1501	4687	73
H18C	6305	2515	3677	73
H19A	-34	1117	4262	46
H20A	-1647	897	5591	63
H21A	-2232	2377	6331	71
H22A	-1156	4060	5670	65
H23A	402	4229	4315	50
H24A	2071	3717	715	56
H25A	3617	3980	-640	83
H26A	5973	3660	-573	88
H27A	6711	3113	913	70
H28A	5088	2841	2250	51
H30A	5967	-1556	959	114
H30B	6655	-416	542	114
H31A	6087	-868	2188	136
H31B	5232	377	1666	136
H31C	4542	-766	2084	136
H32A	4864	963	519	109
H32B	4136	-131	842	109
H33A	5575	-318	1773	179
H33B	6043	-1294	1262	179
H33C	6782	-184	935	179

Table B-21. Crystal data and structure refinement for **14a**.

Empirical formula	C29 H50 N4 P2 Si2 W	
Formula weight	756.70	
Temperature	173(2) K	
Wavelength	0.71073 Å	
Crystal system	Monoclinic	
Space group	P2(1)/n	
Unit cell dimensions	a = 11.4345(7) Å	α= 90°.
	b = 15.920(1) Å	β= 92.176(1)°.
	c = 43.061(3) Å	γ = 90°.
Volume	7833.3(8) $Å^3$	
Z	8	
Density (calculated)	1.283 Mg/m^3	
Absorption coefficient	3.113 mm^{-1}	
F(000)	3072	
Crystal size	0.09 x 0.11 x 0.26 mm^3	
Theta range for data collection	0.95 to 27.50°.	
Index ranges	$-14 \le h \le 14$, $0 \le k \le 20$, $0 \le l \le 55$	
Reflections collected	53105	
Independent reflections	17847 [R(int) = 0.0000]	
Completeness to theta = 27.50°	99.2 %	
Absorption correction	Empirical	
Max. and min. transmission	0.813 and 0.554	
Refinement method	Full-matrix least-squares on F^2	
Data / restraints / parameters	17847 / 0 / 697	
Goodness-of-fit on F^2	1.081	
Final R indices [I>2sigma(I)]	R1 = 0.0428, wR2 = 0.0903 [13661]	
R indices (all data)	R1 = 0.0608, wR2 = 0.0958	
Largest diff. peak and hole	1.608 and -4.146 $e.Å^{-3}$	

$R1 = \Sigma(||F_o| - |F_c||) / \Sigma|F_o|$

$wR2 = [\Sigma[w(F_o^2 - F_c^2)^2] / \Sigma[w(F_o^2)^2]]^{1/2}$

$S = [\Sigma[w(F_o^2 - F_c^2)^2] / (n-p)]^{1/2}$ $w = 1/[\sigma^2(F_o^2)+(0.0370*p)^2+0.31*p]$, $p = [\max(F_o^2,0)+ 2* F_c^2]/3$

Table B-22. Atomic coordinates (x 10^4) and equivalent isotropic displacement parameters ($Å^2$x 10^3) for **14a**. U(eq) is defined as one third of the trace of the orthogonalized U^{ij} tensor.

	x	y	z	U(eq)
W	2119(1)	-8883(1)	-777(1)	21(1)
P1	2571(1)	-10377(1)	-667(1)	29(1)
P2	-33(1)	-9144(1)	-779(1)	26(1)
Si1	1475(1)	-9057(1)	-1603(1)	26(1)
Si2	4891(1)	-7975(1)	-648(1)	33(1)
N1	2041(4)	-8689(3)	-367(1)	25(1)
N2	2285(3)	-9210(3)	-1257(1)	24(1)
N3	3941(4)	-8622(3)	-857(1)	27(1)
N4	1910(4)	-7529(3)	-902(1)	25(1)
C1	1997(5)	-8575(3)	-51(1)	28(1)
C2	1091(5)	-8116(4)	76(1)	36(1)
C3	1074(7)	-7967(4)	396(2)	48(2)
C4	1943(6)	-8273(5)	590(1)	49(2)
C5	2829(6)	-8731(5)	472(1)	52(2)
C6	2874(5)	-8888(4)	153(1)	38(1)
C7	3466(4)	-9482(4)	-1298(1)	31(1)
C8	4336(5)	-9124(4)	-1093(1)	32(1)
C9	5514(5)	-9327(5)	-1144(2)	48(2)
C10	5810(6)	-9888(6)	-1376(2)	65(2)
C11	4961(6)	-10268(6)	-1563(2)	73(3)
C12	3795(6)	-10062(5)	-1522(2)	52(2)
C13	830(6)	-10041(4)	-1782(2)	42(2)
C14	2382(6)	-8562(4)	-1908(1)	48(2)
C15	246(5)	-8291(4)	-1557(1)	37(1)
C16	5803(6)	-7325(5)	-909(2)	50(2)
C17	4125(6)	-7195(4)	-405(2)	47(2)
C18	5864(6)	-8586(5)	-370(1)	47(2)
C19	2465(5)	-7205(4)	-1145(1)	32(1)
C20	2431(6)	-6360(4)	-1217(2)	45(2)
C21	1837(6)	-5817(4)	-1036(2)	52(2)
C22	1291(6)	-6133(4)	-777(2)	46(2)
C23	1355(5)	-6984(3)	-722(1)	34(1)
C24	4125(6)	-10656(5)	-608(2)	57(2)
C25	2017(6)	-10813(4)	-312(2)	49(2)
C26	2083(8)	-11165(4)	-951(2)	64(2)
C27	-1045(5)	-8244(4)	-804(2)	46(2)
C28	-751(5)	-9879(4)	-1053(2)	45(2)
C29	-541(5)	-9588(4)	-417(1)	40(1)
W'	-4229(1)	-8802(1)	-2969(1)	23(1)
P1'	-3387(1)	-7595(1)	-3248(1)	34(1)
P2'	-2360(1)	-9014(1)	-2656(1)	35(1)
Si1'	-2931(1)	-10431(1)	-3420(1)	33(1)
Si2'	-7200(1)	-8530(1)	-3170(1)	25(1)
N1'	-4635(4)	-8143(3)	-2653(1)	31(1)
N2'	-3748(4)	-9515(3)	-3365(1)	25(1)
N3'	-5784(4)	-8743(3)	-3272(1)	23(1)
N4'	-5112(4)	-9950(3)	-2795(1)	25(1)
C1'	-4869(10)	-7697(8)	-2378(3)	23(3)

Table B-22—continued.

C2'	-4633(13)	-7959(10)	-2077(3)	41(3)
C3'	-4910(13)	-7480(11)	-1829(4)	47(4)
C4'	-5440(13)	-6687(12)	-1886(4)	46(4)
C5'	-5701(11)	-6357(8)	-2173(4)	39(3)
C6'	-5422(11)	-6905(8)	-2422(4)	34(3)
C1"	-4963(10)	-7509(8)	-2452(3)	22(3)
C2"	-4848(12)	-7699(10)	-2139(3)	35(3)
C3"	-5143(12)	-7126(11)	-1896(3)	36(3)
C4"	-5588(12)	-6382(9)	-2006(4)	39(4)
C5"	-5714(12)	-6176(10)	-2325(4)	46(4)
C6"	-5397(11)	-6739(8)	-2545(4)	33(3)
C7'	-4387(5)	-9219(3)	-3633(1)	26(1)
C8'	-5496(5)	-8833(3)	-3581(1)	27(1)
C9'	-6182(5)	-8558(4)	-3838(1)	35(1)
C10'	-5791(6)	-8635(4)	-4140(1)	46(2)
C11'	-4712(7)	-8992(4)	-4189(1)	50(2)
C12'	-4026(6)	-9266(4)	-3939(2)	43(2)
C13'	-1461(5)	-10234(4)	-3589(2)	51(2)
C14'	-2738(6)	-11036(4)	-3053(2)	46(2)
C15'	-3706(5)	-11186(4)	-3694(2)	44(2)
C16'	-7620(6)	-7398(4)	-3235(2)	43(2)
C17'	-8288(5)	-9210(4)	-3389(1)	39(1)
C18'	-7444(5)	-8739(4)	-2752(1)	34(1)
C19'	-5585(4)	-10511(3)	-3001(1)	26(1)
C20'	-6172(5)	-11219(4)	-2910(1)	37(1)
C21'	-6319(5)	-11373(4)	-2598(2)	42(2)
C22'	-5872(5)	-10798(4)	-2390(2)	45(2)
C23'	-5277(5)	-10097(4)	-2492(1)	35(1)
C24'	-2973(8)	-6687(4)	-3009(2)	73(3)
C25'	-2069(7)	-7771(5)	-3465(2)	79(3)
C26'	-4291(6)	-7067(4)	-3545(2)	48(2)
C27'	-2373(7)	-9743(5)	-2327(2)	63(2)
C28'	-1859(6)	-8079(4)	-2444(2)	52(2)
C29'	-994(6)	-9297(5)	-2829(2)	60(2)

Table B-23. Bond lengths [Å] and angles [°] for **14a**.

W-N1	1.795(4)
W-N2	2.151(4)
W-N3	2.166(4)
W-N4	2.232(4)
W-P1	2.4757(14)
W-P2	2.4950(13)
P1-C25	1.816(7)
P1-C26	1.822(6)
P1-C24	1.840(6)
P2-C29	1.826(6)
P2-C28	1.833(6)
P2-C27	1.842(6)
Si1-N2	1.740(4)
Si1-C15	1.877(6)
Si1-C14	1.877(6)
Si1-C13	1.883(6)
Si2-N3	1.725(5)
Si2-C17	1.864(7)
Si2-C16	1.873(6)
Si2-C18	1.876(6)
N1-C1	1.378(6)
N2-C7	1.435(6)
N3-C8	1.383(7)
N4-C23	1.341(7)
N4-C19	1.346(7)
C1-C2	1.395(8)
C1-C6	1.398(8)
C2-C3	1.399(8)
C3-C4	1.364(10)
C4-C5	1.361(10)
C5-C6	1.401(8)
C7-C12	1.398(8)
C7-C8	1.422(7)
C8-C9	1.410(8)
C9-C10	1.391(9)
C10-C11	1.379(10)
C11-C12	1.391(9)
C19-C20	1.381(8)
C20-C21	1.365(10)
C21-C22	1.392(9)
C22-C23	1.377(8)
W'-N1'	1.792(5)
W'-N2'	2.137(4)
W'-N3'	2.167(4)
W'-N4'	2.233(4)
W'-P1'	2.4794(15)
W'-P2'	2.5060(15)
P1'-C26'	1.821(7)
P1'-C25'	1.825(7)
P1'-C24'	1.826(7)
P2'-C29'	1.812(7)
P2'-C28'	1.827(6)
P2'-C27'	1.833(7)

Table B-23—continued.

Si1'-N2'	1.752(4)
Si1'-C14'	1.860(7)
Si1'-C15'	1.881(6)
Si1'-C13'	1.884(7)
Si2'-N3'	1.726(4)
Si2'-C18'	1.863(5)
Si2'-C17'	1.876(6)
Si2'-C16'	1.882(6)
N1'-C1"	1.393(13)
N1'-C1'	1.416(12)
N2'-C7'	1.423(7)
N3'-C8'	1.392(6)
N4'-C23'	1.343(7)
N4'-C19'	1.358(7)
C1'-C2'	1.381(19)
C1'-C6'	1.420(17)
C2'-C3'	1.357(19)
C3'-C4'	1.42(2)
C4'-C5'	1.37(2)
C5'-C6'	1.428(19)
C1"-C6"	1.377(18)
C1"-C2"	1.382(18)
C2"-C3"	1.437(19)
C3"-C4"	1.37(2)
C4"-C5"	1.42(2)
C5"-C6"	1.361(19)
C7'-C12'	1.399(7)
C7'-C8'	1.434(7)
C8'-C9'	1.402(8)
C9'-C10'	1.396(8)
C10'-C11'	1.382(10)
C11'-C12'	1.379(9)
C19'-C20'	1.377(7)
C20'-C21'	1.385(8)
C21'-C22'	1.366(9)
C22'-C23'	1.387(8)
N1-W-N2	175.32(17)
N1-W-N3	102.06(17)
N2-W-N3	76.76(15)
N1-W-N4	93.61(17)
N2-W-N4	90.73(16)
N3-W-N4	82.60(16)
N1-W-P1	89.83(13)
N2-W-P1	85.68(12)
N3-W-P1	91.10(12)
N4-W-P1	173.33(12)
N1-W-P2	86.96(14)
N2-W-P2	94.51(11)
N3-W-P2	170.40(11)
N4-W-P2	93.65(11)
P1-W-P2	92.23(5)
C25-P1-C26	101.1(4)
C25-P1-C24	99.0(3)

Table B-23—continued.

C26-P1-C24	101.3(4)
C25-P1-W	116.7(2)
C26-P1-W	118.6(2)
C24-P1-W	116.9(2)
C29-P2-C28	98.8(3)
C29-P2-C27	97.5(3)
C28-P2-C27	101.2(3)
C29-P2-W	114.0(2)
C28-P2-W	121.8(2)
C27-P2-W	119.2(2)
N2-Si1-C15	112.1(2)
N2-Si1-C14	111.6(3)
C15-Si1-C14	103.7(3)
N2-Si1-C13	114.9(3)
C15-Si1-C13	107.5(3)
C14-Si1-C13	106.3(3)
N3-Si2-C17	113.0(2)
N3-Si2-C16	111.8(3)
C17-Si2-C16	104.6(3)
N3-Si2-C18	111.7(3)
C17-Si2-C18	105.4(3)
C16-Si2-C18	109.8(3)
C1-N1-W	177.5(4)
C7-N2-Si1	114.3(3)
C7-N2-W	107.9(3)
Si1-N2-W	136.6(2)
C8-N3-Si2	120.8(4)
C8-N3-W	110.5(3)
Si2-N3-W	128.4(2)
C23-N4-C19	116.7(5)
C23-N4-W	122.2(3)
C19-N4-W	120.6(4)
N1-C1-C2	120.7(5)
N1-C1-C6	121.4(5)
C2-C1-C6	117.9(5)
C1-C2-C3	120.8(6)
C4-C3-C2	120.3(6)
C5-C4-C3	119.9(6)
C4-C5-C6	121.1(6)
C1-C6-C5	119.9(6)
C12-C7-C8	119.5(5)
C12-C7-N2	124.2(5)
C8-C7-N2	116.3(5)
N3-C8-C9	125.9(5)
N3-C8-C7	116.5(5)
C9-C8-C7	117.6(5)
C10-C9-C8	121.2(6)
C11-C10-C9	121.1(6)
C10-C11-C12	118.6(7)
C11-C12-C7	121.9(6)
N4-C19-C20	122.6(6)
C21-C20-C19	119.9(6)
C20-C21-C22	118.5(6)
C23-C22-C21	118.2(6)

Table B-23—continued.

N4-C23-C22	124.0(6)
N1'-W'-N2'	176.21(19)
N1'-W'-N3'	101.55(17)
N2'-W'-N3'	76.92(15)
N1'-W'-N4'	95.20(18)
N2'-W'-N4'	88.06(16)
N3'-W'-N4'	82.33(15)
N1'-W'-P1'	91.72(15)
N2'-W'-P1'	84.83(12)
N3'-W'-P1'	90.00(11)
N4'-W'-P1'	170.56(12)
N1'-W'-P2'	84.89(14)
N2'-W'-P2'	96.75(12)
N3'-W'-P2'	173.35(11)
N4'-W'-P2'	95.53(11)
P1'-W'-P2'	91.47(5)
C26'-P1'-C25'	99.6(4)
C26'-P1'-C24'	99.1(3)
C25'-P1'-C24'	102.1(4)
C26'-P1'-W'	118.5(2)
C25'-P1'-W'	118.2(3)
C24'-P1'-W'	116.0(3)
C29'-P2'-C28'	98.6(3)
C29'-P2'-C27'	101.1(4)
C28'-P2'-C27'	98.1(4)
C29'-P2'-W'	122.9(3)
C28'-P2'-W'	113.9(2)
C27'-P2'-W'	118.0(2)
N2'-Si1'-C14'	111.2(3)
N2'-Si1'-C15'	112.1(3)
C14'-Si1'-C15'	103.9(3)
N2'-Si1'-C13'	113.7(3)
C14'-Si1'-C13'	109.6(3)
C15'-Si1'-C13'	105.7(3)
N3'-Si2'-C18'	112.7(2)
N3'-Si2'-C17'	111.7(2)
C18'-Si2'-C17'	105.1(3)
N3'-Si2'-C16'	112.8(3)
C18'-Si2'-C16'	105.5(3)
C17'-Si2'-C16'	108.5(3)
C1"-N1'-C1'	18.2(6)
C1"-N1'-W'	168.9(7)
C1'-N1'-W'	172.4(7)
C7'-N2'-Si1'	115.1(3)
C7'-N2'-W'	109.3(3)
Si1'-N2'-W'	134.9(2)
C8'-N3'-Si2'	121.4(3)
C8'-N3'-W'	110.6(3)
Si2'-N3'-W'	127.8(2)
C23'-N4'-C19'	117.0(5)
C23'-N4'-W'	123.4(4)
C19'-N4'-W'	119.4(3)
C2'-C1'-N1'	126.8(11)
C2'-C1'-C6'	117.6(12)

Table B-23—continued.

N1'-C1'-C6'	115.5(11)
C3'-C2'-C1'	121.7(15)
C2'-C3'-C4'	118.4(15)
C5'-C4'-C3'	125.2(15)
C4'-C5'-C6'	113.4(13)
C1'-C6'-C5'	123.6(13)
C6"-C1"-C2"	119.9(12)
C6"-C1"-N1'	124.5(11)
C2"-C1"-N1'	115.5(11)
C1"-C2"-C3"	123.6(13)
C4"-C3"-C2"	113.2(13)
C3"-C4"-C5"	124.0(14)
C6"-C5"-C4"	120.1(14)
C5"-C6"-C1"	119.2(14)
C12'-C7'-N2'	125.9(5)
C12'-C7'-C8'	117.6(5)
N2'-C7'-C8'	116.5(4)
N3'-C8'-C9'	125.2(5)
N3'-C8'-C7'	115.9(4)
C9'-C8'-C7'	118.9(5)
C10'-C9'-C8'	121.2(6)
C11'-C10'-C9'	119.9(6)
C12'-C11'-C10'	119.6(6)
C11'-C12'-C7'	122.7(6)
N4'-C19'-C20'	122.5(5)
C19'-C20'-C21'	120.0(6)
C22'-C21'-C20'	117.5(6)
C21'-C22'-C23'	120.5(6)
N4'-C23'-C22'	122.4(6)

Symmetry transformations used to generate equivalent atoms:

Table B-24. Anisotropic displacement parameters ($Å^2 x\ 10^3$) for **14a**. The anisotropic displacement factor exponent takes the form: $-2\pi^2[\ h^2\ a^{*2}U^{11} + ... + 2\ h\ k\ a^*\ b^*\ U^{12}\ ]$.

	U^{11}	U^{22}	U^{33}	U^{23}	U^{13}	U^{12}
W	19(1)	25(1)	19(1)	2(1)	1(1)	-1(1)
P1	31(1)	29(1)	25(1)	2(1)	-2(1)	2(1)
P2	21(1)	31(1)	25(1)	4(1)	3(1)	-3(1)
Si1	28(1)	32(1)	19(1)	2(1)	-2(1)	-4(1)
Si2	25(1)	44(1)	28(1)	4(1)	-3(1)	-10(1)
N1	25(2)	23(2)	27(2)	5(2)	3(2)	-3(2)
N2	19(2)	34(2)	17(2)	-1(2)	2(2)	1(2)
N3	21(2)	38(3)	23(2)	0(2)	4(2)	0(2)
N4	29(2)	28(2)	19(2)	6(2)	-1(2)	-4(2)
C1	34(3)	29(3)	20(2)	-3(2)	3(2)	-6(2)
C2	44(3)	33(3)	31(3)	2(2)	13(3)	3(3)
C3	68(5)	38(3)	41(4)	-13(3)	25(3)	-6(3)
C4	59(4)	66(5)	22(3)	-15(3)	9(3)	-22(4)
C5	44(4)	87(6)	23(3)	-5(3)	-5(3)	-19(4)
C6	25(3)	63(4)	26(3)	-2(3)	2(2)	-11(3)
C7	19(2)	51(4)	24(3)	-5(2)	1(2)	5(2)
C8	24(3)	49(3)	24(3)	5(2)	2(2)	2(2)
C9	20(3)	82(5)	41(4)	-15(3)	0(3)	2(3)
C10	31(4)	118(7)	47(4)	-18(4)	4(3)	21(4)
C11	43(4)	123(8)	51(4)	-45(5)	-5(3)	32(5)
C12	34(3)	85(5)	36(3)	-22(4)	-7(3)	16(3)
C13	43(4)	41(3)	40(3)	-5(3)	-8(3)	-7(3)
C14	59(4)	57(4)	28(3)	11(3)	14(3)	-13(3)
C15	38(3)	43(3)	29(3)	14(3)	-7(2)	-1(3)
C16	39(4)	60(4)	50(4)	10(3)	2(3)	-17(3)
C17	39(4)	57(4)	46(4)	-14(3)	1(3)	-17(3)
C18	39(3)	66(5)	34(3)	6(3)	-12(3)	-12(3)
C19	31(3)	36(3)	30(3)	0(2)	-2(2)	-7(2)
C20	54(4)	39(4)	43(4)	17(3)	2(3)	-16(3)
C21	64(5)	27(3)	64(5)	10(3)	-4(4)	-10(3)
C22	49(4)	31(3)	59(4)	1(3)	5(3)	0(3)
C23	36(3)	30(3)	35(3)	2(2)	3(2)	3(2)
C24	35(4)	58(5)	77(5)	20(4)	6(3)	16(3)
C25	50(4)	39(4)	58(4)	15(3)	3(3)	12(3)
C26	103(6)	35(4)	53(4)	-18(3)	-27(4)	9(4)
C27	30(3)	47(4)	60(4)	15(3)	6(3)	11(3)
C28	33(3)	60(4)	41(4)	1(3)	-3(3)	-17(3)
C29	29(3)	59(4)	33(3)	9(3)	9(2)	-4(3)
W'	23(1)	18(1)	29(1)	0(1)	3(1)	0(1)
P1'	36(1)	21(1)	46(1)	1(1)	9(1)	-4(1)
P2'	27(1)	30(1)	48(1)	-1(1)	-6(1)	1(1)
Si1'	27(1)	22(1)	52(1)	-7(1)	8(1)	2(1)
Si2'	24(1)	25(1)	26(1)	-1(1)	4(1)	2(1)
N1'	25(2)	30(2)	37(3)	-3(2)	1(2)	1(2)
N2'	23(2)	18(2)	34(2)	-3(2)	6(2)	1(2)
N3'	27(2)	23(2)	19(2)	0(2)	5(2)	1(2)
N4'	23(2)	25(2)	26(2)	4(2)	5(2)	1(2)
C7'	35(3)	18(2)	27(3)	0(2)	8(2)	-4(2)
C8'	38(3)	20(2)	23(2)	5(2)	10(2)	-1(2)

Table B-24—continued.

C9'	46(3)	29(3)	30(3)	3(2)	6(3)	1(3)
C10'	71(5)	43(4)	24(3)	4(3)	5(3)	1(3)
C11'	81(5)	42(4)	30(3)	1(3)	30(3)	-3(3)
C12'	54(4)	32(3)	44(4)	2(3)	25(3)	2(3)
C13'	35(3)	50(4)	68(5)	-13(4)	13(3)	9(3)
C14'	43(4)	28(3)	67(4)	-1(3)	1(3)	6(3)
C15'	43(3)	30(3)	58(4)	-11(3)	2(3)	0(3)
C16'	44(4)	35(3)	51(4)	-4(3)	10(3)	14(3)
C17'	34(3)	44(3)	39(3)	-11(3)	3(3)	-5(3)
C18'	29(3)	45(3)	28(3)	-5(3)	7(2)	-1(3)
C19'	27(3)	25(3)	25(3)	2(2)	4(2)	4(2)
C20'	35(3)	28(3)	46(3)	3(3)	1(3)	-7(2)
C21'	43(3)	35(3)	49(4)	12(3)	3(3)	-9(3)
C22'	43(4)	55(4)	36(3)	19(3)	2(3)	-4(3)
C23'	41(3)	36(3)	28(3)	3(2)	-5(2)	-2(3)
C24'	110(7)	36(4)	71(5)	0(4)	-13(5)	-32(4)
C25'	52(5)	51(5)	137(8)	23(5)	52(5)	-6(4)
C26'	65(5)	28(3)	52(4)	10(3)	6(3)	-4(3)
C27'	62(5)	68(5)	58(5)	23(4)	-19(4)	-4(4)
C28'	43(4)	45(4)	65(5)	-15(3)	-15(3)	-4(3)
C29'	31(3)	65(5)	83(6)	-18(4)	-1(4)	14(3)

Table B-25. Hydrogen coordinates (x 10^4) and isotropic displacement parameters ($Å^2$x 10^3) for **14a**.

	x	y	z	U(eq)
H2A	478	-7902	-57	43
H3A	453	-7651	479	58
H4A	1930	-8167	807	59
H5A	3427	-8947	609	62
H6A	3500	-9207	74	45
H9A	6116	-9077	-1017	57
H10A	6611	-10012	-1406	78
H11A	5168	-10662	-1718	87
H12A	3205	-10322	-1650	62
H13A	1393	-10293	-1920	62
H13B	109	-9901	-1901	62
H13C	652	-10440	-1617	62
H14A	2709	-8031	-1830	71
H14B	1889	-8455	-2095	71
H14C	3020	-8943	-1959	71
H15A	-373	-8556	-1440	55
H15B	-70	-8123	-1762	55
H15C	539	-7794	-1444	55
H16A	6199	-7693	-1054	74
H16B	6388	-7013	-783	74
H16C	5299	-6930	-1026	74
H17A	3678	-6807	-540	71
H17B	4704	-6880	-278	71
H17C	3592	-7489	-269	71
H18A	5396	-8818	-204	70
H18B	6468	-8214	-279	70
H18C	6237	-9045	-481	70
H19A	2897	-7572	-1271	39
H20A	2821	-6158	-1393	54
H21A	1798	-5235	-1084	62
H22A	884	-5772	-642	55
H23A	983	-7198	-545	40
H24A	4504	-10257	-464	85
H24B	4509	-10636	-808	85
H24C	4189	-11225	-522	85
H25A	1164	-10865	-333	73
H25B	2225	-10440	-137	73
H25C	2363	-11368	-274	73
H26A	2475	-11700	-903	96
H26B	2278	-10981	-1159	96
H26C	1234	-11239	-941	96
H27A	-1854	-8449	-811	68
H27B	-903	-7921	-992	68
H27C	-916	-7885	-621	68
H28A	-355	-10424	-1040	67
H28B	-710	-9658	-1265	67
H28C	-1573	-9947	-1001	67
H29A	-1391	-9520	-410	60

Table B-25—continued.

H29B	-161	-9296	-240	60
H29C	-344	-10187	-407	60
H2'A	-4269	-8489	-2041	49
H3'A	-4753	-7671	-1623	56
H4'A	-5629	-6359	-1711	55
H5'A	-6034	-5815	-2204	47
H6'A	-5618	-6731	-2629	41
H2"A	-4557	-8238	-2081	42
H3"A	-5040	-7253	-1681	43
H4"A	-5827	-5978	-1859	46
H5"A	-6019	-5644	-2387	55
H6"A	-5474	-6602	-2759	40
H9'A	-6927	-8315	-3806	42
H10B	-6265	-8442	-4311	55
H11B	-4444	-9049	-4394	60
H12B	-3277	-9496	-3976	51
H13D	-1569	-10072	-3808	76
H13E	-988	-10747	-3574	76
H13F	-1060	-9781	-3474	76
H14D	-2141	-10764	-2918	69
H14E	-2489	-11610	-3099	69
H14F	-3481	-11053	-2947	69
H15D	-4522	-11246	-3636	66
H15E	-3318	-11734	-3681	66
H15F	-3681	-10972	-3907	66
H16D	-7125	-7038	-3101	65
H16E	-8442	-7319	-3186	65
H16F	-7512	-7249	-3453	65
H17D	-8257	-9092	-3612	58
H17E	-9076	-9091	-3319	58
H17F	-8099	-9803	-3351	58
H18D	-7398	-9345	-2713	51
H18E	-8219	-8533	-2699	51
H18F	-6842	-8451	-2624	51
H19B	-5507	-10410	-3217	31
H20B	-6477	-11602	-3062	44
H21B	-6716	-11861	-2530	51
H22B	-5969	-10879	-2174	53
H23B	-4976	-9707	-2343	42
H24D	-2192	-6777	-2913	109
H24E	-3541	-6613	-2846	109
H24F	-2966	-6182	-3139	109
H25D	-2215	-8220	-3617	118
H25E	-1424	-7935	-3321	118
H25F	-1862	-7253	-3573	118
H26D	-3888	-6562	-3615	72
H26E	-5040	-6909	-3459	72
H26F	-4431	-7447	-3722	72
H27D	-2688	-10286	-2397	94
H27E	-2865	-9513	-2165	94
H27F	-1573	-9819	-2241	94
H28D	-1260	-8239	-2286	78
H28E	-2522	-7819	-2342	78
H28F	-1527	-7678	-2589	78

Table B-25—continued.

H29D	-820	-8893	-2992	90
H29E	-1064	-9861	-2919	90
H29F	-362	-9292	-2669	90

Table B-26. Crystal data and structure refinement for **15**.

Empirical formula	C32 H37 N3 Si2 W	
Formula weight	703.68	
Temperature	173(2) K	
Wavelength	0.71073 Å	
Crystal system	Monoclinic	
Space group	P2(1)/n	
Unit cell dimensions	a = 12.5177(5) Å	α= 90°.
	b = 15.6686(7) Å	β= 93.285(1)°.
	c = 15.9709(7) Å	γ = 90°.
Volume	3127.3(2) $Å^3$	
Z	4	
Density (calculated)	1.495 Mg/m^3	
Absorption coefficient	3.795 mm^{-1}	
F(000)	1408	
Crystal size	0.23 x 0.15 x 0.03 mm^3	
Theta range for data collection	2.01 to 27.49°.	
Index ranges	$-14 \le h \le 16$, $-20 \le k \le 19$, $-19 \le l \le 20$	
Reflections collected	22400	
Independent reflections	7161 [R(int) = 0.0359]	
Completeness to theta = 27.49°	99.7 %	
Absorption correction	Integration	
Max. and min. transmission	0.8741 and 0.4884	
Refinement method	Full-matrix least-squares on F^2	
Data / restraints / parameters	7161 / 0 / 349	
Goodness-of-fit on F^2	1.038	
Final R indices [I>2sigma(I)]	R1 = 0.0208, wR2 = 0.0487 [6182]	
R indices (all data)	R1 = 0.0271, wR2 = 0.0510	
Largest diff. peak and hole	0.509 and -0.326 e.$Å^{-3}$	

$R1 = \Sigma(||F_o| - |F_c||) / \Sigma|F_o|$

$wR2 = [\Sigma[w(F_o^2 - F_c^2)^2] / \Sigma[w(F_o^2)^2]]^{1/2}$

$S = [\Sigma[w(F_o^2 - F_c^2)^2] / (n-p)]^{1/2}$ $w = 1/[\sigma^2(F_o^2)+(0.0370*p)^2+0.31*p]$, $p = [\max(F_o^2,0)+ 2* F_c^2]/3$

Table B-27. Atomic coordinates (x 10^4) and equivalent isotropic displacement parameters ($Å^2$x 10^3) for **15**. U(eq) is defined as one third of the trace of the orthogonalized U^{ij} tensor.

	x	y	z	U(eq)
W	4890(1)	2139(1)	945(1)	23(1)
Si1	4666(1)	3032(1)	-1005(1)	31(1)
Si2	2853(1)	1047(1)	1860(1)	27(1)
N1	5686(2)	1241(1)	774(1)	28(1)
N2	4185(2)	2751(1)	-25(1)	26(1)
N3	3391(2)	1863(1)	1260(1)	24(1)
C1	6542(2)	672(2)	808(2)	25(1)
C2	7576(2)	966(2)	992(2)	34(1)
C3	8429(2)	405(2)	997(2)	41(1)
C4	8262(2)	-448(2)	826(2)	38(1)
C5	7240(2)	-746(2)	657(2)	37(1)
C6	6378(2)	-196(2)	644(2)	31(1)
C7	3329(2)	3127(2)	382(2)	25(1)
C8	2926(2)	2652(2)	1064(2)	24(1)
C9	2098(2)	3022(2)	1513(2)	30(1)
C10	1665(2)	3797(2)	1283(2)	35(1)
C11	2055(2)	4248(2)	606(2)	36(1)
C12	2878(2)	3929(2)	175(2)	31(1)
C13	5673(3)	2205(2)	-1221(2)	45(1)
C14	5296(2)	4109(2)	-954(2)	46(1)
C15	3563(3)	3006(2)	-1832(2)	53(1)
C16	3588(2)	53(2)	1639(2)	40(1)
C17	3029(2)	1267(2)	3006(2)	35(1)
C18	1404(2)	915(2)	1535(2)	40(1)
C19	5928(2)	3034(2)	1465(2)	28(1)
C20	5281(2)	2772(2)	2047(2)	28(1)
C21	6856(2)	3596(2)	1427(2)	28(1)
C22	7590(2)	3483(2)	810(2)	34(1)
C23	8504(2)	3976(2)	797(2)	41(1)
C24	8687(2)	4608(2)	1386(2)	42(1)
C25	7955(2)	4750(2)	1995(2)	44(1)
C26	7055(2)	4245(2)	2018(2)	37(1)
C27	5072(2)	2868(2)	2935(2)	26(1)
C28	5629(2)	2383(2)	3546(2)	34(1)
C29	5383(2)	2434(2)	4383(2)	38(1)
C30	4567(2)	2962(2)	4614(2)	36(1)
C31	4010(2)	3439(2)	4018(2)	35(1)
C32	4251(2)	3398(2)	3182(2)	31(1)

Table B-28. Bond lengths [Å] and angles [°] for **15**.

W-N1	1.756(2)
W-N2	1.984(2)
W-N3	2.0168(19)
W-C20	2.054(3)
W-C19	2.054(3)
W-C8	2.603(2)
W-C7	2.611(2)
Si1-N2	1.765(2)
Si1-C13	1.854(3)
Si1-C15	1.857(4)
Si1-C14	1.862(3)
Si2-N3	1.755(2)
Si2-C16	1.853(3)
Si2-C17	1.862(3)
Si2-C18	1.869(3)
N1-C1	1.391(3)
N2-C7	1.414(3)
N3-C8	1.396(3)
C1-C2	1.390(4)
C1-C6	1.397(3)
C2-C3	1.382(4)
C3-C4	1.378(4)
C4-C5	1.374(4)
C6-C5	1.380(4)
C7-C12	1.409(3)
C7-C8	1.434(3)
C8-C9	1.418(3)
C9-C10	1.371(4)
C10-C11	1.402(4)
C11-C12	1.367(4)
C19-C20	1.332(4)
C19-C21	1.462(3)
C20-C27	1.466(3)
C21-C22	1.396(3)
C21-C26	1.400(4)
C22-C23	1.382(4)
C23-C24	1.376(4)
C24-C25	1.393(4)
C25-C26	1.378(4)
C27-C28	1.391(4)
C27-C32	1.396(3)
C28-C29	1.392(4)
C29-C30	1.381(4)
C30-C31	1.369(4)
C31-C32	1.387(4)
N1-W-N2	119.74(9)
N1-W-N3	114.27(9)
N2-W-N3	85.42(8)
N1-W-C20	114.24(10)
N2-W-C20	120.62(9)
N3-W-C20	94.05(9)
N1-W-C19	104.97(10)

Table B-28—continued.

N2-W-C19	103.19(9)
N3-W-C19	128.50(9)
C20-W-C19	37.85(10)
N1-W-C8	143.70(9)
N2-W-C8	61.87(8)
N3-W-C8	32.08(8)
C20-W-C8	88.23(9)
C19-W-C8	109.78(9)
N1-W-C7	147.31(9)
N2-W-C7	32.31(8)
N3-W-C7	61.63(8)
C20-W-C7	98.44(9)
C19-W-C7	100.29(9)
C8-W-C7	31.92(7)
N2-Si1-C13	105.13(12)
N2-Si1-C15	110.36(13)
C13-Si1-C15	109.76(17)
N2-Si1-C14	110.69(12)
C13-Si1-C14	110.54(14)
C15-Si1-C14	110.25(16)
N3-Si2-C16	107.29(11)
N3-Si2-C17	112.00(11)
C16-Si2-C17	108.10(14)
N3-Si2-C18	109.03(12)
C16-Si2-C18	109.79(14)
C17-Si2-C18	110.56(13)
C1-N1-W	161.77(18)
C7-N2-Si1	127.55(17)
C7-N2-W	99.06(15)
Si1-N2-W	130.84(12)
C8-N3-Si2	126.86(16)
C8-N3-W	97.79(14)
Si2-N3-W	133.18(12)
C2-C1-N1	120.1(2)
C2-C1-C6	119.1(2)
N1-C1-C6	120.8(2)
C3-C2-C1	120.0(3)
C4-C3-C2	120.5(3)
C5-C4-C3	119.8(3)
C5-C6-C1	120.0(2)
C4-C5-C6	120.6(3)
C12-C7-N2	124.6(2)
C12-C7-C8	119.1(2)
N2-C7-C8	116.2(2)
C12-C7-W	152.98(19)
N2-C7-W	48.63(11)
C8-C7-W	73.74(14)
N3-C8-C9	123.8(2)
N3-C8-C7	118.0(2)
C9-C8-C7	118.1(2)
N3-C8-W	50.13(11)
C9-C8-W	152.08(19)
C7-C8-W	74.35(13)
C10-C9-C8	121.0(2)

Table B-28—continued.

C9-C10-C11	120.2(2)
C12-C11-C10	120.6(3)
C11-C12-C7	120.8(2)
C20-C19-C21	137.0(3)
C20-C19-W	71.05(16)
C21-C19-W	151.72(19)
C19-C20-C27	142.5(3)
C19-C20-W	71.10(16)
C27-C20-W	146.28(19)
C22-C21-C26	118.0(2)
C22-C21-C19	120.6(2)
C26-C21-C19	121.4(2)
C23-C22-C21	121.3(3)
C24-C23-C22	119.8(3)
C23-C24-C25	120.1(3)
C26-C25-C24	119.9(3)
C25-C26-C21	120.9(3)
C28-C27-C32	118.3(2)
C28-C27-C20	120.8(2)
C32-C27-C20	120.7(2)
C27-C28-C29	120.9(3)
C30-C29-C28	119.8(3)
C31-C30-C29	119.9(3)
C30-C31-C32	120.9(3)
C31-C32-C27	120.2(3)

Symmetry transformations used to generate equivalent atoms:

Table B-29. Anisotropic displacement parameters ($Å^2 x\ 10^3$) for **15**. The anisotropic displacement factor exponent takes the form: $-2\pi^2[\ h^2\ a^{*2}U^{11} + ... + 2\ h\ k\ a^*\ b^*\ U^{12}\ ]$

	U^{11}	U^{22}	U^{33}	U^{23}	U^{13}	U^{12}
W	21(1)	25(1)	22(1)	-1(1)	4(1)	1(1)
Si1	32(1)	35(1)	25(1)	3(1)	8(1)	-1(1)
Si2	25(1)	29(1)	27(1)	2(1)	6(1)	-2(1)
N1	26(1)	28(1)	29(1)	-2(1)	5(1)	1(1)
N2	27(1)	29(1)	23(1)	1(1)	6(1)	3(1)
N3	23(1)	26(1)	24(1)	0(1)	5(1)	0(1)
C1	26(1)	28(1)	20(1)	2(1)	3(1)	3(1)
C2	30(1)	31(1)	40(2)	5(1)	1(1)	-1(1)
C3	25(1)	50(2)	48(2)	13(1)	1(1)	2(1)
C4	35(2)	46(2)	33(2)	8(1)	5(1)	18(1)
C5	47(2)	31(1)	33(2)	-4(1)	-5(1)	9(1)
C6	31(1)	33(1)	30(1)	-4(1)	-3(1)	1(1)
C7	24(1)	27(1)	24(1)	-1(1)	2(1)	3(1)
C8	22(1)	27(1)	22(1)	-1(1)	1(1)	1(1)
C9	29(1)	34(1)	26(1)	-3(1)	5(1)	3(1)
C10	32(1)	42(2)	31(1)	-9(1)	3(1)	10(1)
C11	42(2)	30(1)	37(2)	0(1)	-1(1)	10(1)
C12	36(2)	28(1)	30(1)	3(1)	3(1)	2(1)
C13	51(2)	43(2)	43(2)	3(1)	26(2)	5(1)
C14	47(2)	37(2)	55(2)	5(1)	18(2)	-6(1)
C15	53(2)	72(2)	33(2)	10(2)	-1(1)	-1(2)
C16	50(2)	29(1)	41(2)	4(1)	12(1)	4(1)
C17	38(2)	38(2)	30(1)	2(1)	5(1)	-3(1)
C18	29(1)	49(2)	44(2)	2(1)	4(1)	-11(1)
C19	27(1)	27(1)	29(1)	1(1)	2(1)	3(1)
C20	25(1)	30(1)	29(1)	-3(1)	1(1)	4(1)
C21	28(1)	27(1)	28(1)	3(1)	0(1)	-2(1)
C22	31(1)	32(1)	38(2)	-2(1)	8(1)	-1(1)
C23	33(2)	37(2)	53(2)	5(1)	12(1)	-1(1)
C24	31(2)	38(2)	57(2)	8(1)	-3(1)	-7(1)
C25	52(2)	38(2)	40(2)	-4(1)	-8(1)	-12(1)
C26	42(2)	41(2)	28(1)	-3(1)	4(1)	-5(1)
C27	24(1)	31(1)	25(1)	-4(1)	3(1)	-7(1)
C28	31(1)	38(2)	33(2)	3(1)	2(1)	5(1)
C29	39(2)	44(2)	30(1)	8(1)	-5(1)	-4(1)
C30	40(2)	43(2)	24(1)	-3(1)	7(1)	-11(1)
C31	33(1)	39(2)	32(1)	-8(1)	7(1)	1(1)
C32	31(1)	34(1)	28(1)	0(1)	1(1)	3(1)

Table B-30. Hydrogen coordinates (x 10^4) and isotropic displacement parameters ($Å^2$x 10^3) for **15**.

	x	y	z	U(eq)
H2A	7698	1552	1113	40
H3A	9135	609	1120	49
H4A	8851	-830	825	45
H6A	5675	-406	524	38
H5A	7125	-1336	548	45
H9A	1838	2728	1980	35
H10A	1100	4029	1584	41
H11A	1743	4781	446	44
H12A	3149	4251	-270	37
H13A	6267	2235	-795	67
H13B	5944	2303	-1777	67
H13C	5341	1639	-1206	67
H14A	4747	4540	-867	69
H14B	5633	4225	-1481	69
H14C	5839	4127	-488	69
H15A	3231	2439	-1846	79
H15B	3849	3129	-2377	79
H15C	3026	3437	-1709	79
H16A	3510	-73	1037	60
H16B	3295	-420	1955	60
H16C	4348	127	1807	60
H17A	3793	1320	3167	53
H17B	2723	797	3318	53
H17C	2663	1800	3134	53
H18A	1008	1423	1698	61
H18B	1121	412	1812	61
H18C	1322	841	926	61
H22A	7458	3060	391	40
H23A	9006	3878	383	49
H24A	9315	4948	1377	50
H25A	8075	5194	2395	52
H26A	6564	4338	2440	44
H28A	6184	2013	3389	41
H29A	5776	2106	4796	45
H30A	4393	2994	5184	43
H31A	3450	3803	4180	42
H32A	3855	3732	2776	37

Table B-31. Crystal data and structure refinement for **17**.

Empirical formula	C24 H37 N3 Si2 W	
Formula weight	607.60	
Temperature	173(2) K	
Wavelength	0.71073 Å	
Crystal system	Triclinic	
Space group	P-1	
Unit cell dimensions	a = 13.1319(8) Å	α= 72.410(1)°.
	b = 14.0221(9) Å	β= 84.247(1)°.
	c = 15.0036(9) Å	γ = 89.938(1)°.
Volume	2619.0(3) $Å^3$	
Z	4	
Density (calculated)	1.541 Mg/m^3	
Absorption coefficient	4.517 mm^{-1}	
F(000)	1216	
Crystal size	0.17 x 0.15 x 0.03 mm^3	
Theta range for data collection	1.56 to 27.50°.	
Index ranges	$-14 \le h \le 17$, $-18 \le k \le 18$, $-19 \le l \le 16$	
Reflections collected	19003	
Independent reflections	11758 [R(int) = 0.0348]	
Completeness to theta = 27.50°	97.8 %	
Absorption correction	Integration	
Max. and min. transmission	0.8758 and 0.5259	
Refinement method	Full-matrix least-squares on F^2	
Data / restraints / parameters	11758 / 0 / 589	
Goodness-of-fit on F^2	1.005	
Final R indices [I>2sigma(I)]	R1 = 0.0300, wR2 = 0.0655 [9440]	
R indices (all data)	R1 = 0.0434, wR2 = 0.0722	
Largest diff. peak and hole	0.742 and -0.841 $e.Å^{-3}$	

$R1 = \Sigma(||F_o| - |F_c||) / \Sigma|F_o|$

$wR2 = [\Sigma[w(F_o^2 - F_c^2)^2] / \Sigma[w(F_o^2)^2]]^{1/2}$

$S = [\Sigma[w(F_o^2 - F_c^2)^2] / (n-p)]^{1/2}$

$w = 1/[\sigma^2(F_o^2)+(0.0370*p)^2+0.31*p]$, $p = [\max(F_o^2,0)+ 2* F_c^2]/3$

Table B-32. Atomic coordinates (x 10^4) and equivalent isotropic displacement parameters ($Å^2$x 10^3) for **17**. U(eq) is defined as one third of the trace of the orthogonalized U^{ij} tensor.

	x	y	z	U(eq)
W	282(1)	3711(1)	2857(1)	22(1)
Si1	529(1)	3104(1)	800(1)	28(1)
Si2	917(1)	6124(1)	2723(1)	27(1)
N1	-1053(3)	3816(3)	2937(3)	26(1)
N2	985(2)	3669(2)	1594(2)	21(1)
N3	1167(2)	5000(2)	2454(2)	20(1)
C1	-2111(3)	3744(3)	3149(3)	25(1)
C2	-2532(4)	3292(4)	4067(4)	36(1)
C3	-3576(4)	3172(4)	4293(4)	47(1)
C4	-4227(4)	3499(4)	3597(5)	48(1)
C5	-3826(4)	3968(3)	2686(4)	39(1)
C6	-2779(3)	4088(3)	2454(4)	33(1)
C7	1939(3)	4162(3)	1411(3)	21(1)
C8	2038(3)	4896(3)	1887(3)	22(1)
C9	2979(3)	5419(3)	1756(3)	28(1)
C10	3784(3)	5246(3)	1178(4)	33(1)
C11	3687(3)	4541(3)	711(3)	34(1)
C12	2771(3)	4011(3)	816(3)	28(1)
C13	786(4)	3969(4)	-426(4)	41(1)
C14	1133(4)	1884(4)	898(4)	46(1)
C15	-877(3)	2888(4)	1084(4)	41(1)
C16	1235(4)	7197(3)	1632(4)	40(1)
C17	1641(4)	6283(4)	3686(4)	39(1)
C18	-470(3)	6120(4)	3130(4)	38(1)
C19	612(4)	3495(4)	4301(3)	34(1)
C20	1581(4)	3128(3)	3958(3)	34(1)
C21	1495(4)	2411(3)	3512(3)	33(1)
C22	450(4)	2101(3)	3418(4)	36(1)
C23	2588(4)	3602(4)	4017(4)	45(1)
C24	2408(4)	2015(4)	3060(4)	47(1)
W'	5330(1)	9373(1)	2878(1)	22(1)
Si1'	5520(1)	11346(1)	849(1)	28(1)
Si2'	5979(1)	7093(1)	2612(1)	24(1)
N1'	3995(3)	9207(3)	2982(3)	29(1)
N2'	6015(3)	10281(2)	1628(2)	22(1)
N3'	6222(3)	8379(2)	2428(3)	24(1)
C1'	2949(3)	9205(3)	3238(4)	30(1)
C2'	2587(4)	9215(4)	4150(4)	43(1)
C3'	1561(4)	9252(5)	4406(5)	55(2)
C4'	856(4)	9265(4)	3779(5)	50(2)
C5'	1199(4)	9261(4)	2878(5)	46(1)
C6'	2235(4)	9229(3)	2606(4)	41(1)
C7'	6982(3)	9923(3)	1439(3)	22(1)
C8'	7093(3)	8885(3)	1888(3)	22(1)
C9'	8049(3)	8466(3)	1747(3)	29(1)
C10'	8858(3)	9043(3)	1205(4)	32(1)
C11'	8738(3)	10062(4)	748(4)	37(1)
C12'	7809(3)	10489(3)	868(3)	28(1)

Table B-32—continued.

C13'	5817(4)	11301(4)	-384(4)	43(1)
C14'	6069(4)	12523(3)	960(4)	46(1)
C15'	4113(4)	11333(4)	1145(4)	45(1)
C16'	6356(4)	6811(3)	1487(4)	37(1)
C17'	6669(4)	6281(3)	3568(4)	38(1)
C18'	4582(3)	6825(3)	2962(4)	34(1)
C19'	5712(4)	8632(4)	4293(3)	32(1)
C20'	6647(4)	9284(3)	3954(3)	32(1)
C21'	6487(4)	10285(3)	3558(3)	36(1)
C22'	5416(4)	10583(4)	3509(4)	39(1)
C23'	7685(4)	8828(4)	3989(4)	44(1)
C24'	7346(4)	11053(3)	3103(4)	44(1)

Table B-33. Bond lengths [Å] and angles [°] for **17**.

W-N1	1.755(3)
W-N2	2.040(3)
W-N3	2.045(3)
W-C22	2.178(5)
W-C19	2.183(5)
W-C21	2.459(5)
W-C20	2.460(4)
Si1-N2	1.765(3)
Si1-C14	1.856(5)
Si1-C15	1.857(5)
Si1-C13	1.870(5)
Si2-N3	1.764(3)
Si2-C18	1.861(5)
Si2-C16	1.869(5)
Si2-C17	1.874(5)
N1-C1	1.390(5)
N2-C7	1.393(5)
N3-C8	1.390(5)
C1-C2	1.387(6)
C1-C6	1.403(6)
C2-C3	1.376(6)
C3-C4	1.385(8)
C4-C5	1.375(8)
C5-C6	1.383(6)
C7-C12	1.399(6)
C7-C8	1.431(6)
C8-C9	1.405(5)
C9-C10	1.368(6)
C10-C11	1.386(7)
C11-C12	1.385(6)
C19-C20	1.475(7)
C20-C21	1.375(7)
C20-C23	1.503(7)
C21-C22	1.472(7)
C21-C24	1.507(7)
W'-N1'	1.754(4)
W'-N2'	2.042(3)
W'-N3'	2.044(3)
W'-C19'	2.173(5)
W'-C22'	2.186(5)
W'-C20'	2.460(4)
W'-C21'	2.467(4)
Si1'-N2'	1.765(3)
Si1'-C15'	1.855(5)
Si1'-C14'	1.861(5)
Si1'-C13'	1.871(5)
Si2'-N3'	1.764(3)
Si2'-C17'	1.856(5)
Si2'-C18'	1.864(4)
Si2'-C16'	1.867(5)
N1'-C1'	1.388(5)
N2'-C7'	1.398(5)
N3'-C8'	1.392(5)

Table B-33—continued.

C1'-C6'	1.393(7)
C1'-C2'	1.406(7)
C2'-C3'	1.369(7)
C3'-C4'	1.380(8)
C4'-C5'	1.384(8)
C5'-C6'	1.385(7)
C7'-C12'	1.395(6)
C7'-C8'	1.421(5)
C8'-C9'	1.409(5)
C9'-C10'	1.370(6)
C10'-C11'	1.402(6)
C11'-C12'	1.378(6)
C19'-C20'	1.483(6)
C20'-C21'	1.374(6)
C20'-C23'	1.504(7)
C21'-C22'	1.469(7)
C21'-C24'	1.517(7)
N1-W-N2	116.45(15)
N1-W-N3	118.11(14)
N2-W-N3	78.77(13)
N1-W-C22	102.10(17)
N2-W-C22	89.31(18)
N3-W-C22	139.32(16)
N1-W-C19	102.58(18)
N2-W-C19	140.48(16)
N3-W-C19	88.61(17)
C22-W-C19	76.2(2)
N1-W-C21	136.16(16)
N2-W-C21	83.99(14)
N3-W-C21	103.21(14)
C22-W-C21	36.39(17)
C19-W-C21	62.52(18)
N1-W-C20	136.60(17)
N2-W-C20	104.34(15)
N3-W-C20	82.62(14)
C22-W-C20	62.73(18)
C19-W-C20	36.42(17)
C21-W-C20	32.47(16)
N2-Si1-C14	111.2(2)
N2-Si1-C15	108.5(2)
C14-Si1-C15	108.7(2)
N2-Si1-C13	109.5(2)
C14-Si1-C13	110.5(3)
C15-Si1-C13	108.4(2)
N3-Si2-C18	108.29(19)
N3-Si2-C16	108.5(2)
C18-Si2-C16	109.6(2)
N3-Si2-C17	113.7(2)
C18-Si2-C17	106.9(2)
C16-Si2-C17	109.7(2)
C1-N1-W	169.3(3)
C7-N2-Si1	121.6(3)
C7-N2-W	110.2(3)

Table B-33—continued.

Si1-N2-W	128.24(18)
C8-N3-Si2	121.9(3)
C8-N3-W	110.1(2)
Si2-N3-W	128.00(19)
C2-C1-N1	119.8(4)
C2-C1-C6	118.2(4)
N1-C1-C6	121.9(4)
C3-C2-C1	121.2(5)
C2-C3-C4	120.1(5)
C5-C4-C3	119.7(5)
C4-C5-C6	120.5(5)
C5-C6-C1	120.3(5)
N2-C7-C12	126.4(4)
N2-C7-C8	114.6(4)
C12-C7-C8	119.0(4)
N3-C8-C9	126.7(4)
N3-C8-C7	114.7(3)
C9-C8-C7	118.6(4)
C10-C9-C8	121.1(4)
C9-C10-C11	120.4(4)
C12-C11-C10	120.5(4)
C11-C12-C7	120.5(4)
C20-C19-W	82.1(3)
C21-C20-C19	116.2(4)
C21-C20-C23	123.1(5)
C19-C20-C23	120.4(5)
C21-C20-W	73.7(3)
C19-C20-W	61.5(2)
C23-C20-W	130.5(3)
C20-C21-C22	116.8(5)
C20-C21-C24	122.7(4)
C22-C21-C24	120.3(5)
C20-C21-W	73.8(3)
C22-C21-W	61.3(2)
C24-C21-W	131.8(3)
C21-C22-W	82.3(3)
N1'-W'-N2'	117.15(16)
N1'-W'-N3'	118.54(14)
N2'-W'-N3'	79.02(13)
N1'-W'-C19'	103.15(18)
N2'-W'-C19'	139.09(16)
N3'-W'-C19'	88.27(17)
N1'-W'-C22'	99.00(19)
N2'-W'-C22'	90.60(17)
N3'-W'-C22'	141.79(18)
C19'-W'-C22'	75.8(2)
N1'-W'-C20'	136.43(17)
N2'-W'-C20'	102.86(14)
N3'-W'-C20'	84.01(15)
C19'-W'-C20'	36.67(16)
C22'-W'-C20'	62.42(18)
N1'-W'-C21'	133.38(17)
N2'-W'-C21'	83.65(15)
N3'-W'-C21'	105.71(15)

Table B-33—continued.

C19'-W'-C21'	62.52(16)
C22'-W'-C21'	36.18(19)
C20'-W'-C21'	32.38(15)
N2'-Si1'-C15'	108.6(2)
N2'-Si1'-C14'	111.4(2)
C15'-Si1'-C14'	108.1(3)
N2'-Si1'-C13'	109.0(2)
C15'-Si1'-C13'	109.8(3)
C14'-Si1'-C13'	109.9(3)
N3'-Si2'-C17'	112.65(19)
N3'-Si2'-C18'	108.20(18)
C17'-Si2'-C18'	107.5(2)
N3'-Si2'-C16'	108.5(2)
C17'-Si2'-C16'	110.2(2)
C18'-Si2'-C16'	109.8(2)
C1'-N1'-W'	165.1(3)
C7'-N2'-Si1'	122.4(3)
C7'-N2'-W'	109.4(2)
Si1'-N2'-W'	128.20(19)
C8'-N3'-Si2'	122.3(3)
C8'-N3'-W'	108.8(2)
Si2'-N3'-W'	128.78(19)
N1'-C1'-C6'	122.0(5)
N1'-C1'-C2'	119.8(4)
C6'-C1'-C2'	118.2(4)
C3'-C2'-C1'	120.8(5)
C2'-C3'-C4'	120.8(6)
C3'-C4'-C5'	119.1(5)
C4'-C5'-C6'	120.8(5)
C5'-C6'-C1'	120.2(5)
C12'-C7'-N2'	126.0(4)
C12'-C7'-C8'	119.4(4)
N2'-C7'-C8'	114.6(3)
N3'-C8'-C9'	126.3(4)
N3'-C8'-C7'	115.4(3)
C9'-C8'-C7'	118.3(4)
C10'-C9'-C8'	121.2(4)
C9'-C10'-C11'	120.3(4)
C12'-C11'-C10'	119.7(4)
C11'-C12'-C7'	121.1(4)
C20'-C19'-W'	82.3(3)
C21'-C20'-C19'	115.8(4)
C21'-C20'-C23'	124.0(4)
C19'-C20'-C23'	120.0(4)
C21'-C20'-W'	74.1(3)
C19'-C20'-W'	61.1(2)
C23'-C20'-W'	131.2(3)
C20'-C21'-C22'	116.5(4)
C20'-C21'-C24'	123.4(5)
C22'-C21'-C24'	119.8(4)
C20'-C21'-W'	73.5(3)
C22'-C21'-W'	61.4(2)

Symmetry transformations used to generate equivalent atoms:

Table B-34. Anisotropic displacement parameters ($Å^2 x\ 10^3$) for **17**. The anisotropic displacement factor exponent takes the form: $-2\pi^2[\ h^2\ a^{*2}U^{11} + ... + 2\ h\ k\ a^*\ b^*\ U^{12}\ ]$

	U^{11}	U^{22}	U^{33}	U^{23}	U^{13}	U^{12}
W	19(1)	24(1)	21(1)	-7(1)	1(1)	-2(1)
Si1	28(1)	29(1)	28(1)	-14(1)	0(1)	-7(1)
Si2	28(1)	29(1)	29(1)	-15(1)	-6(1)	2(1)
N1	22(2)	29(2)	27(2)	-8(2)	0(2)	-2(1)
N2	20(2)	21(2)	22(2)	-7(1)	-1(1)	-3(1)
N3	25(2)	22(2)	18(2)	-11(1)	-2(1)	1(1)
C1	28(2)	21(2)	28(2)	-9(2)	-1(2)	-1(2)
C2	30(2)	47(3)	32(3)	-14(2)	3(2)	-3(2)
C3	34(3)	63(3)	42(3)	-19(3)	15(2)	-11(2)
C4	24(2)	56(3)	68(4)	-27(3)	6(3)	-3(2)
C5	26(2)	34(2)	62(4)	-18(2)	-13(2)	3(2)
C6	31(2)	31(2)	36(3)	-10(2)	-3(2)	0(2)
C7	22(2)	20(2)	20(2)	-4(2)	-1(2)	0(2)
C8	19(2)	24(2)	20(2)	-5(2)	1(2)	-2(2)
C9	29(2)	29(2)	27(2)	-9(2)	-3(2)	-5(2)
C10	20(2)	36(2)	42(3)	-11(2)	4(2)	-8(2)
C11	26(2)	41(2)	33(3)	-13(2)	9(2)	-3(2)
C12	29(2)	25(2)	29(2)	-10(2)	1(2)	-4(2)
C13	42(3)	54(3)	27(3)	-13(2)	-7(2)	-3(2)
C14	59(3)	36(3)	50(4)	-25(3)	-8(3)	0(2)
C15	30(2)	59(3)	44(3)	-30(3)	0(2)	-13(2)
C16	49(3)	27(2)	46(3)	-11(2)	-7(2)	0(2)
C17	37(3)	50(3)	42(3)	-29(3)	-13(2)	-3(2)
C18	34(3)	46(3)	42(3)	-25(2)	-5(2)	9(2)
C19	41(3)	39(3)	21(2)	-8(2)	1(2)	2(2)
C20	40(3)	35(2)	21(2)	1(2)	-8(2)	8(2)
C21	37(3)	32(2)	21(2)	3(2)	3(2)	1(2)
C22	39(3)	28(2)	36(3)	-4(2)	8(2)	-8(2)
C23	42(3)	54(3)	36(3)	-7(3)	-17(2)	2(2)
C24	44(3)	41(3)	47(3)	-4(2)	5(3)	12(2)
W'	23(1)	22(1)	21(1)	-8(1)	2(1)	0(1)
Si1'	31(1)	25(1)	27(1)	-5(1)	-2(1)	7(1)
Si2'	27(1)	21(1)	25(1)	-7(1)	-3(1)	0(1)
N1'	27(2)	27(2)	33(2)	-12(2)	4(2)	1(2)
N2'	24(2)	21(2)	22(2)	-8(1)	1(1)	-1(1)
N3'	22(2)	19(2)	27(2)	-4(1)	-5(2)	2(1)
C1'	25(2)	19(2)	43(3)	-4(2)	-1(2)	2(2)
C2'	28(2)	54(3)	34(3)	0(2)	7(2)	-2(2)
C3'	38(3)	66(4)	52(4)	-9(3)	13(3)	0(3)
C4'	27(3)	45(3)	68(4)	-10(3)	10(3)	1(2)
C5'	32(3)	36(3)	70(4)	-15(3)	-9(3)	-7(2)
C6'	37(3)	36(2)	50(3)	-18(2)	1(2)	-6(2)
C7'	24(2)	24(2)	19(2)	-8(2)	-3(2)	1(2)
C8'	18(2)	24(2)	25(2)	-11(2)	3(2)	0(2)
C9'	26(2)	30(2)	29(3)	-9(2)	-1(2)	4(2)
C10'	20(2)	36(2)	39(3)	-11(2)	-1(2)	4(2)
C11'	26(2)	40(3)	38(3)	-6(2)	10(2)	-6(2)
C12'	27(2)	23(2)	32(3)	-6(2)	3(2)	-5(2)
C13'	46(3)	51(3)	28(3)	-4(2)	-5(2)	5(2)

Table B-34—continued.

C14'	60(3)	24(2)	55(4)	-8(2)	-13(3)	6(2)
C15'	33(3)	47(3)	45(3)	-3(3)	0(2)	15(2)
C16'	46(3)	32(2)	35(3)	-16(2)	-2(2)	1(2)
C17'	44(3)	27(2)	42(3)	-5(2)	-12(2)	4(2)
C18'	28(2)	33(2)	41(3)	-14(2)	-3(2)	-3(2)
C19'	40(3)	30(2)	21(2)	-5(2)	4(2)	-3(2)
C20'	43(3)	35(2)	18(2)	-7(2)	-7(2)	-7(2)
C21'	58(3)	33(2)	20(2)	-11(2)	-7(2)	-10(2)
C22'	59(3)	27(2)	30(3)	-12(2)	3(2)	1(2)
C23'	48(3)	48(3)	33(3)	-5(2)	-19(2)	-3(2)
C24'	63(3)	29(2)	40(3)	-8(2)	-8(3)	-15(2)

Table B-35. Hydrogen coordinates (x 10^4) and isotropic displacement parameters ($Å^2$x 10^3) for **17**.

	x	y	z	U(eq)
H2A	-2093	3062	4549	43
H3A	-3850	2865	4926	56
H4A	-4946	3399	3749	58
H5A	-4273	4211	2213	47
H6A	-2510	4406	1821	39
H9A	3059	5902	2074	33
H10A	4414	5610	1097	40
H11A	4252	4421	316	40
H12A	2708	3540	481	33
H13A	380	4569	-491	62
H13B	597	3630	-871	62
H13C	1516	4162	-558	62
H14A	1880	1977	823	68
H14B	924	1621	406	68
H14C	914	1410	1517	68
H15A	-1026	2447	1730	62
H15B	-1141	2572	650	62
H15C	-1206	3529	1022	62
H16A	1977	7248	1463	61
H16B	998	7818	1743	61
H16C	895	7087	1117	61
H17A	1465	5723	4259	59
H17B	1457	6913	3807	59
H17C	2378	6294	3496	59
H18A	-876	6050	2639	57
H18B	-628	6749	3264	57
H18C	-634	5557	3703	57
H19A	660(40)	4010(40)	4460(40)	31(13)
H19B	130(40)	3030(40)	4690(40)	39(14)
H22A	370(40)	1660(40)	3030(40)	59(18)
H22B	80(40)	1860(30)	3980(40)	29(13)
H23A	2991	3108	4437	67
H23B	2465	4169	4263	67
H23C	2965	3838	3389	67
H24A	2793	2572	2589	70
H24B	2175	1540	2755	70
H24C	2849	1676	3541	70
H2'A	3061	9196	4593	51
H3'A	1332	9269	5021	66
H4'A	144	9277	3965	59
H5'A	718	9282	2440	55
H6'A	2458	9222	1986	49
H9'A	8133	7771	2032	34
H10B	9503	8751	1139	38
H11B	9294	10456	356	44
H12B	7731	11180	558	34
H13D	5784	11976	-824	65
H13E	5316	10856	-514	65

Table B-35—continued.

H13F	6506	11049	-459	65
H14D	5922	12536	1610	70
H14E	5761	13100	537	70
H14F	6811	12554	793	70
H15D	3807	10719	1089	67
H15E	3827	11916	711	67
H15F	3962	11356	1791	67
H16D	5967	7224	994	55
H16E	6208	6102	1573	55
H16F	7090	6958	1304	55
H17D	7397	6484	3457	58
H17E	6596	5583	3577	58
H17F	6380	6349	4173	58
H18D	4391	6957	3561	50
H18E	4424	6121	3032	50
H18F	4194	7255	2477	50
H19C	5270(40)	8710(40)	4730(40)	42(15)
H19D	5850(40)	7930(40)	4500(40)	45(15)
H22C	5360(30)	11180(30)	3120(30)	22(11)
H22D	5000(30)	10330(30)	4150(40)	28(12)
H23D	8164	9255	3483	66
H23E	7635	8162	3910	66
H23F	7933	8771	4597	66
H24D	7960	10713	2950	66
H24E	7494	11420	3539	66
H24F	7137	11522	2526	66

Table B-36. Crystal data and structure refinement for **19**.

Empirical formula	C27 H43 N3 O Si2 W	
Formula weight	665.67	
Temperature	173(2) K	
Wavelength	0.71073 Å	
Crystal system	Monoclinic	
Space group	P2(1)/n	
Unit cell dimensions	a = 9.8093(4) Å	α= 90°.
	b = 31.089(1) Å	β= 100.321(1)°.
	c = 10.0877(5) Å	γ = 90°.
Volume	3026.6(2) $Å^3$	
Z	4	
Density (calculated)	1.461 Mg/m^3	
Absorption coefficient	3.918 mm^{-1}	
F(000)	1344	
Crystal size	0.08 x 0.13 x 0.28 mm^3	
Theta range for data collection	2.15 to 27.50°.	
Index ranges	$-12 \le h \le 12$, $-28 \le k \le 40$, $-13 \le l \le 12$	
Reflections collected	21831	
Independent reflections	6937 [R(int) = 0.0329]	
Completeness to theta = 27.50°	99.7 %	
Absorption correction	Integration	
Max. and min. transmission	0.7542 and 0.3103	
Refinement method	Full-matrix least-squares on F^2	
Data / restraints / parameters	6937 / 0 / 317	
Goodness-of-fit on F^2	1.111	
Final R indices [I>2sigma(I)]	R1 = 0.0328, wR2 = 0.0675 [6144]	
R indices (all data)	R1 = 0.0392, wR2 = 0.0697	
Largest diff. peak and hole	2.986 and -1.976 $e.Å^{-3}$	

$R1 = \Sigma(||F_o| - |F_c||) / \Sigma|F_o|$

$wR2 = [\Sigma[w(F_o^2 - F_c^2)^2] / \Sigma[w(F_o^2)^2]]^{1/2}$

$S = [\Sigma[w(F_o^2 - F_c^2)^2] / (n-p)]^{1/2}$ $w = 1/[\sigma^2(F_o^2)+(0.0370*p)^2+0.31*p]$, $p = [\max(F_o^2,0)+ 2* F_c^2]/3$

Table B-37. Atomic coordinates (x 10^4) and equivalent isotropic displacement parameters ($Å^2$x 10^3) for **19**. U(eq) is defined as one third of the trace of the orthogonalized U^{ij} tensor.

	x	y	z	U(eq)
W	5872(1)	1448(1)	2434(1)	23(1)
Si1	3986(1)	1099(1)	4790(1)	38(1)
Si2	7319(1)	583(1)	1294(1)	35(1)
O1	6852(3)	1762(1)	1298(3)	32(1)
N1	4255(3)	1414(1)	1389(3)	27(1)
N2	5545(3)	1151(1)	4146(3)	24(1)
N3	7266(3)	960(1)	2585(3)	25(1)
C1	3114(4)	1371(1)	363(4)	27(1)
C2	2468(4)	1737(1)	-253(4)	33(1)
C3	1337(5)	1697(2)	-1278(5)	38(1)
C4	828(5)	1300(2)	-1702(5)	41(1)
C5	1458(5)	938(2)	-1086(5)	43(1)
C6	2589(5)	970(1)	-54(4)	36(1)
C7	6721(4)	925(1)	4781(4)	24(1)
C8	7672(4)	823(1)	3923(4)	23(1)
C9	8894(4)	603(1)	4439(4)	32(1)
C10	9158(4)	471(2)	5776(4)	35(1)
C11	8227(5)	560(2)	6602(4)	37(1)
C12	7025(4)	788(2)	6122(4)	33(1)
C13	4054(7)	1385(3)	6450(6)	79(2)
C14	3633(7)	519(2)	4959(8)	78(2)
C15	2503(5)	1339(2)	3638(6)	60(2)
C16	9112(6)	409(2)	1127(5)	53(1)
C17	6327(7)	103(2)	1664(5)	57(2)
C18	6501(6)	827(2)	-343(4)	47(1)
C19	5746(4)	2043(1)	3511(5)	35(1)
C20	7178(5)	2066(2)	4337(5)	41(1)
C21	8300(5)	2171(2)	3826(6)	49(1)
C22	8229(5)	2330(2)	2402(6)	54(1)
C23	8146(5)	1978(2)	1323(5)	42(1)
C24	7284(7)	1957(2)	5827(5)	60(2)
C25	9735(6)	2175(2)	4672(8)	79(2)
C26	9338(5)	1658(2)	1616(6)	49(1)
C27	8105(6)	2172(2)	-74(6)	63(2)

Table B-38. Bond lengths [Å] and angles [°] for **19**.

W-N1	1.744(3)
W-O1	1.895(3)
W-N3	2.030(3)
W-N2	2.034(3)
W-C19	2.160(4)
Si1-N2	1.773(3)
Si1-C14	1.848(7)
Si1-C15	1.848(5)
Si1-C13	1.887(6)
Si2-N3	1.758(3)
Si2-C17	1.856(6)
Si2-C18	1.863(5)
Si2-C16	1.876(5)
O1-C23	1.431(5)
N1-C1	1.387(5)
N2-C7	1.404(5)
N3-C8	1.403(5)
C1-C6	1.386(6)
C1-C2	1.393(6)
C2-C3	1.379(6)
C3-C4	1.371(7)
C4-C5	1.378(7)
C5-C6	1.382(6)
C7-C12	1.398(5)
C7-C8	1.418(5)
C8-C9	1.396(5)
C9-C10	1.389(6)
C10-C11	1.370(6)
C11-C12	1.387(6)
C19-C20	1.502(6)
C20-C21	1.336(7)
C20-C24	1.527(7)
C21-C22	1.510(8)
C21-C25	1.510(7)
C22-C23	1.536(8)
C23-C26	1.523(6)
C23-C27	1.527(7)
N1-W-O1	99.80(14)
N1-W-N3	121.90(14)
O1-W-N3	91.31(12)
N1-W-N2	102.82(14)
O1-W-N2	157.27(12)
N3-W-N2	78.68(12)
N1-W-C19	103.13(16)
O1-W-C19	86.72(15)
N3-W-C19	134.52(14)
N2-W-C19	86.01(15)
N2-Si1-C14	108.1(2)
N2-Si1-C15	111.5(2)
C14-Si1-C15	108.2(3)
N2-Si1-C13	112.7(2)
C14-Si1-C13	110.8(4)

Table B-38—continued.

C15-Si1-C13	105.5(3)
N3-Si2-C17	107.5(2)
N3-Si2-C18	108.7(2)
C17-Si2-C18	110.3(3)
N3-Si2-C16	114.3(2)
C17-Si2-C16	108.7(3)
C18-Si2-C16	107.4(2)
C23-O1-W	140.9(3)
C1-N1-W	169.0(3)
C7-N2-Si1	118.7(3)
C7-N2-W	111.9(2)
Si1-N2-W	129.05(17)
C8-N3-Si2	118.0(3)
C8-N3-W	111.7(2)
Si2-N3-W	123.42(16)
C6-C1-N1	121.4(4)
C6-C1-C2	119.0(4)
N1-C1-C2	119.7(4)
C3-C2-C1	120.2(4)
C4-C3-C2	120.8(4)
C3-C4-C5	119.1(4)
C4-C5-C6	121.0(4)
C5-C6-C1	119.8(4)
C12-C7-N2	127.5(3)
C12-C7-C8	118.3(3)
N2-C7-C8	114.2(3)
C9-C8-N3	125.7(3)
C9-C8-C7	119.8(3)
N3-C8-C7	114.5(3)
C10-C9-C8	120.3(4)
C11-C10-C9	120.2(4)
C10-C11-C12	120.6(4)
C11-C12-C7	120.9(4)
C20-C19-W	100.8(3)
C21-C20-C19	123.4(5)
C21-C20-C24	121.2(5)
C19-C20-C24	115.3(5)
C20-C21-C22	123.1(5)
C20-C21-C25	122.2(6)
C22-C21-C25	114.5(5)
C21-C22-C23	115.3(4)
O1-C23-C26	110.2(4)
O1-C23-C27	107.0(4)
C26-C23-C27	109.2(4)
O1-C23-C22	106.3(4)
C26-C23-C22	112.8(4)
C27-C23-C22	111.1(5)

Symmetry transformations used to generate equivalent atoms:

Table B-39. Anisotropic displacement parameters ($Å^2 x\ 10^3$) for **19**. The anisotropic displacement factor exponent takes the form: $-2\pi^2[\ h^2\ a^{*2}U^{11} + ... + 2\ h\ k\ a^*\ b^*\ U^{12}\ ]$

	U^{11}	U^{22}	U^{33}	U^{23}	U^{13}	U^{12}
W	21(1)	23(1)	23(1)	3(1)	2(1)	2(1)
Si1	28(1)	53(1)	36(1)	11(1)	14(1)	10(1)
Si2	46(1)	38(1)	23(1)	0(1)	11(1)	12(1)
O1	27(1)	32(2)	38(2)	13(1)	9(1)	1(1)
N1	23(2)	32(2)	25(2)	1(1)	1(1)	1(1)
N2	23(2)	26(2)	23(2)	0(1)	4(1)	3(1)
N3	23(2)	31(2)	21(1)	2(1)	6(1)	4(1)
C1	23(2)	31(2)	26(2)	1(2)	4(1)	-1(2)
C2	32(2)	29(2)	35(2)	3(2)	-2(2)	-1(2)
C3	34(2)	38(3)	40(2)	8(2)	-1(2)	6(2)
C4	30(2)	52(3)	37(2)	2(2)	-6(2)	-1(2)
C5	42(3)	33(2)	49(3)	-5(2)	-6(2)	-9(2)
C6	36(2)	25(2)	42(2)	2(2)	-4(2)	1(2)
C7	22(2)	28(2)	22(2)	2(2)	4(1)	1(2)
C8	26(2)	22(2)	21(2)	-1(1)	1(1)	3(2)
C9	29(2)	36(2)	30(2)	-3(2)	6(2)	8(2)
C10	33(2)	37(2)	31(2)	3(2)	-4(2)	13(2)
C11	41(2)	45(3)	24(2)	4(2)	0(2)	7(2)
C12	35(2)	41(3)	23(2)	4(2)	7(2)	7(2)
C13	62(4)	132(7)	49(3)	-4(4)	27(3)	31(4)
C14	52(3)	70(4)	117(6)	35(4)	31(4)	-8(3)
C15	27(2)	97(5)	61(3)	23(3)	17(2)	17(3)
C16	64(3)	64(4)	36(2)	2(2)	21(2)	32(3)
C17	87(4)	39(3)	46(3)	-10(2)	10(3)	-4(3)
C18	60(3)	59(3)	23(2)	-2(2)	12(2)	15(3)
C19	32(2)	29(2)	43(2)	-3(2)	6(2)	1(2)
C20	43(3)	28(2)	49(3)	-11(2)	-3(2)	4(2)
C21	37(3)	38(3)	67(3)	-11(2)	-4(2)	-4(2)
C22	35(3)	36(3)	91(4)	7(3)	16(3)	-8(2)
C23	30(2)	37(3)	62(3)	16(2)	15(2)	-2(2)
C24	74(4)	51(3)	46(3)	-19(3)	-9(3)	0(3)
C25	42(3)	88(5)	99(5)	-29(4)	-8(3)	-5(3)
C26	26(2)	55(3)	68(3)	10(3)	16(2)	6(2)
C27	48(3)	69(4)	81(4)	41(3)	30(3)	10(3)

Table B-40. Hydrogen coordinates (x 10^4) and isotropic displacement parameters ($Å^2$x 10^3) for **19**.

	x	y	z	U(eq)
H2A	2807	2014	33	40
H3A	906	1949	-1696	46
H4A	52	1275	-2410	50
H5A	1109	662	-1375	52
H6A	3005	717	369	43
H9A	9549	544	3873	38
H10A	9985	319	6119	42
H11A	8405	464	7510	45
H12A	6401	853	6713	39
H13A	4885	1295	7079	119
H13B	3228	1312	6825	119
H13C	4084	1696	6308	119
H14A	3495	383	4069	117
H14B	2795	483	5352	117
H14C	4420	384	5547	117
H15A	2732	1634	3420	91
H15B	1688	1341	4076	91
H15C	2303	1168	2809	91
H16A	9706	663	1134	80
H16B	9075	253	277	80
H16C	9490	221	1882	80
H17A	6818	-38	2479	86
H17B	6235	-97	904	86
H17C	5405	192	1803	86
H18A	5546	911	-302	71
H18B	6498	617	-1068	71
H18C	7028	1082	-521	71
H19A	5553	2290	2888	42
H19B	5029	2029	4087	42
H22A	9059	2509	2370	64
H22B	7407	2519	2169	64
H24A	7896	1708	6052	90
H24B	6361	1889	6012	90
H24C	7663	2204	6375	90
H25A	9894	2451	5144	118
H25B	10424	2136	4089	118
H25C	9818	1941	5332	118
H26A	9340	1522	2492	73
H26B	10218	1809	1631	73
H26C	9225	1437	911	73
H27A	7857	1949	-760	95
H27B	9019	2290	-135	95
H27C	7414	2403	-222	95

Table B-41. Crystal data and structure refinement for **22**.

Empirical formula	C22 H31 N3 S Si2 W	
Formula weight	609.59	
Temperature	173(2) K	
Wavelength	0.71073 Å	
Crystal system	Triclinic	
Space group	P-1	
Unit cell dimensions	a = 9.4647(4) Å	α= 101.246(1)°.
	b = 11.7141(5) Å	β= 111.655(1)°.
	c = 12.4830(5) Å	γ = 93.904(1)°.
Volume	1246.64(9) $Å^3$	
Z	2	
Density (calculated)	1.624 Mg/m^3	
Absorption coefficient	4.826 mm^{-1}	
F(000)	604	
Crystal size	0.15 x 0.08 x 0.04 mm^3	
Theta range for data collection	1.79 to 27.50°.	
Index ranges	$-12 \le h \le 11$, $-15 \le k \le 15$, $-16 \le l \le 15$	
Reflections collected	8979	
Independent reflections	5607 [R(int) = 0.0326]	
Completeness to theta = 27.50°	97.8 %	
Absorption correction	Integration	
Max. and min. transmission	0.8395 and 0.6137	
Refinement method	Full-matrix least-squares on F^2	
Data / restraints / parameters	5607 / 2 / 264	
Goodness-of-fit on F^2	1.024	
Final R indices [I>2sigma(I)]	R1 = 0.0264, wR2 = 0.0647 [5106]	
R indices (all data)	R1 = 0.0305, wR2 = 0.0663	
Largest diff. peak and hole	1.568 and -1.022 $e.Å^{-3}$	

$R1 = \Sigma(||F_o| - |F_c||) / \Sigma|F_o|$

$wR2 = [\Sigma[w(F_o^2 - F_c^2)^2] / \Sigma[w(F_o^2)^2]]^{1/2}$

$S = [\Sigma[w(F_o^2 - F_c^2)^2] / (n-p)]^{1/2}$

$w = 1/[\sigma^2(F_o^2)+(0.0370*p)^2+0.31*p]$, $p = [\max(F_o^2,0)+ 2* F_c^2]/3$

Table B-42. Atomic coordinates (x 10^4) and equivalent isotropic displacement parameters ($Å^2$x 10^3) for **22**. U(eq) is defined as one third of the trace of the orthogonalized U^{ij} tensor.

	x	y	z	U(eq)
W	9027(1)	2056(1)	2801(1)	22(1)
Si1	7351(1)	3929(1)	1014(1)	28(1)
Si2	13013(1)	2288(1)	3832(1)	28(1)
N1	8883(4)	2828(3)	4082(3)	30(1)
N2	8589(4)	2887(3)	1468(3)	26(1)
N3	11127(4)	2167(3)	2749(3)	25(1)
C1	8502(4)	3122(3)	5072(3)	25(1)
C2	7850(5)	2230(3)	5423(3)	30(1)
C3	7403(5)	2520(4)	6364(4)	37(1)
C4	7609(5)	3676(4)	6975(3)	35(1)
C5	8296(5)	4557(3)	6649(4)	33(1)
C6	8731(5)	4288(3)	5701(4)	31(1)
C7	9419(4)	2360(3)	836(3)	27(1)
C8	10795(4)	1969(3)	1536(3)	26(1)
C9	11697(5)	1426(3)	959(4)	34(1)
C10	11275(5)	1298(4)	-238(4)	40(1)
C11	9942(6)	1686(4)	-916(4)	41(1)
C12	9014(5)	2200(4)	-391(4)	37(1)
C13	8311(5)	5027(4)	510(4)	40(1)
C14	5491(5)	3185(4)	-214(5)	49(1)
C15	7006(5)	4672(4)	2328(4)	40(1)
C16	14371(5)	3203(4)	3460(4)	43(1)
C17	13563(5)	785(4)	3873(4)	40(1)
C18	12988(5)	3014(4)	5277(4)	39(1)
S1	6492(3)	1087(2)	1585(3)	32(1)
C19	5977(15)	-102(10)	2057(11)	41(3)
C20	6641(14)	-602(10)	2796(10)	38(3)
C21	8472(12)	-532(8)	3300(8)	32(2)
C22	9340(13)	360(8)	3289(9)	35(3)
S1'	9715(4)	299(2)	3392(3)	28(1)
C19'	8132(14)	-582(10)	3371(11)	34(3)
C20'	6891(16)	-750(12)	2731(12)	37(4)
C21'	5963(17)	103(12)	1924(12)	37(3)
C22'	6705(13)	1052(13)	1824(14)	50(5)

Table B-42. Bond lengths [Å] and angles [°] for **22**.

W-N1	1.734(3)
W-N3	2.008(3)
W-N2	2.016(3)
W-C22'	2.194(10)
W-C22	2.196(9)
W-S1	2.371(3)
W-S1'	2.371(3)
Si1-N2	1.777(3)
Si1-C15	1.853(4)
Si1-C13	1.859(4)
Si1-C14	1.868(5)
Si2-N3	1.773(3)
Si2-C18	1.849(4)
Si2-C16	1.861(4)
Si2-C17	1.873(4)
N1-C1	1.399(4)
N2-C7	1.398(4)
N3-C8	1.396(5)
C1-C6	1.394(5)
C1-C2	1.398(5)
C2-C3	1.380(5)
C3-C4	1.380(6)
C4-C5	1.385(6)
C5-C6	1.379(5)
C7-C12	1.404(5)
C7-C8	1.437(5)
C8-C9	1.415(5)
C9-C10	1.370(6)
C10-C11	1.398(6)
C11-C12	1.381(6)
S1-C19	1.722(12)
C19-C20	1.192(16)
C20-C21	1.600(16)
C21-C22	1.289(14)
S1'-C19'	1.750(13)
C19'-C20'	1.127(18)
C20'-C21'	1.63(2)
C21'-C22'	1.325(19)
N1-W-N3	117.02(14)
N1-W-N2	116.06(13)
N3-W-N2	82.25(12)
N1-W-C22'	101.7(5)
N3-W-C22'	140.7(4)
N2-W-C22'	87.1(5)
N1-W-C22	98.0(3)
N3-W-C22	89.0(3)
N2-W-C22	145.1(3)
C22'-W-C22	78.5(5)
N1-W-S1	104.49(13)
N3-W-S1	138.47(11)
N2-W-S1	80.88(11)
C22'-W-S1	6.2(5)

Table B-42—continued.

C22-W-S1	83.7(3)
N1-W-S1'	99.32(12)
N3-W-S1'	81.79(11)
N2-W-S1'	144.62(11)
C22'-W-S1'	85.5(4)
C22-W-S1'	7.6(3)
S1-W-S1'	90.62(10)
N2-Si1-C15	106.94(17)
N2-Si1-C13	109.44(18)
C15-Si1-C13	109.7(2)
N2-Si1-C14	110.92(18)
C15-Si1-C14	110.2(2)
C13-Si1-C14	109.6(2)
N3-Si2-C18	107.06(18)
N3-Si2-C16	108.95(18)
C18-Si2-C16	110.2(2)
N3-Si2-C17	109.84(18)
C18-Si2-C17	110.0(2)
C16-Si2-C17	110.7(2)
C1-N1-W	162.4(3)
C7-N2-Si1	124.2(2)
C7-N2-W	102.9(2)
Si1-N2-W	132.66(17)
C8-N3-Si2	123.1(2)
C8-N3-W	102.7(2)
Si2-N3-W	133.78(17)
C6-C1-C2	119.4(3)
C6-C1-N1	121.3(3)
C2-C1-N1	119.3(3)
C3-C2-C1	119.6(3)
C4-C3-C2	121.0(4)
C3-C4-C5	119.5(4)
C6-C5-C4	120.4(3)
C5-C6-C1	120.1(3)
N2-C7-C12	125.3(3)
N2-C7-C8	115.2(3)
C12-C7-C8	119.4(3)
N3-C8-C9	125.4(3)
N3-C8-C7	116.1(3)
C9-C8-C7	118.6(3)
C10-C9-C8	120.3(4)
C9-C10-C11	121.0(4)
C12-C11-C10	120.5(4)
C11-C12-C7	120.2(4)
C19-S1-W	112.4(5)
C20-C19-S1	134.5(11)
C19-C20-C21	121.9(11)
C22-C21-C20	121.0(9)
C21-C22-W	136.8(9)
C19'-S1'-W	111.4(4)
C20'-C19'-S1'	129.9(12)
C19'-C20'-C21'	128.1(13)
C22'-C21'-C20'	120.8(13)
C21'-C22'-W	134.1(12)

Table B-43. Anisotropic displacement parameters ($Å^2 x\ 10^3$) for **22**. The anisotropic displacement factor exponent takes the form: $-2\pi^2[\ h^2\ a^{*2}U^{11} + ... + 2\ h\ k\ a^*\ b^*\ U^{12}\ ]$

	U^{11}	U^{22}	U^{33}	U^{23}	U^{13}	U^{12}
W	24(1)	22(1)	22(1)	6(1)	10(1)	6(1)
Si1	30(1)	28(1)	29(1)	11(1)	12(1)	11(1)
Si2	26(1)	29(1)	32(1)	11(1)	10(1)	8(1)
N1	34(2)	28(2)	32(2)	10(1)	16(1)	8(1)
N2	29(2)	28(2)	24(2)	9(1)	11(1)	10(1)
N3	26(2)	26(1)	26(2)	10(1)	12(1)	10(1)
C1	24(2)	26(2)	23(2)	5(1)	9(1)	5(1)
C2	39(2)	25(2)	28(2)	7(1)	13(2)	7(2)
C3	48(3)	35(2)	36(2)	16(2)	22(2)	6(2)
C4	43(2)	40(2)	25(2)	7(2)	18(2)	11(2)
C5	39(2)	25(2)	32(2)	1(2)	13(2)	5(2)
C6	32(2)	26(2)	36(2)	7(2)	16(2)	2(2)
C7	32(2)	25(2)	27(2)	8(1)	13(2)	9(2)
C8	29(2)	25(2)	26(2)	8(1)	12(2)	5(1)
C9	35(2)	35(2)	41(2)	12(2)	20(2)	18(2)
C10	49(3)	43(2)	39(2)	12(2)	27(2)	20(2)
C11	54(3)	43(2)	31(2)	8(2)	20(2)	18(2)
C12	43(2)	39(2)	31(2)	10(2)	14(2)	18(2)
C13	45(3)	42(2)	41(2)	20(2)	21(2)	14(2)
C14	35(2)	42(2)	55(3)	14(2)	-2(2)	10(2)
C15	44(2)	45(2)	41(2)	16(2)	25(2)	20(2)
C16	27(2)	49(2)	57(3)	21(2)	17(2)	5(2)
C17	37(2)	33(2)	53(3)	16(2)	15(2)	16(2)
C18	39(2)	42(2)	32(2)	9(2)	9(2)	9(2)

Table B-44. Hydrogen coordinates (x 10^4) and isotropic displacement parameters ($Å^2$x 10^3) for **22**.

	x	y	z	U(eq)
H2A	7716	1430	5017	36
H3A	6945	1915	6595	44
H4A	7283	3867	7614	42
H5A	8469	5351	7082	40
H6A	9187	4898	5476	37
H9A	12600	1148	1403	41
H10A	11898	941	-612	48
H11A	9673	1595	-1743	49
H12A	8099	2447	-860	44
H13A	9203	5499	1187	59
H13B	7585	5544	171	59
H13C	8651	4617	-94	59
H14A	5693	2748	-883	74
H14B	4844	3778	-471	74
H14C	4959	2639	67	74
H15A	6608	4081	2645	59
H15B	6253	5206	2097	59
H15C	7973	5124	2937	59
H16A	14626	2718	2842	65
H16B	15312	3515	4170	65
H16C	13889	3858	3171	65
H17A	13215	465	4418	60
H17B	14683	840	4146	60
H17C	13077	265	3075	60
H18A	12831	3833	5283	58
H18B	13971	2997	5914	58
H18C	12149	2597	5401	58
H19A	4925	-436	1631	49
H20A	6067	-1055	3094	46
H21A	8927	-1157	3611	38
H22A	10390	256	3566	43
H19B	8351	-981	3994	41
H20B	6317	-1480	2653	44
H21B	4877	-81	1520	44
H22B	6096	1367	1190	60

LIST OF REFERENCES

1. Collman, J. P.; Hegedus, L. S.; Norton, J. R.; Finke, R. G. *Principles and Applications of Organotransition Metal Chemistry;* University Science Books: 1987.

2. Marr, G.; Rockett, B. W. *The Chemistry of the Metal-Carbon Bond;* John Wiley & Sons: New York, 1982.

3. Yamamoto, A. *Organotransition Metal Chemistry*; John Wiley & Sons: New York, 1986.

4. Spessard, G. O.; Miessler, G. L. *Organometallic Chemistry*; Prentice-Hall: New Jersey, 1997.

5. Tolman, C. A. *Chemical Society Reviews* **1972**, *1*, 337.

6. Masters, C. *Homogeneous Transition-Metal Catalysis*; Chapman Hall: London, 1981.

7. Parshall, G. W. *Homogeneous Catalysis*; Wiley Intersience: New York, 1980.

8. Jordan, R. B. *Reaction Mechanisms of Inorganic and Organometallic Systems*; Oxford University Press: Oxford, 1991.

9. Roelen, O. *Angewandte Chemie* **1948**, *60*(3), 6262.

10. Roelen, O. *Angewandte Chemie* **1949**, *61*(11), 448.

11. Falbe, H. *Carbon Monoxide in Organic Synthesis*; Springer-Verlag: Berlin, 1970.

12. Falbe, J. *New Syntheses With Carbon Monoxide*; Springer-Verlag: Berlin, 1980.

13. Wender, I.; Pino, P. *Organic Syntheses Via Metal Carbonyls*; Wiley Interscience: New York, 1977.

14. Elschenbroich, C. H.; Salzer, A. *Organometallics; A Concise Introduction*; VCH: New York, 1992.

15. Crabtree, R. H. *The Organometallic Chemistry of the Transition Metals 2nd Edition*; Wiley Interscience: New York, 1994.

16. Ziegler, T.; Versluis, L. *Advances in Inorganic Chemistry* **1992**, (230), 75.

17. Cawse, J. N.; Fiato, R. A.; Pruett, R. L. *Journal of Organometallic Chemistry* **1979**, *172*(4), 405.

18. Brown, C. K.; Wilkinson, G. *Journal of the Chemical Society a -Inorganic Physical Theoretical* **1970**, (17), 2753.

19. Roth, J. F. *Journal of Organometallic Chemistry* **1985**, *279*(1-2), 1.

20. Roth, J. F.; Craddock, J. H.; Hershman, A.; Paulik, F. E. *Chemical Technology* **1971**, 600.

21. Forster, D. *Advances in Organometallic Chemistry* **1979**, *17*, 255.

22. Forster, D. *Journal of the Chemical Society-Dalton Transactions* **1979**, (11), 1639.

23. Mizoroki, T.; Matsumoto, T.; Ozaki, A. *Bulletin of the Chemical Society of Japan* **1979**, *52*(2), 479.

24. Coffey, R. S. BP 1,121,642, 1966.

25. Young, J. F.; Osborn, J. A.; Jardine, F. H.; Wilkinson, G. *Chemical Communications* **1965** , (7), 131.

26. Chan, A. S. C.; Halpern, J. *Journal of the American Chemical Society* **1980**, *102*(2), 838.

27. Halpern, J. *Science* **1982**, *217*(4558), 401.

28. Halpern, J. *Inorganica Chimica Acta-Articles* **1981**, *50*(1), 11.

29. Halpern, J.; Riley, D. P.; Chan, A. S. C.; Pluth, J. J. *Journal of the American Chemical Society* **1977**, *99*(24), 8055.

30. Boncella, J. M.; Wang, S. Y. S.; Vanderlende, D. D. *Journal of Organometallic Chemistry* **1999**, *591*(1-2), 8.

31. Boncella, J. M.; Wang, S. Y. S.; Vanderlende, D. D.; Huff, R. L.; Abboud, K. A.; Vaughn, W. M. *Journal of Organometallic Chemistry* **1997**, *530*(1-2), 59.

32. Wang, S. Y. S.; Vanderlende, D. D.; Abboud, K. A.; Boncella, J. M. *Organometallics* **1998**, *17*(12), 2628.

33. Wang, S. Y. S. *PhD. Dissertation*; University of Florida: 1998.

34. Fischer, E. O.; Hafner, W. *Z. Naturforschg.* **1955**, *10B*, 665.

35. Calderazzo, F.; Pampaloni, G. *Journal of Organometallic Chemistry* **1992**, *423*(3), 307.

36. Jolly, P. W. *Accounts of Chemical Research* **1996**, *29*(11), 544.

37. Maslowsky, E. *Journal of Chemical Education* **1993**, *70*(12), 980.

38. Green, M. L. H. *Journal of Organometallic Chemistry* **1980**, *200*(1), 119.

39. Yoon, M.; Lin, J. H.; Young, V. G.; Miller, G. J. *Journal of Organometallic Chemistry* **1996**, *507*(1-2), 31.

40. Lockwood, M. A.; Fanwick, P. E.; Eisenstein, O.; Rothwell, I. P. *Journal of the American Chemical Society* **1996**, *118*(11), 2762.

41. Maseras, F.; Lockwood, M. A.; Eisenstein, O.; Rothwell, I. P. *Journal of the American Chemical Society* **1998**, *120*(26), 6598.

42. Ashmore, J.; Green, J. C.; Green, M. L. H.; Smith, M. L.; Mehnert, C.; Wucherer, E. J. *Journal of the Chemical Society-Dalton Transactions* **1995**, (11), 1873.

43. Mehnert, C. P.; Chernega, A. N.; Green, M. L. H. *Journal of Organometallic Chemistry* **1996** , *513*(1-2), 247.

44. Lockwood, M. A.; Fanwick, P. E.; Rothwell, I. P. *Polyhedron* **1995**, *14*(22), 3363.

45. Wexler, P. A.; Wigley, D. E.; Koerner, J. B.; Albright, T. A. *Organometallics* **1991**, *10*(7), 2319.

46. Horton, A. D.; Dewith, J. *Organometallics* **1997**, *16*(25), 5424.

47. Thorn, M. G.; Etheridge, Z. C.; Fanwick, P. E.; Rothwell, I. P. *Organometallics* **1998**, *17*(17), 3636.

48. Musso, F.; Solari, E.; Floriani, C.; Schenk, K. *Organometallics* **1997**, *16*(22), 4889.

49. Calderazzo, F.; Ferri, I.; Pampaloni, G.; Troyanov, S. *Journal of Organometallic Chemistry* **1996**, *518*(1-2), 189.

50. Lancaster, S. J.; Robinson, O. B.; Bochmann, M.; Coles, S. J.; Hursthouse, M. B. *Organometallics* **1995**, *14*(5), 2456.

51. Pellecchia, C.; Grassi, A.; Immirzi, A. *Journal of the American Chemical Society* **1993**, *115*(3), 1160.

52. Troyanov, S. *Journal of Organometallic Chemistry* **1994**, *475*(1-2), 139.

53. Troyanov, S.; Pisarevsky, A.; Struchkov, Y. T. *Journal of Organometallic Chemistry* **1995**, *494*(1-2), C4.

54. Diamond, G. M.; Green, M. L. H.; Walker, N. M.; Howard, J. A. K.; Mason, S. A. *Journal of the Chemical Society-Dalton Transactions* **1992**, (17), 2641.

55. Bruck, M. A.; Copenhaver, A. S.; Wigley, D. E. *Journal of the American Chemical Society* **1987**, *109*(21), 6525.

56. Wang, S. Y. S.; Abboud, K. A.; Boncella, J. M. *Journal of the American Chemical Society* **1997**, *119*(49), 11990.

57. Ortiz, C. G.; Abboud, K. A.; Cameron, T. M.; Boncella, J. M. *Chemical Communications* **2001** , (3), 247.

58. Yasuda, H.; Tatsumi, K.; Nakamura, A. *Accounts of Chemical Research* **1985**, *18*(4), 120.

59. Yasuda, H.; Tatsumi, K.; Okamoto, T.; Mashima, K.; Lee, K.; Nakamura, A.; Kai, Y.; Kanehisa, N.; Kasai, N. *Journal of the American Chemical Society* **1985**, *107*(8), 2410.

60. Kruger, C.; Muller, G.; Erker, G.; Dorf, U.; Engel, K. *Organometallics* **1985**, *4*(2), 215.

61. Blosch, L. L.; Gamble, A. S.; Abboud, K.; Boncella, J. M. *Organometallics* **1992**, *11*(7), 2342.

62. Vanderlende, D. D.; Abboud, K. A.; Boncella, J. M. *Organometallics* **1994**, *13*(9), 3378.

63. Wang, S. Y. S.; Boncella, J. M.; Abboud, K. A. *Acta Crystallographica Section C-Crystal Structure Communications* **1997**, *53*, 436.

64. Erker, G.; Kropp, K. *Journal of the American Chemical Society* **1979**, *101*(13), 3659.

65. Erker, G.; Dorf, U.; Rheingold, A. L. *Organometallics* **1988**, *7*(1), 138.

66. Takahashi, T.; Xi, Z. F.; Rousset, C. J.; Suzuki, N. *Chemistry Letters* **1993**, (6), 1001.

67. Mansel, S.; Thomas, D.; Lefeber, C.; Heller, D.; Kempe, R.; Baumann, W.; Rosenthal, U. *Organometallics* **1997**, *16*(13), 2886.

68. Muhler, M.; Schutze, J.; Wesemann, M.; Rayment, T.; Dent, A.; Schlogl, R.; Ertl, G. *Journal of Catalysis* **1990**, *126*(2), 339.

69. Mills, R. C.; Abboud, K. A.; Boncella, J. M. *Organometallics* **2000**, *19*(16), 2953.

70. Lancaster, S. J.; Robinson, O. B.; Bochmann, M.; Coles, S. J.; Hursthouse, M. B. *Organometallics* **1995**, *14*(5), 2456.

71. Parker, K. G.; Noll, B.; Pierpont, C. G.; Dubois, M. R. *Inorganic Chemistry* **1996**, *35*(11), 3228.

72. Kriley, C. E.; Fanwick, P. E.; Rothwell, I. P. *Journal of the American Chemical Society* **1994**, *116*(12), 5225.

73. Chisholm, M. H.; Cook, C. M.; Folting, K.; Streib, W. E. *Inorganica Chimica Acta* **1992**, *200*, 63.

74. Arnaudet, L.; Bougon, R.; Buu, B.; Lance, M.; Nierlich, M.; Thuery, P.; Vigner, J. *Journal of Fluorine Chemistry* **1995**, *71*(1), 123.

75. Wesemann, L.; Waldmann, L.; Ruschewitz, U.; Ganter, B.; Wagner, T. *Journal of the Chemical Society-Dalton Transactions* **1997**, (6), 1063.

76. Galindo, A.; Ienco, A.; Mealli, C. *New Journal of Chemistry* **2000**, *24*, 73.

77. Mills, R. C.; Abboud, K. A.; Boncella, J. M. *Inorganic Chamistry , In Press.*

78. Buchwald, S. L.; Lum, R. T.; Dewan, J. C. *Journal of the American Chemical Society* **1986**, *108*(23), 7441.

79. Buchwald, S. L.; Watson, B. T.; Huffman, J. C. *Journal of the American Chemical Society* **1987**, *109*(8), 2544.

80. Buchwald, S. L.; Nielsen, R. B. *Chemical Reviews* **1988**, *88*(7), 1047.

81. Ohiff, A.; Pulst, S.; Lefeber, C.; Peulecke, N.; Arndt, P.; Burkalov, V. V.; Rosenthal, U. *Synlett* **1996**, (2), 111.

82. Lefeber, C.; Baumann, W.; Tillack, A.; Kempe, R.; Gorls, H.; Rosenthal, U. *Organometallics* **1996**, *15*(16), 3486.

83. Hiller, J.; Thewalt, U.; Polasek, M.; Petrusova, L.; Varga, V.; Sedmera, P.; Mach, K. *Organometallics* **1996**, *15*(17), 3752.

84. Cotton, F. A.; Hall, W. T. *Inorganic Chemistry* **1981**, *20*(4), 1285.

85. Theopold, K. H.; Holmes, S. J.; Schrock, R. R. *Angewandte Chemie-International Edition in English* **1983**, *22*(12), 1010.

86. Holloway, C. E.; Melnik, M. *Reviews in Inorganic Chemistry* **1985**, *7,* 11161.

87. Walborsky, E. C.; Wigley, D. E.; Roland, E.; Dewan, J. C.; Schrock, R. R. *Inorganic Chemistry* **1987**, *26*(10), 1615.

88. Hartung, J. B.; Pedersen, S. F. *Journal of the American Chemical Society* **1989**, *111*(14), 5468.

89. Curtis, M. D.; Real, J.; Kwon, D. *Organometallics* **1989**, *8*(7), 1644.

90. Cotton, F. A.; Shang, M. *Inorganic Chemistry* **1990**, *29*(3), 508.

91. Maatta, E. A.; Wentworth, R. A. D.; Newton, W. E.; Mcdonald, J. W.; Watt, G. D. *Journal of the American Chemical Society* **1978**, *100*(4), 1320.

92. Maatta, E. A.; Wentworth, R. A. D. *Inorganic Chemistry* **1979**, *18*(2), 524.

93. Newton, W. E.; Mcdonald, J. W.; Corbin, J. L.; Ricard, L.; Weiss, R. *Inorganic Chemistry* **1980**, *19*(7), 1997.

94. Templeton, J. L.; Ward, B. C.; Chen, G. J. J.; Mcdonald, J. W.; Newton, W. E. *Inorganic Chemistry* **1981**, *20*(4), 1248.

95. Morrow, J. R.; Tonker, T. L.; Templeton, J. L. *Organometallics* **1985**, *4*(4), 745.

96. Nielson, A. J.; Ware, D. C. *Polyhedron* **1990**, *9*(4), 603.

97. Nielson, A. J.; Boyd, P. D. W.; Clark, G. R.; Hunt, T. A.; Metson, J. B.; Rickard, C. E. F.; Schwerdtfeger, P. *Polyhedron* **1992**, *11*(11), 1419.

98. Kriley, C. E.; Kerschner, J. L.; Fanwick, P. E.; Rothwell, I. P. *Organometallics* **1993**, *12*(6), 2051.

99. Clark, G. R.; Nielson, A. J.; Rae, A. D.; Rickard, C. E. F. *Journal of the Chemical Society-Dalton Transactions* **1994**, (12), 1783.

100. Nielson, A. J.; Boyd, P. D. W.; Clark, G. R.; Hunt, P. A.; Hursthouse, M. B.; Metson, J. B.; Rickard, C. E. F.; Schwerdtfeger, P. A. *Journal of the Chemical Society-Dalton Transactions* **1995**, (7), 1153.

101. Clark, G. R.; Glenny, M. W.; Nielson, A. J.; Rickard, C. E. F. *Journal of the Chemical Society-Dalton Transactions* **1995**, (7), 1147.

102. Clark, G. R.; Nielson, A. J.; Rickard, C. E. F. *Journal of the Chemical Society-Dalton Transactions* **1995**, (11), 1907.

103. Nielson, A. J.; Rickard, C. E. F. *Journal of the Chemical Society-Dalton Transactions* **1999**, (12), 2021.

104. Crane, T. W.; White, P. S.; Templeton, J. L. *Organometallics* **1999**, *18*(10), 1897.

105. Templeton J. L. *Advances in Organometallic Chemistry* **1989**, *29*, 1.

106. Davidson, J. L. *Reactions of Coordinated Ligands*; Plenum Press: New York, 1986.

107. Elschenbroich, C.; Salzer, A. *Organometallics A Concise Introduction*; VCH: New York, 1991.

108. Erker, G.; Kruger, C.; Muller, G. *Advances in Organometallic Chemistry* **1985**, *24*, 1.

109. Yasuda, H.; Nakamura, A. *Angewandte Chemie-International Edition in English* **1987**, *26*(8), 723.

110. Erker, G.; Wicher, J.; Engel, K.; Rosenfeldt, F.; Dietrich, W.; Kruger, C. *Journal of the American Chemical Society* **1980**, *102*(20), 6344.

111. Akita, M.; Yasuda, H.; Nakamura, A. *Chemistry Letters* **1983**, (2), 217.

112. Mashima, K.; Yasuda, H.; Asami, K.; Nakamura, A. *Chemistry Letters* **1983**, (2), 219.

113. Yasuda, H.; Nagasuna, K.; Asami, K.; Nakamura, A. *Chemistry Letters* **1983**, (7), 955.

114. Yasuda, H.; Kajihara, Y.; Mashima, K.; Nagasuna, K.; Nakamura, A. *Chemistry Letters* **1981** , (5), 671.

115. Yasuda, H.; Kajihara, Y.; Nagasuna, K.; Mashima, K.; Nakamura, A. *Chemistry Letters* **1981** , (6), 719.

116. Erker, G.; Engel, K.; Dorf, U.; Atwood, J. L.; Hunter, W. E. *Angewandte Chemie-International Edition in English* **1982**, *21*(12), 914.

117. Erker, G.; Engel, K.; Atwood, J. L.; Hunter, W. E. *Angewandte Chemie-International Edition in English* **1983**, *22*(6), 494.

118. Erker, G.; Dorf, U. *Angewandte Chemie-International Edition in English* **1983**, *22*(10), 777.

119. Erker, G.; Muhlenbernd, T.; Benn, R.; Rufinska, A.; Tainturier, G.; Gautheron, B. *Organometallics* **1986**, *5*(5), 1023.

120. Erker, G.; Lecht, R.; Petersen, J. L.; Bonnemann, H. *Organometallics* **1987**, *6*(9), 1962.

121. Davies, S. G. *Organotransition Metal Chemistry: Applications to Organic Synthesis*; Pergamon Press: Oxford, 1982.

122. Eaton, B.; King, J. A.; Vollhardt, K. P. C. *Journal of the American Chemical Society* **1986**, *108*(6), 1359.

123. Faller, J. W.; Rosan, A. M. *Journal of the American Chemical Society* **1977**, *99*(14), 4858.

124. Green, M. L. H.; Hare, P. M.; Bandy, J. A. *Journal of Organometallic Chemistry* **1987**, *330*(1-2), 61.

125. Cohen, S. A.; Auburn, P. R.; Bercaw, J. E. *Journal of the American Chemical Society* **1983** , *105*(5), 1136.

126. Erker, G.; Dorf, U.; Rheingold, A. L. *Organometallics* **1988**, *7*(1), 138.

127. Knight, K. S.; Wang, D.; Waymouth, R. M.; Ziller, J. *Journal of the American Chemical Society* **1994**, *116*(5), 1845.

128. Rocklage, S. M.; Schrock, R. R. *Journal of the American Chemical Society* **1982**, *104*(11), 3077.

129. Schultz, A. J.; Brown, R. K.; Williams, J. M.; Schrock, R. R. *Journal of the American Chemical Society* **1981**, *103*(1), 169.

130. Robbins, J.; Bazan, G. C.; Murdzek, J. S.; Oregan, M. B.; Schrock, R. R. *Organometallics* **1991**, *10*(8), 2902.

131. Clark, G. R.; Nielson, A. J.; Rickard, C. E. F.; Ware, D. C. *Journal of the Chemical Society-Dalton Transactions* **1990**, (4), 1173.

132. Ortiz, C. G. *Ph.D. Dissertation*; Universtiy of Florida, 1999.

133. Cameron, T. M.; Ortiz, C. G.; Boncella, J. M. *Unpublished Results* .

134. Fryzuk, M. D.; Haddad, T. S.; Rettig, S. J. *Organometallics* **1989**, *8*(7), 1723.

135. Spencer, M. D.; Wilson, S. R.; Girolami, G. S. *Organometallics* **1997**, *16*(13), 3055.

136. Bachmann, K.; von Philipsborn, W. *Org. Magn. Reson.* **1976**, *8*, 648.

137. Strauch, H. C.; Erker, G.; Frohlich, R. *Organometallics* **1998**, *17*(26), 5746.

138. Strauch, H. C.; Roesmann, R.; Pacheiner, S.; Erker, G.; Frohlich, R.; Wibbeling, B. *Journal of Organometallic Chemistry* **1999**, *584*(2), 318.

139. Strauch, H. C.; Wibbeling, B.; Frohlich, R.; Erker, G.; Jacobsen, H.; Berke, H. *Organometallics* **1999**, *18*(19), 3802.

140. Okamoto, T.; Yasuda, H.; Nakamura, A.; Kai, Y.; Kanehisa, N.; Kasai, N. *Organometallics* **1988**, *7*(11), 2266.

141. Topsøe, H.; Clausen, B. S.; Massoth, F. E. *Hydrotreating Catalysis in Catalysis: Science and Technology;* Springer-Verlag: New York, 1996; Vol. 11.

142. Whitehurst, D. D.; Isoda, T.; Mochida, I. *Advances in Catalysis;* Vol. 42, 345.

143. Bianchini, C.; Meli, A. *Accounts of Chemical Research* **1998**, *31* (3), 109.

144. Angelici, R. J. *Polyhedron* **1997**, *16*(18), 3073.

145. Sanchezdelgado, R. A. *Journal of Molecular Catalysis* **1994**, *86*(1-3), 287.

146. Chen, J. B.; Daniels, L. M.; Angelici, R. J. *Journal of the American Chemical Society* **1990**, *112*(1), 199.

147. Angelici, R. J. *Bulletin Des Societes Chimiques Belges* **1995**, *104*(4-5), 265.

148. Rauchfuss, T. B. *Progress in Inorganic Chemistry* **1991**, *392*, 59.

149. Angelici, R. J. *Coordination Chemistry Reviews* **1990**, *105*, 61.

150. Bianchini, C.; Jimenez, M. V.; Meli, A.; Moneti, S.; Vizza, F.; Herrera, V.; Sanchezdelgado, R. A. *Organometallics* **1995**, *14*(5), 2342.

151. Churchill, D. G.; Bridgewater, B. M.; Parkin, G. *Journal of the American Chemical Society* **2000**, *122*(1), 178.

152. Jones, W. D.; Chin, R. M.; Crane, T. W.; Baruch, D. M. *Organometallics* **1994**, *13*(11), 4448.

153. Dong, L. Z.; Duckett, S. B.; Ohman, K. F.; Jones, W. D. *Journal of the American Chemical Society* **1992**, *114*(1), 151.

154. Jones, W. D.; Dong, L. Z. *Journal of the American Chemical Society* **1991**, *113*(2), 559.

155. Chen, J. B.; Daniels, L. M.; Angelici, R. J. *Polyhedron* **1990**, *9*(15-16), 1883.

156. Chen, J.; Angelici, R. J. *Organometallics* **1990**, *9*(3), 849.

157. Bianchini, C.; Meli, A.; Peruzzini, M.; Vizza, F.; Frediani, P.; Herrera, V.; Sanchezdelgado, R. A. *Journal of the American Chemical Society* **1993**, *115*(7), 2731.

158. Cornils, B.; Herrmann, W. A. *Applied Homogeneous Catalysis With Organometallic Compounds*; VCH: New York, 1996.

159. Aljarallah, A. M.; Anabtawi, J. A.; Siddiqui, M. A. B.; Aitani, A. M.; Alsadoun, A. W. *Catalysis Today* **1992**, *14*(1), R9.

160. Mclain, S. J.; Sancho, J.; Schrock, R. R. *Journal of the American Chemical Society* **1980**, *102*(17), 5610.

161. Piers, W. E.; Shapiro, P. J.; Bunel, E. E.; Bercaw, J. E. *Synlett* **1990**, (2), 74.

162. Hauptman, E.; Saboetienne, S.; White, P. S.; Brookhart, M.; Garner, J. M.; Fagan, P. J.; Calabrese, J. C. *Journal of the American Chemical Society* **1994**, *116*(18), 8038.

163. Christoffers, J.; Bergman, R. G. *Inorganica Chimica Acta* **1998**, *270*(1-2), 20.

164. Andresen, A.; Cordes, H. G.; Herwig, J.; Kaminsky, W.; Merck, A.; Mottweiler, R.; Pein, J.; Sinn, H.; Vollmer, H. J. *Angewandte Chemie-International Edition in English* **1976**, *15*(10), 630.

165. Sinn, H.; Kaminsky, W.; Vollmer, H. J.; Woldt, R. *Angewandte Chemie-International Edition in English* **1980**, *19*(5), 390.

166. Brintzinger, H. H.; Fischer, D.; Mulhaupt, R.; Rieger, B.; Waymouth, R. M. *Angewandte Chemie-International Edition in English* **1995**, *34*(11), 1143.

167. Thorn, M. G.; Hill, J. E.; Waratuke, S. A.; Johnson, E. S.; Fanwick, P. E.; Rothwell, I. P. *Journal of the American Chemical Society* **1997**, *119* (37), 8630.

168. Negishi, E.; Jensen, M. D.; Kondakov, D. Y.; Wang, S. *Journal of the American Chemical Society* **1994**, *116*(18), 8404.

169. Shaughnessy, K. H.; Waymouth, R. M. *Journal of the American Chemical Society* **1995**, *117*(21), 5873.

170. Christoffers, J.; Bergman, R. G. *Journal of the American Chemical Society* **1996**, *118*(19), 4715.

171. Waratuke, S. A.; Thorn, M. G.; Fanwick, P. E.; Rothwell, A. P.; Rothwell, I. P. *Journal of the American Chemical Society* **1999**, *121*(39), 9111.

172. Natta, G.; Dallasta, G.; Donegani, G.; Mazzanti, G. *Angewandte Chemie-International Edition* **1964**, *3*(11), 723.

173. Calderon, N.; Ofstead, E. A.; Ward, J. P.; Judy, W. A.; Scott, K. W. *Journal of the American Chemical Society* **1968**, *90*(15), 4133.

174. Schrock, R. R. *Journal of Organometallic Chemistry* **1986**, *300*(1-2), 249.

175. Schrock, R. R. *Accounts of Chemical Research* **1990**, *23*(5), 158.

176. Carter, E. A.; Goddard III, W. A. *Journal of the American Chemical Society* **1986**, *108*(16), 4746.

177. Menapace, H. R.; Maly, N. A.; Wang, J. L.; Wideman, L. G. *Journal of Organic Chemistry* **1975**, *40*(20), 2983.

178. Menapace, H. R.; Benner, G. S.; Maly, N. A. USP 3,784,629, **1972**.

179. Brown, M.; Menapace, H. R.; Maly, N. A. USP 3,897,512, **1973**.

180. Lawson, G. W. USP 3,813,453, **1974**.

181. Maly, N. A.; Menapace, H. R.; Benner, G. S. USP 3,903,193, **1975**.

182. Hendriksen, D. E. USP 5,059,739, **1989**.

183. Grubbs, R. H.; Miyashita, A. *Journal of the American Chemical Society* **1978**, *100*(23), 7416.

184. Ozawa, F.; Yamamoto, A.; Ikariya, T.; Grubbs, R. H. *Organometallics* **1982**, *1*(11), 1481.

185. McDermott, J. X.; White, J. F.; Whitesides, G. M. *Journal of the American Chemical Society* **1976**, *98*(21), 6521.

186. Brown, M. P.; Hollings, A.; Houston, K. J.; Puddephatt, R. J.; Rashidi, M. *Journal of the Chemical Society-Dalton Transactions* **1976**, (9), 786.

187. Mclain, S. J.; Wood, C. D.; Schrock, R. R. *Journal of the American Chemical Society* **1979** , *101*(16), 4558.

188. Herisson, J. L.; Chauvin, Y. *Makromol. Chem.* **1970**, *141*, 161.

189. Kress, J.; Osborn, J. A. *Angewandte Chemie-International Edition in English* **1992**, *31*(12), 1585.

190. Kiel, W. A.; Lin, G. Y.; Gladysz, J. A. *Journal of the American Chemical Society* **1980**, *102*(9), 3299.

191. Burk, M. J.; Mcgrath, M. P.; Crabtree, R. H. *Journal of the American Chemical Society* **1988**, *110*(2), 620.

192. Freundlich, J. S.; Schrock, R. R.; Cummins, C. C.; Davis, W. M. *Journal of the American Chemical Society* **1994**, *116*(14), 6476.

193. Schrock, R. R.; Sharp, P. R. *Journal of the American Chemical Society* **1978**, *100*(8), 2389.

194. Schrock, R. R. In *Reactions of Coordinated Ligands*; Bratermann, P. S., Ed.; Plenum Press: New York, 1986; p 221.

195. Onopchenko, A.; Cupples, B. L.; Kresge, A. N. *Industrial & Engineering Chemistry Product Research and Development* **1983**, *22*(2), 182.

196. Brennan, J. A. *Industrial & Engineering Chemistry Product Research and Development* **1980**, *19*(1), 2.

197. Shubkin, R. L.; Baylerian, M. S.; Maler, A. R. *Industrial & Engineering Chemistry Product Research and Development* **1980**, *19*(1), 15.

198. Sullivan, F. W.; Vorhees, V.; Neeley, A. W.; Shankland, R. V. *Industrial & Engineering Chemistry Product Research and Development* **1931**, *23*, 604.

199. Garwood, W. E. USP 2,937,129, **1960**.

200. Southern, D.; Milne, C. B.; Moseley, J. C.; Beynon, K. I.; Evans, T. G. BP 873,064, **1961**.

201. Sheldrick, G. M. *SHELLXT* Madison, WI, **1986**.

BIOGRAPHICAL SKETCH

Ryan Christopher Mills was born on August 18th, 1973 in Batavia, NY. Unlike most other chemists, there was no defining moment or individual that was the source of his interest in chemistry. Instead, it just worked out that way. Upon completing high school he moved on to St. Lawrence University where he planned on playing football and baseball while also furthering his education. These priorities soon changed as he was placed on academic probation after his first semester. After taking his first chemistry class during the fall semester of his sophomore year it became apparent that this would make for an interesting and possibly fulfilling career. Wanting more than a career as a B.S. chemist could offer and with the advice of Dr. John J. Rupp, he decided to pursue a graduate degree upon graduation from St. Lawrence in 1996. In the summer of 1996 he moved to the University of Florida where he joined the research group of Dr. James M. Boncella. In the five years since, he has realized that everything eventually falls into place as he has become completely fascinated with the world of organometallic chemistry. After completion of his Ph.D. degree in inorganic/organometallic chemistry in April of 2001, Ryan will assume a position as a research scientist at GE Corporate Research and Development, chemical process and technology division, in Schenectady, NY.

I certify that I have read this study and that in my opinion it conforms to acceptable standards of scholarly presentation and is fully adequate, in scope and quality, as a thesis for the degree of Doctor of Philosophy.

James M. Boncella, Chairman
Professor of Chemistry

I certify that I have read this study and that in my opinion it conforms to acceptable standards of scholarly presentation and is fully adequate, in scope and quality, as a thesis for the degree of Doctor of Philosophy.

David E. Richardson
Professor of Chemistry

I certify that I have read this study and that in my opinion it conforms to acceptable standards of scholarly presentation and is fully adequate, in scope and quality, as a thesis for the degree of Doctor of Philosophy.

Lisa A. McElwee-White
Professor of Chemistry

I certify that I have read this study and that in my opinion it conforms to acceptable standards of scholarly presentation and is fully adequate, in scope and quality, as a thesis for the degree of Doctor of Philosophy.

John R. Reynolds
Professor of Chemistry

I certify that I have read this study and that in my opinion it conforms to acceptable standards of scholarly presentation and is fully adequate, in scope and quality, as a thesis for the degree of Doctor of Philosophy.

Guerry H. McClellan
Professor of Geology

This thesis was submitted to the Graduate Faculty of the Department of Chemistry in the College of Liberal Arts and Sciences and to the Graduate School and was accepted as partial fulfillment of the requirements for the degree of Doctor of Philosophy.

August 2001

Dean, Graduate School